The Unruh-DeWitt Detector Model: Modified Dispersion and Nonlinear Couplings

by

A. Morgan Sachs

A thesis
presented to the University of Waterloo
in fulfillment of the
thesis requirement for the degree of
Doctor of Philosophy
in
Physics (Quantum Information)

Waterloo, Ontario, Canada, 2021

Examining Committee Membership

The following served on the Examining Committee for this thesis. The decision of the Examining Committee is by majority vote.

External Examiner: Stefano Liberati
Full Professor, SISSA, Trieste, Italy

Supervisor(s): Robert B. Mann
Professor, Dept. of Physics and Astronomy, University of Waterloo
Affiliate Faculty, Perimeter Institute for Theoretical Physics

Achim Kempf
Professor and University Research Chair,
Dept. of Applied Mathematics, University of Waterloo
Affiliate Faculty, Perimeter Institute for Theoretical Physics

Internal Member: Robert Spekkens
Senior Faculty, Perimeter Institute for Theoretical Physics
Adjunct faculty, Dept. of Physics and Astronomy, University of Waterloo

Internal Member: Kevin Resch
Professor and Interim Direction,
Institute for Quantum computing, University of Waterloo
Professor, Dept. of Physics and Astronomy, University of Waterloo

Internal-External: Eduardo Martín Martínez
Associate Professor, Dept. of Applied Math, University of Waterloo
Affiliate Faculty, Perimeter Institute for Theoretical Physics
Associate Faculty, Institute for Quantum Computing

Author's Declaration

This thesis consists of material all of which I authored or co-authored: see Statement of Contributions included in the thesis. This is a true copy of the thesis, including any required final revisions, as accepted by my examiners.

I understand that my thesis may be made electronically available to the public.

Statement of Contributions

A. Morgan Sachs was the sole author this thesis, although portions of this thesis are adaptations of collaborative publications, as described below. Methods (chapter 1) and Conclusion (chapter 8) were prepared by AMS for this thesis.

Non-linear Optics with a UDW Detector (chapter 2) is adapted for this thesis from the publication [1]. This publication was prepared in collaboration with Erickson Tjoa, E. Martń-Martínez, and Irene Lopez Gutierrez. At various points through the life of the project AMS held the following roles: mentoring, drafting manuscript, editing manuscripts, and checking calculations. Erickson Tjoa performed the majority of the calculations and drafted, along with E. Martń-Martínez, the majority of the final manuscript. The research problem, originally proposed by E. Martin-Martinez, evolved to its current form through numerous scientific discussions among the collaborators. Erickson Tjoa, Eduardo and AMS critically contributed to the process of developing the conceptual ideas addressed therein.

Fundamental Decoherence in Optical Cavities (chapter 3) are adapted for this thesis from an ongoing collaboration with Agata M. Brańczyk, Olivier Simon and Eduardo Martń-Martínez. AMS performed calculations, took part in scientific discussions, contributed to editing, and drafted an appendix of the manuscript.

Fermionic Entanglement Harvesting (chapter 4) is adapted for this thesis from an ongoing collaboration with one of AMS's supervisors (Robert B. Mann) as well as Eduardo Martín-Martínez. AMS conducted a majority of the research on these projects with some guidance/input from their collaborators. AMS wrote the draft manuscript alone.

UDW pairs with Modified Dispersion (chapter 5) is adapted for this thesis from an ongoing collaboration with one of AMS's supervisors (Robert B. Mann) as well as Silke Weinfurtner. AMS conducted a majority of the research on these projects with some guidance/input from their collaborators. AMS wrote the draft manuscript alone which was then extensively collaboratively edited. This research problem was originally proposed by Achim Kempf, Silke Weinfurtner, and Robert B. Mann.

Techniques in Harvesting (section 6.1) is adapted for this thesis from an ongoing project by AMS. AMS conducted a majority of the research on this project and drafted the manuscript.

Persistent Divergences in Quadratically Coupled Models? (section 7.1) is adapted for this thesis from [2] and an ongoing collaborations with one of AMS's supervisors (Robert B Mann) as well as Eduardo Martín-Martínez. AMS conducted a majority of the research on these projects with guidance/input from their collaborators. AMS wrote the draft manuscript alone which was then collaboratively edited.

Abstract

In this work, we employ the Unruh-DeWitt (UDW) detector model to various ends. We present applications of this relativistic detector model to quantum optics, including decoherence in optical cavities and non-linear quantum optics. We also relate an array of UDW-like models to the usual UDW model, which has the immediate consequence of yielding a tool to probe the entanglement structure of the Fermionic field, as well as many others. We are also able to show that entanglement harvesting is robust under dispersive effects, paving the way for tabletop experiments of the protocol.

Acknowledgements

I would like to thank my supervisor, Robb Mann, especially for his support during critical junctures of my graduate studies. I would also like to thank my supervisor Achim Kempf for stepping in during a stressful transition in my PhD.

To my friends who supported me during the worst and best times, thank you. Especially warm emphatic thanks go to Cary Earnest and to Emma McKay.

I would also like to thank the folks at the Graduate Student Association at the University of Waterloo for the opportunity to do meaningful work when I most needed purpose and a distraction.

Another round of thanks goes to my collaborators, who were patient with me and who gave me opportunities.

The folks in the three RQI research groups at UW were fabulous colleagues, and I'm very thankful for the conversations and ideas that we exchanged.

A thank you goes to the folks at the Louisa street house, especially Julia Amoros Binefa, who put love and effort into building a strong community.

Dedication

Good luck on your norther adventures, Mama Llama.

Table of Contents

List of Figures

Chapter 0

Introduction

All attempts to construct a renormalizable theory of quantum gravity have failed to produce predictive results in accordance with observations of the natural world [3]. Scientists continue to work toward the goal of a theory of quantum gravity, the results of which are ambitious on-going projects such as string theory and loop quantum gravity [3]. Yet, there is much to understand with the more "modest" quantum field theory in curved spacetime. Indeed, while perhaps quantum field theory seems modest next to programs seeking a full theory of quantum gravity, quantum field theory is both very accurate and amazingly predictive as the core of the wildly successful standard model of particle physics [4].

The questions that can be asked (and often answered) through quantum field theory are varied. How much entanglement does a quantum field carry [5]? Can we extract anything useful from the quantum vacuum [6, 7, 8]? What happens near an event horizon [9]? Is information really lost during blackhole evaporation [10]? Can we experiment on quantum field theory in table top experiments [11]?

One of the fields of physics that asks these kinds of questions is relativistic quantum information (RQI). The field is perhaps 15 years old, with the Workshop on Relativistic Quantum Information going online this year (2021) for its 14th iteration in a combined conference with RQI-North, the 11th such conference. It is sometimes said that RQI exists at the intersection of relativity, quantum theory, and information theory. This interdisciplinary field is the one which I consider myself and this work a part.

In the thesis that follows, I will ask questions that are information-theoretic in nature in the setting of quantum field theory, in the realm of what one might term "information theory and information processing in covariant settings." This group applies techniques from classical and quantum information theory to settings where aspects of both relativity

and quantum theory apply. This includes measuring correlations in quantum field theories, defining and studying reference frames defined by quantum systems, bandlimiting in quantum field theory, or pushing the boundaries on our ability to describe non-classical (in the combined general relativistic and quantum mechanicial sense) temporal ordering of operations. While perusing the arxiv for works by this section of the RQI community, you're likely to see many papers discussing the various information-theoretic aspects of black holes, tests of quantum foundations in gravitational fields, and gravitational docoherence.

To speak more on information theory, I'll begin by saying it is a strange beast. It is ever present, yet in most ways it is a tool and not a theory. In our modern world, we're all jacked into the matrix in one form or another. We have social media, Pokémon Go, and constant video conferencing. Our digital lives are as real as our physical ones. So, perhaps it isn't too much of a stretch to the young minds of today to hear that *information is physical*. However, this dictum is different than saying that digital experiences are as valid as physical experiences. Instead, this dictum points to two facets of reality: first, information is carried by physical systems through the physical world; some would say information has *no* existence without the physical systems which carry it. It may seem abstract, but it is very much a part of the world. Next, related to this idea is the fact that information and thermodynamic entropy are linked; storing and then erasing information generates heat. Again, this may seem abstract, but it has direct and profound implications on our ability to pump heat out of the CPU in a modern computer; the heat produced by the erasure of *information* is the biggest hurdle to producing faster computers. Yet a third way we may see that information is physical is by the differences in quantum and classical computing. Information in these theories flows differently. In the quantum theory, we can have the delocalization of information–which cannot be copied in the quantum theory–across multiple systems, we can have correlations that are stronger than those found in classical systems, and we can have superpsoitions of states in subtler ways than in the classical theory. All these differences in the flows of information mean computers work differently. Another way of viewing this fact is to say that the fundamental features of a physical system dictate the information within. Information is physical.

Why all this talk about information? Of course there is the fact that we claim to be studying relativistic quantum *information*, and so of course information theory is relevant. But we won't explicitly mention information terribly often in the following pages. In fact, we will often hide behind terms like "correlations," "entropy," and "entanglement." But these *are* information. These terms are fundamentally about information. The term correlations refers to how much you might learn about one system by measuring another. Entropy, in the specific form of the Shannon entropy, is a measure of information. Finally, entanglement is a specific form of correlation that only occurs in quantum systems. By

choosing to look at these quantities, we are applying the tools of information theory. We are *doing* information theory. That is one of the tricky things about information; it is embedded in physical systems, so we often think we're *just* doing quantum field theory. Remember, information is physical.

Let's dive a little deeper into quantum field theory, and consider some of the challenges the theory presents to itself. First, there is the Reeh-Schlieder theorem. We won't worry about the full precise statement. Generally speaking, the Reeh-Schlieder theorem states that local operations on a quantum field theory do not produce local states [12]. Any state can be arbitrarily well approximated by an operation acting on the vacuum that is confined to a compact region. Additionally, a corollary of the theorem states that there are no local number operators: we can't count particles if we are only looking at a small piece of spacetime [12]! Another theorem, by Malament, also throws a wrench in the works for localizable particles in a relativistic quantum theory [12]. Other problems that ensue are that there aren't any rank-one projectors, which would let us discuss measurements in quantum field theory the same way we do in quantum mechanics [12]. On top of that there is no position operator in quantum field theory [12]. To summarize: our toolset in quantum field theory is *limited* if we want to learn about localized regions of the field.

What does one do in the face of such limitations? Our approach will be to employ a detector to probe the field. The detector will be a non relativistic quantum mechanical system. There are additional reasons to do this beyond those of localization. First, quantities in quantum field theory aren't always convergent [5]. For example, the entanglement entropy between two halves of a quantum field generally diverges, yet that boundless entanglement is not usable and in fact altered UV behaviour is almost certainly required. Another example is the Unruh effect, wherein a non-inertial observer sees particle content in the quantum vacuum. This effect can be shown via Rindler quantization, yet the philosophical issues of the pre-determinism of the forever-accelerated trajectory cast doubt on the results for some [13]. This issue could be said to be analogous to the teleological nature of the event horizon of a black hole.[1] On the other hand, an accelerated detector interacting with Minkowski vacuum shows a thermal response in the adiabatic limit, which only assumes a long, not infinite interaction time. In other words, the infinite pre-determinism of the Rindler quantization is replaced with a detector's time-dependant coupling, which simply must change more slowly than other time scales in the setup! It's the difference between *actual* infinite time in Rindler quantization and an *effective* infinite time in the

[1] See [14]: "For an observer to state that a black hole event horizon has formed requires knowledge of the spacetime outside his or her future light cone, which is impossible to achieve unless the spacetime is stationary, the black hole has existed forever and nothing changes (a common expression is that the event horizon has a teleological nature)."

detector setup.

This is why the information theoretic approach is so powerful in quantum field theories. Most everything else seems to be brick walls and dead ends. Even algebraic quantum field theory seems to produce no-go theorems more than anything else. What do we do when we want to be constructive? When we want to say something that is true of a quantum field, as opposed to providing a list of things that aren't?

We can be creative. So, let's play some tricks with quantum field theory. First, let's keep the information theoretic view of caring about correlations. Indeed, we will find great utility in this view: at least half of the involved calculations in this thesis are calculations of two-point correlators! However, we will also add in a healthy dose of operationalism. When we go to probe, calculate, measure, or what have you, we could ask questions of the fundamental or foundational or mathematical variety. And many do, to interesting ends. However, our focus will instead be the question, "Yes, but if I looked, what would I see?" It may sound naive, but it's also practical. I'm less concerned with the under-the-hood. I want to know: if I put this atom in that field, will it get excited? Will it become entangled? What other correlations will emerge?

We will use particle detectors to answer these kinds questions. In particular, we will use the Unruh-DeWitt (UDW) model. This approach is simple and powerful. It has been used for the Unruh effect, the Hawking effect, and for understanding the entanglement structure of various quantum fields. In this work, we will build on that rich history. In fact, we take this philosophy with us throughout this thesis, preferring operational approaches when we study various phenomena: decoherence, resonance, dispersion, entanglement and mutual information. All will be studied in the context of UDW-like detectors probing some aspect of a full quantum field theory.

We will go beyond the previous works, which primarily studied the linearly coupled UDW. We are interested in more general couplings: quadratic, bilinear, or complex quadratic. Furthermore, we are interested in more general fields, considering Fermionic, massive complex, massless complex, or even dispersive fields. Our goal is to understand the relations between these different paradigms. One of the most central questions in this work is: when can we recover, from various non-linear UDW models, well known results from the real, linear UDW model?

We will begin our journey with a review of the mothods of this thesis, primarily focused on the Unruh-DeWit Detector model. A literature review will allow us to place this thesis in its scientific and historical context. Namely, what started out as a toy model or perhaps a *gedanken* experiment has been shown to be a very good approximation of the light-matter interaction in the absense of exchange of angular momentum. Furthermore, the definition

of the UDW has evolved over time: from cavity to two-level system; from point-like to smeared; from real to complex; from linear to quadratic; and finally, as you will see in the very last part of this thesis, from scalar to spinor. The UDW detector has grown and matured in scope alongside the research field that makes heavy use of it: relativistic quantum information.

On the many other hands, there are folks in the community who build and/or study analog gravity experiments, who spend their time in quantum optics labs, or whose body of work can be neatly packaged on a lab-grown chip. We dip our toes into theoretical aspects of some of that work in this thesis.

After establishing the scientific context for the single UDW detector in Methods (chapter 1), we will use this model to probe our assumptions about quantum optics in Non-linear Optics with a UDW Detector (chapter 2) and Fundamental Decoherence in Optical Cavities (chapter 3). In the chapter on Non-linear optics, the only chapter in which we deal with non-vacuum states, we probe the UDW detector's ability to capture phenomena unique to nonlinear optics. In the decoherence chapter, we move out of our comfort zone (the monopole detector) and stray into intriguing territory, working with the harmonic oscillator UDW detector. We ask: can a perfectly constructed cavity still leak information?

Our foray into quantum optics will be followed up by a string of chapters covering the topic of entanglement harvesting, a protocol which probes the entanglement structure of quantum fields. For some context, many folks discussing entanglement in quantum fields go to the entanglement entropy as a measure of entanglement. However, there are severe limitations to this approach, as we will discuss briefly in our methods chapter. Given the limitations, we suggest the use of two-level systems as probes of entanglement, in the decades long tradition of entanglement harvesting.

Our first chapter on entanglement harvesting is all about Dirac fields: Fermionic Entanglement Harvesting (chapter 4). This chapter delves into the scientific context of Fermionic UDW detectors, tracing their roots back to the 80's. Then more modern context is given, wherein care is taken to regularize divergences and show some remarkable relations between scalar and spinor fields. This chapter combines previous results in novel ways, and the outcome is an elegant method to harvest entanglement from the Fermionic, Minkowski vacuum in any dimension, 1+1 or greater.

Next we will satisfy our curiosity about simulating entanglement harvesting in an analog gravity system. In analog gravity settings, dispersion is always modified, yet it is unknown how strongly dispersion effects the UDW model. We shed light on this in UDW pairs with Modified Dispersion (chapter 5).

Holding up the rear we have Techniques in Harvesting (chapter 6), which is a quick little

extension to a helpful tool for the UDW model, and Persistent Divergences in Quadratically Coupled Models? (chapter 7), which give some updates on some previous work on quadratically coupled UDW detector pairs.

Finally, the conclusion (chapter 8) highlights the results of this thesis and points towards future work.

Chapter 1

Methods

In this chapter, we will cover the general methods employed in this thesis, primarily the UDW Detector model with some additional necessary background. We will consider various couplings and fields, as well as states of the field. Our goal is twofold: to place the UDW detector in its scientific context and to provide the relevant results from the literature that we will build on throughout the rest of this thesis.

1.1 History of the Unruh-DeWitt Model

The precursors to the modern Unruh-DeWitt (UDW) detector model were introduced in the 1970's. Some folks, motivated to their studies by understanding the effects of matter quantization on the gravitational field, realized the definition of particles in curved spacetime was quite subtle. An operational perspective was proposed by Bill Unruh, in which the *detection* of a field quanta was defined to be "the excitation of the detector by the field," in other words, *a particle is that which a particle detector detects.* Unruh then introduced a non-relativistic particle detector model that coupled the detector's wavefunction directly to the the field amplitude for infinite time [15].

Bryce DeWitt took Unruh's Detector and replaced the wave-function coupling with a point-like coupling through the detector's monopole moment [16], producing the Lagrangian

$$\hat{L}_{int} = \hat{m}(\tau)\hat{\phi}(x(t)) \tag{1.1}$$

where $\hat{m}$ is the monopole moment of the two-level detector system and $\hat{\phi}(x(t))$ is the field operator of a massless, real scalar field. Hinton later named this model the "DeWitt detector" [17]. Furhtermore, Hinton defined a particle detector as "a mathematical construct which registers the occupation number of any given mode," which is possibly less influential than the philosophy later outlined by Katherine Freese. A year later the term "Unruh-DeWitt detector" was first published by Freese, referring to both Unruh and DeWitt's detectors as a unified whole. Freese went on to say that "the only real physics is that of experiments and detectors" [18], thus clearly outlying the philosophical assumptions of the UDW model, i.e. the primacy of the operational approach.

The Unruh-DeWitt (UDW) detector is a toy model. It captures many aspects of an atom interacting with an electromagnetic field when orbital angular momentum is not exchanged [19, 20] and is used primarily as a theoretical tool for proof-of-principal calculations or to gain insight into what an observer might "see" when interacting with a quantum field.

Typically research involving UDW-like models also utilizes perturbative methods. While there are non-perturbative UDW techniques, such as the delta switching [21] and the Gaussian formalism [22], they are not applicable to general entanglement harvesting scenarios, which are of great interest in this thesis and discussed later. In the case of the delta switching (also called a kink switching), no-go theorems have been shown for entanglement harvesting [21]. In the case of the Gaussian formalism, there are restrictions on both the interaction Hamiltonian and initial states [22].

In the early literature, it was common for UDW detectors to be point-like and adiabatic (i.e. infinitely long and slow switching functions). However, there is a broader class of UDW detectors (sometimes called UDW-like detectors) that have some spatial smearing and a time-dependent coupling to the field. Often the smearing and switching functions are taken to be either a Gaussian or fully compact.

Furthermore, in the literature in the 80's [23, 24, 25, 26] but also within the last five years [27, 28, 29, 1], there has been interest in different detector couplings. Non-linear couplings model non-linear processes and, more fundamentally, are also the simplest coupling to complex fields that doesn't violate U(1) symmetry [27].

Thus, a very general UDW-like interaction Hamiltonian (for a single detector) is

$$\hat{H}_{int} = \lambda\chi(t)\hat{m}(t)\int \mathrm{d}^n\boldsymbol{x}\, F(\boldsymbol{x})\, f(\hat{\phi}(\boldsymbol{x},t)). \tag{1.2}$$

In this expression, $\hat{m}(t)$ is the monopole operator, which is a Hermitian operator acting on the two-dimensional Hilbert space $\mathbb{C}^2$ (we could generalize further by allowing other

operators or Hilbert spaces here). The function $\chi(t)$ is the switching profile for our detector; thus $\lambda\chi(t)$ can be thought of as a time-dependent coupling (the choice of $\chi(t)$ can effect convergence, see subsection 1.7.3). The switching controls how long (parametrized by T) the detector interacts with the field. $F(\boldsymbol{x})$ is called the spatial profile or smearing function and it controls the shape/localization of the detector. The shape is determined by the functional form of $F(\boldsymbol{x})$, while the size of the detector is controlled by some length parameter σ. Finally, in the results that follow we will consider only functions f that are at most quadratic in the field operator and the appropriate conjugate (e.g. Pauli Adjoint for Dirac fields [30]). However, f may also contain the normal ordering operation, and other regularization schemes may potentially be introduced into the field operator as well, most notably the ϵ-regularization scheme.

1.2 Beyond a Single Detector

Early UDW literature focused on the transition probability or the transition rate of a single detector, illuminating phenomena such as the Unruh effect and Hawking radiation. However, a watershed moment for the UDW detector was the introduction of pairs of detectors for the express purpose of extracting spatio-temporally coded information about entanglement and other correlations in quantum field theories [31, 32].

Quantum fields were known to exhibit entanglement between different spatio-temporal regions [33, 34], but the amount of entanglement is difficult to quantify. Entanglement entropy can only quantify entanglement for pure states. Furhtermore, quantum fields have infinitely many degrees of freedom. There is no known measure of entanglement for arbitrary mixed states of infinitely many degrees of freedom. Separately conceived by [32] and [31], *entanglement harvesting* (named in [35]) showed how to estimate scaling properties of entanglement between two spacetime regions.

Entanglement harvesting has been well studied for the vacuum of a real bosonic field [7], as well as for thermal states, coherent states, and squeezed coherent states [36, 37, 38]. Most studies consider bipartite entanglement, but more detectors have been considered [39]. Additionally, it has been shown that sustainable extraction is theoretically possible via a protocol called *entanglement farming* [40]. Perhaps more interesting is the possibility of harvesting-based ways of distinguishing different background geometries [41, 35, 42] and topologies [43].

These advances in UDW methodology came from a small upgrade to the Hamiltonian,

wherein Eq. (1.2) becomes

$$\hat{H}_{int} = \sum_{\mu\in\{\text{A,B}\}} \lambda_\mu \chi_\mu(t - t_\mu)\hat{m}_\mu(t) \int \mathrm{d}^n\boldsymbol{x}\, F_\mu(\boldsymbol{x} - \boldsymbol{x}_\mu)\, f(\hat{\phi}(\boldsymbol{x}, t)). \tag{1.3}$$

The index we have introduced and summed over designates which of the two detectors, A or B, is in consideration. We have implicitly introduced a second detector Hilbert space.

We will close this section with a note about this Hamiltonian. First, there is no direct interaction between the two detectors. As a result, if the initial state chosen is separable between both of the detectors and the field, then any entanglement that arises throughout the course of interaction via this Hamiltonian must have originated in the field. It is often further assumed that the scaling properties of the entanglement that results from this interaction is indicative of the scaling properties of entanglement in the QFT.

1.3 Beyond Scalar Fields

Much in line with the original detector model by Unruh, in 1980 Iyer and Kuma introduced a UDW-like Fermionic model as a detector consisting of a field confined to a cavity interacting with a Fermionic field [26]. They proposed

$$H_I(\boldsymbol{x}) \propto \lambda\overline{\Psi}\Psi\phi_i^*\phi_j \tag{1.4}$$

as the form for the interaction of a UDW system sensitive to a Fermionic field Ψ. ϕ_i is the Schrodinger wavefunction of the detection system with energy E_i. λ is the coupling parameter. For this detector model, Iyer and Kumar showed an effect for the Fermionic field that is analagous to the Unruh effect in 3+1 dimensions. They find that such a detector, if accelerated, sees an ordinary vacuum as a bath of Dirac quanta (i.e the detector response function in such scenarios is of Fermi-Dirac type) with appropriate statistics at a temperature $a/2\pi$ where a is the proper acceleration of the detector.

In 1985 and following up in 1986, Takagi introduced a simplified model [24, 25] with a detector of the monopole type, analagous to DeWitt's introduction for the scalar model. The Hamiltonian for this model was of the form

$$H_I(\boldsymbol{x}) \propto \hat{m}\overline{\Psi}\Psi, \tag{1.5}$$

where $\hat{m}$ is the monopole operator of the detector. With this model, Takagi studied the vacuum noise as seen by an accelerated observer in Minkowski spacetime and showed that

the transition rate in such scenarios is of Fermi-Dirac type if the dimension of the manifold is even and to be Planckian otherwise.

Twenty years later, Hümmer et al. et al made a comprehensive comparative analysis between different UDW-like models with the aim of understanding how the transition probability (not transition rate) differed between these different models. In addition to the usual linearly coupled UDW detector, and the Monopole Fermion detector introduced by Takagi, they also studied two additional models. One is the UDW detector quadratically coupled to a real scalar field,

$$H_I(\boldsymbol{x}) \propto \hat{m}\phi\phi, \tag{1.6}$$

while the final model studied is that of a particle detector interacting with a *complex* scalar field through the Hamiltonian

$$H_I(\boldsymbol{x}) \propto \hat{m}\phi^\dagger\phi. \tag{1.7}$$

One aspect Hümmer et al uncovered is the existance of a *persistent divergence* in the transititon probability for fields with a quadratic coupling. A *persistent divergence* in a UDW-like model is one that is not regularizable by the use of smooth switching and smearing and the use of a UV regulator (which has a convergent limit after suitable calculations). Hümmer et al studied the Feynman structure of these quadratic models and found a suitable renormalization scheme in analogy with the tadpoles of quantum electrodynamics. In fact, in that work the authors were able to streamline many UDW calculations through the use of extended Feynman rules refined to include localized detector-field interactions.

Working on previous results, Louko and Toussaint proved several interesting perturbative results. They chose as the setting for their studies a detector, coupled to a Dirac field via the Takagi coupling Eq. (1.5), following an arbitrary trajectory in Minkowski spacetime of dimension d with $d \geq 2$. Foremost, they showed that the detector response in d-dimensional Minkowski spacetime is identical to that of a detector coupled linearly to a scalar field in 2d-dimensions. This is notable due to the dimensionally dependent statistics inversion previously known in the Unruh effect literature [25]. For the usual UDW model the response is Planckian in even spacetime dimensions, yet Fermi-Dirac in odd spacetime dimensions. Thus the results by Louko and Toussaint show that the detector response to a Dirac field will be Planckian regardless of the spacetime dimension! Thus, the response to the Dirac field is always Planckian. Furthermore, since the detector response to the Dirac field in 1+1 dimensions matches the detector response to the scalar field in 3+1 dimensions, the Dirac UDW model lacks the IR ambiguitiy discussed previously in subsection 1.7.1. This interesting feature was noted in [28].

1.4 Field Theory

Before moving on to the details of the UDW detector, we will provide a little support for the reader with a quick refresher on quantum field theory (QFT) and our choice of conventions and notation. This section also provides some indication as to the scope of QFTs we are interested in. We will use natural units $c = \hbar = 1$. n will represent the number of spatial dimensions, while $d = n+1$ will be the number of spacetime dimensions. Bold serif font will represent 3-vectors while the bold sans serif fonts will represent a 4-vector, eg. $\mathsf{x} = (t, \boldsymbol{x})$. The Minkowski metric is denoted $\eta_{\mu\nu} = \text{diag}(1, -1, \ldots, -1)$. Throughout this work, we will write a Dirac field as Ψ, a complex scalar field as Φ, and ϕ will represent either an arbitrary field or a real scalar field.

1.4.1 Massless Classical Field Theory

We begin with the action functional,

$$S[\phi] = \int \mathrm{d}^d\mathsf{x} L(\phi(\mathsf{x}), \partial_\mu\phi(\mathsf{x})) \tag{1.8}$$

where

$$L(\phi(\mathsf{x}), \partial_\mu\phi(\mathsf{x})) = \frac{1}{2}\left[\partial^\mu\phi\partial_\mu\phi - m^2\phi^2\right] \tag{1.9}$$

is the Lagrangian density for a classical field with a continuous degree of freedom. An action with the form of a density is assumed since we want an equation of motion which is local[1][2].

A further assumption that goes into this action is that of Lorentz invariance. The volume element is invariant, so the requirement is borne on the shoulders of the Lagrangian density. Lorentz invariance is achieved with polynomials of ϕ, products of derivatives (with all indices contracted), and constant functions. A constant will vanish when taking the Gateaux (or variational) derivative. As a result it will not enter into the equations of motion and we will not include one. The form of the action we have chosen is one of the simplest such forms, with the added benefit of leading to a linear equation of motion.

[1] The equation of motion will have spatial derivatives which cause oscillators near each other in physical space to interact, so the equation is non-local in the sense that the ground state of the quantized theory will be a global state, not a local one.

[2] Also actions of this form are extensively studied and generally easily solvable via the Euler-Lagrange equation.

Hamilton's principle guides us toward the equations of motion of our field. It can be shown that, for a functional of the form

$$J[\phi] = \int \mathrm{d}^d\mathsf{x}\, L(\phi(\mathsf{x}), \partial_\mu\phi(\mathsf{x})), \tag{1.10}$$

the function ϕ^0 is a stationary function if and only if the Euler-Lagrange equation is satisfied. The Euler-Lagrange equation, $\partial L/\partial\phi = \partial_\mu(\partial L/\partial(\partial_\mu\phi))$, is quite simple in the absence of a mass term, i.e. when L lacks direct ϕ-dependence. This version of the Euler-Lagrange equation is called the Klein Gordon equation:

$$(\partial_\mu\partial^\mu - m^2)\phi = 0. \tag{1.11}$$

We will work exclusively with the Hamiltonian formalism in this thesis. Applying the Legendre transform to the Lagrangian density, Eq. (1.9) gives us the Hamiltonian density

$$H(\phi, \pi) = \frac{1}{2}\left(\pi^2 + (\nabla\phi)^2 + m^2\phi^2\right), \tag{1.12}$$

where π is the conjugate momentum $\pi(\boldsymbol{x}, t) = \dot{\phi}(\boldsymbol{x}, t)$. The Hamiltonian defines the energy density of the field. For the massless field, there is not major issue with taking $m \to 0$ for any of the above equations.

1.4.2 Real Scalar Quantum Field Theory

The real scalar quantum field theory arises as a quick transformation from the classical theory. The solutions in the classical theory are scalar functions, while in the quantum theory they are operators satisfying the canonical commutation relations

$$\left[\hat{\phi}(\boldsymbol{x}, t), \hat{\pi}(\boldsymbol{x}', t)\right] = \mathrm{i}\delta^{(n)}(\boldsymbol{x} - \boldsymbol{x}') \tag{1.13}$$

$$\left[\hat{\phi}(\boldsymbol{x}, t), \hat{\pi}(\boldsymbol{x}', t)\right] = 0 \tag{1.14}$$

$$\left[\hat{\phi}(\boldsymbol{x}, t), \hat{\pi}(\boldsymbol{x}', t)\right] = 0. \tag{1.15}$$

The (operator-valued) solution to the Klein-Gordon equation Eq. (1.11) can be expanded in modes

$$\hat{\phi}(t, \boldsymbol{x}) = \int \frac{\mathrm{d}^n\boldsymbol{k}}{\sqrt{2(2\pi)^n|\boldsymbol{k}|}}\left[\hat{a}_{\boldsymbol{k}}\, e^{-\mathrm{i}\omega_{\boldsymbol{k}}t + \mathrm{i}\boldsymbol{k}\cdot\boldsymbol{x}} + \hat{a}^\dagger_{\boldsymbol{k}}\, e^{\mathrm{i}\omega_{\boldsymbol{k}}t - \mathrm{i}\boldsymbol{k}\cdot\boldsymbol{x}}\right] \tag{1.16}$$

where the particle creation and annihilation operators, denoted $\hat{a}^\dagger$ and $\hat{a}$ respectively, satisfy the canonical commutation relations, where the only non-vanishing commutator is

$$[\hat{a}_{\boldsymbol{k}}, \hat{a}^\dagger_{\boldsymbol{p}}] = \delta(\boldsymbol{k} - \boldsymbol{p}). \tag{1.17}$$

The vacuum is defined uniquely as the state annihilated by all $\hat{a}_{\boldsymbol{k}}$. Furthermore, the space of states is built from the vacuum by taking the (infinite) tensor product of all n particle Hilbert spaces (which themselves are tensor products of Hilbert spaces of single particles). This space is called a Fock space.

The free Hamiltonian can be expressed succinctly in terms of an integral over creation and annihilation operators for each mode:

$$\hat{H} = \sum_{\boldsymbol{k}} \omega_{\boldsymbol{k}} \hat{a}^\dagger_{\boldsymbol{k}} \hat{a}_{\boldsymbol{k}}. \tag{1.18}$$

1.4.3 Complex Scalar Quantum Field Theory

We will now note some highlights from the quantization of the free complex field, which follows the same commutation relations as the real field Eq. (1.15). The field can be expanded in modes as

$$\hat{\Phi}(t, \boldsymbol{x}) = \int \mathrm{d}^n \boldsymbol{k} \frac{1}{\sqrt{2(2\pi)^n \omega_{\boldsymbol{k}}}} \left[\hat{a}_{\boldsymbol{k}} e^{-\mathrm{i}\omega_{\boldsymbol{k}} t} \, \varphi_{\boldsymbol{k}}(\boldsymbol{x}) + \hat{b}^\dagger_{\boldsymbol{k}} \, e^{+\mathrm{i}\omega_{\boldsymbol{k}} t} \, \varphi^*_{\boldsymbol{k}}(\boldsymbol{x}) \right] \tag{1.19}$$

The particle and anti-particle creation and annihilation operators satisfy the usual canonical commutation relations

$$[\hat{a}_{\boldsymbol{k}}, \hat{a}^\dagger_{\boldsymbol{p}}] = \delta(\boldsymbol{k} - \boldsymbol{p}), \qquad [\hat{b}_{\boldsymbol{k}}, \hat{b}^\dagger_{\boldsymbol{p}}] = \delta(\boldsymbol{k} - \boldsymbol{p}), \tag{1.20}$$

and all other commutators with $\hat{a}$, $\hat{b}$ or their adjoints are zero. The free Hamiltonian of the free complex field is simple when written in terms of modes $\boldsymbol{k}$

$$\hat{H} = \sum_{\boldsymbol{k}} \omega_{\boldsymbol{k}} \left(\hat{a}^\dagger_{\boldsymbol{k}} \hat{a}_{\boldsymbol{k}} + \hat{b}^\dagger_{\boldsymbol{k}} \hat{b}_{\boldsymbol{k}} \right). \tag{1.21}$$

1.4.4 Dirac Quantum field Theory

The Dirac field Ψ is composed of two left-handed[3] spinor fields χ and ξ as

$$\Psi = \begin{pmatrix} \chi_C \\ \xi^{\dagger \dot{C}} \end{pmatrix}, \tag{1.22}$$

where C and $\dot{C}$ are right and left-handed spinor indices. The field has the following anti-commutation relations

$$\left\{\Psi_a(t,\boldsymbol{x}), \Psi_b(t,\boldsymbol{x}')\right\} = \left\{\Psi_a^\dagger(t,\boldsymbol{x}), \Psi_b^\dagger(t,\boldsymbol{x}')\right\} = 0 \ , \tag{1.23}$$

$$\left\{\Psi_a(t,\boldsymbol{x}), \Psi_b^\dagger(t,\boldsymbol{x}')\right\} = \delta_{ab}\delta^{d-1}(\boldsymbol{x}-\boldsymbol{x}') \ . \tag{1.24}$$

Next, we want to write down the action for a Dirac field, as well as the equation of motion and its solution. Writing these is simpler in terms of the gamma matrices, so we will introduce those first. The gamma matrices γ^i are a set of d traceless, square matrices whose dimension is always even: $N_d \times N_d$ where

$$N_d := \begin{cases} 2^{d/2} & d \text{ even} \\ 2^{(d-1)/2} & d \text{ odd.} \end{cases} \tag{1.25}$$

All γ^i satisfy the anti-commutation relations

$$\{\gamma^\mu, \gamma^\nu\} = 2\eta^{\mu\nu} \tag{1.26}$$

and $\mathrm{Tr}(\gamma^\mu\gamma^\nu) = N_d\eta^{\mu\nu}$. Furthermore, γ^0 is Hermitian, while the remaining γ^i are anti-Hermitian.[4]

The action is the simplest quadratic[5], Hermitian, Lorentz-invariant action that incorporates spin degrees of freedom and leads to a Hamiltonian that is bounded from below.

[3] A $(2j+1, 2j'+1)$ representation of the Lorentz group is the direct sum of two representations of $SU(2)$ (or, I suppose, SO(3) if j or j' is an integer). The representations j and j' of $SU(2)$ are those that are used in quantum *mechanics* for angular momentum. The $(2,1)$ representation of the Lorentz group is the direct sum of the spin-$\frac{1}{2}$ and trivial representations of $SU(2)$. It is called a left-handed Weyl spinor, while the $(1,2)$ representation is a right-handed Weyl spinor; see Section 33 in [44].

[4] As a particular example, the gamma matrices in 3 spatial dimensions are conveniently written in terms of the Pauli matrices as $\gamma^0 = \begin{pmatrix} 1 & 0 \\ 0 & -1 \end{pmatrix} \otimes \sigma^0$ and $\gamma^i = \begin{pmatrix} 0 & 1 \\ -1 & 0 \end{pmatrix} \otimes \sigma^i$.

[5] A quadratic action leads to a linear equation of motion, i.e. a free field with plane-wave solutions.

The following satisfies these requirements, notably for both the Dirac and Majorana fields, although we will not be considering the latter,

$$S = \int \mathrm{d}^d\mathsf{x}\, \overline{\Psi}(\mathsf{x})\, (i\gamma^\mu \partial_\mu - m)\, \Psi(\mathsf{x})\ . \tag{1.27}$$

From the action follows the Dirac equation for Ψ and its Dirac conjugate $\overline{\Psi} = \gamma^0 \Psi^\dagger$,

$$(\mathrm{i}\gamma^\mu \partial_\mu - m)\Psi(\mathsf{x}) = 0 \tag{1.28}$$

$$\mathrm{i}\partial_\mu \overline{\Psi}(\mathsf{x})\gamma^\mu + m\overline{\Psi}(\mathsf{x}) = 0. \tag{1.29}$$

The linear Dirac equation Eq. (1.28) admits a mode expansion

$$\Psi(\mathsf{x}) = \int \widetilde{\mathrm{d}k} \sum_s \left(\hat{b}_s(\boldsymbol{k}) u^{(s)}_{\boldsymbol{k}}(\mathsf{x}) + \hat{d}^\dagger_s(\boldsymbol{k}) v^{(s)}_{\boldsymbol{k}}(\mathsf{x}) \right), \tag{1.30}$$

where $\hat{b}$ and $\hat{d}$ are spinor-valued particle and anti-particle annihilation operators inheriting their anti-commutation relations[6] from Eq. (1.24)

$$\left\{ \hat{b}_s(\mathbf{k}), b^\dagger_{s'}(\mathbf{k}') \right\} = \left\{ \hat{d}_s(\mathbf{k}), d^\dagger_{s'}(\mathbf{k}') \right\} = 2\omega_{\mathbf{k}} (2\pi)^n \delta_{ss'}\, \delta^n(\mathbf{k} - \mathbf{k}'), \tag{1.31}$$

and the mode functions $u^{(s)}(\boldsymbol{k})$ and $v^{(s)}(\boldsymbol{k})$ form a complete orthonormal basis. We will construct them from zero-momentum basis elements, one for each value of the helicity index $s = 1, \ldots, N_d/2$. They have the property

$$\gamma^0 u_{\mathbf{0},s} = u_{\mathbf{0},s} \tag{1.32}$$

$$\gamma^0 v_{\mathbf{0},s} = -v_{\mathbf{0},s}, \tag{1.33}$$

as well as orthogonality,

$$u^\dagger_{\mathbf{0},s} u_{\mathbf{0},s'} = v^\dagger_{\mathbf{0},s} v_{\mathbf{0},s'} = 2m\delta_{s,s'} \tag{1.34}$$

$$u^\dagger_{\mathbf{0},s} v_{\mathbf{0},s'} = 0. \tag{1.35}$$

From them we define the non-zero $\boldsymbol{k}$ spinors

$$u_{\boldsymbol{k},s} = \frac{\gamma^\mu k_\mu + m}{\sqrt{2m(\omega_{\boldsymbol{k}} + m)}} u_{\mathbf{0},s} \tag{1.36}$$

$$v_{\boldsymbol{k},s} = \frac{-\gamma^\mu k_\mu + m}{\sqrt{2m(\omega_{\boldsymbol{k}} + m)}} v_{\mathbf{0},s}. \tag{1.37}$$

[6] The normalization under the Dirac inner product is $\langle \psi, \phi \rangle = \int \mathrm{d}^n \boldsymbol{x}\, \overline{\psi}(t, \boldsymbol{x}) \gamma_0 \psi(t, \boldsymbol{x})$, is $\langle u^{(s)}_{\boldsymbol{k}}, u^{(s')}_{\boldsymbol{k}'} \rangle = 2\omega_{\boldsymbol{k}} (2\pi)^n \delta^{s,s'} \delta^n(\boldsymbol{k} - \boldsymbol{k}')$ as well as $\langle v^{(s)}_{\boldsymbol{k}}, v^{(s')}_{\boldsymbol{k}'} \rangle = 2\omega_{\boldsymbol{k}} (2\pi)^n \delta^{s,s'} \delta^n(\boldsymbol{k} - \boldsymbol{k}')$, and $\langle u^{(s)}_{\boldsymbol{k}}, v^{(s')}_{bk'} \rangle = 0$.

where $\omega_{\boldsymbol{k}}^2 = \boldsymbol{k}^2 + m^2$. The basis spinors $u_{\boldsymbol{k},s}$ and $v_{\boldsymbol{k},s}$ inherit their equations of motion from the full field

$$(\gamma^\mu k_\mu - m)u_{\boldsymbol{k},s} = 0 \tag{1.38}$$
$$(\gamma^\mu k_\mu + m)v_{\boldsymbol{k},s} = 0\ . \tag{1.39}$$

The basis is orthonormal[7]

$$u^\dagger_{\boldsymbol{k},s}u_{\boldsymbol{k},s'} = v^\dagger_{\boldsymbol{k},s}v_{\boldsymbol{k},s'} = 2\omega_{\boldsymbol{k}}\delta_{s,s'} \tag{1.40}$$
$$\overline{u}_{\boldsymbol{k},s}u_{\boldsymbol{k},s'} = -\overline{v}_{\boldsymbol{k},s}v_{\boldsymbol{k},s'} = 2m\delta_{s,s'} \tag{1.41}$$
$$\overline{u}_{\boldsymbol{k},s}v_{\boldsymbol{k},s'} = 0, \tag{1.42}$$

and complete

$$\sum_s (u_{\boldsymbol{k},s})_a(\overline{u}_{\boldsymbol{k},s'})_b = (\gamma^\mu k_\mu + m)_{ab} \tag{1.43}$$
$$\sum_s (v_{\boldsymbol{k},s})_a(\overline{v}_{\boldsymbol{k},s'})_b = (\gamma^\mu k_\mu - m)_{ab}. \tag{1.44}$$

The vacuum is the unique[8] state annihilated by all $\hat{b}_s(\boldsymbol{k})$ and $\hat{d}_s(\boldsymbol{k})$, ie. it is $|0\rangle$ such that $\hat{b}_s(\boldsymbol{k})\,|0\rangle = \hat{d}_s(\boldsymbol{k})\,|0\rangle = 0$

1.5 Monopole UDW Model

Let us consider a quantum field in the state $|\psi\rangle$, whose field operator we will represent with $\hat{\phi}(\boldsymbol{x}, t)$ and whose free dynamics are given by some Hamiltonian $\hat{H}_f$. Furthermore, let us consider two detectors labeled by the symbols A and B in energy eigenstates $|0_\mu\rangle$[9]. The detectors' interaction with the field will be modulated in time and space by switching and smearing functions ($F_\mu(\boldsymbol{x} - \boldsymbol{x}_\mu)$ and $\chi_\mu(t - t_\mu)$), both taken to be real. Let the detectors be two-level systems whose energy gaps are Ω_μ[10], and whose free Hamiltonian is H_μ. Furthermore, $\hat{H}_f$ and H_μ commute and the initial state of the detector-field system is

[7] This equation encompasses Eq. (1.35)

[8] In Minkowski space.

[9] μ will be used to indicate either detector throughout this thesis.

[10] We allow here for the gap to be negative, which can be interpreted as the detector starting in the excited state.

a product state. For more general analyses of UDW-like models, some of these assumptions may be relaxed. We will not do so without prior warning.

The process of deriving the transition probability and the general density matrix for a UDW-like detector has been done many times in the literature for many different detector-field couplings [27, 26, 17, 24, 45]. By contrast, this general derivation, where we do not assume the analytic structure of the field or a particular coupling, is somewhat novel work. However it remains in the literature review because it is not a large leap from previous work and is preliminary for the rest of this thesis.

The interaction Hamiltonian (in the interaction picture) of a UDW-like detector is

$$\hat{H}_{int} = \sum_{\mu\in\{\mathrm{A,B}\}} \lambda_\mu \chi_\mu(t-t_\mu)\hat{m}_\mu(t) \int \mathrm{d}^n\boldsymbol{x}\, F(\boldsymbol{x}-\boldsymbol{x}_\mu)\, f(\hat{\phi}(\boldsymbol{x},t)), \tag{1.45}$$

where $f(\hat{\phi}(\boldsymbol{x},t))$ is a Hermition operator composed of the field operator, possilby with some renormalization scheme incorporated. Note how the detectors do not directly interact. Therefore all correlations between the detectors must come from interaction with the field.

Next, we will consider these two systems when they interact as in the very general UDW-like model shown in Eq. (1.2). The Hamiltonian is the generator of time translations, and as such the (time-ordered) exponential of the interaction Hamiltonian yields the time evolution:

$$\hat{U} = \mathcal{T}\left[\exp\left(\mathrm{i}\int_{-\infty}^{\infty}\mathrm{d}t\hat{H}_I(t)\right)\right] \ . \tag{1.46}$$

We can find an expression for $\hat{U}$ out to arbitrary order in perturbation theory using the Dyson series. In what follows we will expand to second order in the coupling constants λ_μ:

$$\hat{U} = \mathbb{1} - \mathrm{i}\int_{\infty}^{\infty}\mathrm{d}t\hat{H}_I(t) - \int_{\infty}^{\infty}\mathrm{d}t\int_{t}^{\infty}\mathrm{d}t'\,\hat{H}_I(t)\hat{H}_I(t') + \mathcal{O}(\lambda_{\mathrm{A}}^3) \ . \tag{1.47}$$

Given the form above, it is convenient to define

$$\hat{U}^{(0)} := \mathbb{1} \tag{1.48}$$

$$\hat{U}^{(1)} := -\mathrm{i}\int_{\infty}^{\infty}\mathrm{d}t\hat{H}_I(t) \tag{1.49}$$

$$\hat{U}^{(2)} := -\int_{\infty}^{\infty}\mathrm{d}t\int_{-\infty}^{t}\mathrm{d}t'\,\hat{H}_I(t)\hat{H}_I(t') \ . \tag{1.50}$$

Let us apply the time-evolution operator $\hat{U}$ to the initial state of the field-detector system:

$$\rho_0 = |0_{\rm A}\rangle\langle 0_{\rm A}| \otimes |0_{\rm B}\rangle\langle 0_{\rm B}| \otimes |\psi\rangle\langle\psi| \ . \tag{1.51}$$

We will call this state $\hat{\rho}_T = \hat{U}\hat{\rho}_0\hat{U}^\dagger$. Then,

$$\hat{\rho}_T = \hat{\rho}_0 + \hat{\rho}^{(1,0)} + \hat{\rho}^{(0,1)} + \hat{\rho}^{(1,1)} + \hat{\rho}^{(2,0)} + \hat{\rho}^{(0,2)} + \mathcal{O}(\lambda_{\rm A}^3) \tag{1.52}$$

where $\hat{\rho}^{(i,j)} = \hat{U^{(i)}}\hat{\rho}_0\hat{U^{(j)}}^\dagger$. The order in perturbation theory of each $\hat{\rho}^{(i,j)}$ is given by $i+j$. We can compute the expressions for each of these terms. The first order terms, which are Hermitian conjugates of one another, are

$$\begin{aligned}\hat{\rho}^{(1,0)} = &-{\rm i}\lambda_{\rm A}\int{\rm d}t\int{\rm d}\boldsymbol{x}\,\chi_{\rm A}(t-t_{\rm A})F_{\rm A}(\boldsymbol{x}-\boldsymbol{x}_{\rm A})e^{{\rm i}\Omega_{\rm A}t}\,|1_{\rm A}\rangle\langle 0_{\rm A}|\otimes|0_{\rm B}\rangle\langle 0_{\rm B}|\otimes f(\phi(t,\boldsymbol{x}))\,|\psi\rangle\langle\psi| \\ &-{\rm i}\lambda_{\rm B}\int{\rm d}t\int{\rm d}\boldsymbol{x}\,\chi_{\rm B}(t-t_{\rm B})F_{\rm B}(\boldsymbol{x}-\boldsymbol{x}_{\rm B})e^{{\rm i}\Omega_{\rm B}t}\,|0_{\rm A}\rangle\langle 0_{\rm A}|\otimes|1_{\rm B}\rangle\langle 0_{\rm B}|\otimes f(\phi(t,\boldsymbol{x}))\,|\psi\rangle\langle\psi|\end{aligned} \tag{1.53}$$

and $\hat{\rho}^{(0,1)} = \left(\hat{\rho}^{(1,0)}\right)^\dagger$. Two of the second order terms are also Hermitian conjugates of one another,

$$\begin{aligned}\hat{\rho}^{(2,0)} = &-\lambda_{\rm A}^2\int{\rm d}t\int{\rm d}\boldsymbol{x}\int_{-\infty}^{t}{\rm d}t'\int{\rm d}\boldsymbol{x}'\,\chi_{\rm A}(t-t_{\rm A})F_{\rm B}(\boldsymbol{x}-\boldsymbol{x}_{\rm A})\chi_{\rm B}(t'-t_{\rm A})F_{\rm B}(\boldsymbol{x}'-\boldsymbol{x}_{\rm A})e^{{\rm i}\Omega_{\rm A}(t'-t)} \\ &\times|0_{\rm A}\rangle\langle 0_{\rm A}|\otimes|0_{\rm B}\rangle\langle 0_{\rm B}|\otimes f(\phi(t,\boldsymbol{x}))f(\phi(t',\boldsymbol{x}'))\,|\psi\rangle\langle\psi| \\ &-\lambda_{\rm B}^2\int{\rm d}t\int{\rm d}\boldsymbol{x}\int_{-\infty}^{t}{\rm d}t'\int{\rm d}\boldsymbol{x}'\,\chi_{\rm B}(t-t_{\rm B})F_{\rm B}(\boldsymbol{x}-\boldsymbol{x}_{\rm B})\chi_{\rm B}(t'-t_{\rm B})F_{\rm B}(\boldsymbol{x}'-\boldsymbol{x}_{\rm B})e^{{\rm i}\Omega_{\rm B}(t'-t)} \\ &\times|0_{\rm A}\rangle\langle 0_{\rm A}|\otimes|0_{\rm B}\rangle\langle 0_{\rm B}|\otimes f(\phi(t,\boldsymbol{x}))f(\phi(t',\boldsymbol{x}'))\,|\psi\rangle\langle\psi| \\ &-\lambda_{\rm B}\lambda_{\rm A}\int{\rm d}t\int{\rm d}\boldsymbol{x}\int_{-\infty}^{t}{\rm d}t'\int{\rm d}\boldsymbol{x}'\,\chi_{\rm A}(t-t_{\rm A})F_{\rm A}(\boldsymbol{x}-\boldsymbol{x}_{\rm A})\chi_{\rm B}(t'-t_{\rm B})F_{\rm B}(\boldsymbol{x}'-\boldsymbol{x}_{\rm B})e^{{\rm i}(\Omega_{\rm B}t'+\Omega_{\rm A}t)} \\ &\times|1_{\rm A}\rangle\langle 0_{\rm A}|\otimes|1_{\rm B}\rangle\langle 0_{\rm B}|\otimes f(\phi(t,\boldsymbol{x}))f(\phi(t',\boldsymbol{x}'))\,|\psi\rangle\langle\psi| \\ &-\lambda_{\rm B}\lambda_{\rm A}\int{\rm d}t\int{\rm d}\boldsymbol{x}\int_{-\infty}^{t}{\rm d}t'\int{\rm d}\boldsymbol{x}'\,\chi_{\rm B}(t-t_{\rm B})F_{\rm B}(\boldsymbol{x}-\boldsymbol{x}_{\rm B})\chi_{\rm A}(t'-t_{\rm A})F_{\rm A}(\boldsymbol{x}'-\boldsymbol{x}_{\rm A})e^{{\rm i}(\Omega_{\rm A}t'+\Omega_{\rm B}t)} \\ &\times|1_{\rm A}\rangle\langle 0_{\rm A}|\otimes|1_{\rm B}\rangle\langle 0_{\rm B}|\otimes f(\phi(t,\boldsymbol{x}))f(\phi(t',\boldsymbol{x}'))\,|\psi\rangle\langle\psi|\,.\end{aligned} \tag{1.54}$$

and $\hat{\rho}^{(0,2)} = \left(\hat{\rho}^{(2,0)}\right)^\dagger$. The final term is itself Hermitian,

$$\begin{aligned}
\hat{\rho}^{(1,1)} = \lambda_{\mathrm{A}}^2 \int \mathrm{d}t \int \mathrm{d}\boldsymbol{x} \int \mathrm{d}t' \int \mathrm{d}\boldsymbol{x}'\, \chi_{\mathrm{A}}(t - t_{\mathrm{A}}) F_{\mathrm{B}}(\boldsymbol{x} - \boldsymbol{x}_{\mathrm{A}}) \chi_{\mathrm{B}}(t' - t_{\mathrm{A}}) F_{\mathrm{B}}(\boldsymbol{x}' - \boldsymbol{x}_{\mathrm{A}}) e^{\mathrm{i}\Omega_{\mathrm{A}}(t-t')} \\
\times |1_{\mathrm{A}}\rangle \langle 1_{\mathrm{A}}| \otimes |0_{\mathrm{B}}\rangle \langle 0_{\mathrm{B}}| \otimes f(\phi(t, \boldsymbol{x})) |\psi\rangle \langle\psi| f(\phi(t', \boldsymbol{x}'))^\dagger \\
+ \lambda_{\mathrm{B}}^2 \int \mathrm{d}t \int \mathrm{d}\boldsymbol{x} \int \mathrm{d}t' \int \mathrm{d}\boldsymbol{x}'\, \chi_{\mathrm{B}}(t - t_{\mathrm{B}}) F_{\mathrm{B}}(\boldsymbol{x} - \boldsymbol{x}_{\mathrm{B}}) \chi_{\mathrm{B}}(t' - t_{\mathrm{B}}) F_{\mathrm{B}}(\boldsymbol{x}' - \boldsymbol{x}_{\mathrm{B}}) e^{\mathrm{i}\Omega_{\mathrm{B}}(t-t')} \\
\times |0_{\mathrm{A}}\rangle \langle 0_{\mathrm{A}}| \otimes |1_{\mathrm{B}}\rangle \langle 1_{\mathrm{B}}| \otimes f(\phi(t, \boldsymbol{x})) |\psi\rangle \langle\psi| f(\phi(t', \boldsymbol{x}'))^\dagger \\
+ \lambda_{\mathrm{B}} \lambda_{\mathrm{A}} \int \mathrm{d}t \int \mathrm{d}\boldsymbol{x} \int \mathrm{d}t' \int \mathrm{d}\boldsymbol{x}'\, \chi_{\mathrm{A}}(t - t_{\mathrm{A}}) F_{\mathrm{A}}(\boldsymbol{x} - \boldsymbol{x}_{\mathrm{A}}) \chi_{\mathrm{B}}(t' - t_{\mathrm{B}}) F_{\mathrm{B}}(\boldsymbol{x}' - \boldsymbol{x}_{\mathrm{B}}) \\
\times \left(e^{\mathrm{i}(\Omega_{\mathrm{A}} t - \Omega_{\mathrm{B}} t')} |1_{\mathrm{A}}\rangle \langle 0_{\mathrm{A}}| \otimes |0_{\mathrm{B}}\rangle \langle 1_{\mathrm{B}}| + H.c \right) \otimes f(\phi(t, \boldsymbol{x})) |\psi\rangle \langle\psi| f(\phi(t', \boldsymbol{x}'))^\dagger
\end{aligned} \tag{1.55}$$

1.5.1 Density Matrix of UDW Detector Pairs

Typically, one is interested in the state of the detectors after interacting with the field and so performs a partial trace over the field degrees of freedom of the expressions Eq. (1.53), (1.54), and (1.55). We will denote this state by ρ_{AB}.

The first order terms in ρ_{AB} are Hermitian conjugates of one another and are dependent on the one-point function of the state of the field,

$$\begin{aligned}
\mathrm{Tr}_\phi\left(\hat{\rho}^{(1,0)}\right) = -\mathrm{i}\lambda_{\mathrm{A}} \int \mathrm{d}t \int \mathrm{d}\boldsymbol{x}\, \chi_{\mathrm{A}}(t - t_{\mathrm{A}}) F_{\mathrm{A}}(\boldsymbol{x} - \boldsymbol{x}_{\mathrm{A}}) e^{\mathrm{i}\Omega_{\mathrm{A}} t} \langle\psi| f(\phi(t, \boldsymbol{x})) |\psi\rangle |1_{\mathrm{A}}\rangle\langle 0_{\mathrm{A}}| \otimes |0_{\mathrm{B}}\rangle\langle 0_{\mathrm{B}}| \\
- \mathrm{i}\lambda_{\mathrm{B}} \int \mathrm{d}t \int \mathrm{d}\boldsymbol{x}\, \chi_{\mathrm{B}}(t - t_{\mathrm{B}}) F_{\mathrm{B}}(\boldsymbol{x} - \boldsymbol{x}_{\mathrm{B}}) e^{\mathrm{i}\Omega_{\mathrm{B}} t} \langle\psi| f(\phi(t, \boldsymbol{x})) |\psi\rangle |0_{\mathrm{A}}\rangle \langle 0_{\mathrm{A}}| \otimes |1_{\mathrm{B}}\rangle \langle 0_{\mathrm{B}}|
\end{aligned} \tag{1.56}$$

$$\mathrm{Tr}_\phi\left(\hat{\rho}^{(0,1)}\right) = \left(\mathrm{Tr}_\phi\left(\hat{\rho}^{(1,0)}\right)\right)^2 \tag{1.57}$$

The pair of second order terms are dependent on the two-point function of the state of

the field,

$$\begin{aligned}
\mathrm{Tr}\left(\hat{\rho}^{(2,0)}\right) = \Bigg(& -\lambda_{\mathrm{A}}^2 \int \mathrm{d}t \int \mathrm{d}\boldsymbol{x} \int_{-\infty}^{t} \mathrm{d}t' \int \mathrm{d}\boldsymbol{x}'\, \chi_{\mathrm{A}}(t-t_{\mathrm{A}}) F_{\mathrm{B}}(\boldsymbol{x}-\boldsymbol{x}_{\mathrm{A}}) \chi_{\mathrm{B}}(t'-t_{\mathrm{A}}) F_{\mathrm{B}}(\boldsymbol{x}'-\boldsymbol{x}_{\mathrm{A}}) \\
& \times e^{\mathrm{i}\Omega_{\mathrm{A}}(t'-t)} \left\langle \psi \right| f(\phi(t,\boldsymbol{x})) f(\phi(t',\boldsymbol{x}')) \left| \psi \right\rangle \Bigg) \left| 0_{\mathrm{A}} \right\rangle \left\langle 0_{\mathrm{A}} \right| \otimes \left| 0_{\mathrm{B}} \right\rangle \left\langle 0_{\mathrm{B}} \right| \\
& + \Bigg(-\lambda_{\mathrm{B}}^2 \int \mathrm{d}t \int \mathrm{d}\boldsymbol{x} \int_{-\infty}^{t} \mathrm{d}t' \int \mathrm{d}\boldsymbol{x}'\, \chi_{\mathrm{B}}(t-t_{\mathrm{B}}) F_{\mathrm{B}}(\boldsymbol{x}-\boldsymbol{x}_{\mathrm{B}}) \chi_{\mathrm{B}}(t'-t_{\mathrm{B}}) F_{\mathrm{B}}(\boldsymbol{x}'-\boldsymbol{x}_{\mathrm{B}}) \\
& \times e^{\mathrm{i}\Omega_{\mathrm{B}}(t'-t)} \left\langle \psi \right| f(\phi(t,\boldsymbol{x})) f(\phi(t',\boldsymbol{x}')) \left| \psi \right\rangle \Bigg) \left| 0_{\mathrm{A}} \right\rangle \left\langle 0_{\mathrm{A}} \right| \otimes \left| 0_{\mathrm{B}} \right\rangle \left\langle 0_{\mathrm{B}} \right| \\
& + \Bigg(-\lambda_{\mathrm{B}}\lambda_{\mathrm{A}} \int \mathrm{d}t \int \mathrm{d}\boldsymbol{x} \int_{-\infty}^{t} \mathrm{d}t' \int \mathrm{d}\boldsymbol{x}'\, \chi_{\mathrm{A}}(t-t_{\mathrm{A}}) F_{\mathrm{A}}(\boldsymbol{x}-\boldsymbol{x}_{\mathrm{A}}) \chi_{\mathrm{B}}(t'-t_{\mathrm{B}}) F_{\mathrm{B}}(\boldsymbol{x}'-\boldsymbol{x}_{\mathrm{B}}) \\
& \times e^{\mathrm{i}(\Omega_{\mathrm{B}}t'+\Omega_{\mathrm{A}}t)} \left\langle \psi \right| f(\phi(t,\boldsymbol{x})) f(\phi(t',\boldsymbol{x}')) \left| \psi \right\rangle \Bigg) \left| 1_{\mathrm{A}} \right\rangle \left\langle 0_{\mathrm{A}} \right| \otimes \left| 1_{\mathrm{B}} \right\rangle \left\langle 0_{\mathrm{B}} \right| \\
& + \Bigg(-\lambda_{\mathrm{B}}\lambda_{\mathrm{A}} \int \mathrm{d}t \int \mathrm{d}\boldsymbol{x} \int_{-\infty}^{t} \mathrm{d}t' \int \mathrm{d}\boldsymbol{x}'\, \chi_{\mathrm{B}}(t-t_{\mathrm{B}}) F_{\mathrm{B}}(\boldsymbol{x}-\boldsymbol{x}_{\mathrm{B}}) \chi_{\mathrm{A}}(t'-t_{\mathrm{A}}) F_{\mathrm{A}}(\boldsymbol{x}'-\boldsymbol{x}_{\mathrm{A}}) \\
& \times e^{\mathrm{i}(\Omega_{\mathrm{A}}t'+\Omega_{\mathrm{B}}t)} \left\langle \psi \right| f(\phi(t,\boldsymbol{x})) f(\phi(t',\boldsymbol{x}')) \left| \psi \right\rangle \Bigg) \left| 1_{\mathrm{A}} \right\rangle \left\langle 0_{\mathrm{A}} \right| \otimes \left| 1_{\mathrm{B}} \right\rangle \left\langle 0_{\mathrm{B}} \right| \qquad (1.58)
\end{aligned}$$

$$\mathrm{Tr}\left(\hat{\rho}^{(0,2)}\right) = \left(\mathrm{Tr}\left(\hat{\rho}^{(2,0)}\right)\right)^{*} \qquad (1.59)$$

Finally, the last self-adjoint term (second order) is also dependent on the two-point

function of the state of the field,

$$\begin{aligned}
\mathrm{Tr}\left(\hat{\rho}^{(1,1)}\right) = &\left(\lambda_{\mathrm{A}}^2 \int \mathrm{d}t \int \mathrm{d}\boldsymbol{x} \int \mathrm{d}t' \int \mathrm{d}\boldsymbol{x}'\, \chi_{\mathrm{A}}(t-t_{\mathrm{A}}) F_{\mathrm{B}}(\boldsymbol{x}-\boldsymbol{x}_{\mathrm{A}}) \chi_{\mathrm{B}}(t'-t_{\mathrm{A}}) F_{\mathrm{B}}(\boldsymbol{x}'-\boldsymbol{x}_{\mathrm{A}})\right. \\
&\left. \times e^{\mathrm{i}\Omega_{\mathrm{A}}(t-t')} \left\langle\psi\right| f(\phi(t',\boldsymbol{x}'))^\dagger f(\phi(t,\boldsymbol{x})) \left|\psi\right\rangle \right) \left|1_{\mathrm{A}}\right\rangle \left\langle 1_{\mathrm{A}}\right| \otimes \left|0_{\mathrm{B}}\right\rangle \left\langle 0_{\mathrm{B}}\right| \\
+ &\left(\lambda_{\mathrm{B}}^2 \int \mathrm{d}t \int \mathrm{d}\boldsymbol{x} \int \mathrm{d}t' \int \mathrm{d}\boldsymbol{x}'\, \chi_{\mathrm{B}}(t-t_{\mathrm{B}}) F_{\mathrm{B}}(\boldsymbol{x}-\boldsymbol{x}_{\mathrm{B}}) \chi_{\mathrm{B}}(t'-t_{\mathrm{B}}) F_{\mathrm{B}}(\boldsymbol{x}'-\boldsymbol{x}_{\mathrm{B}})\right. \\
&\left. \times e^{\mathrm{i}\Omega_{\mathrm{B}}(t-t')} \left\langle\psi\right| f(\phi(t',\boldsymbol{x}'))^\dagger f(\phi(t,\boldsymbol{x})) \left|\psi\right\rangle \right) \left|0_{\mathrm{A}}\right\rangle \left\langle 0_{\mathrm{A}}\right| \otimes \left|1_{\mathrm{B}}\right\rangle \left\langle 1_{\mathrm{B}}\right| \\
+ &\left(\lambda_{\mathrm{B}}\lambda_{\mathrm{A}} \int \mathrm{d}t \int \mathrm{d}\boldsymbol{x} \int \mathrm{d}t' \int \mathrm{d}\boldsymbol{x}'\, \chi_{\mathrm{A}}(t-t_{\mathrm{A}}) F_{\mathrm{A}}(\boldsymbol{x}-\boldsymbol{x}_{\mathrm{A}}) \chi_{\mathrm{B}}(t'-t_{\mathrm{B}}) F_{\mathrm{B}}(\boldsymbol{x}'-\boldsymbol{x}_{\mathrm{B}})\right. \\
&\left. \times e^{\mathrm{i}(\Omega_{\mathrm{A}}t-\Omega_{\mathrm{B}}t')} \left\langle\psi\right| f(\phi(t',\boldsymbol{x}'))^\dagger f(\phi(t,\boldsymbol{x})) \left|\psi\right\rangle \right) \left|1_{\mathrm{A}}\right\rangle \left\langle 0_{\mathrm{A}}\right| \otimes \left|0_{\mathrm{B}}\right\rangle \left\langle 1_{\mathrm{B}}\right| \\
+ &\left(\lambda_{\mathrm{B}}\lambda_{\mathrm{A}} \int \mathrm{d}t \int \mathrm{d}\boldsymbol{x} \int \mathrm{d}t' \int \mathrm{d}\boldsymbol{x}'\, \chi_{\mathrm{A}}(t'-t_{\mathrm{A}}) F_{\mathrm{A}}(\boldsymbol{x}'-\boldsymbol{x}_{\mathrm{A}}) \chi_{\mathrm{B}}(t-t_{\mathrm{B}}) F_{\mathrm{B}}(\boldsymbol{x}-\boldsymbol{x}_{\mathrm{B}})\right. \\
&\left. \times e^{\mathrm{i}(\Omega_{\mathrm{B}}t-\Omega_{\mathrm{A}}t')} \left\langle\psi\right| f(\phi(t',\boldsymbol{x}'))^\dagger f(\phi(t,\boldsymbol{x})) \left|\psi\right\rangle \right) \left|0_{\mathrm{A}}\right\rangle \left\langle 1_{\mathrm{A}}\right| \otimes \left|1_{\mathrm{B}}\right\rangle \left\langle 0_{\mathrm{B}}\right| . \qquad (1.60)
\end{aligned}$$

While these terms are correct and easily grouped by their order in perturbation theory, another convenient way to group them is by how they enter the bi-partite density matrix of detectors A and B. The density matrix is written as

$$\rho_{\mathrm{AB}} = \begin{pmatrix} 1-\mathcal{L}_{\mathrm{AA}}-\mathcal{L}_{\mathrm{BB}} & \mathcal{L}_{\mathrm{B}}^* & \mathcal{L}_{\mathrm{A}}^* & \mathcal{M}^* \\ \mathcal{L}_{\mathrm{B}} & \mathcal{L}_{\mathrm{AA}} & \mathcal{L}_{\mathrm{BA}} & 0 \\ \mathcal{L}_{\mathrm{A}} & \mathcal{L}_{\mathrm{AB}} & \mathcal{L}_{\mathrm{BB}} & 0 \\ \mathcal{M} & 0 & 0 & 0 \end{pmatrix} + \mathcal{O}(\lambda_\mu^3) \qquad (1.61)$$

were the terms $\mathcal{M}$, $\mathcal{L}_{\mu\nu}$ and $\mathcal{L}_\mu$ are given by

$$\mathcal{M} = -\int \mathrm{d}t \int^t \mathrm{d}t' \int \mathrm{d}^n\boldsymbol{x} \int \mathrm{d}\boldsymbol{x}' M(t,\boldsymbol{x},t',\boldsymbol{x}') W^{f(\phi),|\psi\rangle}(t,\boldsymbol{x},t',\boldsymbol{x}') \qquad (1.62)$$

$$\mathcal{L}_{\mu\nu} = \int \mathrm{d}t \int \mathrm{d}t' \int \mathrm{d}^n\boldsymbol{x} \int \mathrm{d}\boldsymbol{x}' L_\mu(t,\boldsymbol{x}) L_\nu^*(t,\boldsymbol{x}) W^{f(\phi),|\psi\rangle}(t,\boldsymbol{x},t',\boldsymbol{x}') \qquad (1.63)$$

$$\mathcal{L}_\mu = -\mathrm{i} \int \mathrm{d}t \int \mathrm{d}^n\boldsymbol{x} L_\mu(t,\boldsymbol{x}) Y^{f(\phi),|\psi\rangle}(t,\boldsymbol{x}) \qquad (1.64)$$

where the expressions $W^{f(\phi),|\psi\rangle}(t,\boldsymbol{x},t',\boldsymbol{x}')$ and $Y^{f(\phi),|\psi\rangle}(t,\boldsymbol{x})$ are the two- and one-point functions of $f(\phi)$:

$$W^{f(\phi),|\psi\rangle}(t,\boldsymbol{x},) = \langle\psi|\, f(\phi(t,\boldsymbol{x}))f(\phi(t',\boldsymbol{x}'))\,|\psi\rangle \tag{1.65}$$

$$Y^{f(\phi),|\psi\rangle} = \langle\psi|\, f(\phi(t,\boldsymbol{x}))\,|\psi\rangle \ . \tag{1.66}$$

We also further define

$$L_\mu(t,\boldsymbol{x}) = \chi_\mu(t-t_\mu)F_\mu(\boldsymbol{x}-\boldsymbol{x}_\mu)e^{\mathrm{i}\Omega_\mu t} \tag{1.67}$$

$$M(t,\boldsymbol{x},t',\boldsymbol{x}') = L_{\mathrm{A}}(t,\boldsymbol{x})L_{\mathrm{B}}(t',\boldsymbol{x}') + L_{\mathrm{A}}(t',\boldsymbol{x}')L_{\mathrm{B}}(t,\boldsymbol{x}). \tag{1.68}$$

The terms of the density matrix are quite general and can be particularized to any spacetime dimensionality or field, as long as special attention is paid to the assumptions we made at the beginning of this section regarding the switching function, spatial profile, field-state, and initial detector state.

To recover the well-known results for a single detector, simply trace out one of the detector's degrees of freedom. This results in a density matrix for the remaining detector of the form

$$\hat{\rho}_{\mathrm{A},T} = \begin{pmatrix} 1-\mathcal{L}_{\mathrm{AA}} & \mathcal{L}^*_{\mathrm{A}} \\ \mathcal{L}_{\mathrm{A}} & \mathcal{L}_{\mathrm{AA}} \end{pmatrix} + \mathcal{O}(\lambda^3_{\mathrm{A}}). \tag{1.69}$$

were L_{AA} and $\mathcal{L}_{\mathrm{A}}$ are defined above.

The element $\mathcal{L}_{\mathrm{AA}}$ of Eq. (1.69) is the excitation probability of detector A. If the state of the field is the vacuum, then it is called the vacuum excitation probability (VEP), and is denoted $\mathcal{L}_{\mathrm{VAC}}$.

UDW Interacting linearly with vacuum of real, scalar field

Let us turn our attention to the commonly studied point-like UDW model with a linear coupling to a real scalar field in the Minkowski vacuum. The Wightman function is given in [28] as

$$W^{\phi,|0\rangle}(t,\boldsymbol{x},t'\boldsymbol{x}') = \begin{cases} \frac{\Gamma\left(\frac{d}{2}-1\right)}{4\pi^{d/2}\left(z(t,\boldsymbol{x},,t',\boldsymbol{x}')\right)^{d-2}} & \text{for } d>2, \\ -(2\pi)^{-1}\ln\left(\Lambda z(t,\boldsymbol{x},,t',\boldsymbol{x}')\right) & \text{for } d=2, \end{cases}$$

where

$$z(t,\boldsymbol{x},,t',\boldsymbol{x}') := \sqrt{(\boldsymbol{x},-\boldsymbol{x},)^2-(t-t'-i\epsilon)^2}. \tag{1.70}$$

The one-point function for the Minkowski vacuum vanishes.

The $\mathcal{L}_{\text{A}}$ terms vanish due to the vanishing one-point function of the field. The remaining terms $\mathcal{M}$ and $\mathcal{L}_{\mu\nu}$ are expressible in $d>2$ dimensions as

$$\begin{aligned}\mathcal{M} = \lambda_{\text{A}}\lambda_{\text{B}}\frac{\Gamma\left(\frac{d}{2}-1\right)}{4\pi^{d/2}}\int \mathrm{d}t\int^t \mathrm{d}t'\int \mathrm{d}^n\boldsymbol{x}\int \mathrm{d}\boldsymbol{x}'\Bigg(&\frac{\chi_{\text{A}}(t-t_{\text{A}})\chi_{\text{B}}(t'-t_{\text{B}})e^{\mathrm{i}\Omega_{\text{A}}t-\mathrm{i}\Omega_{\text{B}}t'}}{\left(z(t,\boldsymbol{x}_{\text{A}},t',\boldsymbol{x}_{\text{B}})\right)^{d-2}}\\ &+\frac{\chi_{\text{B}}(t-t_{\text{B}})\chi_{\text{A}}(t'-t_{\text{A}})e^{\mathrm{i}\Omega_{\text{B}}t-\mathrm{i}\Omega_{\text{A}}t'}}{\left(z(t,\boldsymbol{x}_{\text{B}},t',\boldsymbol{x}_{\text{A}})\right)^{d-2}}\Bigg)\end{aligned} \tag{1.71}$$

$$\mathcal{L}_{\mu\nu} = \lambda_{\text{A}}\lambda_{\text{B}}\frac{\Gamma\left(\frac{d}{2}-1\right)}{4\pi^{d/2}}\int \mathrm{d}t\int \mathrm{d}t'\frac{\chi_\mu(t-t_\mu)\chi_\nu(t'-t_\nu)e^{\mathrm{i}\Omega_\mu t-\mathrm{i}\Omega_\nu t'}}{\left(z(t,\boldsymbol{x}_\mu,t',\boldsymbol{x}_\nu)\right)^{d-2}}. \tag{1.72}$$

In $1+1$ dimensions, an IR regulator is required,

$$\begin{aligned}\mathcal{M} = \lambda_{\text{A}}\lambda_{\text{B}}(2\pi)^{-1}\int \mathrm{d}t\int^t \mathrm{d}t'\int \mathrm{d}^n\boldsymbol{x}\int \mathrm{d}\boldsymbol{x}'\Bigg(&\frac{\chi_{\text{A}}(t-t_{\text{A}})\chi_{\text{B}}(t'-t_{\text{B}})e^{\mathrm{i}\Omega_{\text{A}}t-\mathrm{i}\Omega_{\text{B}}t'}}{\left(\ln\left(\Lambda z(t,\boldsymbol{x},t',\boldsymbol{x}')\right)\right)^{-1}}\\ &+\frac{\chi_{\text{B}}(t-t_{\text{B}})\chi_{\text{A}}(t'-t_{\text{A}})e^{\mathrm{i}\Omega_{\text{B}}t-\mathrm{i}\Omega_{\text{A}}t'}}{\left(\ln\left(\Lambda z(t,\boldsymbol{x},t',\boldsymbol{x}')\right)\right)^{-1}}\Bigg)\end{aligned} \tag{1.73}$$

$$\mathcal{L}_{\mu\nu} = \lambda_\mu\lambda_\nu(2\pi)^{-1}\int \mathrm{d}t\int \mathrm{d}t'\chi_\mu(t-t_\mu)\chi_\nu(t'-t_\nu)e^{\mathrm{i}\Omega_\mu t-\mathrm{i}\Omega_\nu t'}\ln\left(\Lambda z(t,\boldsymbol{x},t',\boldsymbol{x}')\right). \tag{1.74}$$

General Form for the VEP

We will briefly discuss the single detector model specifically to review a result that will prove useful later. If, instead of calculating the Wightman function as in section 1.5.1, we incorporate it into the vacuum excitation probability (VEP) in its integral form, we can derive a convenient expression for the VEP. We start with $\mathcal{L}_{\mu\nu}$Eq. (1.63) and apply the integral expression of the vacuum Wightman function,

$$\begin{aligned}W^{(f(\hat{\phi}))}(t,\boldsymbol{x},t',\boldsymbol{x}') &= \langle 0|\, f(\phi(t,\boldsymbol{x}))f(\hat{(}t',\boldsymbol{x}'))\,|0\rangle\\ &= \int\frac{\mathrm{d}^n\boldsymbol{k}}{2(2\pi)^n|\boldsymbol{k}|}e^{-\mathrm{i}|\boldsymbol{k}|(t-t')+\boldsymbol{k}\cdot(\boldsymbol{x}-\boldsymbol{x}')}.\end{aligned} \tag{1.75}$$

When W is input into $\mathcal{L}$, the imaginary exponential can be viewed as a Fourier factor. Thus the integrals over space and time are also Fourier transforms of the switching and smearing, $\tilde{\chi}[\Omega + |\boldsymbol{k}|]$ and $\tilde{F}[\boldsymbol{k}]$ respectively. In this light, we may express the vacuum expectation probability as

$$\mathcal{L}_{\text{VAC}} = \frac{\lambda^2}{2(2\pi)^n} \int \frac{\mathrm{d}^n \boldsymbol{k}}{|\boldsymbol{k}|} \left|\tilde{F}[\boldsymbol{k}]\right|^2 |\tilde{\chi}[\Omega + |\boldsymbol{k}|]|^2 , \tag{1.76}$$

where

$$\tilde{F}[\boldsymbol{k}] = \int_{\mathbb{R}^n} \mathrm{d}\boldsymbol{x} F(\boldsymbol{x}) e^{\mathrm{i}\boldsymbol{k}\cdot\boldsymbol{x}} \tag{1.77}$$

$$\tilde{\chi}[\Omega] = \int_{\mathbb{R}} \mathrm{d}t \chi(t) e^{\mathrm{i}\Omega t}. \tag{1.78}$$

1.6 Harvesting Correlations From the Minkowski Vacuum

The vacuum of a free scalar quantum field on Minkowski spacetime exhibits correlations [46, 34, 7]. These correlations can be transferred to two or more spatially separated local probes which interact with the vacuum state of a quantum field.

Now that we have derived general expressions for the state of a pair of UDW detectors after interacting with a quantum field, we can summarize results in the literature regarding the UDW detector's sensitivity to these correlations.

In this section we describe two types of correlations that the two detector models are known to harvest from the field: a) those measured by the mutual information, which quantifies both classical and quantum correlations [47], and b) the negativity, which is a faithful entanglement monotone for bipartite two-level systems [48]. These two types of correlation harvesting were studied for the linear and quadratic models and the real and complex models in [7, 29].

1.6.1 What is entanglement?

Entanglement has a storied history as a counter-intuitive fact about the physical world. Famously discussed by Einstein, Podolsky, and Rosen in their 1935 paper in which they presented non-local correlations as a reason quantum theory couldn't possibly be a complete

theory [49]. Later, it was shown that a theory that is both local and real (has a hidden variable description) cannot violate certain statistical bounds [50]. Determining whether or not this bound can be exceeded is known as a Bell test, and the first experimental Bell test claiming the bound can be exceeded was successfully performed in 1972 [51].

Since then, the field of resource theories as applied to entanglement as a quantum resource has been greatly developed, and it has been found that there are differing notions of entanglement. LOCC (Local Operations and Classical Communication) and LOSR (Local operations and shared randomness) entanglement are differently suited for different tasks [52]. LOCC entanglement is a resource under local operations and classical communication (LOCC), which are "free" operations in quantum computing. LOCC entanglement allows for otherwise impossible tasks, such as super dense coding and quantum teleportation [47]. LOSR entanglement is a resource under local operations and shared randomness (LOSR), which is a more restrictive class of operations than LOCC [52].

Entanglement Harvesting

We consider first the harvesting of entanglement from the vacuum and we quantify it with the negativity acquired between the two (initially uncorrelated) detectors through their interactions with the field while remaining spacelike separated. The entanglement harvesting protocol is sensitive to a variety of features of quantum field theories. For example, it depends on background features, such as spacetime geometry [53, 54, 55] and topology [56].

In our work, we will use negativity , which has been shown to be non-increasing under LOCC operations. Negativity of a bipartite state ρ is an entanglement monotone defined as the sum of the negative eigenvalues of the partial transpose of ρ [48]:

$$\mathcal{N}(\rho) = \sum_{\lambda_i \in \sigma\left[\rho^{\Gamma_A}\right]} \frac{|\lambda_i| - \lambda_i}{2} \,, \tag{1.79}$$

where ρ^{Γ_A} denotes the partial transpose of ρ with respect to subsystem A.

As seen, for instance, in [7], the negativity can be expressed in terms of the vacuum excitation probability, $\mathcal{L}_{\mu\mu}$, of each detector and the non-local term $\mathcal{M}$ (see Eq. (1.63) and Eq. (1.62)). Concretely, it is given by

$$\mathcal{N} = \max\left[\mathcal{N}_{(2)}, 0\right] + \mathcal{O}(\lambda^3), \tag{1.80}$$

where

$$\mathcal{N}_{(2)} = -\frac{1}{2}\left(\mathcal{L}_{\text{AA}} + \mathcal{L}_{\text{BB}} - \sqrt{(\mathcal{L}_{\text{AA}} - \mathcal{L}_{\text{BB}})^2 + 4\,|\mathcal{M}|^2}\right). \tag{1.81}$$

When both detectors are identical (i.e. they have the same spatial profile, switching function, coupling strength, and detector gap), Eq. (1.81) becomes

$$\mathcal{N}_{(2)} = |\mathcal{M}| - \mathcal{L}_{\mu\mu} \tag{1.82}$$

from which we can justify the usual argument that entanglement emerges as a competition between the non-local contribution $\mathcal{M}$ and the noise associated to the vacuum excitation probability $\mathcal{L}_{\mu\mu}$ for each detector [57, 7].

1.6.2 Harvesting Mutual Information

The mutual information $I(\rho_{\text{AB}})$ between two detectors quantifies the amount of uncertainty about one detector that is eliminated if some information about the state of the other is revealed [47].

In general, for a composite quantum system consisting of two subsystems A and B, the mutual information is given by

$$I(\rho_{\text{AB}}) = S(\rho_{\text{A}}) + S(\rho_{\text{B}}) - S(\rho_{\text{AB}}), \tag{1.83}$$

where $\rho_\nu = \text{Tr}_\mu(\rho_{\nu\mu})$ is the partial trace of $\rho_{\nu\mu}$ with respect to subsystem $\mu \in \{A, B\}$ and S is the von Neumann entropy given by $S(\rho) = -\text{Tr}(\rho \log \rho)$.

For a density matrix of the form Eq. (1.61), the mutual information is given by [7]

$$\begin{aligned} I(\rho_{\text{AB}}) = {} & \mathcal{L}_+ \log(\mathcal{L}_+) + \mathcal{L}_- \log(\mathcal{L}_-) \\ & - \mathcal{L}_{\text{AA}} \log(\mathcal{L}_{\text{AA}}) - \mathcal{L}_{\text{BB}} \log(\mathcal{L}_{\text{BB}}) + \mathcal{O}(\lambda_\nu^4) \end{aligned} \tag{1.84}$$

where

$$\mathcal{L}_\pm = \frac{1}{2}\left(\mathcal{L}_{\text{AA}} + \mathcal{L}_{\text{BB}} \pm \sqrt{(\mathcal{L}_{\text{AA}} - \mathcal{L}_{\text{BB}})^2 + 4\,|\mathcal{L}_{\text{AB}}|^2}\right). \tag{1.85}$$

Note how $I(\rho_{\text{AB}})$ only depends on the $\mathcal{L}_{\mu\nu}$ terms at leading order in perturbation theory.

1.7 Regularization in the UDW Model

Infinities abound in quantum field theory, and, while the UDW detector nicely circumvents many of them by using a probe with fewer degrees of freedom, it is no less necessary to proceed carefully. Analysis of the detector response function [58, 59, 60] and a number of investigations of entanglement harvesting and quantum communication with (linear) UDW detectors [32, 31, 57, 7, 61, 62, 63, 64, 19, 35] have found that utilizing smooth switching and smearing functions regularizes all known, leading-order UV divergences present in the time evolution of linearly coupled UDW detectors and detector pairs. Standard results from the UDW literature can be presented regulator-free with suitable choice of detector switching and smearing.

The picture is somewhat different for quadratically coupled detectors. The switching and smearing techniques for the linear detector fail to regularize the quadratically-coupled models [26, 23, 24, 25]. For the single detector, all persistent divergences can be renormalized with the addition of normal ordering [27]. However in [29] it was shown that a straightforward application of the leading-order prescription in [27] does not renormalize persistent leading-order divergences in scenarios with more than a single detector; the entanglement harvesting protocol seems to require the use of a regulator.

1.7.1 UV regularization

The ϵ regularization scheme, which is commonly used with UDW models [65, 29], is a soft UV-regulator. This is the same regularization scheme commonly applied to the Feynman propagator. In this work, high-k (UV) modes will be exponentially suppressed with the regulator $e^{-\epsilon k}$ added to the mode expansion of the field. Later, the limit $\epsilon \to 0$ will be taken where possible. This regulator works for all known linear models (regardless of the number of detectors) and for single quadratically coupled detectors. However, in [2] it was shown that a class of quadratic models all share the same singular behaviour. This behaviour was originally pointed out in [29].

1.7.2 IR regularization

Many researchers work in 1+1 dimensions [66, 65]. In some cases, closed-form or numerically stable solutions are not possible in 3+1, or the researchers turn to the (often simpler) 1+1 dimensional case in order to do exploratory studies or proof-of-principle calculations. In other cases, the authors justify their use of 1+1 dimensions by referencing thin cavities,

although this too might result is some subtleties [67]. When working in 1+1 dimensional free space, one must employ an IR regulator [68, 65]. This type of regulator is not necessary in higher dimensions. Typically this IR cutoff is a small hard cutoff at frequenciy scales much smaller than any other in the setup, for example see [1]

1.7.3 Switching and Smearing

It was shown in [69] that using a box function for the switching function of a detector results in singular behaviour in the linear UDW model. Shortly thereafter, [70] showed that utilizing a smooth switching instead removed divergences found in [69]. Later it was shown in [59] that the transition rate can be regularized by a spatial profile. In [58] the authors obtained a regulator-free integral formula for the total excitation probability of a detector via a smooth switching function. In both of these investigations, the results were regulator free.

While historically the UDW detector has been taken to be a point-like detector in the adiabatic regime (eg. a Gaussian switching that is infinitely wide and a delta smearing), these results show us that there is utility in non-point-like detectors, as they result in finite and regulator free results. As an important aside, the result of giving the detectors some spatial extent is that one must be careful about causality and general covariance issues [71, 72]. However, while the introduction of the smearing function in the UDW model was *ad hoc*, it has been shown that smearing functions arise naturally in more detailed accounts of Hydrogenic atoms coupling to the full electromagnetic field [19]. In these cases, the UDW smearing can be seen as an approximation to the atomic orbital wavefunctions.

Chapter 2

Non-linear Optics with a UDW Detector

In this chapter we will utilize the UDW model in a context reminiscent of quantum optics. We will employ Fock-like quasi-monochromatic states and to them couple detectors both linearly and quadratically. We will thoroughly explore the monochromatic limit, which will help to illuminate that the standard notions of resonance fail to hold in free space.

One reason for this exploration is to analyze the differences between free-field and cavity quantum field theory, which have not been thoroughly understood within the frame work of a particle detector model. In fact, a common intuition for the free-space quantum field theory is to think of it like a field in a very large cavity (see for instance the discussion about vacuum energy in [73]). However, there are fundamental differences and, as we will see in this chapter, they manifest as the (non) normalizability of one-particle Fock states $\hat{a}^\dagger_{\boldsymbol{k}} |0\rangle$. As a result we will pay special attention to the transition from quasi- to fully-monochromatic Fock states.

Another motivation for this project is that the detector response of the non-linear model described here has only been understood in response to the vacuum of a quantum field [24, 27, 29, 2], yet quadratic couplings are useful for modeling non-linear processes in quantum optics, where non-vacuum states are of great interest. Furthermore, quadratic couplings are fundamental to modelling the coupling of a detector to a charged field, Bosonic or Fermionic, without violating the $U(1)$ symmetry of the theory [27].

2.1 Non-linear Optics

This work is inspired by non-linear processes. How close is this work to non-linear optics in the "real world"? Let's take a look.

The interaction Hamiltonian for type II optical parametric processes in a crystal pumped by a laser beam can be written as [74]

$$H_1 = \varepsilon_0 \int_V \mathrm{d}^3\boldsymbol{r}\, \boldsymbol{\chi}\, \boldsymbol{E}_p^{(+)} \boldsymbol{E}_o^{(-)} \boldsymbol{E}_e^{(-)} + H.c. \tag{2.1}$$

We'll explain what each term means, but note that most of the details aren't important and can be explored in [74]. The volume of the crystal is V and the $\boldsymbol{\chi}$ is the non-linear susceptibility tensor. Each $\boldsymbol{E}$ is an electric field. $\boldsymbol{E}_p^{(+)}$ is the pump field, it is sent into the crystal to produce generated fields $\boldsymbol{E}_0^{(-)}$ and $\boldsymbol{E}_e^{(-)}$. The subscripts o and e stand for ordinary and extraordinary, terms corresponding to rays in the (birefringent) crystal. Essentially, $\boldsymbol{E}_0^{(-)}$ and $\boldsymbol{E}_e^{(-)}$ correspond to modes of the same field which have different polarization.

While the analogy is not perfect, since the fields in question are tensorial, this Hamiltonian begins to give some inkling into what a UDW detector modeling a non-linear process might look like. We might consider a simplified Hamiltonian of the form

$$H_2 = \lambda \int_V \mathrm{d}^3\boldsymbol{x}\, \hat{m}(t) :\hat{\phi}^2(\boldsymbol{x}, t): . \tag{2.2}$$

Here, the pump has been replaced with a much simpler two level system. The pair of generated fields are simplified as the scalar field ϕ^2. Furthermore, the interaction is self adjoint (and so Hermitian conjugate term is required). In this model the "smearing function" is played by the volume of integration, i.e. the shape of the bi-refringent crystal. There is no switching function.

Let's make a further change of the model, and add in a switching function. This accounts for turning on and turning off the pump laser. We will also explicitly show the smearing function:

$$H_I = \lambda\chi(t)\hat{m}(t) \int \mathrm{d}^3\boldsymbol{x}\, F(\boldsymbol{x}) :\hat{\phi}^2(\boldsymbol{x}, t): . \tag{2.3}$$

This is the Hamiltonian we will use in this work. While it makes several assumptions and introduces an ad hoc switching function, there is reason to believe that the UDW model can capture salient features of tensorial models, see [19, 20].

In what follows, we will study this Hamiltonian to see if it is able to reproduce features of non-linear optics.

2.2 One and Two Particle States

This work is the rare research in this thesis that utilizes a non-vacuum state. In particular we would like to build one- and two-particle states. In free space these states are completely delocalized and not well-defined. As a result, we will work with Fock wave packets or quasi-monochromatic states, where the spectral function $f_{\boldsymbol{k}_0}$ is real, has some width parameter Δ, and is centered on a peak frequency $\boldsymbol{k}_0$. Given a spectral function $f_{\boldsymbol{k}_0}$, the wave-packet can be described by

$$|1_{f_{k_0}}\rangle \coloneqq \int \mathrm{d}^n\boldsymbol{k}\, f_{\boldsymbol{k}_0}(\boldsymbol{k})\hat{a}^\dagger_{\boldsymbol{k}}\,|0\rangle\ . \tag{2.4}$$

Normalization of the state $|1_{f_{k_0}}\rangle$ requires that the L^2 norm of f is unity, which restricts f to a class of functions whose square is a nascent delta (in the $\Delta \to 0$ sense). Throughout this work we will employ Gaussian spectra

$$f_{\boldsymbol{k}_0}(\boldsymbol{k}) = \frac{e^{-\frac{|\boldsymbol{k}-\boldsymbol{k}_0|^2}{2\Delta^2}}}{(\pi\Delta^2)^{n/4}}. \tag{2.5}$$

Now, for the two-particle state, we will take the one-particle state and apply another spectrally-smeared creation operator,

$$\begin{aligned}|2_{f_{\eta_1,\eta_2}}\rangle &\coloneqq \mathcal{N}\int \mathrm{d}^n\boldsymbol{k}\, f_{\boldsymbol{\eta}_1}(\boldsymbol{k})\hat{a}^\dagger_{\boldsymbol{k}}\,|1_{f,\eta_2}\rangle \\ &= \mathcal{N}\int \mathrm{d}^n\boldsymbol{k}\,\mathrm{d}^n\boldsymbol{k}' f_{\boldsymbol{\eta}_1}(\boldsymbol{k}) f_{\boldsymbol{\eta}_2}(\boldsymbol{k}')\hat{a}^\dagger_{\boldsymbol{k}}\hat{a}^\dagger_{\boldsymbol{k}'}\,|0\rangle\ .\end{aligned} \tag{2.6}$$

We have assumed the spectral functions are the same size and shape, peaked at two (potentially different) frequencies, and both have L^2-norm of 1. To determine the normalization $\mathcal{N}$ we require the self-inner product of $|2_{f_{\eta_1,\eta_2}}\rangle$ to be unity, which is equivalent to

$$\mathcal{N} = \frac{1}{\sqrt{1+C^2_{\boldsymbol{\eta}_1\boldsymbol{\eta}_2}}}\,, \tag{2.7}$$

$$C_{\boldsymbol{\eta}_1\boldsymbol{\eta}_2} \coloneqq \int \mathrm{d}^n\boldsymbol{k}\, f_{\boldsymbol{\eta}_1}(\boldsymbol{k}) f_{\boldsymbol{\eta}_2}(\boldsymbol{k})\,. \tag{2.8}$$

In the case of a cavity, these continuous definitions carry over to the discrete case by replacing the n-dimensional integrals with n summations, and normalization is achieved by the discrete equivalent of the L^2 norm. The Dirac delta is replaced by the Kronecker delta, leading to different physics in cavities than in free space. We will establish the physics expected in a cavity before moving on to the free space case.

2.2.1 Energy Expectation of a One-particle State

We will calculate the energy expectation first in the exactly monochromatic limit, and then in the more general case of an L^2 normalizable function. This analysis helps to understand the transparency exhibited by the field in $n > 1$ dimensions.

In order for the *monochromatic limit* to work, the spectrum $|f_{\boldsymbol{k},\Delta}|^2$ is taken to be a member of a family of nascent delta functions:

$$\lim_{\Delta\to 0} |f_{\boldsymbol{k}_0}|^2 = \delta^{(n)}(\boldsymbol{k}-\boldsymbol{k}_0)\,. \tag{2.9}$$

Given the free Hamiltonian of the scalar field

$$\hat{H}_\phi = \int \mathrm{d}^n\boldsymbol{k}\,|\boldsymbol{k}|\left(\hat{a}^\dagger_{\boldsymbol{k}}\hat{a}_{\boldsymbol{k}} + \frac{1}{2}\right)\,, \tag{2.10}$$

the energy expectation for $|1_{f_{k_0}}\rangle$ with spectrum $f = f_{\boldsymbol{k}_0}$ is then given by

$$\langle 1_f|\,\hat{H}_{0,\phi}\,|1_{f_{k_0}}\rangle = \int \mathrm{d}^n\boldsymbol{k}\,|\boldsymbol{k}|\,|f_{\boldsymbol{k}_0}(\boldsymbol{k})|^2\,. \tag{2.11}$$

In the monochromatic limit $\Delta \to 0$ where $f_{\boldsymbol{k}_0}$ becomes very sharply peaked around $\boldsymbol{k}_0$, the distributional limit gives

$$\lim_{\Delta\to 0}\langle 1_f|\,\hat{H}_{0,\phi}\,|1_{f_{k_0}}\rangle = \int \mathrm{d}^n\boldsymbol{k}\,|\boldsymbol{k}|\delta^{(n)}(\boldsymbol{k}-\boldsymbol{k}_0) = |\boldsymbol{k}_0|\,. \tag{2.12}$$

This agrees with the energy expectation value formally evaluated for the non-normalizable monochromatic state $|1_{\boldsymbol{k}_0}\rangle$.

Now let us consider a particular spectrum, the L^2-normalized Gaussian[75, 76, 77],

$$f_{\boldsymbol{k}_0}(\boldsymbol{k}) = \frac{1}{(\pi\Delta^2)^{n/4}}\exp\left(-\frac{(\boldsymbol{k}-\boldsymbol{k}_0)^2}{2\Delta^2}\right)\,. \tag{2.13}$$

Employing the free-field Hamiltonian, we find

$$\begin{aligned}
&\langle 1_f|\hat{H}_{0,\phi}|1_f\rangle \\
&\quad= \int \mathrm{d}^n\boldsymbol{k}\,|\boldsymbol{k}|\;|f_{\Delta,\boldsymbol{k}_0}(\boldsymbol{k})|^2 \\
&\quad= \frac{1}{\sqrt{\pi\Delta^{2^n}}}\int \mathrm{d}^n\boldsymbol{k}|\boldsymbol{k}|e^{-\frac{(\boldsymbol{k}-\boldsymbol{k}_0)^2}{\Delta^2}} \\
&\quad= \frac{e^{-\frac{|\boldsymbol{k}_0|^2}{\Delta^2}}}{\sqrt{\pi\Delta^{2^n}}}\int \mathrm{d}|\boldsymbol{k}|\mathrm{d}\Omega_{n-1}\,|\boldsymbol{k}|^n e^{-\frac{|\boldsymbol{k}|^2}{\Delta^2}}e^{\frac{2|\boldsymbol{k}||\boldsymbol{k}_0|\cos\theta}{\Delta^2}}\,.
\end{aligned} \tag{2.14}$$

A useful method, the details of which are outlined in subsection 2.4.1, succinctly computes all but one of the angular parts of this expression:

$$\mathrm{d}\Omega_{n-1} = \mathrm{d}\mu_{n-2}\mathrm{d}\theta\,(\sin\theta)^{n-2}\,. \tag{2.15}$$

The integral over θ is given by

$$\int_0^\pi \mathrm{d}\theta\,(\sin\theta)^{n-2} e^{\frac{2|\boldsymbol{k}_0||\boldsymbol{k}|\cos\theta}{\Delta^2}} = \frac{\sqrt{\pi}\Delta^{n-2}}{|\boldsymbol{k}|^{\frac{n-2}{2}}|\boldsymbol{k}_0|^{\frac{n-2}{2}}}\Gamma\left(\frac{n-1}{2}\right) I_{\frac{n-2}{2}}\left(\frac{2|\boldsymbol{k}||\boldsymbol{k}_0|}{\Delta^2}\right)\,, \tag{2.16}$$

where I_n is a modified Bessel function of the first kind [78, 79]. Substituting this expression into Eq. (2.14), we get the energy expectation value for $n \geq 2$,

$$\langle 1_f|\hat{H}_{0,\phi}|1_f\rangle = \Delta\Gamma\left(\frac{n+1}{2}\right)\,{}_1\tilde{F}_1\left(-\frac{1}{2};\frac{n}{2};-\frac{|\boldsymbol{k}_0|^2}{\Delta^2}\right)\,. \tag{2.17}$$

where ${}_p\tilde{F}_q$ is the regularized generalized hypergeometric function [78, 80]. The monochromatic limit reproduces Eq. (2.12) as expected:

$$\lim_{\Delta\to 0}\langle 1_f|\hat{H}_{0,\phi}|1_f\rangle = |\boldsymbol{k}_0|\,. \tag{2.18}$$

The $n = 1$ case admits direct integration, which yields

$$\begin{aligned}&\langle 1_f|\hat{H}_{0,\phi}|1_f\rangle_{n=1}\\ &\quad= \frac{1}{2\sqrt{\pi}}\left[\sqrt{\pi}|k_0|\left(\mathrm{erf}\left(\frac{\Lambda+|k_0|}{\Delta}\right)-\mathrm{erf}\left(\frac{\Lambda-|k_0|}{\Delta}\right)\right)+\Delta\left(e^{-\frac{(\Lambda-|k_0|)^2}{\Delta^2}}+e^{-\frac{(\Lambda+|k_0|)^2}{\Delta^2}}\right)\right],\end{aligned} \tag{2.19}$$

where is the scale of the IR cutoff.

The monochromatic limit $\Delta \to 0$ can be taken while removing the IR cutoff:

$$\lim_{\Delta\to 0}\lim_{\Lambda\to 0}\langle 1_f|\hat{H}_{0,\phi}|1_f\rangle_{n=1} = |k_0|\,. \tag{2.20}$$

The Gaussian wavepacket indeed goes to the expected energy expectation $\hbar|\boldsymbol{k}_0|$ in the monochromatic limit in all dimensions.

In later sections, we will see that the exact monochromatic state of the free field is transparent to the detector for dimensions $n > 1$. The following calculation, in which we calculate the energy density of the field, will aid in our discussion at the end this chapter.

The tt-component from the renormalized stress-energy tensor of the massless scalar field is precisely the Hamiltonian density, which reads

$$\langle 1_f| : \hat{T}_{tt}(\mathsf{x}) : |1_f\rangle = \int \frac{\mathrm{d}^n\boldsymbol{k}\,\mathrm{d}^n\boldsymbol{k}'}{2(2\pi)^n\sqrt{|\boldsymbol{k}||\boldsymbol{k}'|}}(|\boldsymbol{k}||\boldsymbol{k}'| + \boldsymbol{k}\cdot\boldsymbol{k}')f_{\boldsymbol{k}_0}(\boldsymbol{k})f_{\boldsymbol{k}_0}(\boldsymbol{k}')\cos\left[(k_\mu - k'_\mu)x^\mu\right]\,. \tag{2.21}$$

In the above expression, $k_\mu x^\mu = -|\boldsymbol{k}|t + \boldsymbol{k}\cdot\boldsymbol{x}$ and $: \hat{T}_{tt}(\mathsf{x}) :$ is the normal ordered operator $\hat{T}_{tt}(\mathsf{x})$. The energy expectation (2.11) is recovered by performing a spatial integral:

$$\langle 1_f|\hat{H}_{0,\phi}|1_f\rangle = \int \mathrm{d}^n\boldsymbol{x}\,\langle 1_f| : \hat{T}_{tt}(\mathsf{x}) : |1_f\rangle\,. \tag{2.22}$$

A point of note: $f_{\boldsymbol{k}_0}(\boldsymbol{k})$ does not have the correct normalization to define a nascent delta function. However, we can force it into an appropriate form with a scaling factor proportional to Δ. In the case of a Gaussian spectrum (2.13) we can write

$$f_{\boldsymbol{k}_0}(\boldsymbol{k}) = (4\pi\Delta^2)^{n/4}\mathfrak{f}_{\boldsymbol{k}_0}(\boldsymbol{k})\,, \tag{2.23}$$

where

$$\mathfrak{f}_{\boldsymbol{k}_0}(\boldsymbol{k}) = \frac{1}{(2\pi\Delta^2)^{n/2}}e^{-\frac{(\boldsymbol{k}-\boldsymbol{k}_0)^2}{2\Delta^2}}\,. \tag{2.24}$$

Now $\mathfrak{f}_{\boldsymbol{k}_0}$ defines a family of nascent delta function since

$$\int \mathrm{d}^n\boldsymbol{k}\,\mathfrak{f}_{\boldsymbol{k}_0}(\boldsymbol{k}) = 1, \tag{2.25}$$

including in the $\Delta \to 0$ limit. Next, we can write

$$\lim_{\Delta\to 0}\frac{1}{\Delta^n}\langle 1_f| : \hat{T}_{tt}(\mathsf{x}) : |1_f\rangle = \frac{|\boldsymbol{k}_0|}{\pi^{n/2}}\,. \tag{2.26}$$

It follows that

$$\langle 1_f| : \hat{T}_{tt}(\mathsf{x}) : |1_f\rangle \sim |\boldsymbol{k}_0|\Delta^n. \tag{2.27}$$

Hence, in the monochromatic limit, the energy density of the wavepacket vanishes as Δ^n, the inverse spatial-volume scale of the wavepacket.

This reasoning holds for any choice of L^2-normalizable spectrum. Any such spectrum can be transformed into the correct form by an appropriate geometric factor and $\Delta^{n/2}$. We conclude that, for any L^2-normalizable spectrum, the energy density goes to zero in the monochromatic limit.

2.3 The Light-matter Interaction in an Optical Cavity

Much of the intuition of quantum optics is based on cavities, and so we will produce here the transition probability for a point-like UDW detector interacting with a $n+1$-dimensional massless scalar field in an n-dimensional Dirichlet cavity of dimension $L \times \cdots \times L$ with boundaries ($\hat{\phi}(t,x)=0$) at the origin of the coordinate system and along each surface with one spatial coordinate equal to L. This results in a discrete mode decomposition,

$$\hat{\phi}(t,\boldsymbol{x}) = \sum_I \hat{a}_I u_I(t,\boldsymbol{x}) + a_I^\dagger u_I^*(t,\boldsymbol{x})\,, \tag{2.28}$$

where $\hat{a}_I \equiv \hat{a}_{\boldsymbol{k}_I}$ and I is a n-tuple that labels discrete momenta

$$\boldsymbol{k}_I = (k_1,...,k_n) \coloneqq \frac{\pi}{L}(j_1,...,j_n)\,. \tag{2.29}$$

The summation over I is an n-dimensional summation over each $j_i \in \mathbb{N}$. Each mode function $\boldsymbol{k}_I$ takes the form

$$u_I(t,\boldsymbol{x}) = v_I(\boldsymbol{x}) e^{-\mathrm{i}|\boldsymbol{k}_I|t}\,, \tag{2.30}$$

where

$$v_I(\boldsymbol{x}) \coloneqq \frac{1}{\sqrt{2|\boldsymbol{k}_I|}} \left(\frac{L}{2}\right)^{\frac{n}{2}} \prod_{i=1}^{n} \sin\left(\frac{j_i \pi x^i}{L}\right)\,. \tag{2.31}$$

The Wightman two-point function is

$$W^\phi(\mathsf{x},\mathsf{x}') = \mathcal{W}^\phi_{\text{vac}}(\mathsf{x},\mathsf{x}') + \left(\mathcal{K}^*_{\boldsymbol{k}_0}(\mathsf{x})\mathcal{K}_{\boldsymbol{k}_0}(\mathsf{x}') + \text{c.c}\right)\,, \tag{2.32}$$

where

$$\mathcal{W}^\phi_{\text{vac}}(\mathsf{x},\mathsf{x}') = \sum_I u_I(\mathsf{x}) u_I^*(\mathsf{x}')\,, \tag{2.33}$$

$$\mathcal{K}_{\boldsymbol{k}_0}(\mathsf{x}) = \sum_I f_{\boldsymbol{k}_0,\sigma}(\boldsymbol{k}_I) u_I^*(\mathsf{x})\,, \tag{2.34}$$

where $\mathsf{x} = (t,\boldsymbol{x})$.

The excitation probability can be calculated using both $\mathcal{L}_{\mu\nu}$ from Eq. (1.64) and the Wightman function above. The vacuum contribution vanishes in the adiabatic (χ varies slowly) regime,

$$P^{\phi,\text{CAV}} = \lambda^2 \int_{-\infty}^{\infty} \mathrm{d}t \int_{-\infty}^{\infty} \mathrm{d}t' \chi(t)\chi(t') e^{\mathrm{i}\Omega(t-t')} \Bigg(\sum_I f_{\boldsymbol{k}_0,\sigma}(\boldsymbol{k}_I) u_I(\mathsf{x}) \sum_J f_{\boldsymbol{k}_0,\sigma}(\boldsymbol{k}_J) u_J^*(\mathsf{x}') + \sum_I f_{\boldsymbol{k}_0,\sigma}(\boldsymbol{k}_I) u_I^*(\mathsf{x}) \sum_J f_{\boldsymbol{k}_0,\sigma}(\boldsymbol{k}_J) u_J(\mathsf{x}') \Bigg) \tag{2.35}$$

Applying the definition of u and noting that v is real, the integral breaks into two parts,

$$\begin{aligned} P^{\phi,\text{CAV}} = \lambda^2 \int_{-\infty}^{\infty} \mathrm{d}t \int_{-\infty}^{\infty} \mathrm{d}t' \chi(t)\chi(t') e^{\mathrm{i}\Omega(t-t')} \sum_I f_{\boldsymbol{k}_0,\sigma}(\boldsymbol{k}_I) v_I(\boldsymbol{x}_d) e^{-\mathrm{i}|\boldsymbol{k}_I|t} \sum_J f_{\boldsymbol{k}_0,\sigma}(\boldsymbol{k}_J) v_I(\boldsymbol{x}_d) e^{\mathrm{i}|\boldsymbol{k}_I|t'} \\ + \lambda^2 \int_{-\infty}^{\infty} \mathrm{d}t \int_{-\infty}^{\infty} \mathrm{d}t' \chi(t)\chi(t') e^{\mathrm{i}\Omega(t-t')} \sum_I f_{\boldsymbol{k}_0,\sigma}(\boldsymbol{k}_I) v_I(\boldsymbol{x}_d) e^{\mathrm{i}|\boldsymbol{k}_I|t} \sum_J f_{\boldsymbol{k}_0,\sigma}(\boldsymbol{k}_J) v_I(\boldsymbol{x}_d) e^{-\mathrm{i}|\boldsymbol{k}_I|t'} \end{aligned} \tag{2.36}$$

both of which can be re-expressed in terms of the Fourier transform of χ

$$\begin{aligned} P^{\phi,cav} = \lambda^2 \sum_I \widetilde{\chi}[\Omega - |\boldsymbol{k}_I|] f_{\boldsymbol{k}_0,\sigma}(\boldsymbol{k}_I) v_I(\boldsymbol{x}_d) \sum_J \widetilde{\chi}[-\Omega + |\boldsymbol{k}_J|] f_{\boldsymbol{k}_0,\sigma}(\boldsymbol{k}_J) v_I(\boldsymbol{x}_d) \\ + \lambda^2 \sum_I \widetilde{\chi}[\Omega + |\boldsymbol{k}_I|] f_{\boldsymbol{k}_0,\sigma}(\boldsymbol{k}_I) v_I(\boldsymbol{x}_d) \sum_J \widetilde{\chi}[-\Omega - |\boldsymbol{k}_J|] f_{\boldsymbol{k}_0,\sigma}(\boldsymbol{k}_J) v_I(\boldsymbol{x}_d). \end{aligned} \tag{2.37}$$

As the switching approaches a constant value in the long-time limit, $\widetilde{\chi}$ becomes highly peaked where its argument vanishes. All other contributions to $\widetilde{\chi}$ are highly suppressed. The arguments of $\widetilde{\chi}$ in the second term never attain a zero value, and so this term vanishes in the limit. The excitation probability is

$$P^{\phi,\text{CAV}} = \widetilde{\lambda}^2 \left| \sum_I \chi[\Omega - \mathrm{i}|\boldsymbol{k}_I|] f_{\boldsymbol{k}_0,\sigma}(\boldsymbol{k}_I) v_I(\boldsymbol{x}_d) \right|^2 . \tag{2.38}$$

Let's employ a Gaussian spectrum,

$$f_{\boldsymbol{k}_0}(\boldsymbol{k}_I) = \mathcal{N}_\Delta e^{-\frac{|\boldsymbol{k}_I - \boldsymbol{k}_0|^2}{2\Delta^2}} , \tag{2.39}$$

where the Normalization constant is

$$\mathcal{N}_\Delta = \left(\prod_{i=1}^{n} \left[\sum_{m=0}^{j_i^0 - 1} e^{-\left(\frac{\pi}{\Delta L}\right)^2 m^2} + \frac{1}{2} \left(\vartheta_3(0, e^{-\left(\frac{\pi}{\Delta L}\right)^2}) - 1 \right) \right] \right)^{-\frac{1}{2}} , \tag{2.40}$$

where ϑ_3 is the Jacobi theta function, see [78].

Let's look more closely at the monochromatic limit. First, consider that

$$\lim_{\sigma\to 0} \mathcal{N}_\sigma = 1 \tag{2.41}$$

and

$$\lim_{\sigma\to 0} e^{-\frac{|\boldsymbol{k}_I-\boldsymbol{k}_0|^2}{2\sigma^2}} = \delta_{\boldsymbol{k}_I\boldsymbol{k}_0}\,. \tag{2.42}$$

The *Kronecker* delta function is crucial: if $|\boldsymbol{k}_0|$ matches one of the cavity harmonics, then

$$\lim_{\sigma\to 0} |1_{f_{k_0}}\rangle = \hat{a}^\dagger_{\boldsymbol{k}_0}|0\rangle\ . \tag{2.43}$$

This state is physically well-defined (i.e., normalizable) and exactly monochromatic. In this limit, the detector excitation probability is simply

$$\lim_{\sigma\to 0} \mathcal{L}^\phi = \lambda^2 \left|\tilde{\chi}(\Omega - |\boldsymbol{k}_0|)v_{\boldsymbol{k}_0}(\boldsymbol{x}_d)\right|^2 \tag{2.44}$$

for any number of spatial dimensions.

Under the assumption of long switching times, $\tilde{\chi}(\Omega-|\boldsymbol{k}_0|)$ will be sharply peaked around $\Omega = |\boldsymbol{k}_0|$, and thus we expect enhanced transition probability when the field and detector frequencies match, i.e. we get standard resonance behaviour.

2.4 Detector Response to Fock-like states

We recovered the usual intuition in the previous section, and now we will find expressions for the transition probabilities in free space.

Let us pause for a moment to describe our simplifying assumptions, which will be the same for all cases studied. First we will choose a point-like detector for two reasons: this is the case commonly studied in the literature and, furthermore, it leads to closed form expressions for some cases. Second, we will choose the Gaussian spectrum as described previously Eq. (2.5). Next we will work with a Gaussian switching in the long-time limit, which is another common choice in the literature and simplifies calculations. Finally, we will assume the detector is initialized in its ground state, which simplifies calculations.

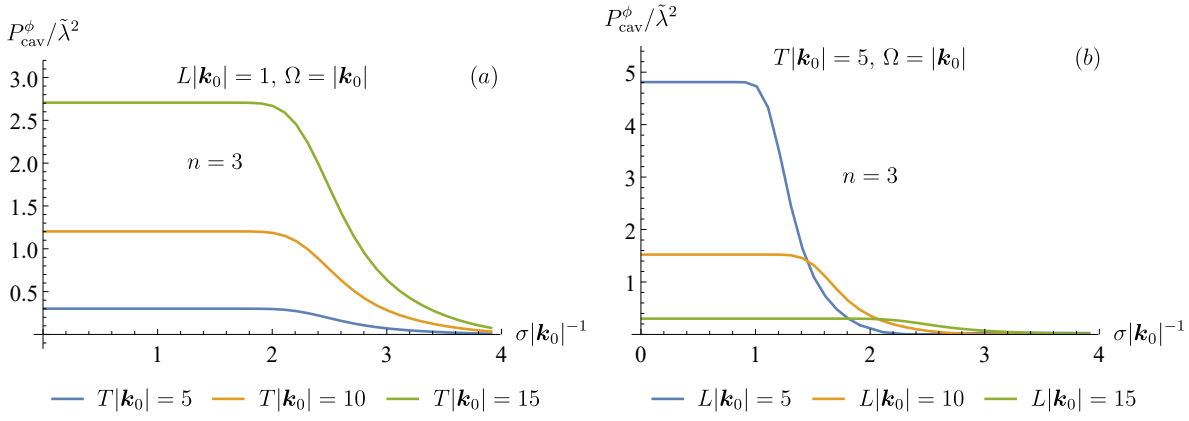

Figure 2.1: Excitation probability when $\Omega = |\boldsymbol{k}_0|$ as a function of the wave-packet width σ in a (3+1)-dimensional Dirichlet cavity. (a) Different curves refer to different interaction time T (in units of $|\boldsymbol{k}_0|^{-1}$). The excitation probability increases with longer interaction time. (b) Different curves refer to different cavity size L (in units of $|\boldsymbol{k}_0|^{-1}$) and the detector is always at the centre of the cavity. Note that the size of the plateau as $\sigma \to 0$ increases with cavity size, while the excitation probability decreases with size. In both cases, however, unlike the free-space setting the probability is always *maximized* in the monochromatic limit. We have chosen T to be large enough so that the result is within the long-time regime: the total probability P^{ϕ}_{cav} is dominated by the co-rotating contribution, while the counter-rotating and vacuum contributions are negligible. Images generated by Erickson Tjoa.

2.4.1 Linear detector model response to one-particle Fock state

In this section we will derive the transition probability for the linearly coupled detector interacting with a one-particle Fock state in free space. We will first derive a simple, general expression, and then particularize to less general assumptions on the switching, smearing, and spectral function.

We derived the excitation probability for a general UDW detector in section 1.5:

$$\mathcal{L}^{\phi}_{\boldsymbol{k}_0} = \lambda^2 \int_{-\infty}^{\infty} \mathrm{d}t \int_{-\infty}^{\infty} \mathrm{d}t' \int \mathrm{d}^n\boldsymbol{x} \int \mathrm{d}^n\boldsymbol{x}' \chi(t) F(\boldsymbol{x}) e^{-\mathrm{i}\Omega t} \chi(t') F(\boldsymbol{x}') e^{\mathrm{i}\Omega t'} W^{\phi,\boldsymbol{k}_0}(t,\boldsymbol{x},t',\boldsymbol{x}').$$

and derived the two-point function for the single particle Fock-like in Appendix 2:

$$W^{\phi}_{k_0}(\mathsf{x},\mathsf{x}') = (K_{\boldsymbol{k}_0}(\mathsf{x})^* K_{\boldsymbol{k}_0}(\mathsf{x}') + c.c) + W^{\phi}_{\mathrm{VAC}}(\mathsf{x},\mathsf{x}).$$

The probability separates into two summands, one dependant on K and the other on the vacuum two-point correlator, W^{ϕ}_{VAC}: $\mathcal{L} = \mathcal{L}_K + \mathcal{L}_{\mathrm{VAC}}$.

The vacuum contribution was already derived in subsection 1.5.1:

$$\mathcal{L}_{\mathrm{VAC}} = \frac{\lambda^2}{2(2\pi)^n} \int \frac{\mathrm{d}^n\boldsymbol{k}}{|\boldsymbol{k}|} \left|\tilde{F}[\boldsymbol{k}]\right|^2 \left|\tilde{\chi}[\Omega + \boldsymbol{k}]\right|^2 .$$

So, let us focus on the the non-vacuum contribution, which can be written

$$\mathcal{L}_K = \lambda^2 \left(\mathcal{I}^2_+(\boldsymbol{k}_0,\tilde{F},\tilde{\chi}) + \mathcal{I}^2_-(\boldsymbol{k}_0,\tilde{F},\tilde{\chi})\right), \tag{2.45}$$

where

$$\mathcal{I}_{\pm}(\boldsymbol{k}_0,\tilde{F},\tilde{\chi}) = \int \frac{\mathrm{d}^n\boldsymbol{k}}{\sqrt{2(2\pi)^n|\boldsymbol{k}|}} f_{\boldsymbol{k}_0}(\boldsymbol{k}) \tilde{F}(\boldsymbol{k}) \tilde{\chi}(\Omega \pm |\boldsymbol{k}|). \tag{2.46}$$

To have any traction in finding a closed form for $\mathcal{L}_K$, we must assume particular forms for the smearing, switching, and spectrum: a delta distribution, a Gaussian function, and a Gaussian function, respectively. Choosing a point-like spatial profile results in the Fourier transform $\tilde{F}$ being unity. As a result, $\tilde{F}$ drops from $\mathcal{I}^2_{\pm}$ and the expression simplifies. The Gaussian switching also produces a simplification on $\mathcal{I}^2_{\pm}$ in the long time limit. Namely, the long-time limit of a Gaussian is a constant function; we will choose $\chi(t) = 1$. In this case the Fourier transform is $\tilde{\chi}[\Omega] = 2\pi\delta[\Omega]$.

Under these two simplications, the function $\mathcal{I}_{\pm}^2$ simplifies, and so too does $\mathcal{L}_K$. We will now write it as

$$\mathcal{L}_K = \lambda^2 \left(\mathcal{I}_+^2(\boldsymbol{k}_0) + \mathcal{I}_-^2(\boldsymbol{k}_0) \right), \tag{2.47}$$

to indicate that the smearing and switching are now fixed. Note this expression has many fewer integrals than the original Eq. (2.45). In other words, $\mathcal{I}_{\pm}(\boldsymbol{k}_0) = \mathcal{I}_{\pm}(\boldsymbol{k}_0, 1, 2\pi\delta)$.

Let us further consider the long-time limit, adding the additional criteria that the detector is initialized to the ground state, $\Omega > 0$. It is known in this case that a detector will thermalize with the vacuum, both in their respective ground states. This can be argued from energy conservation: in the limit, the interaction Hamiltonian is time-independent and energy is conserved (in the sense that no energy is input to the system by the switching mechanism). Additionally the I_+^2 term vanishes under the same assumptions, since the argument of the delta distribution never attains the value of zero: $\Omega + |\boldsymbol{k}| > 0$. Under these assumptions, the transition probability reduces to

$$\mathcal{L}_{\boldsymbol{k}_0}^{\phi} = \lambda^2 \mathcal{I}_-^2(\boldsymbol{k}_0). \tag{2.48}$$

Finally, the L^2-normalized Gaussian spectrum described in Eq. (2.5) will allow for a closed form expression for the transition probability, which we will now derive. Inserting the spectrum into Eq. (2.48) yields

$$\mathcal{L}_{\boldsymbol{k}_0}^{\phi} = \lambda^2 \frac{e^{-\frac{|\boldsymbol{k}_0|^2}{\Delta^2}}}{2^{n-1}\pi^{\frac{3n}{2}-2}\Delta^n} \left(\int \frac{\mathrm{d}^n \boldsymbol{k}}{\sqrt{|\boldsymbol{k}|}} e^{-\frac{|\boldsymbol{k}|^2}{2\Delta^2}} e^{-\frac{|\boldsymbol{k}||\boldsymbol{k}_0|\cos\theta}{\Delta^2}} \delta(\Omega - |\boldsymbol{k}|) \right)^2, \tag{2.49}$$

where θ is the angle between integration variable $\boldsymbol{k}$ and constant $\boldsymbol{k}_0$.

We will consider the integral in parenthesis separately, defining

$$G_n := \int \frac{\mathrm{d}^n \boldsymbol{k}}{\sqrt{|\boldsymbol{k}|}} e^{-\frac{|\boldsymbol{k}|^2}{2\Delta^2}} e^{-\frac{|\boldsymbol{k}||\boldsymbol{k}_0|\cos\theta}{\Delta^2}} \delta(\Omega - |\boldsymbol{k}|). \tag{2.50}$$

Note that for $n = 1$, there is no angular integral. As a result, the integrand exhibits an IR divergence. Asymptotically, it behaves like $1/|\boldsymbol{k}|$ for small $|\boldsymbol{k}|$ (ignoring the δ distribution). We will consider this case separately after considering the more general $n \geq 2$.

Case 1: For $n \geq 2$, the G_n of Eq. (2.50) yields to our attempts at integrations in hyper-spherical coordinates:

$$G_n = \int \mathrm{d}|\boldsymbol{k}| \, \mathrm{d}\Omega_{n-1} |\boldsymbol{k}|^{n-3/2} e^{-\frac{|\boldsymbol{k}|^2}{2\Delta^2}} e^{-\frac{|\boldsymbol{k}||\boldsymbol{k}_0|\cos\theta}{\Delta^2}} \delta(\Omega - |\boldsymbol{k}|), \tag{2.51}$$

where the area element $\mathrm{d}\Omega$ is given by

$$\mathrm{d}\Omega_{n-1} = \prod_{i=1}^{n-1} \mathrm{d}\phi_i \left(\sin\phi_i\right)^{n-1-i}. \tag{2.52}$$

Choosing our coordinate system so that $\phi_1 = \theta$, we can write

$$G_n = \int \frac{\mathrm{d}|\boldsymbol{k}|}{|\boldsymbol{k}|^{3/2-n}} \prod_{i=2}^{n-1} \left(\mathrm{d}\phi_i \left(\sin\phi_i\right)^{n-1-i}\right) \mathrm{d}\theta \left(\sin\theta\right)^{n-2} e^{-\frac{|\boldsymbol{k}|^2}{2\Delta^2}} e^{-\frac{|\boldsymbol{k}||\boldsymbol{k}_0|\cos\theta}{\Delta^2}} \delta(\Omega - |\boldsymbol{k}|). \tag{2.53}$$

The integral $\int \mathrm{d}\Omega_{n-1}$ is known,

$$\int \mathrm{d}\Omega_{n-1} = \frac{2\pi^{n/2}}{\Gamma(n/2)}, \tag{2.54}$$

as is

$$\int \mathrm{d}\theta \left(\sin\theta\right)^{n-2} = \frac{\sqrt{\pi}\Gamma\left(\frac{n-1}{2}\right)}{\Gamma(n/2)}. \tag{2.55}$$

Thus the integral over the ϕ_i is simple to compute since there are no cross-terms between the angular coordinates:

$$\int \mathrm{d}\phi_i \left(\sin\phi_i\right)^{n-1-i} = \frac{\int \mathrm{d}\Omega_{n-1}}{\int \mathrm{d}\theta \left(\sin\theta\right)^{n-2}} = \frac{2\pi^{\frac{n-1}{2}}}{\Gamma\left(\frac{n-1}{2}\right)}. \tag{2.56}$$

As a result, G_n takes the form

$$G_n = \frac{2\pi^{\frac{n-1}{2}}}{\Gamma\left(\frac{n-1}{2}\right)} \int \mathrm{d}|\boldsymbol{k}| \, \mathrm{d}\theta \left(\sin\theta\right)^{n-2} |\boldsymbol{k}|^{n-3/2} e^{-\frac{|\boldsymbol{k}|^2}{2\Delta^2}} e^{-\frac{|\boldsymbol{k}||\boldsymbol{k}_0|\cos\theta}{\Delta^2}} \delta(\Omega - |\boldsymbol{k}|). \tag{2.57}$$

The integral over variable θ has an analytic solution in terms of named functions,

$$\int \mathrm{d}\theta \left(\sin\theta\right)^{n-2} e^{-\frac{|\boldsymbol{k}||\boldsymbol{k}_0|\cos\theta}{\Delta^2}} = \frac{\sqrt{\pi} 2^{\frac{n}{2}-1} \Delta^{n-2}}{|\boldsymbol{k}_0|^{\frac{n}{2}-1} |\boldsymbol{k}|^{\frac{n}{2}-1}} \Gamma\left(\frac{n}{2} - \frac{1}{2}\right) I_{\frac{n-2}{2}}\left(\frac{|\boldsymbol{k}_0||\boldsymbol{k}|}{\Delta^2}\right), \tag{2.58}$$

where I_m is the Modified Bessel Function of the first kind.

G_n now takes the simpler form

$$G_n = \frac{\pi^{\frac{n}{2}} 2^{\frac{n}{2}} \Delta^{n-2}}{|\boldsymbol{k}_0|^{\frac{n}{2}-1}} \int \mathrm{d}|\boldsymbol{k}| \, |\boldsymbol{k}|^{\frac{n-1}{2}} e^{-\frac{|\boldsymbol{k}|^2}{2\Delta^2}} I_{\frac{n-2}{2}}\left(\frac{|\boldsymbol{k}_0||\boldsymbol{k}|}{\Delta^2}\right) \delta(\Omega - |\boldsymbol{k}|). \tag{2.59}$$

Integrating over $\boldsymbol{k}$ is simple due to the δ distribution, and after some manipulations and substituting G_n back into $\mathcal{L}^{\phi}_{\boldsymbol{k}_0}$, we have

$$\mathcal{L}^{\phi}_{\boldsymbol{k}_0} = \lambda^2 \frac{2\Delta^{n-4}}{|\boldsymbol{k}_0|^{n-2}} \frac{\Omega^{n-1}}{\pi^{\frac{n}{2}-2}} e^{-\frac{|\boldsymbol{k}_0|^2+\Omega^2}{\Delta^2}} \left(I_{\frac{n-2}{2}} \left(\frac{|\boldsymbol{k}_0|\Omega}{\Delta^2} \right) \right)^2 . \tag{2.60}$$

Case 2: When $n = 1$, the IR behaviour of the integrand can prove troublesome. However, if we implement an IR cutoff below the detector gap, $\Lambda < \Omega$, then we can evaluate the integral with the delta distribution in the naive way.

$$G_1 = -\frac{2e^{-\frac{\Omega^2}{2\Delta^2}} \sinh\left(\frac{|\boldsymbol{k}_0|\Omega}{\Delta^2}\right)}{\sqrt{\Omega}} \tag{2.61}$$

This results in

$$\mathcal{L}^{\phi,(1)}_{\boldsymbol{k}_0} = \lambda^2 \frac{4e^{-\frac{|\boldsymbol{k}_0|^2+\Omega^2}{\Delta^2}}}{\pi^{\frac{3}{2}-2}\Delta\Omega} \left(\sinh\left(\frac{|\boldsymbol{k}_0|\Omega}{\Delta^2} \right) \right)^2 . \tag{2.62}$$

Notably, this matches exactly the limit

$$\lim_{n\to 1} \mathcal{L}^{\phi,(n)}_{\boldsymbol{k}_0} = \mathcal{L}^{\phi,(1)}_{\boldsymbol{k}_0}. \tag{2.63}$$

and so in future discussions involving $\mathcal{L}^{\phi,(n)}_{\boldsymbol{k}_0}$ we won't treat $n = 1$ separately and instead will assume the IR cutoff is small.

We plot the transition probability for various spatial dimensions in Figure 2.2 to aid in our analysis of Eq. (2.60). We will focus on three aspects of the transition probability. First, for large spectral width $\Delta \gg |\boldsymbol{k}_0|$ (a wave-packet with equal weight for all momenta), the probability vanishes as fast as Δ^n in all spatial dimensions. This is perhaps contrary to expectation: an infinitely wide spectrum Fock wave-packet also has infinite total energy expectation (see subsection 2.2.1), yet that energy does not translate to increased transition probability. This is traced back to the fact that the monochromatic Fock state is not normalizable. In the limit of a fully monochromatic state, the energy density of the state goes to zero.

Second, the maximum of the probability is not at $\Omega = |\boldsymbol{k}_0|$. Instead, the peak drifts toward this value in the monochromatic limit ($\Delta \to 0$). In this limit, the resonant peak also becomes sharper. In $n = 1$ dimensions, this drift is not resolvable, as shown in Figure 2.2.

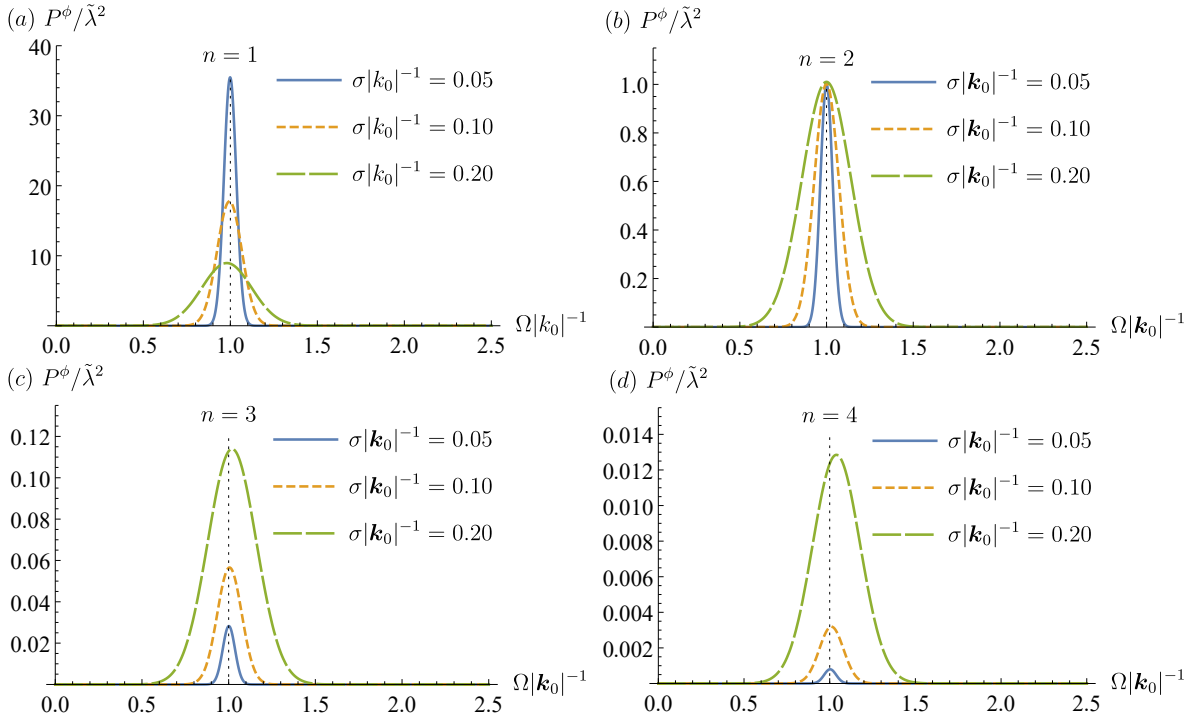

Figure 2.2: Plots of transition probability $\mathcal{L}^\phi/\tilde{\lambda}^2$ as a function of detector energy gap for linear coupling and one-particle state in various spatial dimensions n, for various spectral bandwidths Δ. We vary Ω as we search for resonant peaks while keeping $|\boldsymbol{k}_0|$ fixed. Here $\tilde{\lambda} = \lambda|\boldsymbol{k}_0|^{(n-3)/2}$ is the adimensionalized coupling constant. The vertical lines denote the resonant frequency. Note that in the monochromatic limit $\Delta \to 0$, the peak amplitude *diminishes* for $n \geq 3$, and it approaches a constant value for $n = 2$, while it *increases* for $n = 1$. Images generated by Erickson Tjoa.

However, in solving for the particular value of $|\boldsymbol{k}_0|$ that satisfies $\partial\mathcal{L}^\phi/\partial|\boldsymbol{k}_0| = 0$, the peak can be shown to be offset.

Finally, the amplitude of the resonant peak does not behave the same for all dimensions in the monochromatic limit. For example, in $n = 1$ dimensions the peak of $\mathcal{L}^\phi$ *increases* in amplitude as the spectrum becomes more peaked, while for $n = 2$ the peak approaches a constant value and for $n \geq 3$ the peak *decreases* in amplitude. To see this more explicitly, consider the at-resonance ($\Omega = |\boldsymbol{k}_0|$) asymptotic behaviour of the excitation probability in

the monochromatic limit,

$$\mathcal{L}^{\phi}(\Omega = |\boldsymbol{k}_0|) = \tilde{\lambda}^2 \left(\frac{\Delta/|\boldsymbol{k}_0|}{\sqrt{\pi}} \right)^{n-2} + O((\Delta/|\boldsymbol{k}_0|)^n)\,, \tag{2.64}$$

for all $n \geq 1$ and $\tilde{\lambda} = \lambda |\boldsymbol{k}_0|^{(n-3)/2}$ is a dimensionless coupling constant.

Let us consider for a moment whether the peak vanished completely for finite values of the spectral width. Consider that the peak vanishes in the monochromatic limit for $n \geq 3$. However, it can be shown that in all dimensions

$$\lim_{\Delta \to 0} \frac{\mathcal{L}^{\phi}(\Omega \neq |\boldsymbol{k}_0|)}{\mathcal{L}^{\phi}(\Omega = |\boldsymbol{k}_0|)} = 0\,. \tag{2.65}$$

The off-resonant frequencies decay faster than the resonant frequency, so there is always a resonant peak for finite spectral width.

One may conjecture that the point-like detector is responsible for the vanishing probability. However, this is not the case. Consider a Gaussian smearing function

$$F(\boldsymbol{x}) = \frac{1}{(\pi\sigma^2)^{\frac{n}{2}}} e^{-|\boldsymbol{x}|^2/\sigma^2} \Longrightarrow \tilde{F}(\boldsymbol{k}) = e^{-\frac{1}{4}(\sigma^2 |\boldsymbol{k}|^2)}\,, \tag{2.66}$$

where σ controls the effective size of the detector. The new excitation probability, denoted by P^{ϕ}_{σ}, has a simple relation to the point-like one. Substituting the new spatial profile into Eq. (2.46) yields the relation

$$\mathcal{L}^{\phi}_{\boldsymbol{k}_0,\,\sigma} = \mathcal{L}^{\phi}_{\boldsymbol{k}_0} e^{-\frac{1}{2}\ \sigma^2 \Omega^2}\,, \tag{2.67}$$

from which the point-like result is recovered when $\Delta \to 0$.

Now let us take the monochromatic limit while increasing the size of the detector in proportion, setting $\sigma = \Delta^{-1}$. In this case, the probability decreases *faster* than in the point-like regime. As a result, we cannot argue that the diminishing resonant probability for $n \geq 3$ is due to the fact that the field quanta are simply large in comparison to the detector. Increasing the detector size does not counter the effect!

Instead, the energy density of the wave-packet is the mechanism responsible for the vanishing resonant peak (subsection 2.2.1). The total energy approaches a finite value, k_0, in the monochromatic limit. However, the wave-packet also becomes uniformly delocalized in the limit. As a result, the energy density vanishes (see Eq. (2.27).

So why does the increased detector size not counteract the vanishing energy density? In principle one expects a large enough detector ($\sigma \approx \Delta^{-1}$) would have a non-zero excitation probability. After all, integrating the energy density over the whole of space gives a non-zero value. However, as the detector is delocalized, it becomes more weakly coupled to the field at each point. In the limit of uniform delocalization, the detector response vanishes regardless of the state of the field.

One may wonder: since the units of the coupling strength λ depend on the dimensions of spacetime, does the vanishing response of the detector in the monochromatic limit stem from failing to capture the scaling behaviour of the coupling strength? This is also not the case. Consider allowing the coupling strength λ to run with the wave-packet width Δ. Note λ has units of $[\text{Length}]^{\frac{n-3}{2}}$ for the linear coupling. Define a dimensionless coupling constant $\gamma \coloneqq \lambda\Delta^{\frac{n-3}{2}}$, so that we can rewrite $\mathcal{L}^\phi$ in Eq. (2.60) as

$$\mathcal{L}^\phi = \gamma^2 \frac{2\pi^{\frac{4-n}{2}}}{|\boldsymbol{k}_0|^{n-2}} \frac{\Omega^{n-1}}{\Delta} e^{-\frac{|\boldsymbol{k}_0|^2+\Omega^2}{\Delta^2}} I^2_{\frac{n-2}{2}}\left(\frac{|\boldsymbol{k}_0|\Omega}{\Delta^2}\right) . \tag{2.68}$$

This corresponds to a weakened coupling (for $n > 3$) or a strengthened coupling (for $n < 3$) as we approach the monochromatic limit. In this limit, a running coupling constant yields the universal result

$$\lim_{\Delta\to 0} \mathcal{L}^\phi(\Omega = |\boldsymbol{k}_0|) = 0 \tag{2.69}$$

for *all* $n \geq 1$. The detector becomes transparent when the wave-packet is strictly monochromatic. By forcing the coupling constant to be dimensionless, we force all dimensions to behave qualitatively similar to the $(3+1)$ dimensional case, the coupling of which is dimensionless by default. We conclude that the cancellation of the response of the detector when driven by a quasi-monochromatic wave-packet at resonance is not due to the scaling of the coupling strength in different dimensions.

2.4.2 Linear detector model response to two-particle Fock state

In this section, we will add another particle to our Fock state and see how the linear detector response differs.

First, let us compare the correlation functions between the the two states. Recall the

one-particle Eq. (26) and two-particle Eq. (34) Wightman functions:

$$\begin{aligned} W^{\phi}_{k_0}(\mathsf{x},\mathsf{x}') &= (K_{\boldsymbol{k}_0}(\mathsf{x})^* K_{\boldsymbol{k}_0}(\mathsf{x}') + c.c) + W^{\phi}_{\text{VAC}}(\mathsf{x},\mathsf{x}). \\ W^{\phi}_{\eta_1,\eta_2}(\mathsf{x},\mathsf{x}') &= W^{\phi}_{\text{VAC}}(\mathsf{x},\mathsf{x}') + \mathcal{N}^2\Big[C_{\boldsymbol{\eta}_1\boldsymbol{\eta}_2}\Big(K_{\boldsymbol{\eta}_1}(\mathsf{x}')K^*_{\boldsymbol{\eta}_2}(\mathsf{x}) + K_{\boldsymbol{\eta}_2}(\mathsf{x}')K^*_{\boldsymbol{\eta}_1}(\mathsf{x}) + c.c.\Big) \\ &\quad + \Big(K_{\boldsymbol{\eta}_2}(\mathsf{x}')K^*_{\boldsymbol{\eta}_2}(\mathsf{x}) + K_{\boldsymbol{\eta}_1}(\mathsf{x}')K^*_{\boldsymbol{\eta}_1}(\mathsf{x}) + c.c.\Big)\Big], \end{aligned} \tag{2.70}$$

where $\mathcal{N}$ and $C_{\boldsymbol{\eta}_1\boldsymbol{\eta}_2}$ are defined in Eq. (2.7) and Eq. (2.8).

Note the terms that show up in both correlators: $W^{\phi}_{\text{VAC}}(\mathsf{x},\mathsf{x}')$ and $K_{\boldsymbol{k}}(\mathsf{x})^* K_{\boldsymbol{k}_0}(\mathsf{x}')$. We will exploit this similarity to simplify the calculation. Let us write the excitation probability in a compact form, applying the two-particle correlator to the excitation probability for a general UDW detector derived in section 1.5:

$$\mathcal{L}^{\phi}_{\eta_1,\eta_2} = \mathcal{L}_{\text{VAC}} + 2\mathcal{N}^2 C_{\boldsymbol{\eta}_1\boldsymbol{\eta}_2}\mathcal{L}_{K,\boldsymbol{\eta}_2,\boldsymbol{\eta}_1} + \mathcal{N}^2\mathcal{L}_{K,\boldsymbol{\eta}_2,\boldsymbol{\eta}_2} + \mathcal{N}^2\mathcal{L}_{K,\boldsymbol{\eta}_1,\boldsymbol{\eta}_1}. \tag{2.71}$$

We will be working under the same set of assumptions as in the previous section: a point-like spatial profile, L^2-normalized Gaussian spectrum, uniform switching, and a detector that is initialized to its ground state. As in the previous section, under these assumptions $W^{\phi}_{\text{VAC}}(\mathsf{x},\mathsf{x}')$ vanishes, as do the counter rotating terms $I_+(\boldsymbol{k}_0,\tilde{F},\tilde{\chi})$ (defined in Eq. (2.46)). This leaves only one term, $2\mathcal{N}^2 C_{\boldsymbol{\eta}_1\boldsymbol{\eta}_2}\mathcal{L}_{\boldsymbol{\eta}_2,\boldsymbol{\eta}_1}$, to be calculated. Luckily, the form of this term allows us to re-use definitions from the one-particle case! Recall the function $\mathcal{I}_\pm$ defind in Eq. (2.46):

$$\mathcal{I}_\pm(\boldsymbol{k}_0) = \int \frac{\mathrm{d}^n\boldsymbol{k}}{\sqrt{2(2\pi)^n|\boldsymbol{k}|}} f_{\boldsymbol{k}_0}(\boldsymbol{k})\delta(\Omega \pm |\boldsymbol{k}|).$$

Note we have used the more compact notation $\mathcal{I}_\pm(\boldsymbol{k}_0)$ since we have already fixed the switching and smearing. The re-use of this function allows us to compactly write the remaining term:

$$\mathcal{L}^{\phi}_{K,\boldsymbol{\eta}_2,\boldsymbol{\eta}_1} = \lambda^2\left(I_-(\boldsymbol{\eta}_1)I_-(\boldsymbol{\eta}_2) + I_+(\boldsymbol{\eta}_2)I_+(\boldsymbol{\eta}_1)\right). \tag{2.72}$$

By the same arguments used in the previous section, the counter-rotating terms vanish, so that

$$\mathcal{L}^{\phi}_{K,\boldsymbol{\eta}_2,\boldsymbol{\eta}_1} = 2\lambda^2\mathcal{N}^2 C_{\boldsymbol{\eta}_1\boldsymbol{\eta}_2} I_-(\boldsymbol{\eta}_1)I_-(\boldsymbol{\eta}_2). \tag{2.73}$$

We may now write the linear detector model's response to the two-particle state as:

$$\begin{aligned}\mathcal{L}^{\phi}_{\eta_1,\eta_2} &= \mathcal{N}^2\mathcal{L}^{\phi}_{\boldsymbol{\eta}_1} + \mathcal{N}^2\mathcal{L}^{\phi}_{\boldsymbol{\eta}_2} + 2\lambda^2\mathcal{N}^2 C_{\boldsymbol{\eta}_1\boldsymbol{\eta}_2} I_-(\boldsymbol{\eta}_1) I_-(\boldsymbol{\eta}_2) \\ &= \frac{\mathcal{L}^{\phi}_{\boldsymbol{\eta}_1} + \mathcal{L}^{\phi}_{\boldsymbol{\eta}_2} + 2C_{\boldsymbol{\eta}_1\boldsymbol{\eta}_2}\sqrt{L^{\phi}_{\boldsymbol{\eta}_1}\mathcal{L}^{\phi}_{\boldsymbol{\eta}_2}}}{1 + C_{\boldsymbol{\eta}_1\boldsymbol{\eta}_2}}.\end{aligned} \tag{2.74}$$

where $L^{\phi}_{\boldsymbol{\eta}_j}$ is the detector excitation probability after interacting with a one-particle Fock state with a peak frequency $\boldsymbol{\eta}_j$. We were able to attain the final equality by recalling Eq. (2.48):

$$\mathcal{L} = \lambda^2 \mathcal{I}_-^2(\boldsymbol{k}_0).$$

By our choice of Gaussian spectrum Eq. (2.5), we may write

$$\begin{aligned}C_{\boldsymbol{\eta}_1\boldsymbol{\eta}_2} &= \int \mathrm{d}^n\boldsymbol{k}\, f_{\boldsymbol{\eta}_1}(\boldsymbol{k}) f_{\boldsymbol{\eta}_2}(\boldsymbol{k}) \\ &= \frac{1}{(\pi\Delta^2)^{n/2}} \int \mathrm{d}^n\boldsymbol{k}\, e^{-\frac{|\boldsymbol{k}-\boldsymbol{\eta}_1|^2}{2\Delta^2} - \frac{|\boldsymbol{k}-\boldsymbol{\eta}_2|^2}{2\Delta^2}} \\ &= e^{-\frac{|\boldsymbol{\eta}_2-\boldsymbol{\eta}_1|^2}{4\Delta^2}}.\end{aligned} \tag{2.75}$$

Plugging this into our expression for $\mathcal{L}^{\phi}_{\eta_1,\eta_2}$ reveals the result of this section:

$$\mathcal{L}^{\phi}_{\eta_1,\eta_2} = \frac{\mathcal{L}^{\phi}_{\boldsymbol{\eta}_1} + \mathcal{L}^{\phi}_{\boldsymbol{\eta}_2} + 2e^{-\frac{|\boldsymbol{\eta}_2-\boldsymbol{\eta}_1|^2}{4\Delta^2}}\sqrt{L^{\phi}_{\boldsymbol{\eta}_1}\mathcal{L}^{\phi}_{\boldsymbol{\eta}_2}}}{1 + e^{-\frac{|\boldsymbol{\eta}_2-\boldsymbol{\eta}_1|^2}{4\Delta^2}}}. \tag{2.76}$$

In the case where $\boldsymbol{\eta}_1 = \boldsymbol{\eta}_2$ (a double excitation of the same frequency),

$$\mathcal{L}^{\phi}_{\boldsymbol{\eta}_1,\boldsymbol{\eta}_1} = 2L^{\phi}_{\boldsymbol{\eta}_1}. \tag{2.77}$$

Figure 2.3 presents the transition probability of the detector for $|\boldsymbol{\eta}_2| = 2|\boldsymbol{\eta}_1|$, plotted against Ω. Three facts are readily apparent. First, the resonances occur near $\Omega = |\boldsymbol{\eta}_1|$ and $\Omega = |\boldsymbol{\eta}_2|$. As with the single particle, the peak aligns more closely with Ω as the wave-packet becomes more monochromatic ($\Delta \to 0$). Second, the peaks are not equal in magnitude. The higher frequency peak is smaller than the lower frequency one; it is less likely for a detector to respond to higher frequency excitation of the field. Third, the peaks are dimension-dependent: for $n = 1$, the peak increases in magnitude when the wave-packet is narrower. For $n = 2$ the peaks approach constant values. Finally, for

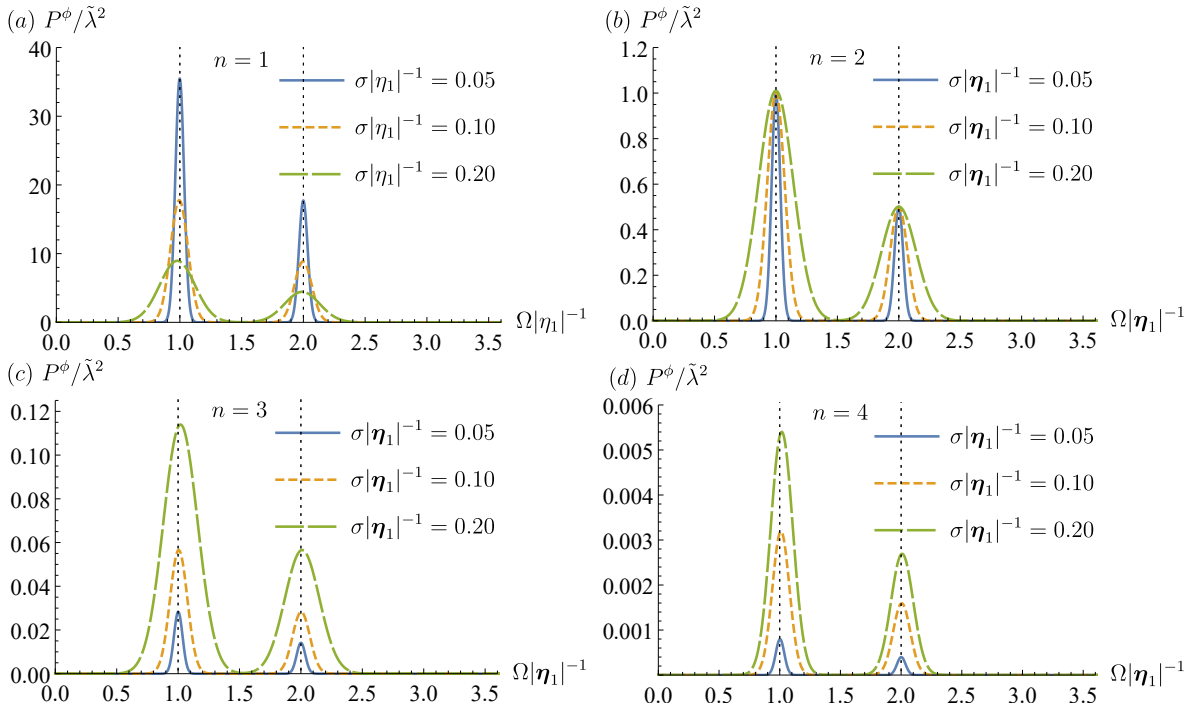

Figure 2.3: Plots of transition probability $P^\phi/\tilde{\lambda}^2$ as a function of frequency for linear coupling and two-particle state for $n \in \{1, 2, 3, 4\}$, where n is the number of spatial dimensions. We vary Ω as we search for resonant peaks while keeping $|\boldsymbol{k}_0|$ fixed. Here $\tilde{\lambda} = \lambda|\boldsymbol{k}_0|^{(n-3)/2}$ is the dimensionless coupling constant. The vertical lines denote the resonant frequencies corresponding to peak frequencies $\Omega = |\boldsymbol{\eta}_1|$ and $\Omega = |\boldsymbol{\eta}_2| = 2|\boldsymbol{\eta}_1|$. As in the one-particle case, in the monochromatic limit $\Delta \to 0$ the $n = 3$ the peak *diminishes* in amplitude, while for $n = 1$ the peak increases as $\Delta \to 0$.

$n \geq 3$, the transition probability near resonance *diminishes* with narrower spectra. The detector is more transparent to sharper wave-packets, similar to what happened with the one-particle case. These results stem directly from the fact that the two-particle model can be written in terms of the transition probability of the one-particle model, and thus the phenomenology is the same.

2.4.3 Quadratic detector model response to one-particle Fock state

In order to find the excitation probability in (as close as possible to a) closed form, we recall the two-point correlator of ϕ^2 for the one-particle Fock-like state, Eq. (50), and plug it into the general expression for UDW transition probability Eq. (1.63). The result separates into two summands,

$$\mathcal{L}^{\phi^2}_{\boldsymbol{k}_0} = \mathcal{L}^{\phi^2}_{\text{VAC}} + \mathcal{L}^{\phi^2}_{K}, \tag{2.78}$$

where

$$\mathcal{L}^{\phi^2}_{\text{VAC}} = 2\big(W^{\phi}_{\text{VAC}}(\mathsf{x},\mathsf{x}')\big)^2 \tag{2.79}$$

and the non-vacuum term, $L^{\phi^2}_K$, can be compactly written

$$\mathcal{L}^{\phi^2}_{K} = \frac{4\lambda^2}{(2\pi)^n}\int \frac{\mathrm{d}^n\boldsymbol{k}}{|\boldsymbol{k}|}\left(\Big(\mathcal{J}_+(\boldsymbol{k},\boldsymbol{k}_0,\tilde{F},\tilde{\chi})\Big)^2 + \Big(\mathcal{J}_-(\boldsymbol{k},\boldsymbol{k}_0,\tilde{F},\tilde{\chi})\Big)^2\right), \tag{2.80}$$

where

$$\mathcal{J}_+(\boldsymbol{k},\boldsymbol{k}_0,\tilde{F},\tilde{\chi}) = \int \frac{\mathrm{d}^n\boldsymbol{p}}{\sqrt{2(2\pi^n)|\boldsymbol{p}|}} f_{\boldsymbol{k}_0}(\boldsymbol{p})\tilde{F}[\boldsymbol{p}-\boldsymbol{k}]\tilde{\chi}[\Omega+|\boldsymbol{k}|\pm|\boldsymbol{p}|]. \tag{2.81}$$

Under the assumptions outlined at the beginning of this section, the quadratic vacuum contribution, $\mathcal{L}^{\phi^2}_{\text{VAC}} = 2\big(W^{\phi}_{\text{VAC}}(\mathsf{x},\mathsf{x}')\big)^2$, vanishes in the adiabatic limit. Furthermore, by the same logic that the counter-rotating term $\mathcal{I}_+$, was shown to vanish in previous sections, $\mathcal{J}_+$ also vanishes. Thus the entire excitation probability is given by

$$\mathcal{L}^{\phi^2}_{\boldsymbol{k}_0} = \frac{4\lambda^2}{(2\pi)^n}\int \frac{\mathrm{d}^n\boldsymbol{k}}{|\boldsymbol{k}|}\Big(\mathcal{J}_-(\boldsymbol{k},\boldsymbol{k}_0,\tilde{F},\tilde{\chi})\Big)^2. \tag{2.82}$$

In order to perform our calculations, let us make a closer comparison of the form of $\mathcal{J}_+$ to that of $\mathcal{I}_+$ Eq. (2.46). Notably, under our assumption of a point-like detector, the (integrated) expression for $\mathcal{I}_+$ can be transformed into $\mathcal{J}_+$ by taking $\Omega \to \boldsymbol{k}' - \Omega$:

$$\begin{aligned}\mathcal{L}^{\phi^2}_{\boldsymbol{k}_0} &= \frac{4}{2(2\pi)^n}\int \frac{\mathrm{d}^n\boldsymbol{k}'}{|\boldsymbol{k}'|}\mathcal{L}^{\phi,[\Omega\to\boldsymbol{k}'-\Omega]}_{\boldsymbol{k}_0} \\ &= \frac{4}{2(2\pi)^n}\frac{2\pi^{n/2}}{\Gamma\left(\frac{n}{2}\right)}\int \mathrm{d}|\boldsymbol{k}'|\,|\boldsymbol{k}'|^{n-1}\mathcal{L}^{\phi,[\Omega\to\boldsymbol{k}'-\Omega]}_{\boldsymbol{k}_0} \\ &= \frac{\lambda^2 e^{-\frac{|\boldsymbol{k}_0|^2}{\Delta^2}}\Delta^{n-4}}{\Gamma\left(\frac{n}{2}\right)2^{n-3}\pi^{n-2}|\boldsymbol{k}_0|^{n-2}}\int \mathrm{d}|\boldsymbol{k}'|\,|\boldsymbol{k}'|^{n-1}(\boldsymbol{k}'-\Omega)^{n-1}e^{-\frac{(\boldsymbol{k}'-\Omega)^2}{\Delta^2}}\left(I_{\frac{n-2}{2}}\left(\frac{|\boldsymbol{k}_0|(\boldsymbol{k}'-\Omega)}{\Delta^2}\right)\right)^2.\end{aligned} \tag{2.83}$$

Unfortunately, a suitable closed-form expression of this final integral was not found and therefore numerical techniques will be applied to produce plots.

Figure 2.4 illustrates the excitation probability for various dimensions. From these plots and Eq. (2.83), we can make two general observations. First, in all but $n = 1$ dimensions, the quadratically coupled detector becomes more transparent to the field quanta as the wave-packet becomes narrower. The second observation is that a resonant-like peak *only* occurs for $n = 1$ dimensions, in contrast to the linear coupling. In two or more spatial dimensions there is *no resonance phenomenon* for quadratic coupling when the field is a one-particle Fock state. Furthermore, the detector's response is maximized when the detector gap is *less than* the frequency of the field quanta. This result highlights that the behaviour of (1+1)-dimensional detector models are the exception rather than the rule.

2.4.4 Quadratic detector model response to two-particle Fock state

In this section we will derive the excitation probability for a detector quadratically coupled to a two-particle quasi-monochromatic state. We begin by recalling the two-point correlator

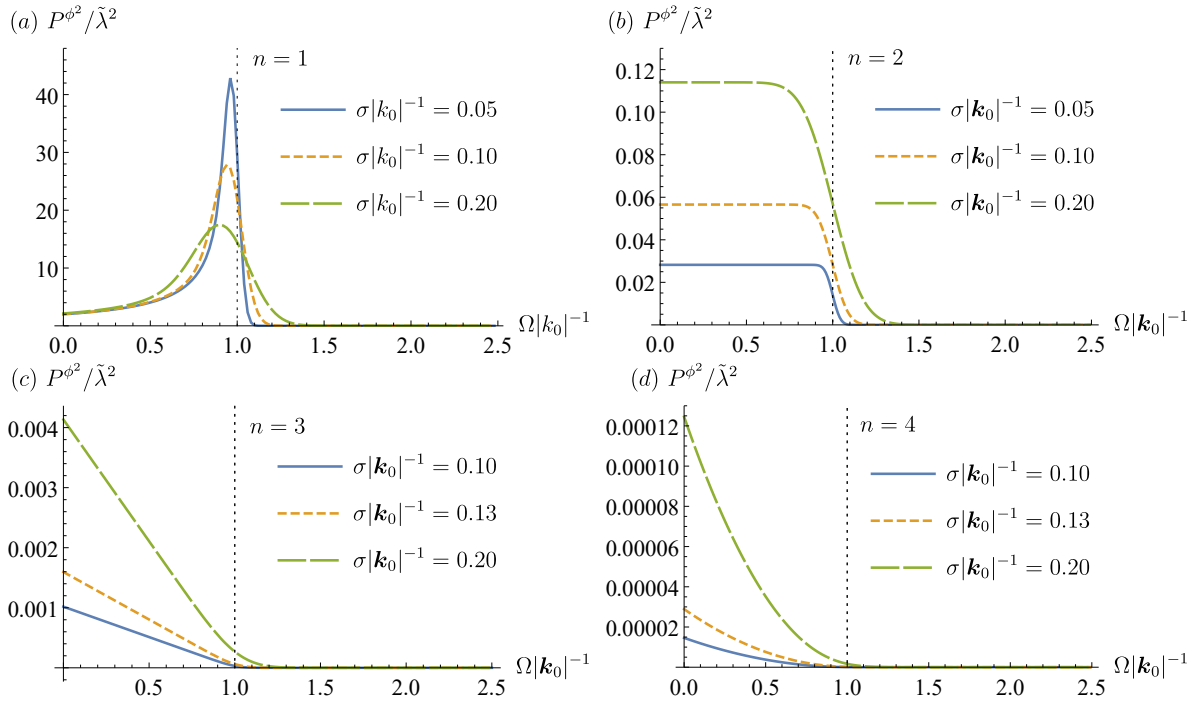

Figure 2.4: Plots of transition probability $\mathcal{L}^{\phi}/\tilde{\lambda}^2$ as a function of frequency for quadratic coupling and one-particle state in various spatial dimensions n, as the spectral bandwidth Δ. We vary Ω as we search for resonant peaks while keeping $|\boldsymbol{k}_0|$ fixed. Here $\tilde{\lambda} = \lambda|\boldsymbol{k}_0|^{(n-2)}$ is the non-dimensionalized coupling constant. The vertical lines denote the resonant frequency $|\boldsymbol{k}_0| = \Omega$. Images generated by Erickson Tjoa.

Eq. (57):

$$W^{\phi^2}_{\eta_1,\eta_2}(\mathsf{x},\mathsf{x}') = 2\left(W^{\phi}_{|0\rangle}(\mathsf{x},\mathsf{x}')\right)^2 + \mathcal{N}^2\Big[4W^{\phi}_{|0\rangle}(\mathsf{x},\mathsf{x}')(K_{\boldsymbol{\eta}_1}(\mathsf{x})K^*_{\boldsymbol{\eta}_1}(\mathsf{x}') + K_{\boldsymbol{\eta}_2}(\mathsf{x})K^*_{\boldsymbol{\eta}_2}(\mathsf{x}') + c.c.)$$
$$+ 4W^{\phi}_{|0\rangle}(\mathsf{x},\mathsf{x}')C_{\boldsymbol{\eta}_1\boldsymbol{\eta}_2}\Big(K_{\boldsymbol{\eta}_1}(\mathsf{x})K^*_{\boldsymbol{\eta}_2}(\mathsf{x}') + K_{\boldsymbol{\eta}_2}(\mathsf{x})K^*_{\boldsymbol{\eta}_1}(\mathsf{x}') + cc\Big)$$
$$+ 4\Big(K^*_{\boldsymbol{\eta}_1}(\mathsf{x})K^*_{\boldsymbol{\eta}_2}(\mathsf{x})K_{\boldsymbol{\eta}_1}(\mathsf{x}')K_{\boldsymbol{\eta}_2}(\mathsf{x}') + K_{\boldsymbol{\eta}_1}(\mathsf{x})K^*_{\boldsymbol{\eta}_2}(\mathsf{x})K^*_{\boldsymbol{\eta}_1}(\mathsf{x}')K_{\boldsymbol{\eta}_2}(\mathsf{x}') + c.c.\Big)$$
$$+ 4|K^*_{\boldsymbol{\eta}_2}(\mathsf{x})|^2|K^*_{\boldsymbol{\eta}_1}(\mathsf{x}')|^2 + 4|K^*_{\boldsymbol{\eta}_1}(\mathsf{x})|^2|K^*_{\boldsymbol{\eta}_2}(\mathsf{x}')|^2\Big],$$

and plugging it into the general expression for UDW transition probability Eq. (1.63). We will condense the resultant expression by writing

$$\mathcal{L}^{\phi^2} = \mathcal{L}^{\phi^2}_{\rm VAC} + \mathcal{N}^2\mathcal{L}^{\phi^2,K^2}_{\boldsymbol{\eta}_1\boldsymbol{\eta}_1} + \mathcal{N}^2\mathcal{L}^{\phi^2,K^2}_{\boldsymbol{\eta}_2\boldsymbol{\eta}_2} + 2\mathcal{N}^2C_{\boldsymbol{\eta}_1\boldsymbol{\eta}_2}\mathcal{L}^{\phi^2,K^2}_{\boldsymbol{\eta}_1\boldsymbol{\eta}_2} + \mathcal{N}^2\mathcal{L}^{\phi^2,K^4}_{\boldsymbol{\eta}_1\boldsymbol{\eta}_2}\,, \tag{2.84}$$

Each of the terms in the above expression is defined by

$$\mathcal{L}^{\phi^2,K^2}_{\boldsymbol{\eta}_i\boldsymbol{\eta}_i} = 4\lambda^2\int\frac{\mathrm{d}^n\boldsymbol{k}}{2(2\pi)^n|\boldsymbol{k}|}\Big[\mathcal{Q}_+(\boldsymbol{k};\boldsymbol{\eta}_i,\tilde{F},\tilde{\chi})^2 + \mathcal{Q}_-(\boldsymbol{k};\boldsymbol{\eta}_i,\tilde{F},\tilde{\chi})^2\Big]\,, \tag{2.85}$$

$$\mathcal{L}^{\phi^2,K^2}_{\boldsymbol{\eta}_1\boldsymbol{\eta}_2} = 4\lambda^2\int\frac{\mathrm{d}^n\boldsymbol{k}}{2(2\pi)^n|\boldsymbol{k}|}\Big[\mathcal{Q}_+(\boldsymbol{k};\Delta,\boldsymbol{\eta}_1,\tilde{F},\tilde{\chi})\mathcal{Q}_+(\boldsymbol{k};\Delta,\boldsymbol{\eta}_2,\tilde{F},\tilde{\chi})$$
$$+ \mathcal{Q}_-(\boldsymbol{k};\boldsymbol{\eta}_1,\tilde{F},\tilde{\chi})\mathcal{Q}_-(\boldsymbol{k};\Delta,\boldsymbol{\eta}_2,\tilde{F},\tilde{\chi})\Big]\,, \tag{2.86}$$

$$\mathcal{L}^{\phi^2,K^4}_{\boldsymbol{\eta}_1\boldsymbol{\eta}_2} = 4\lambda^2\Big[\mathcal{R}^2_+(\boldsymbol{\eta}_1,\boldsymbol{\eta}_2,\tilde{F},\tilde{\chi}) + \mathcal{R}^2_-(\boldsymbol{\eta}_1,\boldsymbol{\eta}_2,\tilde{F},\tilde{\chi}) + \mathcal{S}^2_-(\boldsymbol{\eta}_1,\boldsymbol{\eta}_2,\tilde{F},\tilde{\chi})$$
$$+ \mathcal{S}^2_-(\boldsymbol{\eta}_2,\boldsymbol{\eta}_1,\tilde{F},\tilde{\chi}) + 2\mathcal{S}_-(\boldsymbol{\eta}_1,\boldsymbol{\eta}_1,\tilde{F},\tilde{\chi})\mathcal{S}_-(\boldsymbol{\eta}_2,\boldsymbol{\eta}_2,\tilde{F},\tilde{\chi})\Big]\,. \tag{2.87}$$

with

$$\mathcal{Q}_\pm(\boldsymbol{k};\Delta,\boldsymbol{\eta}_j,\tilde{F},\tilde{\chi}) := \int\frac{\mathrm{d}^n\boldsymbol{k'}}{\sqrt{2(2\pi)^n|\boldsymbol{k'}|}}\tilde{F}[\boldsymbol{k}\pm\boldsymbol{k}']f_{\boldsymbol{\eta}_j,\Delta}(\boldsymbol{k'})\tilde{\chi}(\Omega+|\boldsymbol{k}|\pm|\boldsymbol{k}'|)\,, \tag{2.88}$$

$$\mathcal{R}_\pm(\Delta,\boldsymbol{\eta}_i,\boldsymbol{\eta}_j,\tilde{F},\tilde{\chi}) := \int\frac{\mathrm{d}^n\boldsymbol{k}\,\mathrm{d}^n\boldsymbol{k}'}{2(2\pi)^n\sqrt{|\boldsymbol{k}||\boldsymbol{k}'|}}\tilde{F}[\boldsymbol{k}+\boldsymbol{k}']f_{\boldsymbol{\eta}_i,\Delta}(\boldsymbol{k})f_{\boldsymbol{\eta}_j,\Delta}(\boldsymbol{k}')\tilde{\chi}(\Omega\pm|\boldsymbol{k}|\pm|\boldsymbol{k}'|)\,, \tag{2.89}$$

$$\mathcal{S}(\Delta,\boldsymbol{\eta}_i,\boldsymbol{\eta}_j,\tilde{F},\tilde{\chi}) := \int\frac{\mathrm{d}^n\boldsymbol{k}\,\mathrm{d}^n\boldsymbol{k}'}{2(2\pi)^n\sqrt{|\boldsymbol{k}||\boldsymbol{k}'|}}\tilde{F}[\boldsymbol{k}-\boldsymbol{k}']f_{\boldsymbol{\eta}_i,\Delta}(\boldsymbol{k})f_{\boldsymbol{\eta}_j,\Delta}(\boldsymbol{k}')\tilde{\chi}(\Omega+|\boldsymbol{k}|-|\boldsymbol{k}'|)\,. \tag{2.90}$$

We will now choose a point-like detector $\tilde{F}=1$, adiabatic switching $\tilde{\chi}=2\pi\delta$, Gaussian spectra Eq. (2.5), and the ground state as the initial detector state $\Omega>0$. Then, any term vanishes if the argument of $\tilde{\chi}$ cannot attain zero. The following simplication occurs:

$$\mathcal{L}^{\phi^2,K^2}_{\boldsymbol{\eta}_i\boldsymbol{\eta}_i} = 4\lambda^2\int\frac{\mathrm{d}^n\boldsymbol{k}}{2(2\pi)^n|\boldsymbol{k}|}\mathcal{Q}_-(\boldsymbol{k};\boldsymbol{\eta}_i,\tilde{F},\tilde{\chi})^2, \tag{2.91}$$

$$\mathcal{L}^{\phi^2,K^2}_{\boldsymbol{\eta}_1\boldsymbol{\eta}_2} = 4\lambda^2\int\frac{\mathrm{d}^n\boldsymbol{k}}{2(2\pi)^n|\boldsymbol{k}|}\mathcal{Q}_-(\boldsymbol{k};\boldsymbol{\eta}_1,\tilde{F},\tilde{\chi})\mathcal{Q}_-(\boldsymbol{k};\Delta,\boldsymbol{\eta}_2,\tilde{F},\tilde{\chi}), \tag{2.92}$$

$$\begin{aligned}\mathcal{L}^{\phi^2,K^4}_{\boldsymbol{\eta}_1\boldsymbol{\eta}_2} = 4\lambda^2\Big[&\mathcal{R}^2_-(\boldsymbol{\eta}_1,\boldsymbol{\eta}_2,\tilde{F},\tilde{\chi})+\mathcal{S}^2_-(\boldsymbol{\eta}_1,\boldsymbol{\eta}_2,\tilde{F},\tilde{\chi})\\&+\mathcal{S}^2_-(\boldsymbol{\eta}_2,\boldsymbol{\eta}_1,\tilde{F},\tilde{\chi})+2\mathcal{S}_-(\boldsymbol{\eta}_1,\boldsymbol{\eta}_1,\tilde{F},\tilde{\chi})\mathcal{S}_-(\boldsymbol{\eta}_2,\boldsymbol{\eta}_2,\tilde{F},\tilde{\chi})\Big].\end{aligned} \tag{2.93}$$

Additionally, the expressions for $\mathcal{Q}$, $\mathcal{R}$, and $\mathcal{S}$ can be refined. We have

$$\begin{aligned}\mathcal{Q}_-(\boldsymbol{k};\Delta,\boldsymbol{\eta}_j) &= \int\frac{\mathrm{d}^n\boldsymbol{k'}}{\sqrt{2(2\pi)^n|\boldsymbol{k'}|}}f_{\boldsymbol{\eta}_j,\Delta}(\boldsymbol{k'})\delta(\Omega+|\boldsymbol{k}|-|\boldsymbol{k}'|)\\&=\mathcal{I}_-^{(\Omega\to\Omega+|\boldsymbol{k}|)}(\Delta,\boldsymbol{\eta}_j)\\&=\frac{\sqrt{2}\Delta^{\frac{n}{2}-2}(|\boldsymbol{k}|+\Omega)^{\frac{n-1}{2}}}{\pi^{\frac{n}{4}-1}|\boldsymbol{\eta}_j|^{\frac{n}{2}-1}}e^{-\frac{|\boldsymbol{\eta}_j|^2+(|\boldsymbol{k}|+\Omega)^2}{2\Delta^2}}I_{\frac{n-2}{2}}\left(\frac{|\boldsymbol{\eta}_j|(|\boldsymbol{k}|+\Omega)}{\Delta^2}\right),\end{aligned} \tag{2.94}$$

where $\mathcal{I}_\pm$ is defined as it is used in Eq. (2.60). The next term simplifies as

$$\begin{aligned}\mathcal{R}_-(\boldsymbol{\eta}_i,\boldsymbol{\eta}_j) &= \int\frac{\mathrm{d}^n\boldsymbol{k}\,\mathrm{d}^n\boldsymbol{k}'}{2(2\pi)^n\sqrt{|\boldsymbol{k}||\boldsymbol{k}'|}}f_{\boldsymbol{\eta}_i,\Delta}(\boldsymbol{k})f_{\boldsymbol{\eta}_j,\Delta}(\boldsymbol{k}')\delta(\Omega-|\boldsymbol{k}|-|\boldsymbol{k}'|)\\&=\int_0^\Omega\frac{\mathrm{d}^n\boldsymbol{k}}{\sqrt{2(2\pi)^n|\boldsymbol{k}|}}f_{\boldsymbol{\eta}_j,\Delta}(\boldsymbol{k})\,\mathcal{I}_-^{(\Omega\to\Omega-|\boldsymbol{k}|)}(\Delta,\boldsymbol{\eta}_i)\\&=\frac{\pi^{\frac{2-n}{2}}\Delta^{n-4}}{(|\boldsymbol{\eta}_1||\boldsymbol{\eta}_2|)^{\frac{n-2}{2}}}\int_0^\Omega\mathrm{d}|\boldsymbol{k}|\,\frac{e^{-\frac{|\boldsymbol{k}|^2+(\Omega-|\boldsymbol{k}|)^2}{2\Delta^2}}}{(|\boldsymbol{k}|(\Omega-|\boldsymbol{k}|))^{\frac{1}{2}-n}}I_{\frac{n-2}{2}}\left(\frac{|\boldsymbol{k}||\boldsymbol{\eta}_1|}{\Delta^2}\right)I_{\frac{n-2}{2}}\left(\frac{|\boldsymbol{\eta}_2|(\Omega-|\boldsymbol{k}|)}{\Delta^2}\right),\end{aligned} \tag{2.95}$$

The final term is:

$$\begin{aligned}\mathcal{S}(\boldsymbol{\eta}_i,\boldsymbol{\eta}_j) &= \int\frac{\mathrm{d}^n\boldsymbol{k}\,\mathrm{d}^n\boldsymbol{k}'}{2(2\pi)^n\sqrt{|\boldsymbol{k}||\boldsymbol{k}'|}}f_{\boldsymbol{\eta}_i,\Delta}(\boldsymbol{k})f_{\boldsymbol{\eta}_j,\Delta}(\boldsymbol{k}')\delta(\Omega+|\boldsymbol{k}|-|\boldsymbol{k}'|)\\&=\int\frac{\mathrm{d}^n\boldsymbol{k}}{\sqrt{2(2\pi)^n|\boldsymbol{k}|}}f_{\boldsymbol{\eta}_j,\Delta}(\boldsymbol{k})\,\mathcal{I}_-^{(\Omega\to|\boldsymbol{k}|+\Omega)}(\Delta,\boldsymbol{\eta}_i)\\&=\frac{\pi^{\frac{2-n}{2}}\Delta^{n-4}}{(|\boldsymbol{\eta}_1||\boldsymbol{\eta}_2|)^{\frac{n-2}{2}}}\int_0^\infty\mathrm{d}|\boldsymbol{k}|\,\frac{e^{-\frac{|\boldsymbol{k}|^2+(\Omega+|\boldsymbol{k}|)^2}{2\Delta^2}}}{(|\boldsymbol{k}|(\Omega+|\boldsymbol{k}|))^{\frac{1}{2}-n}}I_{\frac{n-2}{2}}\left(\frac{|\boldsymbol{k}||\boldsymbol{\eta}_1|}{\Delta^2}\right)I_{\frac{n-2}{2}}\left(\frac{|\boldsymbol{\eta}_2|(|\boldsymbol{k}|+\Omega)}{\Delta^2}\right).\end{aligned} \tag{2.96}$$

These expressions are valid for all $n \geq 1$, with the assumption that for $n = 1$ all the energy scales have to be larger than the IR cutoff.

We will re-express the full transition probability as $\mathcal{L}^{\phi^2} = \mathcal{L}^{\phi^2}_{\mathcal{Q}} + \mathcal{L}^{\phi^2}_{\mathcal{R}} + \mathcal{L}^{\phi^2}_{\mathcal{S}}$, where

$$\begin{aligned}
\mathcal{L}^{\phi^2}_{\mathcal{Q}} &= 4\lambda^2\mathcal{N}^2 \int \frac{\mathrm{d}^n\boldsymbol{k}}{2(2\pi)^n|\boldsymbol{k}|}\Big[\mathcal{Q}_-(\boldsymbol{k};\boldsymbol{\eta}_1)^2 + \mathcal{Q}_-(\boldsymbol{k};\boldsymbol{\eta}_2)^2 + 2C_{\boldsymbol{\eta}_1\boldsymbol{\eta}_2}\mathcal{Q}_-(\boldsymbol{k};\boldsymbol{\eta}_1)\mathcal{Q}_-(\boldsymbol{k};\boldsymbol{\eta}_2)\Big] \\
&= 4\lambda^2 \int \frac{\mathrm{d}^n\boldsymbol{k}}{2(2\pi)^n|\boldsymbol{k}|}\mathcal{L}^{\phi,\Omega\to\Omega+\boldsymbol{k}}_{\boldsymbol{\eta}_1,\boldsymbol{\eta}_2}\,, \qquad (2.97) \\
\mathcal{L}^{\phi^2}_{\mathcal{R}} &= 4\lambda^2\mathcal{N}^2\mathcal{R}^2_-(\Delta,\boldsymbol{\eta}_1,\boldsymbol{\eta}_2) \\
&= 4\mathcal{N}^2\left[\int_0^\Omega \frac{\mathrm{d}^n\boldsymbol{k}\, f_{\boldsymbol{\eta}_1,\Delta}(\boldsymbol{k})}{\sqrt{2(2\pi)^n|\boldsymbol{k}|}}\mathcal{L}^{\phi,\Omega\to\Omega-|\boldsymbol{k}|}_{\boldsymbol{\eta}_2}\right]^2, \qquad (2.98) \\
\mathcal{L}^{\phi^2}_{\mathcal{S}} &= 4\lambda^2\mathcal{N}^2\Big[\mathcal{S}^2_-(\Delta,\boldsymbol{\eta}_1,\boldsymbol{\eta}_2) + \mathcal{S}^2_-(\Delta,\boldsymbol{\eta}_2,\boldsymbol{\eta}_1) + 2\mathcal{S}_-(\Delta,\boldsymbol{\eta}_1,\boldsymbol{\eta}_1)\mathcal{S}_-(\Delta,\boldsymbol{\eta}_2,\boldsymbol{\eta}_2)\Big] \\
&= 4\mathcal{N}^2\Bigg(\left[\int \frac{\mathrm{d}^n\boldsymbol{k}\, f_{\boldsymbol{\eta}_1,\Delta}(\boldsymbol{k})}{\sqrt{2(2\pi)^n|\boldsymbol{k}|}}\mathcal{L}^{\phi,\Omega\to|\boldsymbol{k}|+\Omega}_{\boldsymbol{\eta}_2}\right]^2 + \left[\int \frac{\mathrm{d}^n\boldsymbol{k}\, f_{\boldsymbol{\eta}_2,\Delta}(\boldsymbol{k})}{\sqrt{2(2\pi)^n|\boldsymbol{k}|}}\mathcal{L}^{\phi,\Omega\to|\boldsymbol{k}|+\Omega}_{\boldsymbol{\eta}_1}\right]^2 \\
&\quad + 2\left[\int \frac{\mathrm{d}^n\boldsymbol{k}\, f_{\boldsymbol{\eta}_1,\Delta}(\boldsymbol{k})}{\sqrt{2(2\pi)^n|\boldsymbol{k}|}}\mathcal{L}^{\phi,\Omega\to|\boldsymbol{k}|+\Omega}_{\boldsymbol{\eta}_1}\right]\left[\int \frac{\mathrm{d}^n\boldsymbol{k}\, f_{\boldsymbol{\eta}_2,\Delta}(\boldsymbol{k})}{\sqrt{2(2\pi)^n|\boldsymbol{k}|}}\mathcal{L}^{\phi,\Omega\to|\boldsymbol{k}|+\Omega}_{\boldsymbol{\eta}_2}\right]\Bigg). \qquad (2.99)
\end{aligned}$$

We have noted how the two-particle excitation probability is related to previous excitation probabilities where possible. Recall, for the single particle state, the quadratic excitation probability was the integral of the linear excitation probability as described in Eq. (2.83). The term $\mathcal{L}^{\phi^2}_{\mathcal{Q}}$ is related to the linear, two-particle excitation probability in the same way. However, there are additional terms $\mathcal{L}^{\phi^2}_{\mathcal{R}}$ and $\mathcal{L}^{\phi^2}_{\mathcal{S}}$. Therefore the *total* excitation probability does not have this 'simple' relation. Instead, two additional terms incorporate a spectral weighting to the integrals of the one-particle, linear transition probabilities. We will focus our analysis on these three different terms, plotting them separately and discussing their relative weight. Let us first look at three spatial dimensions, shown in Figure 2.5. In this case, there are three interesting observations we can make from Figure 2.5.

First, the dominant contribution comes from the "non-resonant" piece (Eq. (2.97)), which does *not* peak around resonance–it exhibits qualitatively similar behaviour to the quadratic coupling to the one-particle state. Indeed, from plot(a) in Figure 2.5 we see that the peak frequencies of the two-particle Fock wave-packet separate three distinct regimes where the slope of this dominant contribution changes. This is analogous to the two regimes delineated by the quanta frequency in the case of one particle.

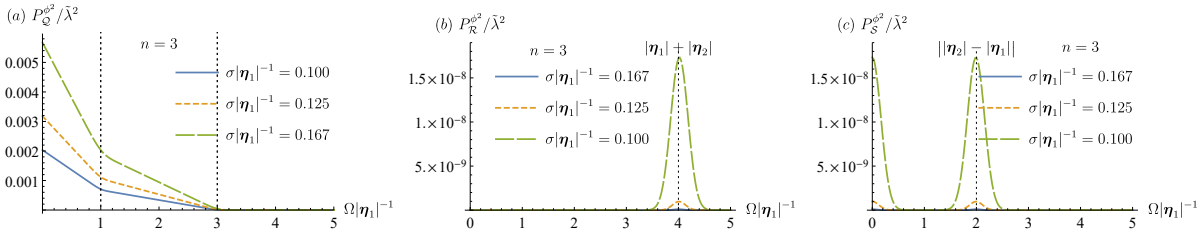

Figure 2.5: Various components of transition probability $\mathcal{L}^{\phi^2}$ for detector interacting with two-particle Fock state in (3+1) dimensions. Here we fix $|\boldsymbol{\eta}_2| = 3|\boldsymbol{\eta}_1|$. We vary Ω as we search for resonant peaks. (a) The dominant part exhibits no resonant peaks. (b) sum-frequency generation (SFG). (c) difference-frequency generation (DFG). Images generated by Erickson Tjoa.

Second, from plot (b) in Figure 2.5, it can be see that Eq. (2.98) contributes to a resonant peak at the *sum* of the dominant frequencies of the two-particle Fock wavepackets. This nonlinear optical effect corresponds to *sum-frequency generation* (SFG), which is known in the quantum optics literature [81].

Finally, in plot (c) of Figure 2.5, the contribution from Eq. (2.99) accounts for two maxima. One peak is not associated to resonance and occurs near zero gap. Within Eq. (2.99), this contribution originates from the final same-frequency term:

$$\mathcal{L}^{\phi^2}_{\mathcal{S},\text{ZERO}} = 4\mathcal{N}^2\left[\int \frac{\mathrm{d}^n\boldsymbol{k}\, f_{\boldsymbol{\eta}_1,\Delta}(\boldsymbol{k})}{\sqrt{2(2\pi)^n|\boldsymbol{k}|}}\mathcal{L}^{\phi,\Omega\to|\boldsymbol{k}|+\Omega}_{\boldsymbol{\eta}_1}\right]\left[\int \frac{\mathrm{d}^n\boldsymbol{k}\, f_{\boldsymbol{\eta}_2,\Delta}(\boldsymbol{k})}{\sqrt{2(2\pi)^n|\boldsymbol{k}|}}\mathcal{L}^{\phi,\Omega\to|\boldsymbol{k}|+\Omega}_{\boldsymbol{\eta}_2}\right]. \tag{2.100}$$

Meanwhile, the second peak corresponds to a resonant peak at the *difference* of the two peak frequencies, stemming from

$$\mathcal{L}^{\phi^2}_{\mathcal{S},\text{DIFF}} = 4\mathcal{N}^2\left(\left[\int \frac{\mathrm{d}^n\boldsymbol{k}\, f_{\boldsymbol{\eta}_1,\Delta}(\boldsymbol{k})}{\sqrt{2(2\pi)^n|\boldsymbol{k}|}}\mathcal{L}^{\phi,\Omega\to|\boldsymbol{k}|+\Omega}_{\boldsymbol{\eta}_2}\right]^2 + \left[\int \frac{\mathrm{d}^n\boldsymbol{k}\, f_{\boldsymbol{\eta}_2,\Delta}(\boldsymbol{k})}{\sqrt{2(2\pi)^n|\boldsymbol{k}|}}\mathcal{L}^{\phi,\Omega\to|\boldsymbol{k}|+\Omega}_{\boldsymbol{\eta}_1}\right]^2\right). \tag{2.101}$$

This is a distinct nonlinear optical phenomena that corresponds to *difference-frequency generation* (DFG) in the quantum optics literature [81]. It is a testament to the relativistic UDW model that it reproduces SFG and DFG in a unified manner.

In Figure 2.6 we consider consider different number of spatial dimensions. Note, the qualitative behaviour for $n = 4$ is similar to $n \geq 5$, so the visual analysis stops at $n = 4$. Some aspects remain as they were in 3 dimensions. $\mathcal{L}^{\phi^2}_{\mathcal{R}}$ is associated with SFG and $\mathcal{L}^{\phi^2}_{\mathcal{S}}$

is associated with DFG. Contrary to the three other cases studied in this chapter, the $\mathcal{L}^{\phi^2}_{\mathcal{R}}$ and $\mathcal{L}^{\phi^2}_{\mathcal{S}}$ terms in the $n = 1$ case do *not* differ from $n > 1$ cases in the follwoing way: the peak probability does not decrease in magnitude as $\Delta \to 0$, and thus *all* dimensions exhibit this same behaviour. Finally, another similarity among all dimensions is that both $\mathcal{L}^{\phi^2}_{\mathcal{R}}$ and $\mathcal{L}^{\phi^2}_{\mathcal{S}}$ are dominated by $\mathcal{L}^{\phi^2}_{\mathcal{Q}}$.

The differences between different dimensions studied are primarily contained in $\mathcal{L}^{\phi^2}_{\mathcal{Q}}$. These differences are analogous to those found with two-particle detection with the linear model, in line with our previous note about their similar forms. For example, when $n \geq 2$, there is no resonant peak at the Fock wave-packet peak frequencies $\omega_1 = |\boldsymbol{\eta}_1|$ and $\omega_2 = |\boldsymbol{\eta}_2|$. Only in $n = 1$ do the detectors have any resonance aligned with the peak frequencies of the wave-packet. In other dimensions, the peak frequencies instead delineate different regimes. Another similarity to previous results is that only in $n = 1$ dimensions does the maximum value of $\mathcal{L}^{\phi^2}_{\mathcal{Q}}$ increase as $\Delta \to 0$, while in $n \geq 2$ dimensions, the dichromatic limit is always associated with a reduction in probability.

While the qualitative behaviour of SFG and DFG in different dimensions is similar, there is one clear difference: the rate at which the magnitude of the peaks diminishes in the dichromatic limit differs for different dimensions. For larger n, the SFG and DFG peaks decrease faster.

2.5 What We Learned from Fock States

We have directed our analysis on understanding the differences between linear and quadratic couplings between light and matter, which we have modelled by a scalar field and a particle detector. Furthermore, we have concentrated on interpreting the phenomenology of detector excitations in both scenarios.

More specifically, we have studied the linearly coupled Unruh-DeWitt detector and its resonance (or lack thereof) with one-particle and two-particle Fock states. Moreover, we investigated the the quadratically coupled model and its similarities to and differences from the linear model. The effects of spacetime dimension and the width of the Fock wavepacket (bandwidth) on the detector's responses to the field's excitations were considered. The converse scenario was included in our analysis, where an excited detector transfers energy into the vacuum state of the field. We noted how the linear and quadratic models differ in how they deposit energy across different modes.

There are three conclusions we can draw. First, in free space, the detector sometimes becomes increasingly transparent to a Fock wavepacket in the monochromatic limit. More

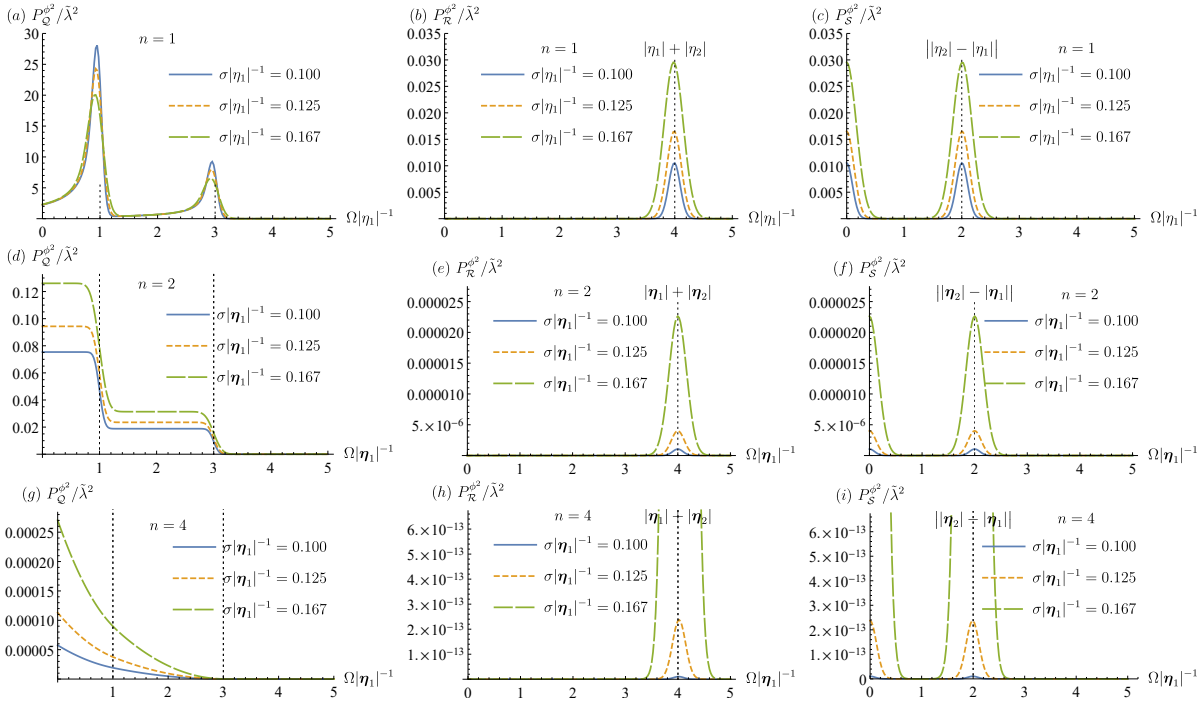

Figure 2.6: Various components of transition probability $\mathcal{L}^{\phi^2}$ for detector interacting with two-particle Fock state in various dimensions. The case for $n = 4$ is qualitatively representative of the higher-dimensional counterparts ($n \geq 5$). Here we set $|\boldsymbol{\eta}_2| = 3|\boldsymbol{\eta}_1|$ for concreteness and we vary Ω in order to search for resonant-like phenomena. In all plots, we see that $\mathcal{L}_{\mathcal{Q}}^{\phi^2}$ exhibits no resonant peaks for $n \geq 2$, $\mathcal{L}_{\mathcal{R}}^{\phi^2}$ contains sum-frequency generation (SFG) and $\mathcal{L}_{\mathcal{S}}^{\phi^2}$ contains difference-frequency generation (DFG). Note the larger spectral width plots (h) and (i) are still peaked. Images generated by Erickson Tjoa.

specifically, for a linearly coupled detector, increased transparency occurs for $(n+1)$-dimensional spacetimes with $n \geq 3$. For a quadratically coupled detector, this happens for $n \geq 2$. Only in the $(1+1)$-dimensional setting do we have larger transition probability for smaller spectral width. This is in contrast to the standard notion of resonance, which stems from the cavity scenario. In our cavity analysis, we found the excitation probability near resonance is amplified for decreased spectral width, regardless of the number of spacial dimensions.

Our second result concerns known non-linear optical phenomena: sum-frequency generation (SFG) and difference-frequency generation (DFG). These phenomena naturally arise within the relativistic particle-detector model formalism that we employed. Thus we conclude that the quadratically coupled UDW model can capture features of non-linear interactions, and further study is required to determine how well this model captures non-linear effects. One wonders if this opens the door for simulating non-linear Higgs dynamics in optical analog systems.

The final lesson from this work is that linearly coupled detectors deposit energy into the field differently than quadratically coupled detectors. The quadratic model prefers to deposit energy in field modes with half the energy of the detector's energy gap. Meanwhile, the linear model deposits energy at resonance.

In summary, for Fock states interacting with matter, there are clear distinctions between free space and cavity, even a large cavity. This is relevant by virtue of results from cavities often being extrapolated to free space. Our results highlight the discrepancy between coupling the detector and then taking the large cavity limit and coupling detectors to a field in free space. This disparity is tied to the discrete vs continuous spectrum, which affects the definition of physically meaningful Fock states.

Let us conclude with a brief reminder that the work that this chapter is based on is the first study of non-linear optical phenomena in the context of relativistic particle detector models. The form of the interaction studied is based on the form of the interaction in non-linear optics. Indeed, we have shown that the connections between the interaction Hamiltonians is enough so that the non-linear UDW detector model is able to capture SFG and DFG effects from non-linear optics.

Chapter 3

Fundamental Decoherence in Optical Cavities

In optics, the quality of a cavity indicates how much light is reflected back into the cavity instead of being transmitted or absorbed by the cavity walls. A higher quality factor (Q factor) is desirable in quantum optics experiments because quantum states of light will maintain coherence for longer times when they are isolated from the external electromagnetic field. However, the electromagnetic field is not the only field permeating spacetime. In fact, the electron field couples to the electromagnetic field via the QED Hamiltonian

$$\hat{H} = -e \int \mathrm{d}^3\boldsymbol{x} \; : \overline{\hat{\Psi}}(\boldsymbol{x}, t)\gamma^\mu \boldsymbol{A}_\mu(\boldsymbol{x}, t)\hat{\Psi}(\boldsymbol{x}, t) : . \tag{3.1}$$

where $\hat{\Psi}$ is defined in 1.4.4 and $\boldsymbol{A}$ is the covariant four-potential of the electromagnetic field.

Even in the absence of field quanta and with a perfect Q-factor, it is theoretically possible that the cavity-confined field can lose information to the electron vacuum. It is not yet known how significant an effect this would have on the coherence of the state of the field in a cavity. This question will be addressed in this chapter.

We will not employ the full QED interaction, but instead use a UDW-like model, where the Dirac field is replaced by a massive complex field (see subsection 1.4.3) in the Minkowski vacuum. The electromagnetic field constitutes the detector and will be modeled by a single mode of a massless, real, scalar field prepared in one of several common states in quantum optics. Furthermore, we will employ a switching and smearing function, as is common in the UDW literature.

3.1 Single Mode Oscillator UDW Model

In this section, we will briefly describe a UDW-like model where the monopole operator $\hat{m}(t)$ associated with a 2-level system is replaced with a single-mode oscillator (analogous so a single mode of the electromagnetic field), a system with countably infinite degrees of freedom. A similar model was studied in [22], wherein the detector interacted with a scalar field confined to a cavity. We will not yet assume a particular form for the field.

We begin with the interaction Hamiltonian for a UDW-like detector:

$$\hat{H}_{int} = \lambda\chi(t)\hat{Q}(t)\int \mathrm{d}^n\boldsymbol{x}\, F(\boldsymbol{x})\, f(\hat{\phi}(\boldsymbol{x},t))., \tag{3.2}$$

where λ is the coupling strength, χ is the switching function, F is the smearing function, and f is a function of the operator of the field with which the detector interacts. Furthermore, we will make a change from the initial general UDW-like interaction Hamiltonian Eq. (1.2) by not taking the detector to interact via the monopole operator $\hat{m}$. Instead, this role will be played by $\hat{Q}$, described by

$$\hat{Q} = \hat{a}e^{-\mathrm{i}\Omega t} + \hat{a}^\dagger e^{\mathrm{i}\Omega t} \tag{3.3}$$

where $[\hat{a}, \hat{a}^\dagger] = 1$. Note that we are working in the interaction picture.

Following the same protocol outlined in section 1.5, the time evolved state can be determined to arbitrary order in perturbation theory using the Dyson expansion. To second order, the state after an interaction time T is

$$\hat{\rho} = \hat{\rho}^{(0)} + \hat{U}_1\hat{\rho}^{(0)} + \hat{\rho}^{(0)}\hat{U}_1 + \hat{U}_1\hat{\rho}^{(0)}\hat{U}_1 + \hat{U}_2\hat{\rho}^{(0)} + \hat{\rho}^{(0)}\hat{U}_2 + \mathcal{O}(e^3) \tag{3.4}$$

where the operators $U^{(i)}$ are defined as in Eq. (1.50). More specifically, they take the form

$$\hat{U}_1 = \mathrm{i}e\int_{-\infty}^{\infty}\mathrm{d}t\,\chi\left(\tfrac{t}{T}\right)\int \mathrm{d}^3\boldsymbol{x}\, F(\boldsymbol{x})\,\hat{Q}(t) : \hat{\phi}(t,\boldsymbol{x})\,\hat{\phi}(t,\boldsymbol{x}) : \tag{3.5}$$

$$\begin{aligned}\hat{U}_2 = -e^2\int_{-\infty}^{\infty}\mathrm{d}t\int_{-\infty}^{t}\mathrm{d}t'\chi\left(\tfrac{t}{T}\right)\chi\left(\tfrac{t'}{T}\right)\int \mathrm{d}^3\boldsymbol{x}\int \mathrm{d}^3\boldsymbol{x}' F(\boldsymbol{x})\,F(\boldsymbol{x}')\,\hat{Q}(t)\,\hat{Q}(t') \\ \times : \hat{\phi}(t,\boldsymbol{x})\hat{\phi}(t,\boldsymbol{x}) : : \hat{\phi}(t',\boldsymbol{x}')\hat{\phi}(t',\boldsymbol{x}') : \ .\end{aligned} \tag{3.6}$$

We are uninterested in the final state of the complex field. We therefore perform a partial trace over its Hilbert space $\mathcal{H}_\mathrm{s}$, leaving only the state of the (simplified) EM field:

$$\hat{\rho}_{\mathrm{EM}} = \mathrm{tr}_\mathrm{s}[\hat{\rho}^{(0)}] + \mathrm{tr}_\mathrm{s}[\hat{U}_1\hat{\rho}^{(0)}] + \mathrm{tr}_\mathrm{s}[\hat{\rho}^{(0)}U_1] + \mathrm{tr}_\mathrm{s}[\hat{U}_2\hat{\rho}^{(0)}] + \mathrm{tr}_\mathrm{s}[\hat{\rho}^{(0)}\hat{U}_2] + \mathrm{tr}_\mathrm{s}[\hat{U}_1\hat{\rho}^{(0)}\hat{U}_1]\,. \tag{3.7}$$

To further specify $\hat{\rho}_{\rm EM}$, we will apply the assumption

$$\hat{\rho}^{(0)} = \hat{\rho}^{(0)}_{\rm EM} \otimes |0\rangle_{\rm S} \langle 0|_{\rm S} \tag{3.8}$$

about our initial state. The first order terms will all vanish, since the vacuum one-point function is zero.

Clearly the post-interaction zeroth-order term is

$$\mathrm{tr}_{\rm S}[\hat{\rho}^{(0)}] = \hat{\rho}^{(0)}_{\rm EM}\,, \tag{3.9}$$

while the first first-order terms take the form

$$\mathrm{tr}_{\rm S}[\hat{U}_1\hat{\rho}^{(0)}] = \mathrm{tr}_{\rm S}[\hat{\rho}^{(0)}\hat{U}_1]^\dagger = ie\int_{-\infty}^{\infty} \mathrm{d}t\, \chi\big(\tfrac{t}{T}\big) \int \mathrm{d}^3\boldsymbol{x}\, F(\boldsymbol{x})\hat{Q}(t)\hat{\rho}^{(0)}_{\rm EM}\mathrm{tr}[:\hat{\phi}(t,\boldsymbol{x})\hat{\phi}^\dagger(t,\boldsymbol{x}):\hat{\rho}^{(0)}_{\rm S}]. \tag{3.10}$$

We will define

$$Y_n^{:\phi\phi^\dagger:}(t,\boldsymbol{x}) := \mathrm{tr}[:\hat{\phi}(t,\boldsymbol{x})\hat{\phi}^\dagger(t',\boldsymbol{x}'):\hat{\rho}^{(0)}_{\rm S}]\,, \tag{3.11}$$

where n indicates the number of spatial dimensions. This is the one-point function of the operator $:\phi\phi^\dagger:$. Next note that we are working with the vacuum expectation of a normal ordered operator! This must vanish, and so we will find there is no first order contribution,

$$\mathrm{tr}_{\rm S}[\hat{U}_1\hat{\rho}^{(0)}] = \mathrm{tr}_{\rm S}[\hat{\rho}^{(0)}\hat{U}_1] = 0\,. \tag{3.12}$$

Now let us move on to second order. The first second-order term of Eq. (3.7) is

$$\begin{aligned}\mathrm{tr}_{\rm S}[\hat{U}_2\hat{\rho}^{(0)}] = &-e^2\int_{-\infty}^{\infty}\mathrm{d}t\int_{-\infty}^{t}\mathrm{d}t'\chi\big(\tfrac{t}{T}\big)\chi\big(\tfrac{t'}{T}\big)\int\mathrm{d}^3\boldsymbol{x}\int\mathrm{d}^3\boldsymbol{x}' F(\boldsymbol{x})F(\boldsymbol{x}')\hat{Q}(t)\hat{Q}(t')\hat{\rho}^{(0)}_{\rm EM}\\ &\times\mathrm{tr}_{\rm S}[:\hat{\phi}(t,\boldsymbol{x})\hat{\phi}^\dagger(t,\boldsymbol{x}):\hat{\phi}(t',x')\hat{\phi}^\dagger(t',x'):\hat{\rho}^{(0)}_{\rm S}].\end{aligned} \tag{3.13}$$

The second order Dyson operator contains two copies of the Hamiltonian, and therefore two copies of $:\hat{\phi}\hat{\phi}^\dagger:$. thus instead of having the (vanishing) one-point function in this term, we have the function

$$W_n^{:\phi\phi^\dagger:}(t,\boldsymbol{x},t',\boldsymbol{x}') := \mathrm{tr}_{\rm S}[:\hat{\phi}(t,\boldsymbol{x})\hat{\phi}^\dagger(t,\boldsymbol{x}):\hat{\phi}(t',x')\hat{\phi}^\dagger(t',x'):\hat{\rho}^{(0)}_{\rm S}]. \tag{3.14}$$

This is the two-point correlator of the operator $:\phi\phi^\dagger:$ for the field ϕ in the state $\rho_{\rm S}^{(0)}$. Inserting this definition into the second order term, we get

$$\begin{aligned}\mathrm{tr}_{\rm S}[\hat{U}_2\hat{\rho}^{(0)}] =& -e^2\int_{-\infty}^{\infty}\mathrm{d}t\int_{-\infty}^{t}\mathrm{d}t'\,\chi\big(\tfrac{t}{T}\big)\chi\big(\tfrac{t'}{T}\big)\int\mathrm{d}^3\boldsymbol{x}\int\mathrm{d}^3\boldsymbol{x}'\,F(\boldsymbol{x})F(\boldsymbol{x}')\hat{Q}(t)\hat{Q}(t')\hat{\rho}_{\rm EM}^{(0)}\\ &\times W_n^{:\phi\phi^\dagger:}(t,\boldsymbol{x},t',\boldsymbol{x}').\end{aligned} \tag{3.15}$$

It has been shown (see [29] and [2]) that $W_n^{:\phi\hat{\phi}^\dagger:}(t,\boldsymbol{x},t',\boldsymbol{x}') = (W_n^{\phi}(t,\boldsymbol{x},t',\boldsymbol{x}'))^2$ where

$$W_n^{\phi}(t,\boldsymbol{x},t',\boldsymbol{x}') = \mathrm{tr}[\hat{\phi}(t,\boldsymbol{x})\hat{\phi}^\dagger(t',\boldsymbol{x}')\hat{\rho}_{\rm S}^{(0)}]\,, \tag{3.16}$$

Applying this relation to our second order term, we find

$$\begin{aligned}\mathrm{tr}_{\rm S}[\hat{U}_2\hat{\rho}^{(0)}] =& -e^2\int_{-\infty}^{\infty}\mathrm{d}t\int_{-\infty}^{t}\mathrm{d}t'\,\chi\big(\tfrac{t}{T}\big)\chi\big(\tfrac{t'}{T}\big)\int\mathrm{d}^3\boldsymbol{x}\int\mathrm{d}^3\boldsymbol{x}'\,F(\boldsymbol{x})F(\boldsymbol{x}')\\ &\times\hat{Q}(t)\hat{Q}(t')\hat{\rho}_{\rm EM}^{(0)}\left(W_n^{\phi}(t,\boldsymbol{x},t',\boldsymbol{x}')\right)^2\,.\end{aligned} \tag{3.17}$$

The next second-order term is

$$\begin{aligned}\mathrm{tr}_{\rm S}[\hat{U}_2\hat{\rho}^{(0)}] =& -e^2\int_{-\infty}^{\infty}\mathrm{d}t\int_{-\infty}^{t}\mathrm{d}t'\,\chi\big(\tfrac{t}{T}\big)\chi\big(\tfrac{t'}{T}\big)\int\mathrm{d}^3\boldsymbol{x}\int\mathrm{d}^3\boldsymbol{x}'\,F(\boldsymbol{x})F(\boldsymbol{x}')\\ &\times\hat{\rho}_{\rm EM}^{(0)}\hat{Q}(t)\hat{Q}(t')\left(W_n^{\phi}(t,\boldsymbol{x},t',\boldsymbol{x}')\right)^2\,.\end{aligned} \tag{3.18}$$

Finally, the remaining second-order term is

$$\begin{aligned}\mathrm{tr}_{\rm S}[\hat{U}_1\hat{\rho}^{(0)}\hat{U}_1] =& e^2\int_{-\infty}^{\infty}\mathrm{d}t\int_{-\infty}^{\infty}\mathrm{d}t'\chi\big(\tfrac{t}{T}\big)\chi\big(\tfrac{t'}{T}\big)\int\mathrm{d}^3\boldsymbol{x}\int\mathrm{d}^3\boldsymbol{x}'F(\boldsymbol{x})F(\boldsymbol{x}')\\ &\times\hat{Q}(t)\hat{\rho}_{\rm EM}^{(0)}\hat{Q}(t')\left(W_n^{\phi}(t',\boldsymbol{x}',t,\boldsymbol{x})\right)^2\,.\end{aligned} \tag{3.19}$$

Combining these expressions for the second order terms as well as the fact that the first order terms vanish, we find that the full state of the oscillator, to second order and after an interaction time T, is

$$\begin{aligned}\hat{\rho}_{\rm EM} =& \hat{\rho}_{\rm EM}^{(0)} - e^2\int_{-\infty}^{\infty}\mathrm{d}t\int_{-\infty}^{t}\mathrm{d}t'\,\chi\big(\tfrac{t}{T}\big)\chi\big(\tfrac{t'}{T}\big)\int\mathrm{d}^3\boldsymbol{x}\int\mathrm{d}^3\boldsymbol{x}'\,F(\boldsymbol{x})F(\boldsymbol{x}')\\ &\times\{\hat{Q}(t)\hat{Q}(t'),\hat{\rho}_{\rm EM}^{(0)}\}\left(W_n^{\phi}(t,\boldsymbol{x},t',\boldsymbol{x}')\right)^2\\ &+e^2\int_{-\infty}^{\infty}\mathrm{d}t\int_{-\infty}^{\infty}\mathrm{d}t'\chi\big(\tfrac{t}{T}\big)\chi\big(\tfrac{t'}{T}\big)\int\mathrm{d}^3\boldsymbol{x}\int\mathrm{d}^3\boldsymbol{x}'F(\boldsymbol{x})F(\boldsymbol{x}')\\ &\times\hat{Q}(t)\hat{\rho}_{\rm EM}^{(0)}\hat{Q}(t')\left(W_n^{\phi}(t',\boldsymbol{x}',t,\boldsymbol{x})\right)^2\,,\end{aligned} \tag{3.20}$$

where $\{\cdot,\cdot\}$ is the anticomutator. It doesn't make much sense to have the order of primed and unprimed co-ordinates be reversed in one of the terms if we can help it, and so we perform a change of coordinates to fix that minor inconsistency. We are thus able to write the expression

$$\hat{\rho}_{\text{EM}} = \hat{\rho}^{(0)}_{\text{EM}} - e^2 \int_{-\infty}^{\infty} \mathrm{d}t \left(\int_{-\infty}^{t} \mathrm{d}t' \{\hat{Q}(t)\hat{Q}(t'), \hat{\rho}^{(0)}_{\text{EM}}\} - \int_{-\infty}^{\infty} \mathrm{d}t' \hat{Q}(t') \hat{\rho}^{(0)}_{\text{EM}} \hat{Q}(t) \right) \chi\left(\tfrac{t}{T}\right) \chi\left(\tfrac{t'}{T}\right) w(t,t') \,, \tag{3.21}$$

where

$$w(t,t') = \int \mathrm{d}^3\boldsymbol{x} \int \mathrm{d}^3\boldsymbol{x}' F(\boldsymbol{x}) F(\boldsymbol{x}') \left(W^{\phi}_n(t,\boldsymbol{x},t',\boldsymbol{x}') \right)^2 \tag{3.22}$$

is the smeared two-point correlator of the field operator to which the detector couples.

The exact form of $W^{\phi}_n(t,\boldsymbol{x},t',\boldsymbol{x}')$ is calculated in Appendix 7, where we find

$$W^{\phi}(\boldsymbol{x},t,\boldsymbol{x}',t') = \frac{m K_1\left(m\sqrt{|\boldsymbol{x}'-\boldsymbol{x}|^2 - (t'-t+\mathrm{i}\epsilon)^2}\right)}{(2\pi)^2 \sqrt{|\boldsymbol{x}'-\boldsymbol{x}|^2 - (t'-t+\mathrm{i}\epsilon)^2}} \,. \tag{3.23}$$

Here, K_1 is the modified Bessel function of the second kind, and ϵ is a soft UV cutoff that has been introduced to regularize the expression.

3.2 Purity

If a state, represented by the density matrix ρ is pure, then it can be represented by a vector in a Hilbert space. Such a state also has the property that $\mathrm{Tr}(\rho^2) = 1$. A state that is not pure is mixed and has the property $\frac{1}{d} \leq \mathrm{Tr}(\rho^2) < 1$. The lower bound $\frac{1}{d}$ is attained for the completely mixed state $\rho = I/d$.

If an initially pure state loses coherence, that means it becomes mixed. It is important to note that, while coherences are basis dependent, the purity is not. It is unitarily invariant. As a result, it turns out that a decline in purity is actually a better indicator that a particular state has "leaked information" to the environment.

Thus in what follows we will measure the purity of the UDW detector after interacting with the vacuum of the complex field. We will do so after setting up the initial state of the UDW detector to be several different common states in quantum optics.

First, we will compute the purity of the state $\hat{\rho}_{\rm EM}$ for an arbitrary pure input state $\hat{\rho}^{(0)}_{\rm EM} = |\psi\rangle\langle\psi|$. We will do this by expanding $\{\hat{Q}(t)\hat{Q}(t'), \hat{\rho}^{(0)}_{\rm EM}\}$ and $\hat{Q}(t)\hat{\rho}^{(0)}_{\rm EM}\hat{Q}(t')$. Next we will transition from the view of various operators ($\hat{Q}$, $\rho_{\rm EM}$, etc) to the view of coefficients of the density matrix $\hat{\rho}_{\rm EM}$. After, we will derive restrictions on the coefficients, thus expressing the purity in a simplified form. Finally, in several short subsections, we will derive the particular form of the purity for more specific input states.

The following definitions will be helpful in this process

$$|\psi_{--}\rangle := \hat{a}\hat{a}\,|\psi\rangle \tag{3.24}$$
$$|\psi_{-+}\rangle := \hat{a}\hat{a}^\dagger\,|\psi\rangle \tag{3.25}$$
$$|\psi_{+-}\rangle := \hat{a}^\dagger\hat{a}\,|\psi\rangle \tag{3.26}$$
$$|\psi_{++}\rangle := \hat{a}^\dagger\hat{a}^\dagger\,|\psi\rangle\ , \tag{3.27}$$

and

$$|\psi_{+}\rangle := \hat{a}^\dagger\,|\psi\rangle \tag{3.28}$$
$$|\psi_{-}\rangle := \hat{a}\,|\psi\rangle\ . \tag{3.29}$$

Additionally, we will use the following identities

$$\langle\psi|\psi_{--}\rangle = \langle\psi_{++}|\psi\rangle \tag{3.30}$$
$$\langle\psi|\psi_{+-}\rangle = \langle\psi_{+-}|\psi\rangle \tag{3.31}$$
$$\langle\psi|\psi_{+}\rangle = \langle\psi_{-}|\psi\rangle\,. \tag{3.32}$$

We expand the anti-commutator as

$$\begin{aligned}\{\hat{Q}(t)\hat{Q}(t'), \hat{\rho}^{(0)}_{\rm EM}\} &= \hat{Q}(t)\hat{Q}(t')\,|\psi\rangle\langle\psi| + \text{h.c.} \qquad (3.33)\\ =&\frac{1}{2V\Omega}(\hat{a}e^{-\mathrm{i}\Omega t} + \hat{a}^\dagger e^{\mathrm{i}\Omega t})(\hat{a}e^{-\mathrm{i}\Omega t'} + \hat{a}^\dagger e^{\mathrm{i}\Omega t'})\,|\psi\rangle\langle\psi| + \text{h.c.}\\ =&\frac{1}{2V\Omega}\Big(e^{-\mathrm{i}\Omega(t-t')}\,|\psi_{-+}\rangle\langle\psi| + e^{\mathrm{i}\Omega(t-t')}\,|\psi_{+-}\rangle\langle\psi| + e^{-\mathrm{i}\Omega(t+t')}\,|\psi_{--}\rangle\langle\psi| + e^{\mathrm{i}\Omega(t+t')}\,|\psi_{++}\rangle\langle\psi|\\ &+ e^{\mathrm{i}\Omega(t-t')}\,|\psi\rangle\langle\psi_{-+}| + e^{-\mathrm{i}\Omega(t-t')}\,|\psi\rangle\langle\psi_{+-}| + e^{\mathrm{i}\Omega(t+t')}\,|\psi\rangle\langle\psi_{--}| + e^{-\mathrm{i}\Omega(t+t')}\,|\psi\rangle\langle\psi_{++}|\Big)\,,\end{aligned}$$

while the remaining term can be written

$$\begin{aligned}\hat{Q}(t)\hat{\rho}^{(0)}_{\rm EM}\hat{Q}(t') &= \frac{1}{2V\Omega}(\hat{a}e^{-\mathrm{i}\Omega t} + \hat{a}^\dagger e^{\mathrm{i}\Omega t})\,|\psi\rangle\langle\psi|\,(\hat{a}e^{-\mathrm{i}\Omega t'} + \hat{a}^\dagger e^{\mathrm{i}\Omega t'})\\ =&\frac{1}{2V\Omega}(e^{-\mathrm{i}\Omega(t-t')}\,|\psi_-\rangle\langle\psi_-| + e^{\mathrm{i}\Omega(t-t')}\,|\psi_+\rangle\langle\psi_+| + e^{-\mathrm{i}\Omega(t+t')}\,|\psi_-\rangle\langle\psi_+| + e^{\mathrm{i}\Omega(t+t')}\,|\psi_+\rangle\langle\psi_-|)\,.\end{aligned} \tag{3.34}$$

Next we will define the following eight expressions,

$$A = \frac{e^2}{2V\Omega}\int_{-\infty}^{\infty}\mathrm{d}t\int_{-\infty}^{\infty}\mathrm{d}t' e^{-\mathrm{i}\Omega(t-t')}\chi\big(\tfrac{t}{T}\big)\chi\big(\tfrac{t'}{T}\big)w(t,t') \tag{3.35a}$$

$$B = \frac{e^2}{2V\Omega}\int_{-\infty}^{\infty}\mathrm{d}t\int_{-\infty}^{\infty}\mathrm{d}t' e^{-\mathrm{i}\Omega(t+t')}\chi\big(\tfrac{t}{T}\big)\chi\big(\tfrac{t'}{T}\big)w(t,t') \tag{3.35b}$$

$$C = \frac{e^2}{2V\Omega}\int_{-\infty}^{\infty}\mathrm{d}t\int_{-\infty}^{\infty}\mathrm{d}t' e^{\mathrm{i}\Omega(t-t')}\chi\big(\tfrac{t}{T}\big)\chi\big(\tfrac{t'}{T}\big)w(t,t') \tag{3.35c}$$

$$D = \frac{e^2}{2V\Omega}\int_{-\infty}^{\infty}\mathrm{d}t\int_{-\infty}^{\infty}\mathrm{d}t' e^{\mathrm{i}\Omega(t+t')}\chi\big(\tfrac{t}{T}\big)\chi\big(\tfrac{t'}{T}\big)w(t,t') \tag{3.35d}$$

$$a = \frac{e^2}{2V\Omega}\int_{-\infty}^{\infty}\mathrm{d}t\int_{-\infty}^{t}\mathrm{d}t' e^{-\mathrm{i}\Omega(t-t')}\chi\big(\tfrac{t}{T}\big)\chi\big(\tfrac{t'}{T}\big)w(t,t') \tag{3.35e}$$

$$b = \frac{e^2}{2V\Omega}\int_{-\infty}^{\infty}\mathrm{d}t\int_{-\infty}^{t}\mathrm{d}t' e^{-\mathrm{i}\Omega(t+t')}\chi\big(\tfrac{t}{T}\big)\chi\big(\tfrac{t'}{T}\big)w(t,t') \tag{3.35f}$$

$$c = \frac{e^2}{2V\Omega}\int_{-\infty}^{\infty}\mathrm{d}t\int_{-\infty}^{t}\mathrm{d}t' e^{\mathrm{i}\Omega(t-t')}\chi\big(\tfrac{t}{T}\big)\chi\big(\tfrac{t'}{T}\big)w(t,t') \tag{3.35g}$$

$$d = \frac{e^2}{2V\Omega}\int_{-\infty}^{\infty}\mathrm{d}t\int_{-\infty}^{t}\mathrm{d}t' e^{\mathrm{i}\Omega(t+t')}\chi\big(\tfrac{t}{T}\big)\chi\big(\tfrac{t'}{T}\big)w(t,t')\,. \tag{3.35h}$$

which we will combine with $\{\hat{Q}(t)\hat{Q}(t'), \hat{\rho}^{(0)}_{\text{EM}}\}$ and $\hat{Q}(t)\hat{\rho}^{(0)}_{\text{EM}}\hat{Q}(t')$ to recast our expression of $\hat{\rho}_{\text{EM}}$ in terms of coefficients of a density matrix. Doing so, we find

$$\begin{aligned}\hat{\rho}_{\text{EM}} = {}& |\psi\rangle\langle\psi| + A\,|\psi_-\rangle\langle\psi_-| + C\,|\psi_+\rangle\langle\psi_+| + B\,|\psi_-\rangle\langle\psi_+| + D\,|\psi_+\rangle\langle\psi_-| \\ & - \Big(a\big(\,|\psi_{-+}\rangle\langle\psi| + |\psi\rangle\langle\psi_{+-}|\,\big) + b\big(\,|\psi_{+-}\rangle\langle\psi| + |\psi\rangle\langle\psi_{-+}|\,\big) \\ & + c\big(\,|\psi_{--}\rangle\langle\psi| + |\psi\rangle\langle\psi_{++}|\,\big) + d\big(\,|\psi_{++}\rangle\langle\psi| + |\psi\rangle\langle\psi_{--}|\,\big)\Big)\,.\end{aligned} \tag{3.36}$$

Density matrices, by definition, are trace-one Hermitian operators. This will allow for further refinement of this expression. In particular, Hermiticity implies the following relationships between the off-diagonal elements: $D = B^*$, $b = a^*$, and $d = c^*$. Furthermore, A and C (the diagonal elements) must be real. Now we may write $\hat{\rho}_{\text{EM}}$ as

$$\begin{aligned}\hat{\rho}_{\text{EM}} = {}& |\psi\rangle\langle\psi| + A\,|\psi_-\rangle\langle\psi_-| + C\,|\psi_+\rangle\langle\psi_+| + B\,|\psi_-\rangle\langle\psi_+| + B^*\,|\psi_+\rangle\langle\psi_-| \\ & - \Big(a\big(\,|\psi_{-+}\rangle\langle\psi| + |\psi\rangle\langle\psi_{+-}|\,\big) + a^*\big(\,|\psi_{+-}\rangle\langle\psi| + |\psi\rangle\langle\psi_{-+}|\,\big) \\ & + c\big(\,|\psi_{--}\rangle\langle\psi| + |\psi\rangle\langle\psi_{++}|\,\big) + c^*\big(\,|\psi_{++}\rangle\langle\psi| + |\psi\rangle\langle\psi_{--}|\,\big)\Big)\,.\end{aligned} \tag{3.37}$$

Next, the trace, which must be unity, can be expressed as

$$\begin{aligned}\mathrm{tr}[\hat{\rho}_{\mathrm{EM}}] =& 1 + A\,\langle\psi_-|\psi_-\rangle + C\,\langle\psi_+|\psi_+\rangle + B\,\langle\psi_+|\psi_-\rangle + B^*\,\langle\psi_-|\psi_+\rangle \\ &- \Big(a(\langle\psi|\psi_{-+}\rangle + \langle\psi_{+-}|\psi\rangle) + a^*(\langle\psi|\psi_{+-}\rangle + \langle\psi_{-+}|\psi\rangle) \\ &+ c(\langle\psi|\psi_{--}\rangle + \langle\psi_{++}|\psi\rangle) + c^*(\langle\psi|\psi_{++}\rangle + \langle\psi_{--}|\psi\rangle)\Big)\,. \end{aligned} \tag{3.38}$$

We will next simplify using the identities provided at the beginning of this section:

$$\begin{aligned}\mathrm{tr}[\hat{\rho}_{\mathrm{EM}}] =& 1 + A\,\langle\psi|\psi_{+-}\rangle + C\,\langle\psi|\psi_{-+}\rangle + B\,\langle\psi|\psi_{--}\rangle + B^*\,\langle\psi|\psi_{++}\rangle \\ &- \Big(a(\langle\psi|\psi_{-+}\rangle + \langle\psi|\psi_{+-}\rangle) + a^*(\langle\psi|\psi_{+-}\rangle + \langle\psi|\psi_{-+}\rangle) \qquad (3.39) \\ &+ c(\langle\psi|\psi_{--}\rangle + \langle\psi|\psi_{--}\rangle) + c^*(\langle\psi|\psi_{++}\rangle + \langle\psi|\psi_{++}\rangle)\Big) \qquad (3.40) \\ =& 1 + (A - 2\mathrm{Re}[a])\,\langle\psi|\psi_{+-}\rangle + (C - 2\mathrm{Re}[a])\,\langle\psi|\psi_{-+}\rangle \\ &+ (B - 2c)\,\langle\psi|\psi_{--}\rangle + (B^* - 2c^*)\,\langle\psi|\psi_{++}\rangle\Big)\,. \qquad (3.41)\end{aligned}$$

Requiring this whole expression to be unity for any normalized input state imposes the following:

$$A = C = 2\mathrm{Re}[a] \tag{3.42}$$

$$B = 2c\,. \tag{3.43}$$

Let us re-write the output state as the sum of the input state and a perturbative correction: $\hat{\rho}_{\mathrm{EM}} = |\psi\rangle\langle\psi| + \hat{\rho}^{(2)}_{\mathrm{EM}}$,

$$\begin{aligned}\hat{\rho}^{(2)}_{\mathrm{EM}} =& A(|\psi_-\rangle\langle\psi_-| + |\psi_+\rangle\langle\psi_+|) + B\,|\psi_-\rangle\langle\psi_+| + B^*\,|\psi_+\rangle\langle\psi_-| \\ &- \Big(a(|\psi_{-+}\rangle\langle\psi| + |\psi\rangle\langle\psi_{+-}|) + a^*(|\psi_{+-}\rangle\langle\psi| + |\psi\rangle\langle\psi_{-+}|) \\ &+ \frac{B}{2}(|\psi_{--}\rangle\langle\psi| + |\psi\rangle\langle\psi_{++}|) + \frac{B^*}{2}(|\psi_{++}\rangle\langle\psi| + |\psi\rangle\langle\psi_{--}|)\Big)\,. \end{aligned} \tag{3.44}$$

Recall that we are specifically interested in the purity, $\mathrm{tr}[\hat{\rho}^2_{\mathrm{EM}}]$. First we expand $\hat{\rho}^2_{\mathrm{EM}}$ to second order,

$$\hat{\rho}^2_{\mathrm{EM}} = |\psi\rangle\langle\psi| + \Big\{\hat{\rho}^{(2)}_{\mathrm{EM}}, \langle\psi|\psi\rangle\Big\} + \mathcal{O}(e^4),\,. \tag{3.45}$$

Then we apply the trace operation

$$\mathrm{tr}[\hat{\rho}^2_{\mathrm{EM}}] = 1 + 2\,\langle\psi|\,\hat{\rho}^{(2)}_{\mathrm{EM}}\,|\psi\rangle + \mathcal{O}(e^4). \tag{3.46}$$

Applying the expression we derived for $\hat{\rho}^{(2)}_{\text{EM}}$, then applying the identities from earlier in this section (Eq. (3.32) and Eq. (3.42)), we find the following expression

$$\begin{aligned}\text{tr}[\hat{\rho}^2_{\text{EM}}] =& 1 + 2A\Big(2|\langle\psi|\psi_-\rangle|^2 - \langle\psi|\psi_{-+}\rangle - \langle\psi|\psi_{+-}\rangle\Big) \\ &+ 2B\Big(\big(\langle\psi|\psi_-\rangle\big)^2 - \langle\psi|\psi_{--}\rangle\Big) + 2B^*\Big(\big(\langle\psi|\psi_+\rangle\big)^2 - \langle\psi|\psi_{++}\rangle\Big) + \mathcal{O}(e^4). \quad (3.47)\end{aligned}$$

which conveniently is only dependent on A and B. A relatively simple final form is achieved by transforming from the plus/minus states to the input state $|\psi\rangle$ and creation and annihilation operators:

$$P = 1 - 2A + 2A\Big(2|\langle\psi|\hat{a}|\psi\rangle|^2 - \langle\psi|\hat{a}^\dagger\hat{a}|\psi\rangle\Big) + 4\text{Re}\Big[B\Big(\big(\langle\psi|\hat{a}|\psi\rangle\big)^2 - \langle\psi|\hat{a}\hat{a}|\psi\rangle\Big)\Big] + \mathcal{O}(e^4)\,. \quad (3.48)$$

Note that we have used the fact that $\langle\psi|\psi_{-+}\rangle = \langle\psi|\hat{a}\hat{a}^\dagger|\psi\rangle = \langle\psi_+|\psi_+\rangle = 1$. This can't be applied to $\langle\psi|\psi_{+-}\rangle$, since inputting the vacuum state would cause that term to vanish.

This equation is as specific as we can get without further specifying the input state, which we will do in the next sections.

3.2.1 Vacuum state

We set the input state to the ground state $|\psi\rangle = |0\rangle$ and compute the purity

$$P = 1 - 2A + 2A\Big(2|\langle 0|\hat{a}|0\rangle|^2 - \langle 0|\hat{a}^\dagger\hat{a}|0\rangle\Big) + 4\text{Re}\Big[B\Big(\big(\langle 0|\hat{a}|0\rangle\big)^2 - \langle 0|\hat{a}\hat{a}|0\rangle\Big)\Big] + \mathcal{O}(e^4). \quad (3.49)$$

All of the inner products vanish, leaving

$$P = 1 - 2A + \mathcal{O}(e^4)\,. \quad (3.50)$$

This expression tells us that even inputting the vacuum state, we find decoherence (i.e. purity less than one) due to creation of a single photon. This can be seen from Eq. (3.44), where for the vacuum as the input state, we find

$$\hat{\rho}_{\text{EM}} = |0\rangle\langle 0| + A\left(\hat{a}^\dagger|0\rangle\langle 0|\hat{a}\right) - \left(\left(a\left(\hat{a}\hat{a}^\dagger|0\rangle\langle 0|\right) + H.c\right) + \left(\frac{B}{2}\left(|0\rangle\langle 0|\hat{a}\hat{a}\right) + H.c\right)\right), \quad (3.51)$$

where $A\,\hat{a}^\dagger|0\rangle\langle 0|\hat{a}$ is a single particle state.

3.2.2 Coherent state

The next input state we will consider is a coherent state $|\psi\rangle = |\alpha\rangle$, defined by being an eigenvector of the annihilation operator, $\hat{a}\,|\alpha\rangle = \alpha\,|\alpha\rangle$. Applying this to our expression for purity reveals that coherent states decohere exactly as does the vacuum state.

$$P = 1 - 2A + \mathcal{O}(e^4)\,. \tag{3.52}$$

3.2.3 Fock state

Let us now consider inputting an n-particle Fock state $|\psi\rangle = |n\rangle$, which is generated by applying a creation operator to the vacuum n times. The action of the creation and annihilation operators on an n-particle fock state are $\hat{a}\,|n\rangle = \sqrt{n}\,|n{-}1\rangle$ and $\hat{a}^\dagger\,|n\rangle = \sqrt{n+1}\,|n{+}1\rangle$. The purity that results is

$$P = 1 - 2A(n+1) + \mathcal{O}(e^4)\,. \tag{3.53}$$

The $n = 0$ Fock state is the vacuum state, thus we expect the purity for these two states to match, which they do.

3.2.4 Squeezed Vacuum

Next consider the squeezed vacuum. First we define the squeezing operator

$$\hat{S}(\zeta) = \exp(\frac{1}{2}(\zeta^* \hat{a}^2 - \zeta \hat{a}^{\dagger 2})), \tag{3.54}$$

where $\zeta = re^{2i\phi}$ is the squeezing parameter with magnitude r and phase ϕ. The squeezing operator obeys the identities

$$\hat{S}(\zeta)^\dagger \hat{S}(\zeta) = \hat{S}(\zeta)\hat{S}(\zeta)^\dagger = \mathbb{1}, \tag{3.55}$$

$$S^\dagger(\zeta)\hat{a}\hat{S}(\zeta) = (h\hat{a} + s\hat{a}^\dagger), \tag{3.56}$$

$$S^\dagger(\zeta)\hat{a}^\dagger\hat{S}(\zeta) = (h\hat{a}^\dagger + s^*\hat{a}), \tag{3.57}$$

where s and h are defined as $s := -e^{2i\phi}\sinh(r)$, and $h := \cosh(r)$. Then the squeezed vacuum can be expressed as $|\psi\rangle = |S0\rangle = \hat{S}(\zeta)\,|0\rangle$.

In this case, the purity is somewhat more involved to calculate that the previous input states considered. We start with plugging the squeezed vacuum state into the expression we derived for purity:

$$\begin{aligned} P =& 1 - 2A + A\Big(2|\left\langle 0\right|\hat{S}(\zeta)^\dagger \hat{a}\hat{S}(\zeta)\left|0\right\rangle|^2 - \left\langle 0\right|\hat{S}(\zeta)^\dagger\hat{a}^\dagger\hat{S}(\zeta)\hat{S}(\zeta)^\dagger\hat{a}\hat{S}(\zeta)\left|0\right\rangle\Big) \\ &+ 4\mathrm{Re}\Big[B\Big(\big(\left\langle 0\right|\hat{S}(\zeta)^\dagger\hat{a}\hat{S}(\zeta)\left|0\right\rangle\big)^2 - \left\langle 0\right|\hat{S}(\zeta)^\dagger\hat{a}\hat{S}(\zeta)\hat{S}(\zeta)^\dagger\hat{a}\hat{S}(\zeta)\left|0\right\rangle\Big)\Big] + \mathcal{O}(e^4). \quad (3.58) \end{aligned}$$

From here, we apply the squeezing operator identities, finding the state to be:

$$\begin{aligned} P =& 1 - 2A + 2A\Big(2|\left\langle 0\right|(h\hat{a} + s\hat{a}^\dagger)\left|0\right\rangle|^2 - \left\langle 0\right|(h\hat{a}^\dagger + s^*\hat{a})(h\hat{a} + s\hat{a}^\dagger)\left|0\right\rangle\Big) \quad (3.59) \\ &+ 4\mathrm{Re}\Big[B\Big(\big(\left\langle 0\right|(h\hat{a} + s\hat{a}^\dagger)\left|0\right\rangle\big)^2 - \left\langle 0\right|(h\hat{a} + s\hat{a}^\dagger)(h\hat{a} + s\hat{a}^\dagger)\left|0\right\rangle\Big)\Big] + \mathcal{O}(e^4). \quad (3.60) \end{aligned}$$

Simplifying, we find,

$$P = 1 - 2A - 2As^*s - 4\mathrm{Re}\Big[Bhs\Big] + \mathcal{O}(e^4). \quad (3.61)$$

Now apply the definitions of h and s

$$P = 1 - 2A - 2A\left|-e^{2i\phi}\sinh(r)\right|^2 - 4\mathrm{Re}\Big[B\cosh(r)\left(-e^{2i\phi}\sinh(r)\right)\Big] + \mathcal{O}(e^4). \quad (3.62)$$

simplify one more time, noting that $\sinh(r)^2 = -\frac{1}{2} + \frac{1}{2}\cosh(2r)$:

$$P = 1 - A - A\cosh(2r) + 4\mathrm{Re}\Big[Be^{2i\phi}\Big]\cosh(r)\sinh(r) + \mathcal{O}(e^4). \quad (3.63)$$

3.2.5 Cat State

The final state we will consider is called a cat state. It is defined as $|\mathrm{cat}\rangle := \mathcal{N}_+(|\alpha\rangle + |-\alpha\rangle)$ where $|\alpha\rangle$ is a coherent state that satisfies $\hat{a}\,|\alpha\rangle = \alpha\,|\alpha\rangle$, $|-\alpha\rangle$ satisfies $\hat{a}\,|-\alpha\rangle = -\alpha\,|-\alpha\rangle$, and $\mathcal{N}_\pm = 1/\sqrt{2(1 \pm e^{-2|\alpha|^2})}$ is a normalization factor dependent on the overlap of the coherent states:

$$\langle\alpha|-\alpha\rangle = \exp(-2|\alpha|^2). \quad (3.64)$$

One can see how the overlap enters the normalization by looking at the inner product

$$(\langle\alpha| \pm \langle-\alpha|)(|\alpha\rangle \pm |-\alpha\rangle) = \mathcal{N}_\pm^{-2}. \quad (3.65)$$

Furthermore, the following identity is useful

$$\left(\langle\alpha| + \langle -\alpha|\right)\left(|\alpha\rangle - |-\alpha\rangle\right) = 0. \tag{3.66}$$

Now we will apply our definition of a cat state to the expression we derived for the purity.

$$\begin{aligned} P =& 1 - 2A + 2A\Big(2\mathcal{N}_+^4|\big(\langle\alpha| + \langle -\alpha|\big)\hat{a}\big(|\alpha\rangle + |-\alpha\rangle\big)|^2 - \mathcal{N}_+^2\big(\langle\alpha| + \langle -\alpha|\big)\hat{a}^\dagger\hat{a}\big(|\alpha\rangle + |-\alpha\rangle\big)\Big) \\ &+ 4\mathrm{Re}\Big[B\Big(\mathcal{N}_+^4\big(\big(\langle\alpha| + \langle -\alpha|\big)\hat{a}\big(|\alpha\rangle + |-\alpha\rangle\big)\big)^2 - \mathcal{N}_+^2\big(\langle\alpha| + \langle -\alpha|\big)\hat{a}\hat{a}\big(|\alpha\rangle + |-\alpha\rangle\big)\Big)\Big] \\ &+ \mathcal{O}(e^4) \end{aligned} \tag{3.67}$$

We'll also go ahead and act the creation and annihilation operators on the coherent states therein, resulting in

$$\begin{aligned} P =& 1 - 2A + 2A\Big(2\mathcal{N}_+^4|\big(\langle\alpha| + \langle -\alpha|\big)\alpha\big(|\alpha\rangle - |-\alpha\rangle\big)|^2 - \mathcal{N}_+^2\big(\langle\alpha| - \langle -\alpha|\big)\alpha^*\alpha\big(|\alpha\rangle - |-\alpha\rangle\big)\Big) \\ &+ 4\mathrm{Re}\Big[B\Big(\mathcal{N}_+^4\big(\big(\langle\alpha| + \langle -\alpha|\big)\alpha\big(|\alpha\rangle - |-\alpha\rangle\big)\big)^2 - \mathcal{N}_+^2\big(\langle\alpha| + \langle -\alpha|\big)\alpha\alpha\big(|\alpha\rangle + |-\alpha\rangle\big)\Big)\Big] \\ &+ \mathcal{O}(e^4) \end{aligned} \tag{3.68}$$

the mixed cat state inner products vanish

$$\begin{aligned} P =& 1 - 2A + 2A\Big(-\mathcal{N}_+^2\big(\langle\alpha| - \langle -\alpha|\big)\alpha^*\alpha\big(|\alpha\rangle - |-\alpha\rangle\big)\Big) \\ &+ 4\mathrm{Re}\Big[B\Big(-\mathcal{N}_+^2\big(\langle\alpha| + \langle -\alpha|\big)\alpha\alpha\big(|\alpha\rangle + |-\alpha\rangle\big)\Big)\Big] + \mathcal{O}(e^4) \end{aligned} \tag{3.69}$$

while the other inner products return the overlap

$$P = 1 - 2A - 2A|\alpha|^2\Big(\mathcal{N}_+^2\mathcal{N}_-^{-2}\Big) - 4\mathrm{Re}\Big[\alpha^2 B\Big] + \mathcal{O}(e^4) \tag{3.70}$$

Next consider that

$$\mathcal{N}_+^2\mathcal{N}_-^{-2} = \frac{2 - 2e^{-2|\alpha|^2}}{2e^{-2|\alpha|^2} + 2} = \tanh(|\alpha|^2) \tag{3.71}$$

This results in the following form for the purity of a cat state after interacting with the vacuum of a massive complex field,

$$P = 1 - 2A(|\alpha|^2\tanh(|\alpha|^2) + 1) - 4\mathrm{Re}\left[B\alpha^2\right] + \mathcal{O}(e^4) \tag{3.72}$$

3.3 Results

Coefficients A and B, detailed in appendix 6, are difficult to calculate and exact numerical results are yet to be obtained. Ideally, an intermediate stage could be found wherein the absolute magnitude of A and B are approximated. In what follows, we will simply assume that $A, B \ll 1$, since we are working in the perturbative regime.

First, for the Fock state, the purity after interaction is

$$P = 1 - 2A(n+1) + \mathcal{O}(e^4)\,. \tag{3.73}$$

The effects of decoherence due to interacting with the external field increases with the photon-number n. Indeed, $n = 1$ doubles the decohering effect when comparing to inputting the oscillator in its the ground state. For $n = 0$, we recover the purity for both the vacuum and coherent states.

It is perhaps surprising that the purity for the coherent state is independent of the amplitude. This is potentially interesting, since while $n = 1$ and $\alpha = 1$ have the same particle number expectation value, the Fock state will decohere at twice the rate of the coherent state. This could be related to the fact that higher amplitude coherent states have more overlap, thus offsetting the enhanced decohering effects of a greater amplitude state.

Consider the purity from a squeezed vacuum input state

$$P = 1 - A(\cosh(2r) + 1) + 4\mathrm{Re}[Be^{2i\phi}]\sinh(r)\cosh(r) + \mathcal{O}(e^4). \tag{3.74}$$

The purity depends on the magnitude of the squeezing parameter r. In fact, for sufficiently large r, the positive term can dominate and drive the purity back up. The decoherence also depends on the phase ϕ, in fact the terms ϕ and B can interfere to either add to or remove purity from the system. We can also conclude that the coupling between the cavity mode and the massive complex vacuum is sensitive to the phase of the squeezed state. The unsqueezed vacuum is attained by setting $r = 0$. Thus, we expect to recover (and do) the same purity as the vacuum input state, $P = 1 - 2A + \mathcal{O}(e^4)$.

Lastly, let us consider the cat state input, whose output has purity

$$P = 1 - 2A(|\alpha|^2\tanh(|\alpha|^2) + 1) - 4\mathrm{Re}\left[B\alpha^2\right] + \mathcal{O}(e^4) \tag{3.75}$$

While the coherent state did not output a state whose purity depends on the amplitude α, the cat state does. It also depends on the phase, through the term α^2 (note there is no

modulus), and so once again we find the oscillator-field coupling is sensitive to the phase of the input state. We expect, and indeed do, recover the same result as the vacuum when $\alpha = 0$.

If we compare the cat state to the Fock state, taking $n = \alpha = 1$, we find that the cat state can exhibit much stronger or weaker decoherence effects depending on the phase of B. If $|A| = |B|$, we find the worst-case scenario exhibits a reduction in purity of ≈ 3.7 times larger for the cat state than for the Fock state. However, if A and B have equal magnitude and opposite phase, we find that the cat state exhibits roughly 30% less of a reduction in purity.

From this analysis, we conclude that decoherence of systems in quantum optics due to the presence of the vacuum of an ancilliary field is theretically possible. We were able to show the scaling properties of such effects for different states common in quantum optics, generally finding that the larger the amplitude or higher the excitations of the state, the more purity was reduced. Additionally, we conclude that tuning the parameters of the model to achieve different relative magnitude or phase of elements of the density matrix of the output state could result in drastically different decoherence effects. However, it remains to be shown how the magnitude of this effect compares to other decoherence effects for quantum states of light confined to cavities, and at what scales the effects may be come significant. Further work towards estimating the absolute magnitude of A and B must be done.

Chapter 4

Fermionic Entanglement Harvesting

The UDW detector response to a fermionic field in the d-dimensional Minkowski vacuum was derived in [28]. In particular, the scenario described above is related linearly to the UDW detector response to a scalar bosonic field in the $2d$-dimensional Minkowski vacuum. Here, we will show how this same technique can be applied to a pair of detectors to harvest entanglement from a fermionic field. We will relate these results to the well-studied entanglement harvesting protocol from a bosonic vacuum [19].

4.1 Why do this?

Entanglement in the Fermionic field presents some complications over its Bosonic counterpart. The anti-commuting nature of the field is difficult to map to commuting degrees of freedom. In particular, the Jordan-Wigner transformation results in non-physical mappings (local degrees of freedom map to non-local degrees of freedom) from Fermionic to qubit degrees of freedom. For a more in depth discussion, see [82]. Superselection rules prevent ambiguities in defining the trace and assessing the local nature of operations. However, the Jordan-Wigner transformation has not been shown to perserve locality even paired with the Wigner parity superselection rule [82]. More specifically, notions of entanglement and separability that are equivalent in qubit systems have been shown to be different when superselection rules are present: there exist convex combinations of Fermionic product states that are not locally preparable [82].

In this chapter, we present an alternative method to probe the entanglement structure of the Fermionic field. Instead of trying to map Fermionic states to Bosonic states or trying to

create a unique and universal definition of entanglement in Fermionic systems, we will take an operational approach and ask: how much entanglement can we extract from fermionic systems with the entanglement harvesting protocol? For entanglement harvesting, if the detectors are never in causal contact, any entanglement must have originated in non-local correlations in the field. Thus, through the use of the UDW model, we can provide some insight into the scaling behaviour of entanglement in a Fermionic field. In particular we will focus on how the Fermionic field differs in this respect from the Bosonic field. While this will not be explored indepth, this could be amenable to a resource theoretic perspective; what can we learn if we define entanglement via the yield of the entanglement harvesting protocol?

4.2 UDW Detector Pairs and the Fermionic Field

We begin with a free fermionic field (see subsection 1.4.4) and a two-level detector interacting via the Hamiltonian in Eq. (1.2), where the coupling to the field is given by the renormalized scalar density

$$f(\Psi(\mathsf{x})) = :\overline{\Psi}(\mathsf{x})\Psi(\mathsf{x}): \,. \tag{4.1}$$

The form of a UDW detector's density matrix after time evolution with an arbitrary field in an *arbitrary state* is given in Eq. (1.61), while the entries in that matrix are given by Eq. (1.62)-(1.64). Applying Eq. (4.1) and setting the state of the field to the vacuum, Eq. (1.64) vanishes. The remaining terms are dependent upon the two-point function of $:\overline{\Psi}\Psi:$, given by

$$W^{:\overline{\Psi}\Psi:,|0\rangle}(t,\boldsymbol{x},) = \langle 0| :\overline{\Psi}(t,\boldsymbol{x})\Psi(t,\boldsymbol{x}):\overline{\Psi}(t',\boldsymbol{x}')\Psi(t',\boldsymbol{x}'): |0\rangle \ , \tag{4.2}$$

which, in appendix 6, is shown to be

$$W^{:\overline{\Psi}\Psi:,|0\rangle}(t,\boldsymbol{x},t'\boldsymbol{x}') = \frac{N_d(\Gamma(d/2))^2}{4\pi^d(z(t,\boldsymbol{x},t',\boldsymbol{x}'))^{2d-2}} \tag{4.3}$$

where

$$z(t,\boldsymbol{x},,t',\boldsymbol{x}') := \sqrt{(\boldsymbol{x}-\boldsymbol{x}')^2-(t-t'-\mathrm{i}\epsilon)^2} \tag{4.4}$$

and N_d is defined in Eq. (1.25).

Combining expressions Eq. (1.62) and Eq. (1.63) with the two point correlator yields the following two expressions, which completely characterize the Fermionic UDW model,

$$\mathcal{M}^{:\overline{\Psi}\Psi:,d} = \frac{-N_d(\Gamma(d/2))^2}{4\pi^d}\int \mathrm{d}t \int^t \mathrm{d}t' \int \mathrm{d}^n\boldsymbol{x} \int \mathrm{d}\boldsymbol{x}' \frac{M(t,\boldsymbol{x},t',\boldsymbol{x}')}{(z(t,\boldsymbol{x},t',\boldsymbol{x}'))^{2d-2}} \tag{4.5}$$

$$\mathcal{L}^{:\overline{\Psi}\Psi:,d}_{\mu\nu} = \frac{-N_d(\Gamma(d/2))^2}{4\pi^d}\int \mathrm{d}t \int \mathrm{d}t' \int \mathrm{d}^n\boldsymbol{x} \int \mathrm{d}\boldsymbol{x}' \frac{L_\mu(t,\boldsymbol{x})L^*_\nu(t,\boldsymbol{x})}{(z(t,\boldsymbol{x},t',\boldsymbol{x}'))^{2d-2}}, \tag{4.6}$$

where we have modified notation so that dependence on the vacuum $|0\rangle$ is implied while dependence on spacetime dimension d is explicitly noted in the superscript.

Comparing these expressions to similar ones derived for the scalar bosonic field, i.e. $\mathcal{M}^{\phi,2d}$ given in Eq. (1.71) and $\mathcal{L}^{\phi,2d}_{\mu\nu}$ given in Eq. (1.72), we find that the following identities hold:

$$\mathcal{M}^{:\overline{\Psi}\Psi:,d} = \frac{N_d(\Gamma(d/2))^2}{\Gamma\big(d-1\big)}\mathcal{M}^{\phi,2d} \tag{4.7}$$

$$\mathcal{L}^{:\overline{\Psi}\Psi:,d}_{\mu\nu} = \frac{N_d(\Gamma(d/2))^2}{\Gamma\big(d-1\big)}\mathcal{L}^{\phi,2d}_{\mu\nu}. \tag{4.8}$$

This result, which extends the single detector result found in [28], tells us that, up to some geometric factors, the coupling to the scalar density of a fermionic field is the same as coupling to a scalar field in twice as many spacetime dimensions. In other words, the UDW model is insensitive to the spinor structure of the Dirac field. This is consistent with the model's coupling to the scalar density.

It was noted in [28] that there is no IR ambiguity in the Fermionic UDW model in 1+1-dimensional Minkowski vacuum. We add to that claim, and find that this holds, unsurprisingly, for a pair of detectors as well.

4.3 Negativity for fermions

In this section, we will derive an expression for the leading order correction to the negativity of a pair of point-like UDW detectors interacting with the vacuum of a Fermionic field. We will do so in spacetime dimension $d \geq 2$. We take as our starting point the expression for negativity Eq. (1.81) found in Entanglement Harvesting (subsection 1.6.1),

$$\mathcal{N}_{(2)} = -\frac{1}{2}\left(\mathcal{L}_{\mathrm{AA}} + \mathcal{L}_{\mathrm{BB}} - \sqrt{(\mathcal{L}_{\mathrm{AA}} - \mathcal{L}_{\mathrm{BB}})^2 + 4\,|\mathcal{M}|^2}\right).$$

Next we will substitute in the expressions for $\mathcal{L}_{\rm AA}$ Eq. (4.8) and $\mathcal{M}$ Eq. (4.7) derived in the previous section, which yields

$$\mathcal{N}^{:\overline{\Psi}\Psi:,d}_{(2)} = -\frac{1}{2}\Bigg[\frac{N_d(\Gamma(d/2))^2}{\Gamma\big(d-1\big)}\mathcal{L}^{\phi,2d}_{\rm AA} + \frac{N_d(\Gamma(d/2))^2}{\Gamma\big(d-1\big)}\mathcal{L}^{\phi,2d}_{\rm BB} - \sqrt{\left(\frac{N_d(\Gamma(d/2))^2}{\Gamma\big(d-1\big)}\mathcal{L}^{\phi,2d}_{\rm AA} - \frac{N_d(\Gamma(d/2))^2}{\Gamma\big(d-1\big)}\mathcal{L}^{\phi,2d}_{\rm BB}\right)^2 + 4\left|\frac{N_d(\Gamma(d/2))^2}{\Gamma\big(d-1\big)}\mathcal{M}^{\phi,2d}\right|^2}\Bigg].$$

For real arguments, the pre-factor $\frac{N_d(\Gamma(d/2))^2}{\Gamma\big(d-1\big)}$ is real and non-negative. Therefore, we may pull it out of the Modulus and square root. What remains inside the expression is exactly that expression for the leading order negativity of a pair of UDW detectors interacting with the massless scalar Minkowski vacuum in twice as many dimensions as the orginal Fermionic model:

$$\begin{aligned}\mathcal{N}^{:\overline{\Psi}\Psi:,d}_{(2)} &= \frac{N_d(\Gamma(d/2))^2}{\Gamma\big(d-1\big)}\left(-\frac{1}{2}\left(\mathcal{L}^{\phi,2d}_{\rm AA} + \mathcal{L}^{\phi,2d}_{\rm BB} - \sqrt{\left(\mathcal{L}^{\phi,2d}_{\rm AA} - \mathcal{L}^{\phi,2d}_{\rm BB}\right)^2 + 4\left|\mathcal{M}^{\phi,2d}\right|^2}\right)\right)\\ &= \frac{N_d(\Gamma(d/2))^2}{\Gamma\big(d-1\big)}\mathcal{N}^{\phi,2d}_{(2)}.\end{aligned} \tag{4.9}$$

Thus we have proved the following theorem, analogous to **Theorem 1** in [28].

Theorem *The leading-order negativity resulting from the entanglement harvesting protocol for a pair of point-like Unruh-DeWitt detectors coupled to the renormalized scalar density of a massless Dirac field in Minkowski vacuum in $d \geq 2$ spacetime dimensions equals*

$$\frac{N_d(\Gamma(d/2))^2}{\Gamma(d-1)}, \tag{4.10}$$

times the negativity resulting from the entanglement harvesting protocol for a pair of point-like Unruh-DeWitt detectors coupled linearly to a massless scalar field in Minkowski vacuum in $2d$ spacetime dimensions.

This result allows us to immediately relate Fermionic entanglement harvesting to the extant literature. Namely, in [7], a pair of point-like detectors is coupled to the vacuum of a scalar field in 3+1 dimensional Minkowski space. By Eq.(4.9), we may apply those results to 1+1 dimensional Fermionic model (see Figure 1.(b) in [7]). In particular, it was shown that for a Gaussian switching function and point-like smearing, in 3+1-dimensional

spacetime, the UDW model can harvest entanglement at arbitrary distances, while for a sudden switching the output of the entanglement harvesting protocol is severely limited. We conclude the same behaviour will appear in the 1+1-dimensional Fermionic model described here.

One potentially interesting path forward is to develop a spinor UDW model for the Dirac field, much like was done in [45] for the electromagnetic field. In that work, the vector UDW model recovered the physics as the scalar model, with the addition that it was sensitive to the relative orientation of the detectors. Such a difference could also manifest in a vector-Fermionic UDW model.

4.4 Mutual information for Fermions

In this section we consider the mutual information harvested from a fermionic field. This is used somewhat as a bench mark. The mutual information represents total correlations and has been shown in the past to have different scaling properties (in the harvesting scenario) than negativity; mutual information harvesting is generally non-zero; while entanglement harvesting generally dies out with increasing detector separation of decreasing detector gap, for example. Thus, the harvesting protocol captures different features of the quantum field depending on the measure of correlations that is studied.

Mutual information measures the total correlations, both classical and quantum in a given system. Recall from section subsection 1.6.2 that the leading order contribution to the mutual information between a pair of UDW detectors is given by

$$\begin{aligned} I(\rho_{\text{AB}}) = &\mathcal{L}_+ \log(\mathcal{L}_+) + \mathcal{L}_- \log(\mathcal{L}_-) \\ &- \mathcal{L}_{\text{AA}} \log(\mathcal{L}_{\text{AA}}) - \mathcal{L}_{\text{BB}} \log(\mathcal{L}_{\text{BB}}) + \mathcal{O}(\lambda_\nu^4) \end{aligned}$$

where

$$\mathcal{L}_\pm = \frac{1}{2}\left(\mathcal{L}_{\text{AA}} + \mathcal{L}_{\text{BB}} \pm \sqrt{(\mathcal{L}_{\text{AA}} - \mathcal{L}_{\text{BB}})^2 + 4\,|\mathcal{L}_{\text{AB}}|^2}\right).$$

For the fermionic model, $L_{\mu\nu}$ is defined in Eq. (4.6) and obeys the identity Eq. (4.8).

According to Eq. (4.8) and the same rationale provided in the the previous section, $\mathcal{L}_\pm$ can be written as

$$\mathcal{L}_\pm^{:\overline{\Psi}\Psi:,d} = \frac{N_d(\Gamma(d/2))^2}{\Gamma\big(d-1\big)}\mathcal{L}_\pm^{\phi,2d}. \tag{4.11}$$

We may write

$$I(\rho_{\text{AB}})^{:\overline{\Psi}\Psi:,d} = \frac{N_d(\Gamma(d/2))^2}{\Gamma\big(d-1\big)}\Bigg[\mathcal{L}_+^{\phi,2d}\log\left(\frac{N_d(\Gamma(d/2))^2}{\Gamma\big(d-1\big)}\mathcal{L}_+^{\phi,2d}\right) + \mathcal{L}_-^{\phi,2d}\log\left(\frac{N_d(\Gamma(d/2))^2}{\Gamma\big(d-1\big)}\mathcal{L}_-^{\phi,2d}\right)$$
$$- \mathcal{L}_{\text{AA}}^{\phi,2d}\log\left(\frac{N_d(\Gamma(d/2))^2}{\Gamma\big(d-1\big)}\mathcal{L}_{\text{AA}}^{\phi,2d}\right) - \mathcal{L}_{\text{BB}}^{\phi,2d}\log\left(\frac{N_d(\Gamma(d/2))^2}{\Gamma\big(d-1\big)}\mathcal{L}_{\text{BB}}^{\phi,2d}\right)\Bigg] + \mathcal{O}(\lambda_\nu^4),$$

which is reducible to

$$I(\rho_{\text{AB}})^{:\overline{\Psi}\Psi:,d} = \frac{N_d(\Gamma(d/2))^2}{\Gamma\big(d-1\big)}\log\left(\frac{N_d(\Gamma(d/2))^2}{\Gamma\big(d-1\big)}\right)\left[\mathcal{L}_+^{\phi,2d} + \mathcal{L}_-^{\phi,2d} - \mathcal{L}_{\text{AA}}^{\phi,2d} - \mathcal{L}_{\text{BB}}^{\phi,2d}\right]$$
$$+ \frac{N_d(\Gamma(d/2))^2}{\Gamma\big(d-1\big)}I(\rho_{\text{AB}})^{\phi,2d} + \mathcal{O}(\lambda_\nu^4),$$

When the detectors have the same energy gap and switching function, then $\mathcal{L}_{\text{AA}} = \mathcal{L}_{\text{BB}}$ and $\mathcal{L}_\pm$ simplifies to

$$\mathcal{L}_\pm = \mathcal{L}_{\text{AA}} \pm |\mathcal{L}_{\text{AB}}|\,.$$

In this case, the expression $\mathcal{L}_+^{\phi,2d} + \mathcal{L}_-^{\phi,2d} - \mathcal{L}_{\text{AA}}^{\phi,2d} - \mathcal{L}_{\text{BB}}^{\phi,2d}$ vanishes and the mutual information has the form

$$I(\rho_{\text{AB}})^{:\overline{\Psi}\Psi:,d} = \frac{N_d(\Gamma(d/2))^2}{\Gamma\big(d-1\big)}I(\rho_{\text{AB}})^{\phi,2d} + \mathcal{O}(\lambda_\nu^4), \tag{4.12}$$

Thus, like the Negativity, the mutual information is (to leading order) equivalent up to a geometric factor for the d-dimensonal Fermionic and 2d-dimensional Bosonic models. One intuitive explanation of the difference in dimensions is to simply point to the spinor structure and subsequent calculation of the Wightman function. When the contracting the spinor-valued propagators in Eq. (74), we end up with double the number of copies of the scalar Wightman function (or, more specifically, more copies of the function $z(t, \boldsymbol{x}, t', \boldsymbol{x}')$).

In conclusion, the Fermionic model as employed here is not sensitive to the spinor nature of the field. We find this to be succinctly explained by the scalar nature of the coupling.

Chapter 5

UDW pairs with Modified Dispersion

In this chapter, we will investigate the possibility of using such systems to study entanglement harvesting protocols. This work was motivated by recent proposals for UDW-like detectors in analogue gravity models. Our approach is to account for the dispersion in analogue gravity systems, apply that to a large class of disperive quantum field theories residing on a n-dimensional Minkowski spacetime, and derive a theoretical entanglement measure for two Unruh-Dewit detectors coupled to such a field. Our main result is that, at leading order in perturbation theory, our calculations indicate that entanglement harvesting can be tuned to be insensitive to the effects of dispersion.

5.1 Introduction

In subsection 1.6.1, we discussed the theoretical extraction of entanglement from the quantum vacuum. However an experimental implementation thereof has yet to be realized. In this chapter we investigate the possibility of employing laboratory systems as a path to confirm entanglement harvesting [83, 84, 85].

The laboratory systems we will be considering are those referred to as analogue gravity experiments. Analog gravity systems are a wide class of physical systems, such as fluids, superfluids and optical systems, whose excitations experience an effective spacetime geometry. In these systems, one can map between the dynamical equations for the perturbations and a scalar field theory coupling minimally to a metric tensor. In principle, any physical system that allows for this kind of mapping can be used to simulate classical and quantum field theory processes in the laboratory. For example, air-water interface analogue gravity

systems have been used to simulate Hawking radiation [86, 87], superradiance [88] and black hole quasinormal modes [89]. Ultra-cold atoms system have been used to mimic the dynamical Casimir effect [90], Hawking radiation [91] and Hubble friction [92], and optical analogues were used to mimic Hawking radiation [93, 94]. A more complete list of analogue gravity experiments can be found in a recent review article [95].

Recently, experimentally feasible UDW-like models have been developed, primarily to study the Unruh effect, for ultra cold atoms [96, 97, 98, 99]. These studies considered both two-level (e.g. atomic quantum dots [96]) and continuous field (i.e. optical interferometers [97]) detectors. However, in these experiments, the acceleration of the detectors can present a challenge, and so detectors taken to be static or inertial may in fact be more experimentally feasible.

One of the main differences between analogue gravity systems and quantum field theory in curved spacetimes is that the effective field theory in analog gravity systems exhibit additional terms that involve more than two spatial derivatives. These terms can be neglected in the low-energy limit, resulting in an equation of motion resembling a relativistic scalar field in an effective curved spacetime geometry. The role of the speed of light is played by the low-energetic propagation limit of the perturbations, e.g. emergent sound-cone structure in ultra-cold atomic systems [100]. However, analogue gravity systems are intrinsically dispersive, and as such are an important aspect of modelling efforts to propose future and/or support current analogue gravity experiments.

In this chapter we will employ a pair of Unruh-DeWitt detectors to study the entanglement harvesting protocol for a large class of dispersive systems in order to understand if simulating entanglement harvesting in analog gravity is experimentally feasible. We will discuss causality in dispersive or non-local emergent field theories on system sizes and time-scales relevant for experiments.

5.2 Why Simulate Harvesting?

An experimental realization of the entanglement harvesting protocol has yet to be realized. In fact, a spacelike version of this protocol may prove difficult to implement due to the large value of the speed of light. However, analog gravity systems offer a path to potential confirmation via simulation in laboratory experiments [101, 102, 103]. In these experiments, the speed of sound replaces the speed of light [100] thus enabling more feasible experimental access to spacelike separation. However, it is important to note that entanglement harvesting is still possible with causal contact, where the detectors are allowed to pass

signals through the field. In fact it has been shown that the channel between two detectors coupled via the UDW Hamiltonian has non-zero channel capacity [61, 104, 105, 106].

The speed of sound in analog gravity systems can be as much as a dozen orders of magnitude slower than the speed of light. Typically, the large magnitude of the speed of light makes it very difficult to ensure spacelike separation at distances where the entanglement harvesting protocol produces non-zero entanglement. Thus analog gravity systems offer a test bed where spacelike entanglement harvesting will be more readily achievable than in non-simulated systems.

This justification emphasizes the spacelike-separated regime of entanglement harvesting, but timelike harvesting is also a subject of study [107]. Spacelike separation is emphasized because it is simple to directly infer that entanglement stemmed from the quantum field if the detectors were uncorrelated beofre the interaction, and remained out of causal contact for the duration of the interaction. However, in scenarios where causal separation is not maintained, there is potential for utilizing a causality estimator to separate a common cause (in the field) from one detector's influence on the other (through the field) [108]. However, to the author's knowledge this technique has not been applied to harvesting scenarios. It is, however, an interesting possibility. [1]

Analog gravity experiments offer another advantage over more traditional confirmation studies. This advantage is the ability to repeat experiments many times in quick secession. This ability aids in overcoming two hurdles, both of which increase the number of times an experiment must be performed. First, entanglement is not an observable, and thus cannot be directly measured. Instead, self-testing quantum systems for genuine bi-partite entanglement requires many experimental repetitions to gain sufficient statistics. These statistics then show that a classical bound, such as the CHSH inequality, can be violated. The next challenge is that the amount of entanglement is small. In order to break classical bounds with statistical certainty, it may be necessary to run an experiment many times and perform entanglement distillation on the series of resulting detector states. This further increases the number of experimental repetitions required to self-test the entangled qubits produced by the entanglement harvesting protocol. In summary, laboratory control of a system in analog gravity allows for repeated, high-fidelity preparations of initial states of the simulated field. The same level of control and repeatability is not currently possible on quantum fields at the length scales prescribed by the speed of light combined with a requirement of spacelike separation.

Confirmation of the entanglement harvesting protocol is in itself worth exploring in analog gravity systems, but it is not the only benefit. Entanglement harvesting is a tool to

[1] I'd like to thank Robert Spekkens for pointing out this tool.

characterize the entanglement structure of a relativistic quantum field, such as those that live on curved spacetimes or the effective field theories of many condensed matter systems.

As with other analysis with application to analog gravity experiments [109], we will be working in 2+1 dimensions.

5.3 Why Dispersion?

In this section, we will introduce the equations of motion for a wide class of analogue gravity systems. we consider a generalised wave equation for our effective quantum field $\hat{\phi}(t, \mathbf{x})$,

$$\mathcal{D}_t^2 \hat{\phi}(t, \mathbf{x}) + G(-\mathrm{i}\nabla)\hat{\phi}(t, \mathbf{x}) = 0\,, \tag{5.1}$$

where $\mathcal{D}_t = \partial^2 + \boldsymbol{v}_0 \cdot \nabla$ is the material derivative and where G is an arbitrary function of the ∇-operator, so that G controls the order of this differential equation and, as we will see, the dispersion as well. Here $\boldsymbol{v}_0 = \boldsymbol{v}_0(t, \boldsymbol{x})$ is the flow velocity and is in general a function of time and space. In superfluid analog gravity systems $\boldsymbol{v}_0 = \nabla\Phi_0$ represents an irrotational background flow. The emergent quantum field theory (5.1) applies to quantum fluctuations of the scalar field Φ_0.

To mimic Minkowski spacetime scenarios, we set the background flow to zero, $\boldsymbol{v}_0 = \mathbf{0}$, and thus the material derivative simplifies to a partial time derivative. The wave equation (5.1) on Minkowski spacetime exhibits plane wave solutions $u_k(t, \mathbf{x}) = e^{-\mathrm{i}(\omega_{\boldsymbol{k}} t - \boldsymbol{k}\cdot\boldsymbol{x})}$, and the field modes may be expanded as follows

$$\hat{\phi}(t, \boldsymbol{x}) = \int \frac{\mathrm{d}^n \boldsymbol{k}}{\sqrt{(2\pi)^n}} \frac{(\hat{a}_{\boldsymbol{k}} u_k(t, \mathbf{x}) + \hat{a}^\dagger_{\boldsymbol{k}} u^*_k(t, \mathbf{x}))}{\sqrt{2\omega_{\boldsymbol{k}}}}\,, \tag{5.2}$$

where $\hat{a}_k$ and $\hat{a}^\dagger_k$ are the standard annihilation and creation operators, i.e. $[a_k, a_{k'}] = [a^\dagger_k, a^\dagger_{k'}] = 0$ and $[a_k, a^\dagger_k] = \delta_{kk'}$. Note that all the extra complication of the higher-order spatial derivatives are hidden in the dispersion relation

$$\omega^2_{\boldsymbol{k}} = G(\boldsymbol{k})\,. \tag{5.3}$$

We are interested in situations where $G(k)$ is an analytic and even function in k and for which

$$\lim_{k\to 0} G(k^2) = ck^2. \tag{5.4}$$

For a similar analysis for a classical field theory, see [110]. This type of dispersion is very general and applicable to most analogue gravity systems. To list a couple of examples, the dispersion relation for sound waves in Bose-Einstein condensates is given by,

$$\omega_k^2 = c^2 k^2 + \left(\frac{\hbar}{2m}\right)^2 k^4 \,, \tag{5.5}$$

where $\hbar$ is the reduced Planck constant and m the mass of the atoms that form the condensate. Furthermore interface waves on fluids or superfluids is given by,

$$\omega_k^2 = (g\,k + \gamma k^3)\tanh(h_0\,k)\,, \tag{5.6}$$

where g is the gravitational acceleration, γ the surface tension and h_0 the height of the fluid.

In what follows, we will work in units with $c = \hbar = 1$.

5.4 Switching and Smearing function

In our analysis, the form of the switching and smearing will play an important role.

To begin, we will allow switching function $\chi_{\rm I}(t)$ to be any function which peaks when its argument is zero and decays monotonically as the magnitude of the argument increases. We will take both detectors to have the same switching function, i.e. $\chi(t) := \chi_{\rm A}(t) = \chi_{\rm B}(t)$.

Next we will assume the smearing functions, which represent how strong a detector couples to the field at each point in space, to be identical $F(\boldsymbol{x}) := F_{\rm A}(\boldsymbol{x}) = F_{\rm B}(\boldsymbol{x})$ and spherically symmetric $F(\boldsymbol{x}) = F(|\boldsymbol{x}|)$. We will assume that $F(\boldsymbol{x})$ is normalized to unity such that

$$\int \mathrm{d}^n\boldsymbol{x}\,\left|F\left(\tfrac{|\boldsymbol{x}|}{\sigma}\right)\right| = 1\,. \tag{5.7}$$

These assumptions lead to a Fourier transform obeying the identity,

$$\int \mathrm{d}^n\boldsymbol{x}\,F\left(\frac{\boldsymbol{x}-\boldsymbol{x}_{\rm I}}{\sigma}\right)\,e^{\mathrm{i}\boldsymbol{k}\cdot\boldsymbol{x}} = \widetilde{F}[\boldsymbol{k}\,\sigma]\,e^{\mathrm{i}\boldsymbol{k}\cdot\boldsymbol{x}_{\rm I}}. \tag{5.8}$$

5.5 Results

The process to apply the UDW model to a dispersive field of the kind described in the previous section is the same as that in subsection 1.5.1. The time-evolved state is given by the density matrix Eq. (1.61). For the vacuum state, the element $\mathcal{L}_\mu$ in Eq. (1.64) vanishes, and the remaining two elements $\mathcal{M}$ Eq. (1.62) and $\mathcal{L}$ Eq. (1.63) depend on the two-point correlator

$$W^{\phi_{\omega_k},|0\rangle}(t,\boldsymbol{x},) = \langle\psi|\,\phi_{\omega_k}(t,\boldsymbol{x})\phi_{\omega_k}(t',\boldsymbol{x}')\,|\psi\rangle \tag{5.9}$$

where the subscript ω_k emphasizes that the field in question is dispersive.

For the UDW model with a dispersive field, we can express the two-point correlator as

$$W(t,\boldsymbol{x},t',\boldsymbol{x}') = \int \mathrm{d}^n\boldsymbol{k}\frac{e^{\mathrm{i}\omega_{\boldsymbol{k}}(t-t')-i\boldsymbol{k}\cdot(\boldsymbol{x}-\boldsymbol{x}')}}{2(2\pi)^n\omega_{\boldsymbol{k}}}\,. \tag{5.10}$$

When we apply this to $\mathcal{M}$ and $\mathcal{L}$, we will find that the imaginary exponential functions can act as Fourier factors. Doing so, we find that we may write $\mathcal{M}$ and $\mathcal{L}$ as

$$\mathcal{M} = \int \frac{\mathrm{d}\boldsymbol{k}}{2(2\pi)^n\omega_{\boldsymbol{k}}}M(\boldsymbol{k}) \tag{5.11}$$

$$\mathcal{L}_{\mu\nu} = \int \frac{\mathrm{d}\boldsymbol{k}}{2(2\pi)^n\omega_{\boldsymbol{k}}}L_\mu(\boldsymbol{k})\,(L_\nu(\boldsymbol{k}))^* \tag{5.12}$$

where

$$M^{(n)} = -\lambda_{\mathrm{A}}\lambda_{\mathrm{B}}\frac{\widetilde{F}(\sigma|\boldsymbol{k}|)\widetilde{F}(\sigma|\boldsymbol{k}|)}{e^{-\mathrm{i}\boldsymbol{k}\cdot(\boldsymbol{x}_{\mathrm{A}}-\boldsymbol{x}_{\mathrm{B}})}}\int_{-\infty}^{\infty}\mathrm{d}t\int_{-\infty}^{t}\mathrm{d}t' e^{-\mathrm{i}\omega_{\boldsymbol{k}}(t_{\mathrm{A}}-t_{\mathrm{B}})}\left(\frac{\chi(\frac{t-t_{\mathrm{A}}}{T})\,\chi(\frac{t'-t_{\mathrm{B}}}{T})}{e^{-\mathrm{i}(\Omega_{\mathrm{B}}t'+\Omega_{\mathrm{A}}t)}}+\frac{\chi(\frac{t'-t_{\mathrm{A}}}{T})\,\chi(\frac{t-t_{\mathrm{B}}}{T})}{e^{-\mathrm{i}(\Omega_{\mathrm{B}}t'+\Omega_{\mathrm{A}}t)}}\right) \tag{5.13}$$

while for $L(\boldsymbol{k})$, we find

$$L_\mu^{(n)} = \frac{\lambda_\mu\widetilde{F}(\sigma|\boldsymbol{k}|)}{e^{\mathrm{i}\boldsymbol{k}\cdot\boldsymbol{x}_\mu}}\int_{-\infty}^{\infty}\mathrm{d}t\chi(\tfrac{t-t_{\mathrm{A}}}{T})\,e^{\mathrm{i}((\Omega_{\mathrm{A}}+\omega_{\boldsymbol{k}})t)}, \tag{5.14}$$

Now if we particularize to Gaussian switching and smearing

$$F(\boldsymbol{x}) = \frac{e^{-x^2}}{\left(\sqrt{2}\pi\right)^n} \tag{5.15}$$

$$\chi(t) = e^{-t^2}. \tag{5.16}$$

The Fourier transform is

$$\widetilde{F}(\boldsymbol{k}) = e^{-\frac{1}{4}\boldsymbol{k}^2}. \tag{5.17}$$

We will proceed by applying these functions in a similar way as [7] (see equations (23) and (24) in that work, which are for 3+1 dimensional UDW detectors with Gaussian switching and smearing and that do not take into account dispersion). We find

$$L_\mu^{(n)} = \lambda_\mu e^{-\frac{1}{4}\sigma^2|\boldsymbol{k}|^2} e^{-\mathrm{i}\boldsymbol{k}\cdot\boldsymbol{x}_\mu} G_1(\boldsymbol{k}, t_\mu) \tag{5.18}$$

$$M^{(n)} = -\lambda_{\mathrm{A}}\lambda_{\mathrm{B}} e^{-\frac{1}{2}\sigma^2|\boldsymbol{k}|^2} e^{\mathrm{i}\boldsymbol{k}\cdot(\boldsymbol{x}_{\mathrm{A}}-\boldsymbol{x}_{\mathrm{B}})} G_2(\boldsymbol{k}) \tag{5.19}$$

where G_i are defined as

$$G_1(\boldsymbol{k}, t_\mu) := \int_{-\infty}^{\infty} \mathrm{d}t e^{-(\frac{t-t_\mu}{T})^2} e^{\mathrm{i}((\Omega_{\mathrm{A}}+\omega_{\boldsymbol{k}})t)} \tag{5.20}$$

$$G_1(\boldsymbol{k}, t_\mu) := \int_{-\infty}^{\infty}\mathrm{d}t \int_{-\infty}^{t}\mathrm{d}t' e^{-\mathrm{i}\omega_{\boldsymbol{k}}(t_{\mathrm{A}}-t_{\mathrm{B}})} \left(\frac{e^{-\left((\frac{t-t_{\mathrm{A}}}{T}\right)^2} e^{-\left((\frac{t'-t_{\mathrm{B}}}{T}\right)^2}}{e^{-\mathrm{i}(\Omega_{\mathrm{B}}t'+\Omega_{\mathrm{A}}t)}} + \frac{e^{-\left((\frac{t'-t_{\mathrm{A}}}{T}\right)^2} e^{-\left((\frac{t-t_{\mathrm{B}}}{T}\right)^2}}{e^{-\mathrm{i}(\Omega_{\mathrm{B}}t'+\Omega_{\mathrm{A}}t)}} \right). \tag{5.21}$$

A closed-form expression for G_1 follows from straightforward integral calculations

$$G_1(\boldsymbol{k}, t_\mu) = T\sqrt{\pi} e^{-\frac{1}{4}(\Omega+\omega_{\boldsymbol{k}})^2} e^{\mathrm{i}(\Omega+\omega_{\boldsymbol{k}})t_\mu}. \tag{5.22}$$

Next, we can evaluate G_2 for a dispersive field using the techniques outlined in the appendix A of [7], we find

$$\begin{aligned} G_2(\boldsymbol{k}) =& \frac{\pi T^2}{2} e^{-2\mathrm{i}\Omega t_{\mathrm{A}}} \Big[e^{-\frac{1}{2}(\Omega^2+\omega_{\boldsymbol{k}}^2)+\mathrm{i}(t_{\mathrm{B}}-t_{\mathrm{A}})(\Omega-\omega_{\boldsymbol{k}}))} - e^{\frac{(t_{\mathrm{A}}-t_{\mathrm{B}})^2}{T^2}} I\Big(\omega_{\boldsymbol{k}}+\Omega, \omega_{\boldsymbol{k}}-\Omega+2\mathrm{i}(t_{\mathrm{B}}-t_{\mathrm{A}})\Big) \\ &+ e^{-\frac{1}{2}(\Omega^2+\omega_{\boldsymbol{k}}^2)+\mathrm{i}(t_{\mathrm{B}}-t_{\mathrm{A}})(\Omega-\omega_{\boldsymbol{k}}))} - e^{\frac{(t_{\mathrm{A}}-t_{\mathrm{B}})^2}{T^2}} I\Big(\omega_{\boldsymbol{k}}+\Omega-2\mathrm{i}(t_{\mathrm{B}}-t_{\mathrm{A}}), \omega_{\boldsymbol{k}}-\Omega\Big) \Big] \end{aligned} \tag{5.23}$$

where

$$I(a,b) = \mathrm{i} e^{-\frac{a^2+b^2}{4}} \mathrm{Erfi}\left(\frac{a+b}{2\sqrt{2}}\right). \tag{5.24}$$

5.5.1 2+1 Dimensions

Applying our results to 2+1 dimensions is straightforward, due to the angular part of the integral over $\boldsymbol{k}$ being rather simple. It depends only on the imaginary exponential of the detector separation. Thus we calculate

$$\int_0^{2\pi} |\boldsymbol{k}| e^{-\mathrm{i}|\boldsymbol{k}||\boldsymbol{x}_\mu|\cos[\theta]} = 2\pi k J_0(|\boldsymbol{k}||\boldsymbol{x}_\mu|), \tag{5.25}$$

where J_0 a Bessel function of the first kind [78]. Thus particularizes the previous expressions to 2+1 dimensions

$$\mathcal{M}^{(2)} = -\lambda_{\mathrm{A}}\lambda_{\mathrm{B}} \int_0^\infty \frac{\mathrm{d}|\boldsymbol{k}|}{2(2\pi)\omega_{\boldsymbol{k}}} e^{-\frac{1}{2}\sigma^2|\boldsymbol{k}|^2} J_0(|\boldsymbol{k}||\boldsymbol{x}_{\mathrm{A}} - \boldsymbol{x}_{\mathrm{B}}|) G_2(\boldsymbol{k}) \tag{5.26}$$

$$\mathcal{L}^{(2)}_{\mathrm{AB}} = \lambda_{\mathrm{A}}\lambda_{\mathrm{B}} \int_0^\infty \frac{\mathrm{d}|\boldsymbol{k}|\ |\boldsymbol{k}|}{2(2\pi)\omega_{\boldsymbol{k}}} e^{-\frac{1}{2}\sigma^2|\boldsymbol{k}|^2} J_0(|\boldsymbol{k}||\boldsymbol{x}_{\mathrm{A}} - \boldsymbol{x}_{\mathrm{B}}|) G_1(\boldsymbol{k}, t_{\mathrm{A}}) G_1(\boldsymbol{k}, t_{\mathrm{B}}) \tag{5.27}$$

$$\mathcal{L}^{(2)}_{\mathrm{AA}} = \lambda_{\mathrm{A}}\lambda_{\mathrm{A}} \int_0^\infty \frac{\mathrm{d}|\boldsymbol{k}|\ |\boldsymbol{k}|}{2(2\pi)^2\omega_{\boldsymbol{k}}} e^{-\frac{1}{2}\sigma^2|\boldsymbol{k}|^2} G_1(\boldsymbol{k}, t_{\mathrm{A}}) G_1(\boldsymbol{k}, t_{\mathrm{A}}). \tag{5.28}$$

5.5.2 Entanglement Harvesting

Now that we have derived the density matrix elements above, we will plot the negativity (Entanglement Harvesting (section 1.6.1)) for both the linear dispersion and for small positive and small negative corrections. Our interest is two fold: first, we ask if the linear and corrected dispersive fields result in qualitatively similar output of the entanglement harvesting protocol and secondly we do a quantitative comparison. The results of this numerical study are shown in figure 5.1. We also make plots that show the broad-strokes differences between linear dispersion and the two types of modified dispersion, highlighting the areas of the parameter space where the largest differences occur. This data is shown in figure 5.2.

The qualitative behaviour of the harvesting protocol is unchanged upon correcting the dispersion, either with the Bogoliubov or subsonic correction. The curve indicating where the negativity goes to zero in the plotted parameter space has the same general form in both cases. The scaling properties with detector gap are also nearly unchanged: the negativity drops multiple orders of magnitude with order 1 increases to the detector gap, and the decrease in negativity is more extreme for larger detector gaps. We also see that entanglement harvesting is not possible for degenerate detectors (zero detector gap, $\Omega = 0$)

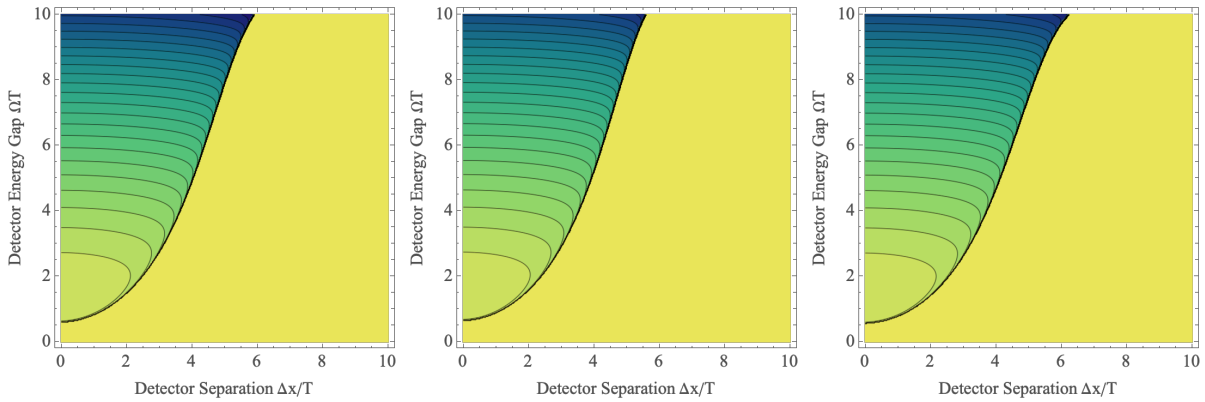

Figure 5.1: These three plots show the magnitude of the entanglement harvesting protocol given three different dispersion relations. On the left is linear dispersion $\omega_{\boldsymbol{k}}^2 = |\boldsymbol{k}|^2$. In the middle is a small subtractive correction to dispersion $\omega_{\boldsymbol{k}}^2 = |\boldsymbol{k}|^2 - \epsilon^2|\boldsymbol{k}|^4$. On the right is a small additive correction to dispersion $\omega_{\boldsymbol{k}}^2 = |\boldsymbol{k}|^2 + \epsilon^2|\boldsymbol{k}|^4$. The color scales on these plots refer to the magnitude of the negativity between the detectors. The large block of yellow in each plot indicates zero negativity. Each contour represents an order of magnitude drop in the negativity. For regions of non-zero negativity, the darker colors indicate less negativity.

for the given parameter set for all three dispersion types. These behaviours are shared by all types of dispersion studied in this work, including linear as shown in Figure 5.1.

The area of the greatest quantitative difference between all the dispersion types studied is located near the curve where the negativity goes to zero. While the curve traces out a nearly identical path through the energy-gap-spatial-separation parameter space, we find that, for a fixed detector gap, negativity drops off to zero more rapidly in the case of Bogoliubov dispersion and more slowly in the case of subsonic dispersion. This region is indicated by a middle band of darker color in Figure 5.2. In both figures, these bands indicate that the negativity differs by more than on part in 100 as compared to the case of linear dispersion.

5.5.3 Large Detector Limit

One of the notable features of $\mathcal{M}$ and $\mathcal{L}$ is that the fourier transforms of F and χ seem to modulate the sensitivity of the detector to various field modes. In this section, we will study this model when the detector size is much larger than all of the other scales in the problem. We will do a numerical exploration of the expressions for $\mathcal{M}$ and $\mathcal{L}$ for Gaussian switching

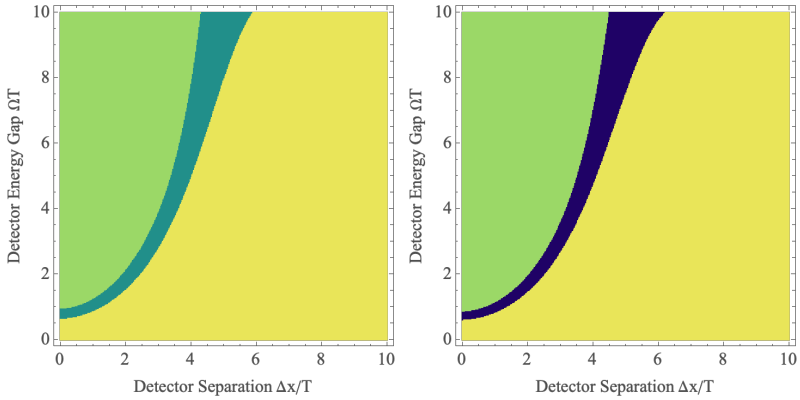

Figure 5.2: These two plots compare each compare one type modified dispersion to linear dispersion. The left shows a small negative correction to dispersion, while the right shows a small positive correction to dispersion. The lighter (yellow and green) regions show where the negativity changes very little (less than 10%). The darker band shows where the magnitude changes by more than 10%.

and smearing decribed above. In particular, we will focus on the relative difference between $\mathcal{M}$ (or $\mathcal{L}$) for a detector interacting with a dispersive and non-dispersive field:

$$\frac{\left|\left|\mathcal{M}_{\omega_k^2=G(\boldsymbol{k})}\right| - \left|\mathcal{M}_{\omega_k^2=\boldsymbol{k}^2}\right|\right|}{\left|\mathcal{M}_{\omega_k^2=\boldsymbol{k}^2}\right|} \tag{5.29}$$

and

$$\frac{\left|\left|\mathcal{L}_{\omega_k^2=G(\boldsymbol{k})}\right| - \left|\mathcal{L}_{\omega_k^2=\boldsymbol{k}^2}\right|\right|}{\left|\mathcal{L}_{\omega_k^2=\boldsymbol{k}^2}\right|}, \tag{5.30}$$

where the subscript indicates the type of dispersion. The results of this study for various parameter combinations is shown in Figure 5.3

What we find is a supression of the differences arising from dispersion for the UDW detector functions $\mathcal{M}$ and $\mathcal{L}_{\text{IJ}}$ when the spot size of the detector is larger than the other scales in the problem. Thus in any scenario when this can be the case, the effects of the dispersive field can be made to vanish. However, one must note that the spot size of the detector must also be larger than the detector separation. This is consistent with the data shown in figures 5.1 and 5.2. In those plots, for a given detector gap, the differences between the two models are greater for larger detector separations (excluding the cases where both detectors exhibit no negativity).

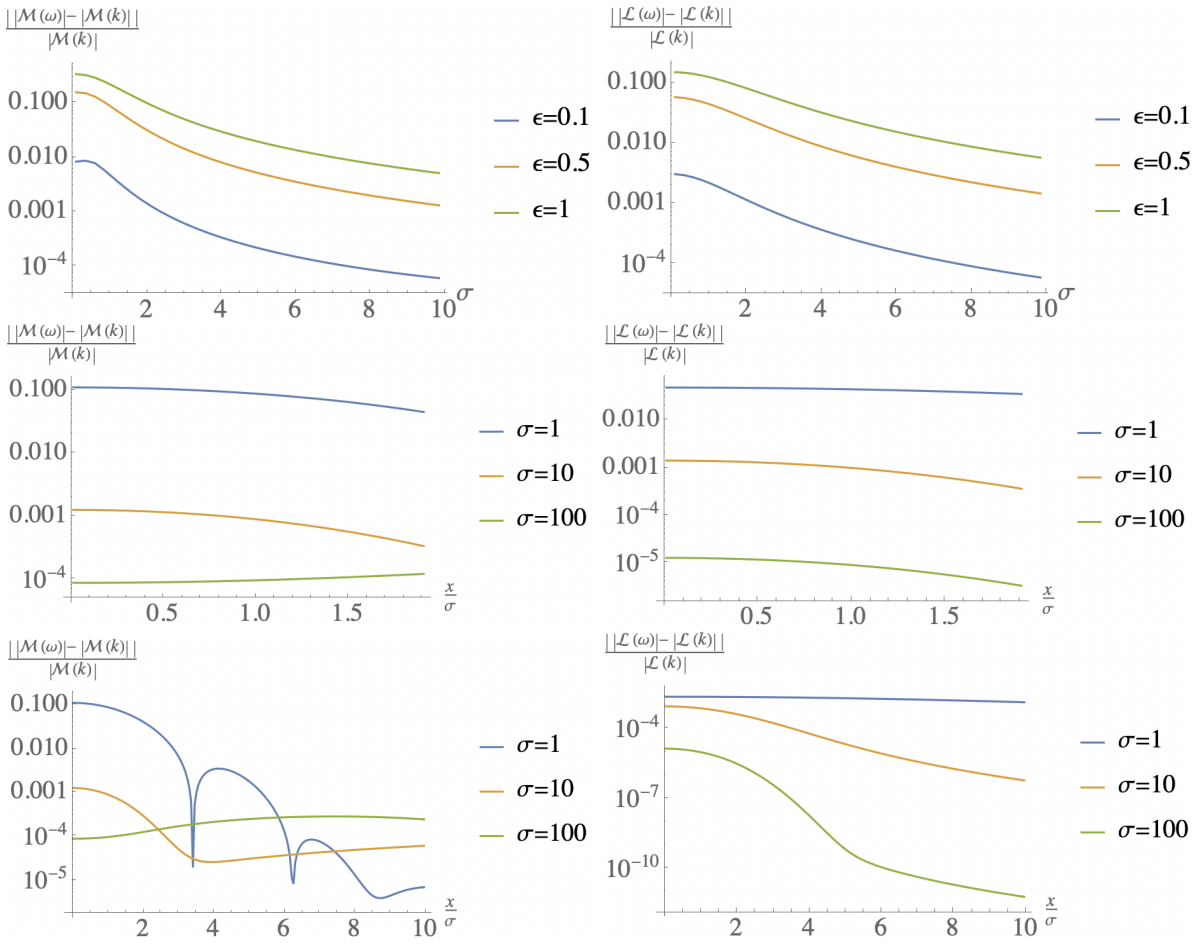

Figure 5.3: The top two plots show that the difference in the detector functions $\mathcal{M}$ and $\mathcal{L}_{\text{IJ}}$ between the dispersive field and non-dispersive field decays as σ increases. This is shown for various values of ϵ for a dispersion relation with a small correction $\omega_{\boldsymbol{k}}^2 = k^2 + \epsilon^2 k^4$. In the middle row of plots, this same phenomena is viewed from a different perspective: the difference function for $\mathcal{M}$ and $\mathcal{L}_{\text{IJ}}$ is plotted against the non-dimensionalized detector separation, $\frac{x}{\sigma}$, for various detector widths. We find that each successively larger detector yields results which are strictly less than the smaller detectors in the range of detector separations which are on the order of the detector size or smaller. However, the bottom plot shows us that, in the realm of detectors which are separated much farther than their width, we find that difference function for $\mathcal{M}$ and $\mathcal{L}_{\text{IJ}}$ to behave quite differently. We find the difference between $\mathcal{L}_{\text{IJ}}$ for dispersive and non-dispersive fields shrinks as σ increases regardless of the separation of the detectors; this no longer holds for $\mathcal{M}$

5.6 Discussion

We will now summarize and analyze our results, then draw conclusions about the robustness of the entanglement harvesting protocol under the given modifications to dispersion.

We have studied the entanglement harvesting protocol with small corrections to the dispersion relations with a hard UV cutoffs. We found the protocol to be qualitatively unaffected by modified dispersion, and significantly quantitatively affected in a small band of the parameter space.

We began this study by noting that analog gravity systems are dispersive. It follows that testing sensitivity to dispersion is a necessary precursor to simulating anything in an analog gravity experiment. We tested the entanglement harvesting protocol's sensitivity to corrections to dispersion, and found that it was not sensitive. Thus, we conclude that it may be possible to simulate entanglement harvesting in analog gravity experiments.

Chapter 6

Techniques in Harvesting

In [111] a technique, which we call the *Ng technique*, was developed, which de-nested the nested integrals in the density matrix element $\mathcal{M}$ of Eq. (1.62) in the time-evolved detector state. These nested integrals originate from the second order terms of the Dyson expansion and can make finding a closed form for the density matrix element $\mathcal{M}$ difficult. The work [111] focused on applying this de-nesting technique in curved spacetimes, which is where much of the difficulty may arise if one is using a linearly coupled detector.

However, we have largely focused on non-linear couplings in this work, and as such we found it was necessary to extend the Ng technique to arbitrary couplings as well. While much of the work in this thesis is presented without direct use of the Ng technique, a great deal of it was first calculated with this technique, and only later generalized to cases when the Ng technique does not apply. Thus the Ng technique, and the generalization presented here, are great tools for initial exploration with simplified calculations that still apply to a broad range of scenarios.

In this short chapter, we present a version of the Ng technique for arbitrary coupling to an arbitrary field in flat spacetime. Alongside that, we have a primer on the original technique as applied to Minkowski spacetime. We will leave the extension of the technique to arbitrary couplings *and* curved spacetimes to another enterprising student.

6.1 Background: The *Ng Technique*

The *Ng technique* focuses on the expression $\mathcal{M}$,

$$\mathcal{M} = -\int \mathrm{d}t \int^{t} \mathrm{d}t' \int \mathrm{d}^{n}\boldsymbol{x} \int \mathrm{d}\boldsymbol{x}' M(t,\boldsymbol{x},t',\boldsymbol{x}') W^{\phi,|\psi\rangle}(t,\boldsymbol{x},t',\boldsymbol{x}') \tag{6.1}$$

where

$$M(t,\boldsymbol{x},t',\boldsymbol{x}') = L_{\mathrm{A}}(t,\boldsymbol{x})L_{\mathrm{B}}(t',\boldsymbol{x}') + L_{\mathrm{A}}(t',\boldsymbol{x}')L_{\mathrm{B}}(t,\boldsymbol{x}) \tag{6.2}$$

$$L_{\mu}(t,\boldsymbol{x}) = \chi_{\mu}(t-t_{\mu})F_{\mu}(\boldsymbol{x}-\boldsymbol{x}_{\mu})e^{\mathrm{i}\Omega_{\mu}t}. \tag{6.3}$$

The expressions $W^{f(\phi),|\psi\rangle}(t,\boldsymbol{x},t',\boldsymbol{x}')$ denote the two-point functions of the real scalar field ϕ in the state $|\psi\rangle$:

$$W^{\phi,|\psi\rangle}(t,\boldsymbol{x},) = \langle\psi|\,\phi(t,\boldsymbol{x})\phi(t',\boldsymbol{x}')\,|\psi\rangle \ . \tag{6.4}$$

The expression $\mathcal{M}$ is often difficult to compute due to the nested time integrals. There are at least two ways to de-nest these integrals. The first is to apply a coordinate transformation $u = t + t'$ and $v = t - t'$, as was done in [29, 2]. The second method is the *Ng technique*, which is our focus.

It was noted that Eq. (6.2) is symmetric under exchange of primed and unprimed coordinates. Next, they split the two-point correlator Eq. (6.4) into its symmetric and anti-symmetric parts, corresponding to its real and imaginary parts. Once the Wightman function was split in this way, it is possible to extend the domain of integration by application of the sign function $\varepsilon(t) = 2\Theta(t) - 1$ to the imaginary (antisymmetric) portion of the Wightman function:

$$\begin{aligned}\mathcal{M} = -\frac{1}{2}\int \mathrm{d}t \int \mathrm{d}t' \int \mathrm{d}^{n}\boldsymbol{x} \int \mathrm{d}\boldsymbol{x}' M(t,\boldsymbol{x},t',\boldsymbol{x}') \\ \times \left[Re\left(W^{\phi,|\psi\rangle}(t,\boldsymbol{x},t',\boldsymbol{x}')\right) + \mathrm{i}\varepsilon(t-t') Im\left(W^{\phi,|\psi\rangle}(t,\boldsymbol{x},t',\boldsymbol{x}')\right)\right]\end{aligned} \tag{6.5}$$

Next it was noted that the real and imaginary parts of the correlator corresponded nicely with the anti-commutator and commutator, respectively. Namely,

$$\mathcal{C}^{+}(t,\boldsymbol{x},t',\boldsymbol{x}') = 2Re\left(W^{\phi,|\psi\rangle}(t,\boldsymbol{x},t',\boldsymbol{x}')\right) \tag{6.6}$$

$$\mathcal{C}^{-}(t,\boldsymbol{x},t',\boldsymbol{x}') = 2Im\left(W^{\phi,|\psi\rangle}(t,\boldsymbol{x},t',\boldsymbol{x}')\right) \tag{6.7}$$

where C^+ and C^- are defined via

$$\mathcal{C}^+(t,\boldsymbol{x},t',\boldsymbol{x}') := \left\langle \left[\hat{\phi}(t,\boldsymbol{x}),\hat{\phi}(t',\boldsymbol{x}')\right]_+ \right\rangle_{|\psi\rangle} \tag{6.8}$$

$$\mathcal{C}^-(t,\boldsymbol{x},t',\boldsymbol{x}') := \left\langle \left[\hat{\phi}(t,\boldsymbol{x}),\hat{\phi}(t',\boldsymbol{x}')\right]_- \right\rangle_{|\psi\rangle} . \tag{6.9}$$

With this notation, we can write $2W^{\phi,|\psi\rangle}(t,\boldsymbol{x},t',\boldsymbol{x}') = \mathcal{C}^+(t,\boldsymbol{x},t',\boldsymbol{x}') + \mathrm{i}\mathcal{C}^-(t,\boldsymbol{x},t',\boldsymbol{x}')$. Furthermore, while $W^{\phi,|\psi\rangle}(t,\boldsymbol{x},t',\boldsymbol{x}')$ is not an even function, we find that integrating $W^{\phi,|\psi\rangle}(t,\boldsymbol{x},t',\boldsymbol{x}')$ over the full domain is equivalent to integrating just the symmetric part over the full domain. This allows us to recast Eq. (6.5) into the form,

$$\begin{aligned}\mathcal{M} = -\frac{1}{2}\int \mathrm{d}t \int \mathrm{d}t' \int \mathrm{d}^n\boldsymbol{x} \int \mathrm{d}\boldsymbol{x}' M(t,\boldsymbol{x},t',\boldsymbol{x}') \\ \times \left[W^{\phi,|\psi\rangle}(t,\boldsymbol{x},t',\boldsymbol{x}') + \frac{\mathrm{i}}{2}\varepsilon(t-t')\mathcal{C}^-(t,\boldsymbol{x},t',\boldsymbol{x}')\right] .\end{aligned} \tag{6.10}$$

Let us define the following convenient functions:

$$\mathcal{M}^+(\Omega_{\mathrm{A}},\Omega_{\mathrm{B}}) = -\frac{1}{2}\int \mathrm{d}^n\boldsymbol{x}\int \mathrm{d}^n\boldsymbol{x}'\int_{-\infty}^{\infty}\mathrm{d}t\int_{-\infty}^{\infty}\mathrm{d}t'\, M(\boldsymbol{x},t,\boldsymbol{x}',t',\Omega_{\mathrm{A}},\Omega_{\mathrm{B}})W^{\hat{\phi}}(\boldsymbol{x},t,\boldsymbol{x}',t') \tag{6.11}$$

$$\mathcal{M}^-(\Omega_{\mathrm{A}},\Omega_{\mathrm{B}}) = -\frac{\mathrm{i}}{2}\int \mathrm{d}^n\boldsymbol{x}\int \mathrm{d}^n\boldsymbol{x}'\int_{-\infty}^{\infty}\mathrm{d}t\int_{-\infty}^{\infty}\mathrm{d}t'\, M(\boldsymbol{x},t,\boldsymbol{x}',t',\Omega_{\mathrm{A}},\Omega_{\mathrm{B}})\epsilon(t-t')\mathrm{Im}(W^{\hat{\phi}}(\boldsymbol{x},t,\boldsymbol{x}',t')) \tag{6.12}$$

Taking the complex conjugate of $L_\mu(t,\boldsymbol{x})$ has the same effect as inverting the sign of the energy gap,

$$L_\mu^*(\Omega_\mu;t,\boldsymbol{x}) = L_\mu(-\Omega_\mu;t,\boldsymbol{x}) , \tag{6.13}$$

where now Eq. (6.3) is used:

$$L_\mu(\Omega_\mu;t,\boldsymbol{x}) = \chi_\mu(t-t_\mu)F_\mu(\boldsymbol{x}-\boldsymbol{x}_\mu)e^{\mathrm{i}\Omega_\mu t}. \tag{6.14}$$

Next make one more change to notation,

$$\mathcal{L}_{\mu\nu}[\Omega_\mu,\Omega_\nu] = \int \mathrm{d}t \int \mathrm{d}t' \int \mathrm{d}^n\boldsymbol{x} \int \mathrm{d}\boldsymbol{x}' L_\mu(\Omega_\mu;t,\boldsymbol{x})L_\nu^*(\Omega_\mu;t,\boldsymbol{x})W^{f(\phi),|\psi\rangle}(t,\boldsymbol{x},t',\boldsymbol{x}'). \tag{6.15}$$

this particular form of $\mathcal{L}_{\mu\nu}[\Omega_\mu, \Omega_\nu]$, with its explicit dependence on the detector gaps, allows us to write $\mathcal{M}^+$ as

$$\mathcal{M}^+ = -\frac{1}{2}\left(\mathcal{L}_{\mathrm{AB}}[\Omega_{\mathrm{A}}, -\Omega_{\mathrm{B}}] + \mathcal{L}_{\mathrm{BA}}[\Omega_{\mathrm{B}}, -\Omega_{\mathrm{A}}]\right) \ . \tag{6.16}$$

Of particular interest is *when the commutator vanishes*, $C^-(t, \boldsymbol{x}, t', \boldsymbol{x}') = 0$. In this case $\mathcal{M}^-$ also vanishes, so that $\mathcal{M} = \mathcal{M}^+$, and the above expression can also be used for $\mathcal{M}$.

6.2 Generalizing the *Ng Technique*

In the previous section, we assumed a linear coupling to a real scalar field. Can we break this assumption and still apply this technique?

There are good reasons for extending this result to other couplings and fields. For example, for the quadratically coupled UDW model, $\mathcal{M}$ (Eq. (1.62)) was found to be divergent, while $\mathcal{L}_{\mu\nu}$ (Eq. (1.63)) remains finite [29]. Meanwhile, the *Ng technique* indicates that the two expressions should perhaps have the same UV behaviour. This prompts the question: can the $\hat{\phi}^2$ coupling (studied in [27, 29]) have the domain extension technique from [111] applied to it, and if so, does this process illuminate the source of the divergence for the non-linear coupling, or eliminate the divergence entirely? The results of this exploration we will see in chapter 7.

Additionally, the technique in [111] seemed likely to prove fruitful when combined with recent results [28] concerning the Fermionic UDW-like detector. In fact, the first results presented on the Fermionic UDW model (presented at RQI-N 2018) relied on this method. Only later was the general version presented in chapter 4 found.

6.2.1 The General *Ng Technique*

Our starting point is the collection of expressions Eq. (1.61)-Eq. (1.68) from subsection 1.5.1, which define the detector state after interaction with an arbitrary field in an arbitrary state. In general, the detector part of the integrand of $\mathcal{M}$, given in Eq. (1.68), is symmetric under exchange of primed and un-primed coordinates. Thus, in analogy with the *Ng technique*, we would like to break up the two-point correlator $W(\boldsymbol{x}, t, \boldsymbol{x}', t')$ into a sum of symmetric and anti-symmetric parts. Note we are momentarily dropping the superscript notation for the two-point correlator.

Let us consider now that the function $f(\hat{\phi}(t,\boldsymbol{x}))$, as defined in Eq. (1.2), is clearly restricted to being self-adjoint, $f = f^\dagger$, due to its appearance in the UDW interaction Hamiltonian. Observables are self adjoint. This is important, as it allows us the identity

$$W(t,\boldsymbol{x},t',\boldsymbol{x}') = W(t',\boldsymbol{x}',t,\boldsymbol{x})^\dagger, \tag{6.17}$$

which implies precisely that the real part of $W(t,\boldsymbol{x},t',\boldsymbol{x}')$ is symmetric while its imaginary part is anti-symmetric. This simple observation allows us derive a generalization of the *Ng technique* without straying too far from the original derivation.

First, we decompose $\mathcal{M}$, defined in Eq. (1.62), into symmetric and anti-symmetric parts corresponding to the real and imaginary parts of W,

$$\begin{aligned}\mathcal{M}(\Omega_{\rm A},\Omega_{\rm B}) = -\int \mathrm{d}^n\boldsymbol{x}\int \mathrm{d}^n\boldsymbol{x}'\int_{-\infty}^{\infty}\mathrm{d}t\int_{-\infty}^{t}\mathrm{d}t'\, M(\boldsymbol{x},t,\boldsymbol{x}',t',\Omega_{\rm A},\Omega_{\rm B})\\ \left(Re(W(\boldsymbol{x},t,\boldsymbol{x}',t')) + \mathrm{i}Im(W(\boldsymbol{x},t,\boldsymbol{x}',t'))\right).\end{aligned} \tag{6.18}$$

These symmetries allow us to extend the domain of integration by use of the function $\epsilon(t-t') = 2\Theta(t-t')-1$. Furthermore, we may add a scalar multiple of the anti-symmetric part of the integral, since under the extended domain such an addition will vanish. This allows us to substitute in the function $W(\boldsymbol{x},t,\boldsymbol{x}',t')$:

$$\begin{aligned}\mathcal{M}(\Omega_{\rm A},\Omega_{\rm B}) = -\frac{1}{2}\int \mathrm{d}^n\boldsymbol{x}\int \mathrm{d}^n\boldsymbol{x}'\int_{-\infty}^{\infty}\mathrm{d}t\int_{-\infty}^{\infty}\mathrm{d}t'\, M(\boldsymbol{x},t,\boldsymbol{x}',t',\Omega_{\rm A},\Omega_{\rm B})\\ \times\left(W(\boldsymbol{x},t,\boldsymbol{x}',t') + \mathrm{i}\,\epsilon(t-t')Im(W(\boldsymbol{x},t,\boldsymbol{x}',t'))\right).\end{aligned} \tag{6.19}$$

Next decompose the expression as $\mathcal{M} = \mathcal{M}^+ + \mathcal{M}^-$, with

$$\mathcal{M}^+(\Omega_{\rm A},\Omega_{\rm B}) = -\frac{1}{2}\int \mathrm{d}^n\boldsymbol{x}\int \mathrm{d}^n\boldsymbol{x}'\int_{-\infty}^{\infty}\mathrm{d}t\int_{-\infty}^{\infty}\mathrm{d}t'\, M(\boldsymbol{x},t,\boldsymbol{x}',t',\Omega_{\rm A},\Omega_{\rm B})W(\boldsymbol{x},t,\boldsymbol{x}',t') \tag{6.20}$$

$$\mathcal{M}^-(\Omega_{\rm A},\Omega_{\rm B}) = -\frac{\mathrm{i}}{2}\int \mathrm{d}^n\boldsymbol{x}\int \mathrm{d}^n\boldsymbol{x}'\int_{-\infty}^{\infty}\mathrm{d}t\int_{-\infty}^{\infty}\mathrm{d}t'\, M(\boldsymbol{x},t,\boldsymbol{x}',t',\Omega_{\rm A},\Omega_{\rm B})\epsilon(t-t')Im(W(\boldsymbol{x},t,\boldsymbol{x}',t')) \tag{6.21}$$

Now we may finally write $\mathcal{M}^+$ in terms of $\mathcal{L}_{\rm A,B}$

$$\mathcal{M}^+(\Omega_{\rm A},\Omega_{\rm B}) = -\frac{1}{2}\left(\mathcal{L}_{\rm A,B}(-\Omega_{\rm A},\Omega_{\rm B}) + \mathcal{L}_{\rm BA}(-\Omega_{\rm B},\Omega_{\rm A})\right)\ . \tag{6.22}$$

And of course, if the function W has no anti-symmetric part, then $\mathcal{M} = \mathcal{M}^+$:

$$\mathcal{M}(\Omega_{\rm A}, \Omega_{\rm B}) = -\frac{1}{2}\left(\mathcal{L}_{\rm A,B}(-\Omega_{\rm A}, \Omega_{\rm B}) + \mathcal{L}_{\rm BA}(-\Omega_{\rm B}, \Omega_{\rm A})\right) \ . \tag{6.23}$$

Under what circumstance does $Im(W(\boldsymbol{x}, t, \boldsymbol{x}', t'))$ vanish? Actually, quite a similar one, as was shown earlier in this chapter and originally found in [111]. We will show that $Im(W(\boldsymbol{x}, t, \boldsymbol{x}', t'))$ vanishes when the expectation value of $[f, f']$ vanishes.

Consider that the imaginary part of $W(\boldsymbol{x}, t, \boldsymbol{x}', t')$ may be written $Im(W) = \frac{1}{2}(W - W^\dagger)$, so that

$$Im(W(\boldsymbol{x}, t, \boldsymbol{x}', t')) = \frac{1}{2}\Big[\, \langle\psi|\, ff' \,|\psi\rangle - \langle\psi|\, f'f \,|\psi\rangle \,\Big] \ , \tag{6.24}$$

where we have used the self-adjoint property of f. Next, we may further refine the expression:

$$Im(W(\boldsymbol{x}, t, \boldsymbol{x}', t')) = \frac{1}{2}\Big[\, \langle\psi|\, ff' - f'f \,|\psi\rangle \,\Big] \ . \tag{6.25}$$

Now we may note that the expression in the bra-ket is the commutator, $[f, f'] = ff' - f'f$. Thus we have proved the identity,

$$Im(W(\boldsymbol{x}, t, \boldsymbol{x}', t')) = \frac{1}{2}\Big\langle \Big[f, f'\Big] \Big\rangle_{|\psi\rangle} \ , \tag{6.26}$$

where the angle brakets with subscript indicates the expectation value for the state $|\psi\rangle$. From this we may conclude the function $\mathcal{M}^-$ vanishes if and only if the commutator of f vanishes, or more importantly we have proved the following:

Theorem *Let a pair of UDW detectors couple to the field with the (self-adjoint) Hamiltonian Eq. (1.2). Then the non-local term $\mathcal{M}$ in the detectors' density matrix may be written in terms of the functions $\mathcal{L}_{\rm A,B}(-\Omega_{\rm A}, \Omega_{\rm B})$, i.e.*

$$\mathcal{M}(\Omega_{\rm A}, \Omega_{\rm B}) = -\frac{1}{2}\left(\mathcal{L}_{\rm A,B}(-\Omega_{\rm A}, \Omega_{\rm B}) + \mathcal{L}_{\rm BA}(-\Omega_{\rm B}, \Omega_{\rm A})\right) \ , \tag{6.27}$$

if and only if the expectation value of the commutator of f vanishes, i.e.

$$\Big\langle \Big[f(\hat{\phi}(t, \boldsymbol{x})), f(\hat{\phi}((t', \boldsymbol{x}'))\Big] \Big\rangle_{|\psi\rangle} \ . \tag{6.28}$$

Chapter 7

Persistent Divergences in Quadratically Coupled Models?

In this section we consider a UDW-like model coupled to a complex scalar field, previously studied for the single UDW detector scenario in [27]. The motivation to study this model is two-fold. Primarily, the interest here is to establish a baseline when we compare the Bosonic and Fermionic models. When differences inevitably arise between the models, we will be interested in whether those differences arise from the analytic structure (scalar vs. spinor), the statistics (Bosonic v.s Fermionic), or the fact of the field being real or complex. Studying the real and complex scalar model may help to establish the origin of such differences. Another reason for studying the complex model is to understand the divergence that arose in [29]. Do the same persistent divergences found in the real quadratic model also appear in the complex model? This chapter answers that question.

Anticipating Fermionic Entanglement Harvesting, the UDW detector coupled quadraticaly to a scalar field was studied [29]. In that work, a new type of divergence was shown to be present in detectors coupled quadratically to a real scalar field in its vacuum state. In this chapter we will briefly describe this divergence, and potential routes toward regularization.

Analysis of the detector response function [58, 59, 60] and a number of investigations of entanglement harvesting and quantum communication with (linear) UDW detectors [32, 31, 57, 7, 61, 62, 63, 64, 19, 35] indicate that all leading order UV divergences present in the time evolution of linearly coupled UDW detectors are regularizable. While this is not the case for quadratically coupled detectors [26, 23, 24, 25], it has been shown that all persistent divergences can also be renormalized for an individual quadratically coupled

detector [27]. We will demonstrate below that a straightforward application of the leading-order prescription in [27] cannot renormalize persistent leading-order divergences in more complex scenarios with several detectors.

In this chapter, we will work toward two goals. First, we will attempt to establish a relationship between the different non-linear UDW models. Then we will relate these to the linear model. Finally, we hope to shed light on the persistent divergence of the quadratic model described in [29]. We aim to do this with the various tools we have developed up to now in this thesis.

In particular, we will relate the density matrix elements for the quadratically coupled model $f(\phi) =: \phi^2 :$ with real $\hat{\phi}$ to other quadratically coupled models, $f(\phi) =: \phi^\dagger \phi :$ with complex ϕ and $f(\phi) = \phi_1 \phi_2$ with real fields ϕ_1 and ϕ_2. This will show that the divergence found in [29] (if it is in fact a persistent divergence) is not unique to the UDW model with $f(\phi) =: \phi^2 :$. The goal of this particular project is to further understand the divergence of the quadratic model.

In a later part of this chapter we will trak back to the $f(\phi) =: \phi^2 :$ model and, inspired by the *Ng technique*, we will find expressions for the model when the detector gaps are not equal.

7.1 Divergences in Quadratically Coupled Detector Pairs

In this section, we will recall the details of the divergences discussed in [29]. In particular, we will consider the UDW detector model described in Monopole UDW Model (section 1.5) with the function f in the general interaction Hamiltonian set to $f(\hat{\phi}(\boldsymbol{x}, t)) =: \hat{\phi}(\boldsymbol{x}, t)^2 :$, i.e. the normal-ordered square of the field operator. The normal-ordering is required to renormalize the single detector model [27]. We will take the field ϕ to be in its vacuum state. The time evolved state of the detectors after interacting with the vacuum is described by the expressions

$$\mathcal{M} = -\int \mathrm{d}t \int^t \mathrm{d}t' \int \mathrm{d}^n\boldsymbol{x} \int \mathrm{d}\boldsymbol{x}' M(t, \boldsymbol{x}, t', \boldsymbol{x}') W^{:\hat{\phi}(\boldsymbol{x},t)^2:,|0\rangle}(t, \boldsymbol{x}, t', \boldsymbol{x}') \tag{7.1}$$

$$\mathcal{L}_{\mu\nu} = \int \mathrm{d}t \int \mathrm{d}t' \int \mathrm{d}^n\boldsymbol{x} \int \mathrm{d}\boldsymbol{x}' L_\mu(t, \boldsymbol{x}) L^*_\nu(t, \boldsymbol{x}) W^{:\hat{\phi}(\boldsymbol{x},t)^2:,|0\rangle}(t, \boldsymbol{x}, t', \boldsymbol{x}'). \tag{7.2}$$

It has been shown [29] that the two-point correlator of $:\phi^2:$ can be written in terms of the two-point correlator of ϕ:

$$W^{:\hat{\phi}(\boldsymbol{x},t)^2:,|0\rangle}(t,\boldsymbol{x},t',\boldsymbol{x}') = 2\left(W^{\phi(\boldsymbol{x},t):,|0\rangle}(t,\boldsymbol{x},t',\boldsymbol{x}')\right)^2 \tag{7.3}$$

Then, the expressions for $\mathcal{M}$ and $\mathcal{L}_{\mu\nu}$ can be written

$$\mathcal{M} = -2\int \mathrm{d}t \int^t \mathrm{d}t' \int \mathrm{d}^n\boldsymbol{x} \int \mathrm{d}\boldsymbol{x}' M(t,\boldsymbol{x},t',\boldsymbol{x}') \left(W^{\phi(\boldsymbol{x},t):,|0\rangle}(t,\boldsymbol{x},t',\boldsymbol{x}')\right)^2 \tag{7.4}$$

$$\mathcal{L}_{\mu\nu} = 2\int \mathrm{d}t \int \mathrm{d}t' \int \mathrm{d}^n\boldsymbol{x} \int \mathrm{d}\boldsymbol{x}' L_\mu(t,\boldsymbol{x}) L^*_\nu(t,\boldsymbol{x}) \left(W^{\phi(\boldsymbol{x},t):,|0\rangle}(t,\boldsymbol{x},t',\boldsymbol{x}')\right)^2 \ . \tag{7.5}$$

Unlike the linear model, the term $\mathcal{M}$ for the quadratically coupled model is not free of UV divergences, despite the fact that the detector has a smooth switching function and spatial smearing, and despite the renormalization process that removed the single-detector divergences. Concretely, the expression Eq. (7.1) is numerically found to be logarithmically divergent with the UV cutoff scale.

Notably, the expression Eq. (7.2) is found to converge in the UV cutoff-free limit. This is perhaps surprising in light of the *Ng technique* showing us we can write $\mathcal{M}$ in terms of $\mathcal{L}_{\mu\nu}$, with the only difference being in the sign of the energy gap.

To gain insight on the logarithmic divergence in $\mathcal{M}$, one can calculate all integrals in $\mathcal{M}$ except a single integral in the variable $q = |x - x'|$ (this integral proved rather unyielding

to analytic approaches). The full expression, labeled $G(\xi)$ is

$$\begin{aligned}
\mathrm{G}\left(q\right) \coloneqq & \frac{\sinh\left(\left(\frac{q}{T}\right)\left(|\boldsymbol{x}_{\mathrm{A}}-\boldsymbol{x}_{\mathrm{B}}|/T\right)/\left(\frac{\sigma}{T}\right)^{2}\right)}{\left(\frac{q}{T}\right)^{2}\left((\epsilon T)^{2}+\left(\frac{q}{T}\right)^{2}\right)e^{\left(\frac{q}{T}\right)^{2}/\left(2\left(\frac{\sigma}{T}\right)^{2}\right)}}\Bigg[-4\left(\frac{q}{T}\right)\left(\sqrt{2\pi}(\epsilon T)^{2}-2\mathrm{i}\epsilon T+\sqrt{2\pi}\left(\frac{q}{T}\right)^{2}\right) \\
& +\frac{(\epsilon T)^{2}+\left(\frac{q}{T}\right)^{2}}{e^{\left(\frac{q}{T}\right)^{2}/2}}\Bigg(\Bigg[\mathrm{Chi}\left(\frac{(\epsilon T+\mathrm{i}\left(\frac{q}{T}\right))^{2}}{2}\right)+\mathrm{i}\pi\,\mathrm{erf}\left(\frac{\epsilon T+\mathrm{i}\left(\frac{q}{T}\right)}{\sqrt{2}}\right)+2\log\left(\frac{\left(\frac{q}{T}\right)-\mathrm{i}\epsilon T}{(\epsilon T+\mathrm{i}\left(\frac{q}{T}\right))^{2}}\right) \\
& \quad -\mathrm{Shi}\left(\frac{1}{2}(\epsilon T+\mathrm{i}\left(\frac{q}{T}\right))^{2}\right)\Bigg]2\mathrm{i}e^{\frac{1}{2}\epsilon T(\epsilon T+2\mathrm{i}\left(\frac{q}{T}\right))}\left(\epsilon T\left(\frac{q}{T}\right)+\mathrm{i}\left(\left(\frac{q}{T}\right)^{2}+1\right)\right) \\
& \quad +e^{\frac{1}{2}\epsilon T(\epsilon T-2\mathrm{i}\left(\frac{q}{T}\right))}\Bigg[2\left(\mathrm{i}\epsilon T\left(\frac{q}{T}\right)+\left(\frac{q}{T}\right)^{2}+1\right)\mathrm{Chi}\left(\frac{1}{2}(\epsilon T-\mathrm{i}\left(\frac{q}{T}\right))^{2}\right) \\
& \quad +\log\left(-(\epsilon T-\mathrm{i}\left(\frac{q}{T}\right))^{2}\right)+4\left(\mathrm{i}\epsilon T\left(\frac{q}{T}\right)+\left(\frac{q}{T}\right)^{2}+1\right)\log(-\left(\frac{q}{T}\right)-\mathrm{i}\epsilon T) \\
& \quad -2\log(\left(\left(\frac{q}{T}\right)+\mathrm{i}\epsilon T\right)(\epsilon T-\mathrm{i}\left(\frac{q}{T}\right))^{2}\Big)-2\mathrm{i}\left(\frac{q}{T}\right)(\epsilon T-\mathrm{i}\left(\frac{q}{T}\right))\log\left((\epsilon T-\mathrm{i}\left(\frac{q}{T}\right))^{2}\right) \\
& \quad +2\left(-\mathrm{i}\epsilon T\left(\frac{q}{T}\right)-\left(\frac{q}{T}\right)^{2}-1\right)\mathrm{Shi}\left(\frac{1}{2}(\epsilon T-\mathrm{i}\left(\frac{q}{T}\right))^{2}\right) \\
& \quad +2\pi\left(-\epsilon T\left(\frac{q}{T}\right)+\mathrm{i}\left(\left(\frac{q}{T}\right)^{2}+1\right)\right)\mathrm{erf}\left(\frac{\epsilon T-\mathrm{i}\left(\frac{q}{T}\right)}{\sqrt{2}}\right)\Bigg]\Bigg)\Bigg],
\end{aligned} \tag{7.6}$$

where Shi and Chi are defined as

$$\mathrm{Shi}(z) := \int_{0}^{z}\frac{\sinh(t)}{t}\mathrm{d}t \tag{7.7}$$

$$\mathrm{Chi}(z) := \gamma+\log(z)+\int_{0}^{z}\left(\cosh(t)-1\right)\mathrm{d}t \tag{7.8}$$

where γ is Euler's constant. We will now briefly recount the behaviour of this integrand in the limit of no UV cutoff. It was also shown that $G(q)$ has the following limiting behaviour:

$$\lim_{\epsilon\to 0}G(q)=\frac{4}{q^{2}}e^{-\frac{\left(\sigma^{2}+T^{2}\right)}{2\sigma^{2}q^{-2}}}\sinh\left(\frac{q|\boldsymbol{x}_{\mathrm{A}}-\boldsymbol{x}_{\mathrm{B}}|}{\sigma^{2}}\right)\left[-\sqrt{2\pi}e^{\frac{q^{2}}{2T^{2}}}qT+\mathrm{i}\pi\left(q^{2}+T^{2}\right)\mathrm{erfc}\left(\frac{\mathrm{i}q}{\sqrt{2T}}\right)\right], \tag{7.9}$$

where Erfc is defined via

$$\mathrm{Erfc}(z)=1-\mathrm{Erf}(z). \tag{7.10}$$

Furthermore, ϵ controls the UV cutoff with $\epsilon \to 0$ corresponding to no cutoff. T is the switching time of the detector, σ is the size of the detector, $|\boldsymbol{x}_{\mathrm{A}} - \boldsymbol{x}_{\mathrm{B}}|$ is the spatial distance between detectors, and it is assumed that the detectors are switched on simultaneously.

The leading order term in the Laurent series of $G(q)$ is order $\mathcal{O}(q^{-1})$,

$$\lim_{\epsilon \to 0} G \sim \frac{4\mathrm{i}\pi |\boldsymbol{x}_{\mathrm{A}} - \boldsymbol{x}_{\mathrm{B}}| T^2}{\sigma^2 q} \ , \tag{7.11}$$

which will dominate the expression $\lim_{\epsilon \to 0} G(q)$ for large q. Thus the expression (7.9) diverges as $1/q$ as $q \to 0$. Recall that the variable q has units of length, thus $q \to 0$ is associated with the UV regime. Numerical analysis shown in [29] supports the analysis that the divergence is logarithmic in ϵ.

This divergence is peculiar due to the fact that it shows up only in the two-detector model, in spite of the fact that the vacuum excitation probability for a single quadratic detector is finite [27]. Thus, while a single quadratically coupled detector does not require additional UV regularization, a cutoff is required for certain quantities describing detector pairs, namely $\mathcal{M}$ Eq. (7.1).

7.2 Bilinear coupling to real fields

We will utilize the general UDW Hamiltonian Eq. (1.2), particularized to what we will call a "bilinear" coupling. We define this coupling by setting $f(\phi) = \phi_1 \phi_2$ with ϕ_i both real. The time evolved state, derived for the general case in section 1.5, is given by the density matrix Eq. (1.61) with elements

$$\mathcal{M} = -\lambda_{\mathrm{A}} \lambda_{\mathrm{B}} \int_{-\infty}^{\infty} \mathrm{d}t \int_{-\infty}^{t} \mathrm{d}t' \int \mathrm{d}^n \boldsymbol{x} \int \mathrm{d}^n \boldsymbol{x}' \, M(t, \boldsymbol{x}, t', \boldsymbol{x}') W^{\phi_1 \phi_2, |\psi\rangle}(t, \boldsymbol{x}, t', \boldsymbol{x}') \tag{7.12}$$

$$\mathcal{L}_{\mu\nu} = \lambda_\nu \lambda_\mu \int_{-\infty}^{\infty} \mathrm{d}t \int_{-\infty}^{\infty} \mathrm{d}t' \int \mathrm{d}^n \boldsymbol{x} \int \mathrm{d}^n \boldsymbol{x}' \, L_\mu^*(t, \boldsymbol{x}) \, L_\nu(t', \boldsymbol{x}') \, W^{\phi_1 \phi_2, |\psi\rangle}(t, \boldsymbol{x}, t', \boldsymbol{x}') \tag{7.13}$$

$$\mathcal{L}_\mu = -\mathrm{i} \int \mathrm{d}t \int \mathrm{d}^n \boldsymbol{x} L_\mu(t, \boldsymbol{x}) Y^{\phi_1 \phi_2, |\psi\rangle}(t, \boldsymbol{x}), \tag{7.14}$$

where M and L_μ are defined as in Eq. (1.67) andEq. (1.68).

If the fields ϕ_1 and ϕ_2 are in a product of pure states, then the expression for W

$$W^{\phi_1 \phi_2, |\psi\rangle}(t, \boldsymbol{x}, t', \boldsymbol{x}') := \langle \psi | \, \hat{\phi}_1(\boldsymbol{x}, t) \hat{\phi}_2(\boldsymbol{x}, t) \hat{\phi}_1(\boldsymbol{x}', t') \hat{\phi}_2(\boldsymbol{x}', t') \, | \psi \rangle \ , \tag{7.15}$$

can be further refined:

$$W^{\phi_1\phi_2,|\psi_1\rangle\otimes|\psi_2\rangle}(t,\boldsymbol{x},t',\boldsymbol{x}') = \langle\psi_1|\,\hat{\phi}_1(\boldsymbol{x},t)\hat{\phi}_1(\boldsymbol{x}',t')\,|\psi_1\rangle\,\langle\psi_2|\,\hat{\phi}_2(\boldsymbol{x},t)\hat{\phi}_2(\boldsymbol{x}',t')\,|\psi_2\rangle\ . \tag{7.16}$$

In particular, if ψ_1 and ψ_2 are in their respective vacuum states, then

$$W^{\phi_1\phi_2,|0\rangle\otimes|0\rangle}(t,\boldsymbol{x},t',\boldsymbol{x}') = \left(W^{\phi,|0\rangle}(t,\boldsymbol{x},t',\boldsymbol{x}')\right)^2\ . \tag{7.17}$$

This allows for us to rewrite Eq. (7.12) as

$$\mathcal{M} = -\,\lambda_{\text{A}}\lambda_{\text{B}}\int_{-\infty}^{\infty}\!\mathrm{d}t\int_{-\infty}^{t}\!\mathrm{d}t'\int\mathrm{d}^n\boldsymbol{x}\int\mathrm{d}^n\boldsymbol{x}'\,L_\mu(t,\boldsymbol{x})L_\nu(t',\boldsymbol{x}')\,\left(W^{\phi,|0\rangle}(t,\boldsymbol{x},t',\boldsymbol{x}')\right)^2\ , \tag{7.18}$$

which can be compared directly to Eq. (7.4). We find that

$$\mathcal{M}^{\phi_1\phi_2,|0\rangle\otimes|0\rangle} = \frac{1}{2}\mathcal{M}^{:\phi^2:,|0\rangle}, \tag{7.19}$$

where the superscript indicates the coupling and state of the field as it does for W.

From Eq. (7.19) we infer that the bilinear coupling exhibits the same singular behaviour as the quadratic model studied in [29].

7.3 Complex field quadratic coupling

We now turn our attention to the UDW detector interacting with the vacuum of a complex scalar field. The simplest self-adjoint UDW Hamiltonian that maintains $U(1)$ symmetry can be found by setting

$$f(\hat{\Phi}(\boldsymbol{x},t)) =: \hat{\Phi}(\boldsymbol{x},t)\hat{\Phi}^\dagger(\boldsymbol{x},t)\,: \tag{7.20}$$

in the the general UDW Hamiltonian Eq. (1.2).

In appendix 1, we relate the two-point correlators of the real and complex fields in their respective vacua, and find

$$W^{:\Phi\Phi^\dagger:}(t,\boldsymbol{x},t',\boldsymbol{x}') = \left(\langle 0|\,\hat{\Phi}(\boldsymbol{x},t)\hat{\Phi}^\dagger(\boldsymbol{x}',t')\,|0\rangle\right)^2.$$

Applying this relation to the general form of the time-evolved UDW model Eq. (1.61), and further taking the field to be in its vacuum state, we find

$$\mathcal{M} = -\lambda_{\mathrm{A}}\lambda_{\mathrm{B}} \int_{-\infty}^{\infty}\mathrm{d}t \int_{-\infty}^{t}\mathrm{d}t' \int \mathrm{d}^d\boldsymbol{x} \int \mathrm{d}^d\boldsymbol{x}'\, M(t,\boldsymbol{x},t',\boldsymbol{x}') \left(W^{\phi}(t,\boldsymbol{x},t',\boldsymbol{x}')\right)^2 \tag{7.21}$$

$$\mathcal{L}_{\gamma\nu} = \lambda_\nu\lambda_\mu \int_{-\infty}^{\infty}\mathrm{d}t \int_{-\infty}^{\infty}\mathrm{d}t' \int \mathrm{d}^d\boldsymbol{x} \int \mathrm{d}^d\boldsymbol{x}'\, L^*_\gamma(t,\boldsymbol{x})\, L_\nu(t',\boldsymbol{x}') \left(W^{\phi}(t,\boldsymbol{x},t',\boldsymbol{x}')\right)^2 . \tag{7.22}$$

We can immediately see that the UDW density matrix elements shown here have the same form as the bilinear model, Eq. (7.18), such that we can compare it directly to Eq. (7.4). We find that

$$\mathcal{M}^{:\Phi^\dagger\Phi:,|0\rangle} = \mathcal{M}^{\phi_1\phi_2,|0\rangle\otimes|0\rangle} = \frac{1}{2}\mathcal{M}^{:\phi^2:,|0\rangle}, \tag{7.23}$$

where the superscript indicates the coupling and state of the field, ϕ are real fields and Φ is complex. Furthermore, where the quadratic model studied in [29] exhibits a divergence, so too does this model.

7.4 Relationship to the linear model

Much like the Fermionic and real, linear models can be related for point-like detectors, the three models we just studied can also be related to the real linear model.

First let us recall the two-point correlator for the linear coupling Eq. (64).

$$W^{\phi,|0\rangle}(t,\boldsymbol{x},t'\boldsymbol{x}') = \begin{cases} \dfrac{\Gamma\left(\frac{d}{2}-1\right)}{4\pi^{d/2}\left(z(t,\boldsymbol{x},,t',\boldsymbol{x}')\right)^{d-2}} & \text{for } d>2, \\ -(2\pi)^{-1}\ln\left(\Lambda z(t,\boldsymbol{x},,t',\boldsymbol{x}')\right) & \text{for } d=2, \end{cases}$$

where

$$z(t,\boldsymbol{x},,t',\boldsymbol{x}') := \sqrt{(\boldsymbol{x},-\boldsymbol{x},)^2-(t-t'-i\epsilon)^2}. \tag{7.24}$$

Applying this expression to the quadratic two-point function Eq. (7.3), we find

$$W^{:\hat{\phi}^2:,|0\rangle}(t,\boldsymbol{x},t',\boldsymbol{x}') = \frac{\left(\Gamma\left(\frac{d}{2}-1\right)\right)^2}{8\pi^d}\frac{1}{z(t,\boldsymbol{x},,t',\boldsymbol{x}')^{2d-4}}. \tag{7.25}$$

Next, we note the power of z is the same as it would be for the linear coupling in $2d-2$ dimensions. Therefore,

$$W^{:\hat{\phi}^2:,d}(t,\boldsymbol{x},t',\boldsymbol{x}') = \frac{\left(\Gamma\left(\frac{d}{2}-1\right)\right)^2}{2\pi\Gamma\left(d-2\right)} W^{\phi,2d-2}, \tag{7.26}$$

where we have dropped the notation indicating we are working in the vacuum and picked up (superscript) notation indicating the dimension of the spacetime in which each field resides.

Applying this expression to the density matrix elements for the quadratically coupled model Eq. (7.1)-(7.2) and taking the detectors to be point-like (spatial spearking becomes $F(\boldsymbol{x}) = \delta(\boldsymbol{x})$), it is straightforward to show that

$$\mathcal{M}^{:\hat{\phi}^2:,d} = \frac{\left(\Gamma\left(\frac{d}{2}-1\right)\right)^2}{2\pi\Gamma\left(d-2\right)} \mathcal{M}^{\hat{\phi},2d-2} \tag{7.27}$$

$$\mathcal{L}_{\mu\nu}^{:\hat{\phi}^2:,d} = \frac{\left(\Gamma\left(\frac{d}{2}-1\right)\right)^2}{2\pi\Gamma\left(d-2\right)} \mathcal{L}_{\mu\nu}^{\hat{\phi},2d-2}. \tag{7.28}$$

Furthermore, from Eq. (7.23) and Eq. (7.19), nearly the same identity holds for both the complex and bilinear models. The only difference is a factor of 2. The identity for the complex model is

$$\mathcal{M}^{:\hat{\Phi}^\dagger\hat{\Phi}:,d} = \frac{\left(\Gamma\left(\frac{d}{2}-1\right)\right)^2}{\pi\Gamma\left(d-2\right)} \mathcal{M}^{\hat{\phi},2d-2} \tag{7.29}$$

$$\mathcal{L}_{\mu\nu}^{:\hat{\Phi}^\dagger\hat{\Phi}:,d} = \frac{\left(\Gamma\left(\frac{d}{2}-1\right)\right)^2}{\pi\Gamma\left(d-2\right)} \mathcal{L}_{\mu\nu}^{\hat{\phi},2d-2}, \tag{7.30}$$

while the same identity for the bilinear model can be written

$$\mathcal{M}^{\phi_1\phi_2,d} = \frac{\left(\Gamma\left(\frac{d}{2}-1\right)\right)^2}{\pi\Gamma\left(d-2\right)} \mathcal{M}^{\hat{\phi},2d-2} \tag{7.31}$$

$$\mathcal{L}_{\mu\nu}^{\phi_1\phi_2,d} = \frac{\left(\Gamma\left(\frac{d}{2}-1\right)\right)^2}{\pi\Gamma\left(d-2\right)} \mathcal{L}_{\mu\nu}^{\hat{\phi},2d-2}. \tag{7.32}$$

From these expressions follow similar identities for the Negativity and Mutual information (similar to Eq. (4.12) and Eq. (4.9)).

Note that these expressions only hold in the vacuum and only for point-like detectors.

7.5 Discussion

In this section, we will analyze and compare the results derived from the four models in the previous section. Relying on the previous study [29], we will draw conclusions about the divergent behaviour (if any) of the models' predictions, considering in particular *persistent* divergences in the correlation terms. Then, we will discuss the nature of the divergences as they relate to distribution theory and operator algebras, which will also have bearing on possible regularization schemes.

Before further discussion, however, we would like to note that we do not consider the persistent divergence to be physical. Rather, we assume it to be a mathematical or model artifact that can be potentially resolved via, for example, a suitable regularization or renormalization scheme or by careful attention being paid to the commutation properties of the operations used in calculations.

The first observation we make is simple. Recall from Eq. (7.23) that the forms of $\mathcal{M}$ for the bilinear and complex models are precisely the same and differ from that of the real quadratic model by a constant factor. Thus in any case where the real quadratic model presents persistent divergences, so too will the complex and bilinear models. Concretely, these models will exhibit the same persistent divergences as the quadratically coupled detector model studied in [29]. This will lead to divergent negativity unless further regularization schemes are employed or a satisfactory renormalization technique is found. Furthermore, we can conclude that the regularization methods or renormalization techniques used to tame the divergences for the quadratic model should work equally well for the complex scalar field.

In addition to illustrating parallel divergences in all of the quadratic models studied here, we also find that entanglement harvesting from a complex field is less efficient by a factor of two than from a real field if both models utilize quadratic coupling. One could also study the hierarchy of entanglement harvesting efficiency, where harvesting from a complex field or bilinear real fields is less efficient than from a detector coupled quadratically to a real field. If the persistent divergence exhibited in the quadratic models is regularized, the linear model can enter the hierarchy. It is presumed that it will be the most efficient based on the higher mutual information that can be extracted from the linear model [29], but this is still an open question.

Our final observation is about the nature of the higher-order multi-linear interactions, which was left out of this thesis but is simple to show (and is in [2]). Simply put, if the UDW model couples to n scalar fields in their respective vacua, then the two-point

correlator will be the n-th power of the Wightman function:

$$W^{\prod_i \phi_i, \prod_i |0\rangle_i} = \left(W^{\phi, |0\rangle}\right)^n \ . \tag{7.33}$$

Considering that the linear interaction is free of persistent divergences and the bi-linear case has been shown to exhibit persistent divergences, it might be that we can appeal to the distributional nature of the Wightman function to understand the divergence; the only difference between the two is the power to which the Wightman funciton is raised. However, it should be noted that the single detector quadratically coupled model is free of persistent divergences as well as the $\mathcal{L}_{\mu\nu}$ term of the quadratic model, both of which contain terms quadratic in the Wightman function.

We have not yet answered the question of whether the multi-linear models with more than two fields exhibit persistent divergences, but it is productive to point out that, even for the quadratic model, it might perhaps be surprising that *any* of the density matrix elements of the quadratic models are convergent at all. This is because the role that the Wightman function plays for a linear detector in the detector's matrix elements is played by *products* of Wightman functions in the quadratic and bilinear cases. However, the Wightman function is a distribution, and the product of two distributions that are well-defined in a reasonable test space is not guaranteed to be a well-defined distribution on the same space.

Finally, another way of looking at this issue of divergences is via considering algebras of operators. Smeared field operators are well-defined objects [112]. However, a smeared *product* of field operators (as we see in the quadratic models studied in this paper) is not, a-priori, a well-defined object in the algebra of field operators. One method to give the quadratic Hamiltonian a well-defined interpretations is as a limit of well-defined non-local Hamiltonians, as in

$$\int \mathrm{d}y \int \mathrm{d}x F(\boldsymbol{x}) \hat{\phi}(\boldsymbol{x}) G_\delta(\boldsymbol{y} - \boldsymbol{x}) \hat{\phi}(\boldsymbol{y}) \ , \tag{7.34}$$

where $G_\delta(\boldsymbol{x})$ is a nascent delta distribution. This technique is known as point-splitting, and as yet we have not explored its effectiveness on these various singular quadratic models.

A more intriguing alternative regularization scheme might exploit recent work [111] demonstrating that for general spacetimes and spacelike-separated pairs of detectors following arbitrary timelike trajectories, it is possible to de-nest the nested integrals in $\mathcal{M}$ and write them as functions of slightly-altered $\mathcal{L}_{\gamma\nu}$. Since all functions $\mathcal{L}_{\gamma\nu}$ for pairs of quadratically coupled detectors have been found to be free of persistent divergences, it may be possible regularize the quadratic models through analyzing this de-nesting process.

It has been pointed out that altogether different techniques could help, and so we briefly discuss the use of a smooth approximation to the theta function as well as the position-space approach as in Scharf's book in section Regularizing the Heaviside,

A final, perhaps more elegant, regularization scheme (still different from a UV cutoff) is applying *multiple smearings*, one for each instance of the field operator in the interaction Hamiltonian. Under this regularization scheme, the smeared field operators would be rigorously defined in terms of operator algebras. More concretely, every field operator appearing in the Hamiltonian is smeared under an integral separately. For example, instead of a multi-linear Hamiltonian,

$$\hat{H}(t) = \sum_{\gamma\in\{A,B\}} \int \mathrm{d}^d\boldsymbol{x} \hat{D}_\gamma(\boldsymbol{x},t) \prod_{i=1}^{n} \hat{\phi}_i(\boldsymbol{x},t) \ , \tag{7.35}$$

one could use the following multiply-smeared detector model,

$$\hat{H}(t) = \sum_{\gamma\in\{A,B\}} \hat{D}_\gamma(t) \prod_{i=1}^{n} \int \mathrm{d}^d\boldsymbol{x}_i \, F_{i,\gamma}(\boldsymbol{x}_i) \, \hat{\phi}_i(\boldsymbol{x}_i,t), \tag{7.36}$$

where $F_{i,\gamma}$ is the smearing associated with the ith field and the detector γ. This particular idea has yet to be worked out.

Finally, the last possibility is that the divergence exhibited by these models is spurious and due to the order integration applied, and the form of the integrals when the author resorted to numerical study. There are a few factors pointing toward this being the case.

First, in some cases, the term $\mathcal{M}$ can be related to $\mathcal{L}_{\mu\nu}$ with a modified energy gap. Since the divergence in $\mathcal{M}$ for the non-linear models does not show up in $\mathcal{L}_{\mu\nu}$, the divergence could be related to the assumption that the detector gaps are equal, which was used in the study which showed convergence.

The next interesting fact to note is that, for the point-like model, we can equate any of the non-linear models to the linear model in a different spacetime dimension. In particular, the (supposedly divergent) $d = 4$ dimensional quadratic model should be equivalent (up to a finite, constant geometric factor) to the linear model in 6 spacetime dimensions. The linear UDW model in $d = 6$ spacetime dimensions remains finite for stationary trajectories. Therefore, we begin to question the need for renormalization and instead look toward the possibility of non-commuting limits. However, more study is required to determine which, if any of these is at the heart of the apparently divergent model.

Chapter 8

Conclusion

In Non-linear Optics with a UDW Detector (chapter 2) and Fundamental Decoherence in Optical Cavities (chapter 3) we explored the application of the UDW model to the domain of quantum optics. In particular, we showed that the quadratic model can capture known features of non-linear quantum optics: sum frequency generation and difference frequency generation. We also established new results: the fundamental interaction of the electron and electromagnetic fields may cause unavoidable decoherence in optical cavities. However, at the same time we were able to relate the quadratic UDW model to the usual linear model in a different number of spacetime dimensions, potentially pointing to some interesting connections between coupling and dimension. A clear route forward for the work on decoherence would be to refine the numerical methods applied to the matrix coefficients A and B of the model, or to employ approximate methods to estimate the magnitude of this effects relative to other known effects. An interesting avenue forward would be to find states which maximize or minimize the decoherence effects of this fundamental interaction. Another interesting problem would be to do a full QED calculation, or to employ the scalar-coupled Dirac UDW model, to explore any refinements that can be made to the model. Regarding the results in this work that apply to quantum optics, an obvious line of inquiry is that of seeing if UDW-like models can capture any other known effects from non-linear optics, such as self focusing, third harmonic generation, and stimulated Brillouin scattering and many others [113].

The relation between the linear model and non-standard couplings goes beyond the quadratic coupling to a real field. In Fermionic Entanglement Harvesting (chapter 4), we showed that the coupling to the scalar density of a Fermionic field in d spacetime dimensions can be related back to the linear coupling in $2d$ spacetime dimensions. This result allows one to understand the entanglement structure of the Fermionic field just by looking at

the (much simpler to compute) real scalar field. Moving forward, an immediate goal for building on this result would be to expand our knowledge of non-point-like detectors. Furthermore, this result presents exciting opportunities to broaden our understanding of the fermionic vacuum. Future work includes exploring the entangling properties of non-vacuum states of the Fermionic field, applying this Fermionic model to the question of optical decoherence, or even expanding the repertoire of UDW-like models to include a vector coupling to a Fermionic field.

Perhaps the most exciting prospect to emerge from this thesis is the possibility of entanglement harvesting in the lab. The work in UDW pairs with Modified Dispersion (chapter 5) has laid the foundations for such an investigation. Indeed, the robustness of entanglement harvesting to dispersion indicates that the basic effects of the protocol should be simulable in the laboratory for large detectors that are not separated by a distance much larger than the detector size. There are a number promising routes toward avenues of exploration from this work. The use of the Gaussian formalism[22], which utilizes a harmonic oscillator detector, would be a step towards aligning theoretical calculations more closely with the experimental proposals for UDW-like detectors. Indeed, an oscillator detector model would be more in line with the interferometric detector proposed in [97]. In fact, another clear route forward is to to alter the proposed experimental setup to incorporate a second detector to do entanglement harvesting.

In Techniques in Harvesting (chapter 6), we extended a technique by Ng to arbitrary UDW field-couplings. An additional avenue of research would be to pursue this extension to arbitrary curved spacetimes as well, which should be a rather straightforward calculation.

Finally, in Persistent Divergences in Quadratically Coupled Models? (chapter 7) we showed that the three non-linear models studied are equivalent up to a constant factor, regardless of the detector smearing function or other detector parameters used for the comparison. Additionally, we showed that, for the point-like spatial profile, these models (in d dimensions) can be written in terms of the linear model (in $d-2$ dimensions), times a geometric factor. That discussion of the persistent divergences also addressed a divergence exhibited by pairs of quadratically coupled detectors, which presents an ongoing research question. Future work on these models includes tackling the various potential regularization schemes outlined at the end of that chapter. Expanding our focus to also include the mapping of the Fermionic mode to the linear model, we highlight the fact that we were able to write all fields and coupling types that we studied (linear, quadratic, bilinear, fermionic etc) in terms of the linear UDW model. This was achieved via various manipulations of the Wightman function, generally via applications of Wick's theorem. Is it possible to prove, via Wick's theorem, that this connection is possible to prove for arbitrary UDW couplings? This connection bears scrutinizing, and is a potential well of

future work.

Bibliography

[1] Erickson Tjoa, Irene López Gutiérrez, Allison Sachs, and Eduardo Martín-Martínez. What makes a particle detector click, 2021.

[2] Allison M Sachs, Robert B Mann, and Eduardo Martin-Martinez. Entanglement harvesting from multiple massless scalar fields and divergences in unruh-dewitt detector models. *arXiv preprint arXiv:1808.05980*, 2018.

[3] S Carlip. Quantum gravity: a progress report. *Reports on Progress in Physics*, 64(8):885–942, jul 2001.

[4] Matthew D. Schwartz. *Quantum Field Theory and the Standard Model*. Cambridge University Press, 3 2014.

[5] Pasquale Calabrese and John Cardy. Entanglement entropy and quantum field theory: a non-technical introduction, May 2005.

[6] Astrid Lambrecht. The casimir effect: a force from nothing. *Physics World*, 15(9):29–32, sep 2002.

[7] Alejandro Pozas-Kerstjens and Eduardo Martín-Martínez. Harvesting correlations from the quantum vacuum. *Phys. Rev. D*, 92:064042, Sep 2015.

[8] Masahiro Hotta, Jiro Matsumoto, and Go Yusa. Quantum energy teleportation without a limit of distance. *Phys. Rev. A*, 89:012311, Jan 2014.

[9] L C Barbado, C Barceló, and L J Garay. Hawking radiation as perceived by different observers. *Classical and Quantum Gravity*, 28(12):125021, may 2011.

[10] William G Unruh and Robert M Wald. Information loss. *Reports on Progress in Physics*, 80(9):092002, jul 2017.

[11] M. J. Jacquet, S. Weinfurtner, and F. König. Experimental black-hole evaporation? *Phil. Trans. R. Soc.*, 378:0239, August 2020.

[12] Papageorgiou, Maria-Eftychia. What is a field, what is a particle?...what about algebras? Master's thesis, University of Waterloo, 2019.

[13] HRVOJE NIKOLIĆ. Inappropriateness of the rindler quantization. *Modern Physics Letters A*, 16(09):579–581, 2001.

[14] Valerio Faraoni. Evolving black hole horizons in general relativity and alternative gravity. *Galaxies*, 1(3):114–179, 2013.

[15] W. G. Unruh. Notes on black-hole evaporation. *Phys. Rev. D*, 14:870–892, Aug 1976.

[16] Bryce Seligman DeWitt. Quantum gravity: The new synthesis. In S. W. Hawking and W. Israel, editors, *General Relativity: An Einstein Centenary Survey*, page 680. Cambridge University Press, 1979.

[17] K J Hinton. Particle detectors in rindler and schwarzchild space-times. *Journal of Physics A: Mathematical and General*, 16(9):1937–1946, jun 1983.

[18] Katherine Freese, Christopher T. Hill, and Mark Mueller. Covariant functional schrödinger formalism and application to the hawking effect. *Nuclear Physics B*, 255:693–716, 1985.

[19] Alejandro Pozas-Kerstjens and Eduardo Martín-Martínez. Entanglement harvesting from the electromagnetic vacuum with hydrogenlike atoms. *Phys. Rev. D*, 94:064074, Sep 2016.

[20] Eduardo Martín-Martínez and Pablo Rodriguez-Lopez. Relativistic quantum optics: The relativistic invariance of the light-matter interaction models. *Physical Review D*, 97(10):105026, 2018.

[21] Petar Simidzija, Robert H. Jonsson, and Eduardo Martín-Martínez. General no-go theorem for entanglement extraction. *Phys. Rev. D*, 97:125002, Jun 2018.

[22] Eric G. Brown, Eduardo Martín-Martínez, Nicolas C. Menicucci, and Robert B. Mann. Detectors for probing relativistic quantum physics beyond perturbation theory. *Phys. Rev. D*, 87:084062, Apr 2013.

[23] K J Hinton. Particle detector equivalence. *Classical Quant. Grav.*, 1(1):27, 1984.

[24] Shin Takagi. On the response of a rindler particle detector. iii. *Prog. Theor. Phys.*, 74(3):501–510, 1985.

[25] Shin Takagi. Vacuum noise and stress induced by uniform acceleration: Hawking-unruh effect in rindler manifold of arbitrary dimension. *Prog. Theor. Phys. Supp.*, 88:1–142, 1986.

[26] B R Iyer and A Kumar. Detection of dirac quanta in rindler and black hole spacetimes and the xi quantisation scheme. *Journal of Physics A: Mathematical and General*, 13(2):469, 1980.

[27] Daniel Hümmer, Eduardo Martín-Martínez, and Achim Kempf. Renormalized unruh-dewitt particle detector models for boson and fermion fields. *Phys. Rev. D*, 93:024019, Jan 2016.

[28] Jorma Louko and Vladimir Toussaint. Unruh-dewitt detector's response to fermions in flat spacetimes. *Phys. Rev. D*, 94(6):064027, Sep 2016.

[29] Allison Sachs, Robert B. Mann, and Eduardo Martín-Martínez. Entanglement harvesting and divergences in quadratic unruh-dewitt detector pairs. *Phys. Rev. D*, 96:085012, Oct 2017.

[30] L. Parker and D. Toms. *Quantum Field Theory in Curved Spacetime: Quantized Fields and Gravity*. Cambridge Monographs on Mathematical Physics. Cambridge University Press, 2009.

[31] Benni Reznik. Entanglement from the vacuum. *Foundations of Physics*, 33(1):167–176, 2003.

[32] Antony Valentini. Non-local correlations in quantum electrodynamics. *Physics Letters A*, 153(6):321–325, 1991.

[33] Stephen J. Summers and Reinhard Werner. The vacuum violates bell's inequalities. *Physics Letters A*, 110(5):257 – 259, 1985.

[34] S. J. Summers and R. Werner. Maximal violation of bell's inequalities is generic in quantum field theory. *Comm. Math. Phys.*, 110, 1987.

[35] Grant Salton, Robert B Mann, and Nicolas C Menicucci. Acceleration-assisted entanglement harvesting and rangefinding. *New J. Phys.*, 17(3):035001, 2015.

[36] Eric G. Brown. Thermal amplification of field-correlation harvesting. *Phys. Rev. A*, 88:062336, Dec 2013.

[37] Petar Simidzija and Eduardo Martín-Martínez. All coherent field states entangle equally. *Phys. Rev. D*, 96:025020, Jul 2017.

[38] Petar Simidzija and Eduardo Martín-Martínez. Harvesting correlations from thermal and squeezed coherent states. *Phys. Rev. D*, 98:085007, Oct 2018.

[39] Shingo Kukita and Yasusada Nambu. Harvesting large scale entanglement in de sitter space with multiple detectors. *Entropy*, 19(9), 2017.

[40] Eduardo Martín-Martínez, Eric G. Brown, and and Achim Kempf William Donnelly. Sustainable entanglement production from a quantum field. *Phys. Rev. A*, 88:052310, Nov 2013.

[41] Greg Ver Steeg and Nicolas C. Menicucci. Entangling power of an expanding universe. *Phys. Rev. D*, 79:044027, Feb 2009.

[42] Keith K. Ng, Robert B. Mann, and Eduardo Martín-Martínez. Over the horizon: Distinguishing the schwarzschild spacetime and the $\mathbb{RP}^3$ spacetime using an unruh-dewitt detector. *Phys. Rev. D*, 96:085004, Oct 2017.

[43] Eduardo Martín-Martínez, Alexander R. H. Smith, and Daniel R. Terno. Spacetime structure and vacuum entanglement. *Phys. Rev. D*, 93:044001, Feb 2016.

[44] M.A. Srednicki. *Quantum Field Theory*. Cambridge University Press, 2007.

[45] Alejandro Pozas-Kerstjens, Jorma Louko, and Eduardo Martín-Martínez. *Degenerate detectors are unable to harvest spacelike entanglement*. To appear in Phys. Rev. D - arXiv:1703.02982, 2017.

[46] Grant Salton, Robert B Mann, and Nicolas C Menicucci. Acceleration-assisted entanglement harvesting and rangefinding. *New J. Phys.*, 17(035001), 2015.

[47] Michael A. Nielsen and Isaac L. Chuang. *Quantum Computation and Quantum Information*. Cambridge University Press, 2011.

[48] G. Vidal and R. F. Werner. Computable measure of entanglement. *Phys. Rev. A*, 65:032314, Feb 2002.

[49] A. Einstein, B. Podolsky, and N. Rosen. Can quantum-mechanical description of physical reality be considered complete? *Phys. Rev.*, 47:777–780, May 1935.

[50] John S Bell. On the einstein podolsky rosen paradox. *Physics Physique Fizika*, 1(3):195, 1964.

[51] Stuart J. Freedman and John F. Clauser. Experimental test of local hidden-variable theories. *Phys. Rev. Lett.*, 28:938–941, Apr 1972.

[52] David Schmid, Thomas C. Fraser, Ravi Kunjwal, Ana Belen Sainz, Elie Wolfe, and Robert W. Spekkens. Why standard entanglement theory is inappropriate for the study of bell scenarios, 2020.

[53] Greg Ver Steeg and Nicolas C. Menicucci. Entangling power of an expanding universe. *Phys. Rev. D*, 79:044027, Feb 2009.

[54] Keith K. Ng, Robert B. Mann, and Eduardo Martín-Martínez. Over the horizon: Distinguishing the schwarzschild spacetime and the $\mathbb{RP}^3$ spacetime using an unruh-dewitt detector. *Phys. Rev. D*, 96:085004, Oct 2017.

[55] Wan Cong, Ji ří Bičák, David Kubizňák, and Robert B. Mann. Quantum distinction of inertial frames: Local versus global. *Phys. Rev. D*, 101:104060, May 2020.

[56] Eduardo Martín-Martínez, Alexander R. H. Smith, and Daniel R. Terno. Spacetime structure and vacuum entanglement. *Phys. Rev. D*, 93:044001, Feb 2016.

[57] Jonathan Silman Benni Reznik, Alex Retzker. Violating bell's inequalities in the vacuum. *Phys. Rev. A*, 2005.

[58] Jorma Louko and Alejandro Satz. Transition rate of the unruh–dewitt detector in curved spacetime. *Classical Quant. Grav.*, 25(5):055012, 2008.

[59] Jorma Louko and Alejandro Satz. How often does the unruh–dewitt detector click? regularization by a spatial profile. *Classical Quant. Grav.*, 23(22):6321, 2006.

[60] Alejandro Satz. Then again, how often does the unruh–dewitt detector click if we switch it carefully? *Classical Quant. Grav.*, 24(7):1719, 2007.

[61] Robert H. Jonsson, Eduardo Martín-Martínez, and Achim Kempf. Information transmission without energy exchange. *Phys. Rev. Lett.*, 114:110505, Mar 2015.

[62] Ana Blasco, Luis J. Garay, Mercedes Martín-Benito, and Eduardo Martín-Martínez. Violation of the strong huygen's principle and timelike signals from the early universe. *Phys. Rev. Lett.*, 114:141103, Apr 2015.

[63] Eduardo Martín-Martínez and Jorma Louko. $(1+1)$D calculation provides evidence that quantum entanglement survives a firewall. *Phys. Rev. Lett.*, 115:031301, Jul 2015.

[64] Masahiro Hotta. Quantum energy teleportation in spin chain systems. *J. Phys. Soc. Jpn.*, 78(3):034001, 2009.

[65] Wan Cong, Erickson Tjoa, and Robert B. Mann. Entanglement harvesting with moving mirrors. *Journal of High Energy Physics*, 2019(6):21, 2019.

[66] Benito A Juárez-Aubry and Jorma Louko. Onset and decay of the 1+1 hawking-unruh effect: what the derivative-coupling detector saw. *Classical and Quantum Gravity*, 31(24):245007, nov 2014.

[67] Richard Lopp, Eduardo Martín-Martínez, and Don N Page. Relativity and quantum optics: accelerated atoms in optical cavities. *Classical and Quantum Gravity*, 35(22):224001, oct 2018.

[68] Kensuke Gallock-Yoshimura, Erickson Tjoa, and Robert B. Mann. Harvesting entanglement with detectors freely falling into a black hole. *Phys. Rev. D*, 104:025001, Jul 2021.

[69] B. F. Svaiter and N. F. Svaiter. Inertial and noninertial particle detectors and vacuum fluctuations. *Phys. Rev. D*, 46:5267–5277, Dec 1992.

[70] A. Higuchi, G. E. A. Matsas, and C. B. Peres. Uniformly accelerated finite-time detectors. *Phys. Rev. D*, 48:3731–3734, Oct 1993.

[71] Richard Lopp and Eduardo Martín-Martínez. Quantum delocalization, gauge, and quantum optics: Light-matter interaction in relativistic quantum information. *Phys. Rev. A*, 103:013703, Jan 2021.

[72] José de Ramón, Maria Papageorgiou, and Eduardo Martín-Martínez. Relativistic causality in particle detector models: Faster-than-light signaling and impossible measurements. *Phys. Rev. D*, 103:085002, Apr 2021.

[73] VIATCHESLAV F. MUKHANOV and SERGEI WINITZKI. *Introduction to Quantum Effects in Gravity*. Cambridge University Press, 2007.

[74] Morton H. Rubin, David N. Klyshko, Y. H. Shih, and A. V. Sergienko. Theory of two-photon entanglement in type-ii optical parametric down-conversion. *Phys. Rev. A*, 50:5122–5133, Dec 1994.

[75] Dionigi M T Benincasa, Leron Borsten, Michel Buck, and Fay Dowker. Quantum information processing and relativistic quantum fields. *Classical and Quantum Gravity*, 31(7):075007, mar 2014.

[76] Jan Kohlrus, David Edward Bruschi, Jorma Louko, and Ivette Fuentes. Quantum communications and quantum metrology in the spacetime of a rotating planet. *EPJ Quantum Technology*, 4:2196–0763, 2017.

[77] David Edward Bruschi and Frank K. Wilhelm. Self gravity affects quantum states, 2020.

[78] *NIST Digital Library of Mathematical Functions.* http://dlmf.nist.gov/, Release 1.0.25 of 2019-12-15. F. W. J. Olver, A. B. Olde Daalhuis, D. W. Lozier, B. I. Schneider, R. F. Boisvert, C. W. Clark, B. R. Miller, B. V. Saunders, H. S. Cohl, and M. A. McClain, eds.

[79] Besseli, 2002. Accessed: 20-May-2021.

[80] Hypergeometricpfqregularized, 1996. Accessed: 08-June-2021.

[81] R.W. Boyd and D. Prato. *Nonlinear Optics.* Elsevier Science, 2008.

[82] Mari-Carmen Bañuls, J. Ignacio Cirac, and Michael M. Wolf. Entanglement in fermionic systems. *Phys. Rev. A*, 76:022311, Aug 2007.

[83] Carlos Barceló, Stefano Liberati, and Matt Visser. Analogue gravity. *Living Reviews in Relativity*, 2011.

[84] Grigory E. Volovik. *The Universe in a Helium Droplet.* Oxford University Press, 2009.

[85] Petr O. Fedichev and Uwe R. Fischer. Gibbons-hawking effect in the sonic de sitter space-time of an expanding bose-einstein-condensed gas. *Phys. Rev. Lett.*, 91:240407, Dec 2003.

[86] Silke Weinfurtner, Edmund W. Tedford, Matthew C. J. Penrice, William G. Unruh, and Gregory A. Lawrence. Measurement of stimulated hawking emission in an analogue system. *Phys. Rev. Lett.*, 106:021302, Jan 2011.

[87] L.-P. Euvé, F. Michel, R. Parentani, T. G. Philbin, and G. Rousseaux. Observation of noise correlated by the hawking effect in a water tank. *Phys. Rev. Lett.*, 117:121301, Sep 2016.

[88] Theo Torres, Sam Patrick, Antonin Coutant, Maurício Richartz, Edmund W. Tedford, and Silke Weinfurtner. Rotational superradiant scattering in a vortex flow. *Nature Physics*, 13(9):833–836, 2017.

[89] Theo Torres, Sam Patrick, Maurício Richartz, and Silke Weinfurtner. Quasinormal mode oscillations in an analogue black hole experiment. *Phys. Rev. Lett.*, 125:011301, Jul 2020.

[90] J.-C. Jaskula, G. B. Partridge, M. Bonneau, R. Lopes, J. Ruaudel, D. Boiron, and C. I. Westbrook. Acoustic analog to the dynamical casimir effect in a bose-einstein condensate. *Phys. Rev. Lett.*, 109:220401, Nov 2012.

[91] Juan Ramón Muñoz de Nova, Katrine Golubkov, Victor I. Kolobov, and Jeff Steinhauer. Observation of thermal hawking radiation and its temperature in an analogue black hole. *Nature*, 569:688–691, 2019.

[92] Stephen Eckel and Ted Jacobson. Phonon redshift and Hubble friction in an expanding BEC. *SciPost Phys.*, 10:064, 2021.

[93] Jonathan Drori, Yuval Rosenberg, David Bermudez, Yaron Silberberg, and Ulf Leonhardt. Observation of stimulated hawking radiation in an optical analogue. *Phys. Rev. Lett.*, 122:010404, Jan 2019.

[94] F. Belgiorno, S. L. Cacciatori, M. Clerici, V. Gorini, G. Ortenzi, L. Rizzi, E. Rubino, V. G. Sala, and D. Faccio. Hawking radiation from ultrashort laser pulse filaments. *Phys. Rev. Lett.*, 105:203901, Nov 2010.

[95] M. J. Jacquet, S. Weinfurtner, and F. König. The next generation of analogue gravity experiments. *Philosophical Transactions of the Royal Society A: Mathematical, Physical and Engineering Sciences*, 378(2177):20190239, 2020.

[96] A. Retzker, J. I. Cirac, M. B. Plenio, and B. Reznik. Methods for detecting acceleration radiation in a bose-einstein condensate. *Phys. Rev. Lett.*, 101:110402, Sep 2008.

[97] Cisco Gooding, Steffen Biermann, Sebastian Erne, Jorma Louko, William G. Unruh, Jörg Schmiedmayer, and Silke Weinfurtner. Interferometric unruh detectors for bose-einstein condensates. *Phys. Rev. Lett.*, 125:213603, Nov 2020.

[98] Steffen Biermann, Sebastian Erne, Cisco Gooding, Jorma Louko, Jörg Schmiedmayer, William G. Unruh, and Silke Weinfurtner. Circular motion unruh and analogue unruh temperatures in 3+1 and 2+1 dimensions, 2020.

[99] Jamir Marino, Gabriel Menezes, and Iacopo Carusotto. Zero-point excitation of a circularly moving detector in an atomic condensate and phonon laser dynamical instabilities. *Phys. Rev. Research*, 2:042009, Oct 2020.

[100] T. Langen, R. Geiger, M. Kuhnert, B. Rauer, and J. Schmiedmayer. Local emergence of thermal correlations in an isolated quantum many-body system. *Nature Physics*, 9, 2013.

[101] Carlos Barceló, Stefano Liberati, and Matt Visser. Analogue gravity. *Living Reviews in Relativity*, 2011.

[102] Grigory E. Volovik. *The Universe in a Helium Droplet*. Oxford University Press, 2009.

[103] Petr O. Fedichev and Uwe R. Fischer. Gibbons-hawking effect in the sonic de sitter space-time of an expanding bose-einstein-condensed gas. *Phys. Rev. Lett.*, 91:240407, Dec 2003.

[104] Robert H. Jonsson. Information travels in massless fields in 1+1 dimensions where energy cannot. *arXiv:1512.05065*, 2015.

[105] Robert H. Jonsson, Eduardo Martín-Martínez, and Achim Kempf. Quantum signaling in cavity qed. *Phys. Rev. A*, 89:022330, Feb 2014.

[106] Robert Jonsson. *Decoupling of Information Propagation from Energy Propagation*. PhD thesis, University of Waterloo, 2016.

[107] S. Jay Olson and Timothy C. Ralph. Entanglement between the future and the past in the quantum vacuum. *Phys. Rev. Lett.*, 106:110404, Mar 2011.

[108] Kean-Philippe W MacLean, Katja Ried, Robert W. Spekkens, and Kevin J. Resch. Quantum-coherent mixtures of causal relations. *Nature Communications*, 1(8):15149, 2017.

[109] Matthew P. G. Robbins, Laura J. Henderson, and Robert B. Mann. Entanglement Amplification from Rotating Black Holes, 10 2020.

[110] Theo Torres, Antonin Coutant, Sam Dolan, and Silke Weinfurtner. Waves on a vortex: rays, rings and resonances. *Journal of Fluid Mechanics*, 857:291–311, 2018.

[111] Keith K. Ng, Robert B. Mann, and Eduardo Martín-Martínez. New techniques for entanglement harvesting in flat and curved spacetimes. *Phys. Rev. D*, 97:125011, Jun 2018.

[112] Robert M. Wald. *General Relativity*. The University of Chicago Press, 1984.

[113] Boris I. Lembrikov. Introductory chapter: Nonlinear optical phenomena. In Boris I. Lembrikov, editor, *Nonlinear Optics*, chapter 1. IntechOpen, Rijeka, 2019.

[114] Zhang Hong-Hao, Feng Kai-Xi, Qiu Si-Wei, Zhao An, and Li Xue-Song. On analytic formulas of feynman propagators in position space. *Chinese Physics C*, 34(10):1576, 2010.

[115] I Gradshteyn. Table of integrals, series and products, 1962.

Appendix: Two Point Correlators

The basis of many of these calculations is the two-point correlator of the operator to which the detector couples. In this section we calculate the various correlators which appear through out the thesis.

1 Two-point correlator of the quadratic coupling to a complex field

In this section, we will breifly relate the two point correlator of a real scalar field to the two-point correlator of the function

$$f(\hat{\Phi}(t,\boldsymbol{x})) =: \hat{\Phi}\hat{\Phi}^\dagger : \ , \tag{1}$$

where $\hat{\Phi}$ is complex.

We begin with the relationship between an operator $\hat{A}$ and its normal ordered version is given by

$$: \hat{A} := \hat{A} - \langle 0|\hat{A}\,|0\rangle\, \mathbb{1} \tag{2}$$

Using this identity, $W^{:\hat{\Phi}\hat{\Phi}^\dagger:}$ can be rewritten as

$$\begin{aligned} W^{:\hat{\Phi}\hat{\Phi}^\dagger:}(t,\boldsymbol{x},t',\boldsymbol{x}') = \langle 0|\, \hat{\Phi}(\boldsymbol{x},t)\hat{\Phi}^\dagger(\boldsymbol{x},t)\hat{\Phi}(\boldsymbol{x}',t')\hat{\Phi}^\dagger(\boldsymbol{x}',t')\,|0\rangle \\ - \langle 0|\, \hat{\Phi}(\boldsymbol{x},t)\hat{\Phi}^\dagger(\boldsymbol{x},t)\,|0\rangle\, \langle 0|\, \hat{\Phi}(\boldsymbol{x}',t')\hat{\Phi}^\dagger(\boldsymbol{x}',t')\,|0\rangle\,. \end{aligned} \tag{3}$$

The first term of $W^{:\hat{\Phi}\hat{\Phi}^\dagger:}(t,\boldsymbol{x},t',\boldsymbol{x}')$ can be simplified. To do so, we will write the field

operator as $\hat{\Phi} = \hat{\Phi}^+ + \hat{\Phi}^-$, where $\hat{\Phi}^+$ and $\hat{\Phi}^-$ are defined as

$$\hat{\Phi}^+(\boldsymbol{x}, t) = \int \frac{\mathrm{d}^d \boldsymbol{k}\, e^{-\epsilon|\boldsymbol{k}|/2}}{\sqrt{2(2\pi)^n |\boldsymbol{k}|}}\, \hat{a}_k^\dagger\, e^{\mathrm{i}(|\boldsymbol{k}|t - \boldsymbol{k}\cdot\boldsymbol{x})}, \tag{4}$$

$$\hat{\Phi}^-(\boldsymbol{x}, t) = \int \frac{\mathrm{d}^d \boldsymbol{k}\, e^{-\epsilon|\boldsymbol{k}|/2}}{\sqrt{2(2\pi)^n |\boldsymbol{k}|}}\, \hat{b}_k\, e^{-\mathrm{i}(|\boldsymbol{k}|t - \boldsymbol{k}\cdot\boldsymbol{x})}\ , \tag{5}$$

where the operators $\hat{\Phi}^+$ and $\hat{\Phi}^-$ satisfy the commutation relation

$$\left[\hat{\Phi}^-(\boldsymbol{x}_\mu, t_\mu), \hat{\Phi}^+(\boldsymbol{x}_\nu, t_\nu)\right] = 0, \tag{6}$$

and

$$\left[\hat{\Phi}^-(\boldsymbol{x}_\mu, t_\mu), \hat{\Phi}^{-\dagger}(\boldsymbol{x}_\nu, t_\nu)\right] = \mathcal{C}_{\mu\nu}\mathbb{1}, \tag{7}$$

$$\left[\hat{\Phi}^+(\boldsymbol{x}_\mu, t_\mu), \hat{\Phi}^{+\dagger}(\boldsymbol{x}_\nu, t_\nu)\right] = \mathcal{C}_{\nu\mu}\mathbb{1}\ , \tag{8}$$

where $\mathcal{C}_{\mu\nu} \in \mathbb{C}$ is precisely

$$\mathcal{C}_{\mu\nu} = \int \frac{\mathrm{d}^d \boldsymbol{k}\, e^{-\epsilon|\boldsymbol{k}|/2}}{2(2\pi)^n |\boldsymbol{k}|} e^{\mathrm{i}(|\boldsymbol{k}|(t_\nu - t_\mu) - \boldsymbol{k}\cdot(\boldsymbol{x}_\nu - \boldsymbol{x}_\mu))}$$

Furthermore, to simplify notation we define $\hat{\Phi}_\nu$ such that

$$\langle 0|\hat{\Phi}(\boldsymbol{x}, t)\hat{\Phi}^\dagger(\boldsymbol{x}, t)\hat{\Phi}(\boldsymbol{x}', t')\hat{\Phi}^\dagger(\boldsymbol{x}', t')\,|0\rangle = \langle 0|\,\hat{\Phi}_1\hat{\Phi}_2^\dagger\hat{\Phi}_3\hat{\Phi}_4^\dagger\,|0\rangle\,, \tag{9}$$

we can use $\hat{\Phi}^+$ and $\hat{\Phi}^-$ (and their adjoints) to rewrite the first term in Eq. (3) as

$$\langle 0|\hat{\Phi}_1\hat{\Phi}_2^\dagger\hat{\Phi}_3\hat{\Phi}_4^\dagger\,|0\rangle = \langle 0|\,\hat{\Phi}_1^-\hat{\Phi}_2^{-\dagger}\hat{\Phi}_3^-\hat{\Phi}_4^{-\dagger}\,|0\rangle + \langle 0|\,\hat{\Phi}_1^-\hat{\Phi}_2^{+\dagger}\hat{\Phi}_3^-\hat{\Phi}_4^{+\dagger}\,|0\rangle\ . \tag{10}$$

Note that here the expression differs from the real scalar field case (see equation (A7) of [29]), although we still use that

$$\hat{\Phi}_\mu^{+\dagger}\,|0\rangle = \langle 0|\,\hat{\Phi}_\nu^+ = \hat{\Phi}_\mu^-\,|0\rangle = \langle 0|\,\hat{\Phi}_\nu^{-\dagger} = 0, \tag{11}$$

and that only summands with as many $\hat{\Phi}^-$ as $\hat{\Phi}^{-\dagger}$ and $\hat{\Phi}^+$ as $\hat{\Phi}^{+\dagger}$ give a non-vanishing vacuum expectation

By commuting operators using Eq. (6), we can write the following

$$\begin{aligned}\langle 0|\,\hat{\Phi}_1^-\hat{\Phi}_2^{-\dagger}\hat{\Phi}_3^-\hat{\Phi}_4^{-\dagger}\,|0\rangle &= \mathcal{C}_{23}\mathcal{C}_{14}\\ \langle 0|\,\hat{\Phi}_1^-\hat{\Phi}_2^+\hat{\Phi}_3^-\hat{\Phi}_4^+\,|0\rangle &= \mathcal{C}_{12}\mathcal{C}_{34}\ .\end{aligned} \tag{12}$$

Thus Eq. (10) can be written as

$$\langle 0|\hat{\Phi}_1\hat{\Phi}_2\hat{\Phi}_3\hat{\Phi}_4\,|0\rangle = \mathcal{C}_{23}\mathcal{C}_{14} + \mathcal{C}_{12}\mathcal{C}_{34}. \tag{13}$$

We can rewrite the $\mathcal{C}_{\mu\nu}$ coefficients as

$$\mathcal{C}_{\mu\nu} = \langle 0|\left[\hat{\Phi}_\mu^-, \hat{\Phi}_\nu^{-\dagger}\right]|0\rangle = \langle 0|\,\hat{\Phi}_\mu^-\hat{\Phi}_\nu^{-\dagger}\,|0\rangle = \langle 0|\,\hat{\Phi}_\mu\hat{\Phi}_\nu^\dagger\,|0\rangle \ , \tag{14}$$

which allows us to write the following relation

$$\langle 0|\,\hat{\Phi}_1\hat{\Phi}_2\hat{\Phi}_3\hat{\Phi}_4\,|0\rangle = \langle 0|\,\hat{\Phi}_1\hat{\Phi}_2^\dagger\,|0\rangle\,\langle 0|\,\hat{\Phi}_3\hat{\Phi}_4^\dagger\,|0\rangle + \langle 0|\,\hat{\Phi}_1\hat{\Phi}_3^\dagger\,|0\rangle\,\langle 0|\,\hat{\Phi}_2\hat{\Phi}_4^\dagger\,|0\rangle \ . \tag{15}$$

Using our definition of $\hat{\Phi}_\nu$ in Eq. (9), this becomes

$$\begin{aligned}\langle 0|\,\hat{\Phi}(\boldsymbol{x},t)\hat{\Phi}^\dagger(\boldsymbol{x},t)\hat{\Phi}(t',\boldsymbol{x}')\hat{\Phi}^\dagger(t',\boldsymbol{x}')\,|0\rangle &= \langle 0|\,\hat{\Phi}(\boldsymbol{x},t)\hat{\Phi}^\dagger(\boldsymbol{x},t)\,|0\rangle\,\langle 0|\,\hat{\Phi}(t',\boldsymbol{x}')\hat{\Phi}^\dagger(t',\boldsymbol{x}')\,|0\rangle \\ &\quad + \langle 0|\,\hat{\Phi}(\boldsymbol{x},t)\hat{\Phi}^\dagger(t',\boldsymbol{x}')\,|0\rangle\,\langle 0|\,\hat{\Phi}(\boldsymbol{x},t)\hat{\Phi}^\dagger(t',\boldsymbol{x}')\,|0\rangle \ .\end{aligned} \tag{16}$$

Thus the complex correlation function, originally expressed in Eq. (3), is

$$W^{:\Phi\Phi^\dagger:}(t,\boldsymbol{x},t',\boldsymbol{x}') = \Big(\langle 0|\,\hat{\Phi}(\boldsymbol{x},t)\hat{\Phi}^\dagger(\boldsymbol{x}',t')\,|0\rangle\Big)^2 . \tag{17}$$

2 Two point correlator of the linear coupling to a one-particle Fock state

In this section we will calculate the following two-point correlator

$$W_{k_0}^\phi(\mathsf{x},\mathsf{x}') = \langle 1_f|\,\phi(\mathsf{x})\phi(\mathsf{x}')\,|1_{f_{k_0}}\rangle\,. \tag{18}$$

First we will expand the field operator and insert our definition of the one-particle Fock state Eq. (2.4):

$$\begin{aligned}W_{k_0}^\phi(\mathsf{x},\mathsf{x}') = &\int \mathrm{d}^n\boldsymbol{p} f_{\boldsymbol{k}_0}(\boldsymbol{p}) \int \mathrm{d}^n\boldsymbol{p}' f_{\boldsymbol{k}_0}(\boldsymbol{p}') \int \widetilde{\mathrm{d}^n\boldsymbol{k}} \int \widetilde{\mathrm{d}^n\boldsymbol{k}'} \\ &\times \langle 0|\,\hat{a}_{\boldsymbol{p}'}\left(\hat{a}_{\boldsymbol{k}}e^{-\mathrm{i}|\boldsymbol{k}|t+\boldsymbol{k}\cdot\boldsymbol{x}} + \hat{a}_{\boldsymbol{k}}^\dagger e^{\mathrm{i}|\boldsymbol{k}|t-\boldsymbol{k}\cdot\boldsymbol{x}}\right)\left(\hat{a}_{\boldsymbol{k}'}e^{-\mathrm{i}|\boldsymbol{k}|t+\boldsymbol{k}'\cdot\boldsymbol{x}'} + \hat{a}_{\boldsymbol{k}'}^\dagger e^{\mathrm{i}|\boldsymbol{k}'|t'-\boldsymbol{k}'\cdot\boldsymbol{x}'}\right)\hat{a}_{\boldsymbol{p}}^\dagger\,|0\rangle\,,\end{aligned} \tag{19}$$

where $\widetilde{\mathrm{d}^n\boldsymbol{k}} = \mathrm{d}^n\boldsymbol{k}/\sqrt{2(2\pi)^n|\boldsymbol{k}|}$. We must have the same number of creation and annihilation operators in order for an inner product to not vanish, and thus the above expression immediately simplifies,

$$W^{\phi}_{k_0}(\mathsf{x},\mathsf{x}') = \int \mathrm{d}^n\boldsymbol{p} \int \mathrm{d}^n\boldsymbol{p}' \int \widetilde{\mathrm{d}^n\boldsymbol{k}} \int \widetilde{\mathrm{d}^n\boldsymbol{k}'} f_{\boldsymbol{k}_0}(\boldsymbol{p}) f_{\boldsymbol{k}_0}(\boldsymbol{p}') \tag{20}$$
$$\times \left(e^{-\mathrm{i}|\boldsymbol{k}|t+\boldsymbol{k}\cdot\boldsymbol{x}} e^{\mathrm{i}|\boldsymbol{k}'|t'-\boldsymbol{k}'\cdot\boldsymbol{x}'} \langle 0|\, \hat{a}_{\boldsymbol{p}'}\hat{a}_{\boldsymbol{k}}\hat{a}^{\dagger}_{\boldsymbol{k}'}\hat{a}^{\dagger}_{\boldsymbol{p}}\, |0\rangle + e^{\mathrm{i}|\boldsymbol{k}|t-\boldsymbol{k}\cdot\boldsymbol{x}} e^{-\mathrm{i}|\boldsymbol{k}|t+\boldsymbol{k}'\cdot\boldsymbol{x}'} \langle 0|\, \hat{a}_{\boldsymbol{p}'}\hat{a}^{\dagger}_{\boldsymbol{k}}\hat{a}_{\boldsymbol{k}'}\hat{a}^{\dagger}_{\boldsymbol{p}}\, |0\rangle \right).$$

Consider for a moment $\langle 0|\, \hat{a}_{\boldsymbol{p}'}\hat{a}_{\boldsymbol{k}}\hat{a}^{\dagger}_{\boldsymbol{k}'}\hat{a}^{\dagger}_{\boldsymbol{p}}\, |0\rangle$. We will show how the commutation relation of the creation and anihilation operators may be applied in order to simplify the expressions:

$$\begin{aligned}
\langle 0|\, \hat{a}_{\boldsymbol{p}'}\hat{a}_{\boldsymbol{k}}\hat{a}^{\dagger}_{\boldsymbol{k}'}\hat{a}^{\dagger}_{\boldsymbol{p}}\, |0\rangle &= \langle 0|\, \hat{a}_{\boldsymbol{p}'} \left(\hat{a}^{\dagger}_{\boldsymbol{k}'}\hat{a}_{\boldsymbol{k}} + \delta(\boldsymbol{k}'-\boldsymbol{k}) \right) \hat{a}^{\dagger}_{\boldsymbol{p}}\, |0\rangle \\
&= \langle 0| \left(\hat{a}^{\dagger}_{\boldsymbol{k}'}\hat{a}_{\boldsymbol{p}'} + \delta(\boldsymbol{k}'-\boldsymbol{p}') \right) \left(\hat{a}^{\dagger}_{\boldsymbol{p}}\hat{a}_{\boldsymbol{k}} + \delta(\boldsymbol{p}-\boldsymbol{k}) \right) |0\rangle \\
&\quad + \langle 0|\, \hat{a}^{\dagger}_{\boldsymbol{p}}\hat{a}_{\boldsymbol{p}'} + \delta(\boldsymbol{p}-\boldsymbol{p}')\, |0\rangle\, \delta(\boldsymbol{k}'-\boldsymbol{k}) \\
&= \delta(\boldsymbol{k}'-\boldsymbol{p}')\delta(\boldsymbol{p}-\boldsymbol{k}) + \delta(\boldsymbol{p}-\boldsymbol{p}')\delta(\boldsymbol{k}'-\boldsymbol{k}),
\end{aligned} \tag{21}$$

where the first equality is due to the definition of the commutator. The second equality is an additional application of the same definition after some minor arithmetic. Creation and annihilation operators on the right and left of the vacuum, respectively, cause the associated terms to vanish, resulting in the third equality.

Now we will consider the second inner product, $\langle 0|\, \hat{a}_{\boldsymbol{p}'}\hat{a}^{\dagger}_{\boldsymbol{k}}\hat{a}_{\boldsymbol{k}'}\hat{a}^{\dagger}_{\boldsymbol{p}}\, |0\rangle$. If we commute the left and right pairs of operators and anihilate the vacuume where appropriate, we find

$$\langle 0|\, \hat{a}_{\boldsymbol{p}'}\hat{a}^{\dagger}_{\boldsymbol{k}}\hat{a}_{\boldsymbol{k}'}\hat{a}^{\dagger}_{\boldsymbol{p}}\, |0\rangle = \delta(\boldsymbol{p}'-\boldsymbol{k})\delta(\boldsymbol{k}'-\boldsymbol{p}). \tag{22}$$

Both of the above expressions can be substituted into Eq. (21). The result is

$$\begin{aligned}
W^{\phi}_{k_0}(\mathsf{x},\mathsf{x}') &= \int \mathrm{d}^n\boldsymbol{p} \int \mathrm{d}^n\boldsymbol{p}' \int \widetilde{\mathrm{d}^n\boldsymbol{k}} \int \widetilde{\mathrm{d}^n\boldsymbol{k}'} f_{\boldsymbol{k}_0}(\boldsymbol{p}) f_{\boldsymbol{k}_0}(\boldsymbol{p}') \\
&\quad \times e^{-\mathrm{i}|\boldsymbol{k}|t+\boldsymbol{k}\cdot\boldsymbol{x}} e^{\mathrm{i}|\boldsymbol{k}'|t'-\boldsymbol{k}'\cdot\boldsymbol{x}'} \delta(\boldsymbol{k}'-\boldsymbol{p}')\delta(\boldsymbol{p}-\boldsymbol{k}) \\
&\quad + \int \mathrm{d}^n\boldsymbol{p} \int \mathrm{d}^n\boldsymbol{p}' \int \widetilde{\mathrm{d}^n\boldsymbol{k}} \int \widetilde{\mathrm{d}^n\boldsymbol{k}'} f_{\boldsymbol{k}_0}(\boldsymbol{p}) f_{\boldsymbol{k}_0}(\boldsymbol{p}') e^{-\mathrm{i}|\boldsymbol{k}|t+\boldsymbol{k}\cdot\boldsymbol{x}} e^{\mathrm{i}|\boldsymbol{k}'|t'-\boldsymbol{k}'\cdot\boldsymbol{x}'} \delta(\boldsymbol{p}-\boldsymbol{p}')\delta(\boldsymbol{k}'-\boldsymbol{k}) \\
&\quad + \int \mathrm{d}^n\boldsymbol{p} \int \mathrm{d}^n\boldsymbol{p}' \int \widetilde{\mathrm{d}^n\boldsymbol{k}} \int \widetilde{\mathrm{d}^n\boldsymbol{k}'} f_{\boldsymbol{k}_0}(\boldsymbol{p}) f_{\boldsymbol{k}_0}(\boldsymbol{p}') e^{\mathrm{i}|\boldsymbol{k}|t-\boldsymbol{k}\cdot\boldsymbol{x}} e^{-\mathrm{i}|\boldsymbol{k}|t+\boldsymbol{k}'\cdot\boldsymbol{x}'} \delta(\boldsymbol{p}'-\boldsymbol{k})\delta(\boldsymbol{k}'-\boldsymbol{p}).
\end{aligned} \tag{23}$$

Applying the delta distributions reduces the number of integrals, yielding

$$\begin{aligned} W^{\phi}_{k_0}(\mathsf{x},\mathsf{x}') = &\int \widetilde{\mathrm{d}^n\boldsymbol{k}} f_{\boldsymbol{k}_0}(\boldsymbol{k}) e^{-\mathrm{i}|\boldsymbol{k}|t+\boldsymbol{k}\cdot\boldsymbol{x}} \int \widetilde{\mathrm{d}^n\boldsymbol{k}'} f_{\boldsymbol{k}_0}(\boldsymbol{k}') e^{\mathrm{i}|\boldsymbol{k}'|t'-\boldsymbol{k}'\cdot\boldsymbol{x}'} \\ &+ \int \mathrm{d}^n\boldsymbol{p} (f_{\boldsymbol{k}_0}(\boldsymbol{p}))^2 \int \widetilde{\widetilde{\mathrm{d}^n\boldsymbol{k}}} e^{-\mathrm{i}|\boldsymbol{k}|(t-t')+\boldsymbol{k}\cdot(\boldsymbol{x}-\boldsymbol{x}')} \\ &+ \int \widetilde{\mathrm{d}^n\boldsymbol{k}} f_{\boldsymbol{k}_0}(\boldsymbol{k}) e^{\mathrm{i}|\boldsymbol{k}|t-\boldsymbol{k}\cdot\boldsymbol{x}} \int \widetilde{\mathrm{d}^n\boldsymbol{k}'} f_{\boldsymbol{k}_0}(\boldsymbol{k}') e^{-\mathrm{i}|\boldsymbol{k}|t+\boldsymbol{k}'\cdot\boldsymbol{x}'}, \end{aligned} \tag{24}$$

where the double tilde simply indicates that that normalization factor indicated by the single tilde is squared. Let us now define

$$K_{\boldsymbol{k}_0}(\mathsf{x}) = \int \widetilde{\mathrm{d}^n\boldsymbol{k}} f_{\boldsymbol{k}_0}(\boldsymbol{k}) e^{\mathrm{i}|\boldsymbol{k}|t-\boldsymbol{k}\cdot\boldsymbol{x}}, \tag{25}$$

and recall that state-normalization forces the L^2 norm of f to unity. Furthermore, we can recognise the integral with the double tilde as the vacuum Wightman Eq. (1.75):

$$W^{\phi}_{\mathrm{VAC}}(\mathsf{x},\mathsf{x}) = \int \widetilde{\widetilde{\mathrm{d}^n\boldsymbol{k}}} e^{-\mathrm{i}|\boldsymbol{k}|(t-t')+\boldsymbol{k}\cdot(\boldsymbol{x}-\boldsymbol{x}')}.$$

These notes allow us to simplify the notation of our expression:

$$W^{\phi}_{k_0}(\mathsf{x},\mathsf{x}') = (K_{\boldsymbol{k}_0}(\mathsf{x})^* K_{\boldsymbol{k}_0}(\mathsf{x}') + c.c) + W^{\phi}_{\mathrm{VAC}}(\mathsf{x},\mathsf{x}). \tag{26}$$

This is the expression that we will use in later sections when the two-point (Wightman) function for the one-particle state is called for.

3 Two point correlator of the linear coupling to a two-particle Fock state

In this section we will calculate the following two-point correlator

$$W^{\phi}_{\eta_1,\eta_2}(\mathsf{x},\mathsf{x}') = \langle 2_f |\, \phi(\mathsf{x})\phi(\mathsf{x}')\, |2_{f_{\eta_1,\eta_2}}\rangle\,, \tag{27}$$

where $|2_{f_{\eta_1,\eta_2}}\rangle$ is defined in Eq. (2.6).

The method of finding a simplified expression for the correlator will be similar to that in the previous section. However, now the inner product has two additional operators from

the two-particle Fock state. Additionally, we will have a second peak frequency to track.

$$W^{\phi}_{\eta_1,\eta_2}(\mathsf{x},\mathsf{x}') = \mathcal{N}^2 \int \mathrm{d}^n\boldsymbol{k}_1\,\mathrm{d}^n\boldsymbol{k}_2\,\mathrm{d}^n\boldsymbol{k}_3\,\mathrm{d}^n\boldsymbol{k}_4\,\widetilde{\mathrm{d}^n\boldsymbol{k}}\,\widetilde{\mathrm{d}^n\boldsymbol{k}'} f_{\eta_1}(\boldsymbol{k}_1) f_{\eta_2}(\boldsymbol{k}_2) f_{\eta_1}(\boldsymbol{k}_3) f_{\eta_2}(\boldsymbol{k}_4)$$
$$\times \langle 0|\, \hat{a}_{\boldsymbol{k}_3}\hat{a}_{\boldsymbol{k}_4}\left(\hat{a}_{\boldsymbol{k}} e^{-\mathrm{i}|\boldsymbol{k}|t+\boldsymbol{k}\cdot\boldsymbol{x}} + \hat{a}^\dagger_{\boldsymbol{k}} e^{\mathrm{i}|\boldsymbol{k}|t-\boldsymbol{k}\cdot\boldsymbol{x}}\right)\left(\hat{a}_{\boldsymbol{k}'} e^{-\mathrm{i}|\boldsymbol{k}|t+\boldsymbol{k}'\cdot\boldsymbol{x}'} + \hat{a}^\dagger_{\boldsymbol{k}'} e^{\mathrm{i}|\boldsymbol{k}'|t'-\boldsymbol{k}'\cdot\boldsymbol{x}'}\right)\hat{a}^\dagger_{\boldsymbol{k}_1}\hat{a}^\dagger_{\boldsymbol{k}_2}\,|0\rangle \tag{28}$$

Only terms with equal numbers of creation and anihilation operators contribute, and so

$$\begin{aligned} W^{\phi}_{\eta_1,\eta_2}(\mathsf{x},\mathsf{x}') &= \mathcal{N}^2 \int \mathrm{d}^n\boldsymbol{k}_1\,\mathrm{d}^n\boldsymbol{k}_2\,\mathrm{d}^n\boldsymbol{k}_3\,\mathrm{d}^n\boldsymbol{k}_4\,\widetilde{\mathrm{d}^n\boldsymbol{k}}\,\widetilde{\mathrm{d}^n\boldsymbol{k}'} f_{\eta_1}(\boldsymbol{k}_1) f_{\eta_2}(\boldsymbol{k}_2) f_{\eta_1}(\boldsymbol{k}_3) f_{\eta_2}(\boldsymbol{k}_4) \\ &\quad\times e^{-\mathrm{i}|\boldsymbol{k}|t+\boldsymbol{k}\cdot\boldsymbol{x}} e^{\mathrm{i}|\boldsymbol{k}'|t'-\boldsymbol{k}'\cdot\boldsymbol{x}'}\,\langle 0|\,\hat{a}_{\boldsymbol{k}_3}\hat{a}_{\boldsymbol{k}_4}\hat{a}_{\boldsymbol{k}}\hat{a}^\dagger_{\boldsymbol{k}'}\hat{a}^\dagger_{\boldsymbol{k}_1}\hat{a}^\dagger_{\boldsymbol{k}_2}\,|0\rangle \\ &\quad+\mathcal{N}^2 \int \mathrm{d}^n\boldsymbol{k}_1\,\mathrm{d}^n\boldsymbol{k}_2\,\mathrm{d}^n\boldsymbol{k}_3\,\mathrm{d}^n\boldsymbol{k}_4\,\widetilde{\mathrm{d}^n\boldsymbol{k}}\,\widetilde{\mathrm{d}^n\boldsymbol{k}'} f_{\eta_1}(\boldsymbol{k}_1) f_{\eta_2}(\boldsymbol{k}_2) f_{\eta_1}(\boldsymbol{k}_3) f_{\eta_2}(\boldsymbol{k}_4) \\ &\quad\times e^{\mathrm{i}|\boldsymbol{k}|t-\boldsymbol{k}\cdot\boldsymbol{x}} e^{-\mathrm{i}|\boldsymbol{k}|t+\boldsymbol{k}'\cdot\boldsymbol{x}'}\,\langle 0|\,\hat{a}_{\boldsymbol{k}_3}\hat{a}_{\boldsymbol{k}_4}\hat{a}^\dagger_{\boldsymbol{k}}\hat{a}_{\boldsymbol{k}'}\hat{a}^\dagger_{\boldsymbol{k}_1}\hat{a}^\dagger_{\boldsymbol{k}_2}\,|0\rangle\,. \end{aligned} \tag{29}$$

Let us quickly permute the middle two creation and annihilation operators in the first summand:

$$\begin{aligned} W^{\phi}_{\eta_1,\eta_2}(\mathsf{x},\mathsf{x}') &= \mathcal{N}^2 \int \mathrm{d}^n\boldsymbol{k}_1\,\mathrm{d}^n\boldsymbol{k}_2\,\mathrm{d}^n\boldsymbol{k}_3\,\mathrm{d}^n\boldsymbol{k}_4\,\widetilde{\mathrm{d}^n\boldsymbol{k}}\,\widetilde{\mathrm{d}^n\boldsymbol{k}'} f_{\eta_1}(\boldsymbol{k}_1) f_{\eta_2}(\boldsymbol{k}_2) f_{\eta_1}(\boldsymbol{k}_3) f_{\eta_2}(\boldsymbol{k}_4) \\ &\quad\times e^{-\mathrm{i}|\boldsymbol{k}|t+\boldsymbol{k}\cdot\boldsymbol{x}} e^{\mathrm{i}|\boldsymbol{k}'|t'-\boldsymbol{k}'\cdot\boldsymbol{x}'}\,\langle 0|\,\hat{a}_{\boldsymbol{k}_3}\hat{a}_{\boldsymbol{k}_4}\hat{a}^\dagger_{\boldsymbol{k}'}\hat{a}_{\boldsymbol{k}}\hat{a}^\dagger_{\boldsymbol{k}_1}\hat{a}^\dagger_{\boldsymbol{k}_2}\,|0\rangle \\ &\quad+\mathcal{N}^2 \int \mathrm{d}^n\boldsymbol{k}_1\,\mathrm{d}^n\boldsymbol{k}_2\,\mathrm{d}^n\boldsymbol{k}_3\,\mathrm{d}^n\boldsymbol{k}_4\,\widetilde{\mathrm{d}^n\boldsymbol{k}}\,\widetilde{\mathrm{d}^n\boldsymbol{k}'} f_{\eta_1}(\boldsymbol{k}_1) f_{\eta_2}(\boldsymbol{k}_2) f_{\eta_1}(\boldsymbol{k}_3) f_{\eta_2}(\boldsymbol{k}_4) \\ &\quad\times e^{-\mathrm{i}|\boldsymbol{k}|t+\boldsymbol{k}\cdot\boldsymbol{x}} e^{\mathrm{i}|\boldsymbol{k}'|t'-\boldsymbol{k}'\cdot\boldsymbol{x}'}\,\langle 0|\,\hat{a}_{\boldsymbol{k}_3}\hat{a}_{\boldsymbol{k}_4}\hat{a}^\dagger_{\boldsymbol{k}_1}\hat{a}^\dagger_{\boldsymbol{k}_2}\,|0\rangle\,\delta(\boldsymbol{k}-\boldsymbol{k}') \\ &\quad+\mathcal{N}^2 \int \mathrm{d}^n\boldsymbol{k}_1\,\mathrm{d}^n\boldsymbol{k}_2\,\mathrm{d}^n\boldsymbol{k}_3\,\mathrm{d}^n\boldsymbol{k}_4\,\widetilde{\mathrm{d}^n\boldsymbol{k}}\,\widetilde{\mathrm{d}^n\boldsymbol{k}'} f_{\eta_1}(\boldsymbol{k}_1) f_{\eta_2}(\boldsymbol{k}_2) f_{\eta_1}(\boldsymbol{k}_3) f_{\eta_2}(\boldsymbol{k}_4) \\ &\quad\times e^{\mathrm{i}|\boldsymbol{k}|t-\boldsymbol{k}\cdot\boldsymbol{x}} e^{-\mathrm{i}|\boldsymbol{k}|t+\boldsymbol{k}'\cdot\boldsymbol{x}'}\,\langle 0|\,\hat{a}_{\boldsymbol{k}_3}\hat{a}_{\boldsymbol{k}_4}\hat{a}^\dagger_{\boldsymbol{k}}\hat{a}_{\boldsymbol{k}'}\hat{a}^\dagger_{\boldsymbol{k}_1}\hat{a}^\dagger_{\boldsymbol{k}_2}\,|0\rangle \end{aligned} \tag{30}$$

We will simplify the first and last summands in the above expression by studying the inner product $\langle 0|\,\hat{a}_{\boldsymbol{p}_3}\hat{a}_{\boldsymbol{p}_4}\hat{a}^\dagger_{\boldsymbol{p}'}\hat{a}_{\boldsymbol{p}}\hat{a}^\dagger_{\boldsymbol{p}_1}\hat{a}^\dagger_{\boldsymbol{p}_2}\,|0\rangle$. We consruct the following string of equalities,

$$\begin{aligned} \langle 0|\,\hat{a}_{\boldsymbol{p}_3}\hat{a}_{\boldsymbol{p}_4}\hat{a}^\dagger_{\boldsymbol{p}'}\hat{a}_{\boldsymbol{p}}\hat{a}^\dagger_{\boldsymbol{p}_1}\hat{a}^\dagger_{\boldsymbol{p}_2}\,|0\rangle &= \langle 0|\,\hat{a}_{\boldsymbol{p}_3}(\hat{a}^\dagger_{\boldsymbol{p}'}\hat{a}_{\boldsymbol{p}_4}+\delta(\boldsymbol{p}_4-\boldsymbol{p}'))(\hat{a}^\dagger_{\boldsymbol{p}_1}\hat{a}_{\boldsymbol{p}}+\delta(\boldsymbol{p}-\boldsymbol{p}_1))\hat{a}^\dagger_{\boldsymbol{p}_2}\,|0\rangle \\ &= \langle 0|\,\hat{a}_{\boldsymbol{p}_3}\hat{a}^\dagger_{\boldsymbol{p}'}\hat{a}_{\boldsymbol{p}_4}\hat{a}^\dagger_{\boldsymbol{p}_1}\hat{a}_{\boldsymbol{p}}\hat{a}^\dagger_{\boldsymbol{p}_2}\,|0\rangle + \langle 0|\,\hat{a}_{\boldsymbol{p}_3}\hat{a}^\dagger_{\boldsymbol{p}_1}\hat{a}_{\boldsymbol{p}}\hat{a}^\dagger_{\boldsymbol{p}_2}\,|0\rangle\,\delta(\boldsymbol{p}_4-\boldsymbol{p}') \\ &\quad+\langle 0|\,\hat{a}_{\boldsymbol{p}_3}\hat{a}^\dagger_{\boldsymbol{p}'}\hat{a}_{\boldsymbol{p}_4}\hat{a}^\dagger_{\boldsymbol{p}_2}\,|0\rangle\,\delta(\boldsymbol{p}-\boldsymbol{p}_1) + \langle 0|\,\hat{a}_{\boldsymbol{p}_3}\hat{a}^\dagger_{\boldsymbol{p}_2}\,|0\rangle\,\delta(\boldsymbol{p}_4-\boldsymbol{p}')\delta(\boldsymbol{p}-\boldsymbol{p}_1) \\ &= \delta(\boldsymbol{p}_3-\boldsymbol{p}')\delta(\boldsymbol{p}_4-\boldsymbol{p}_1)\delta(\boldsymbol{p}-\boldsymbol{p}_2) + \delta(\boldsymbol{p}_3-\boldsymbol{p}_1)\delta(\boldsymbol{p}-\boldsymbol{p}_2)\delta(\boldsymbol{p}_4-\boldsymbol{p}') \\ &\quad+\delta(\boldsymbol{p}_3-\boldsymbol{p}')\delta(\boldsymbol{p}_4-\boldsymbol{p}_2)\delta(\boldsymbol{p}-\boldsymbol{p}_1) + \delta(\boldsymbol{p}_3-\boldsymbol{p}_2)\delta(\boldsymbol{p}_4-\boldsymbol{p}')\delta(\boldsymbol{p}-\boldsymbol{p}_1) \end{aligned} \tag{31}$$

where the first holds because of the form of the commutator of the creation and annihilation operators. The second equality follows from arithmetic. The final equality results from a final application of the commutator.

The next expression of interest is $\langle 0| \hat{a}_{\boldsymbol{k}_3} \hat{a}_{\boldsymbol{k}_4} \hat{a}^\dagger_{\boldsymbol{k}_1} \hat{a}^\dagger_{\boldsymbol{k}_2} |0\rangle$, where

$$\begin{aligned}
\langle 0| \hat{a}_{\boldsymbol{k}_3} \hat{a}_{\boldsymbol{k}_4} \hat{a}^\dagger_{\boldsymbol{k}_1} \hat{a}^\dagger_{\boldsymbol{k}_2} |0\rangle &= \langle 0| \hat{a}_{\boldsymbol{k}_3} (\hat{a}^\dagger_{\boldsymbol{k}_1} \hat{a}_{\boldsymbol{k}_4} + \delta(\boldsymbol{k}_1 - \boldsymbol{k}_4)) \hat{a}^\dagger_{\boldsymbol{k}_2} |0\rangle \\
&= \langle 0| \hat{a}_{\boldsymbol{k}_3} \hat{a}^\dagger_{\boldsymbol{k}_1} \hat{a}_{\boldsymbol{k}_4} \hat{a}^\dagger_{\boldsymbol{k}_2} |0\rangle + \langle 0| \hat{a}_{\boldsymbol{k}_3} \hat{a}^\dagger_{\boldsymbol{k}_2} |0\rangle \, \delta(\boldsymbol{k}_1 - \boldsymbol{k}_4) \\
&= \langle 0| (\hat{a}^\dagger_{\boldsymbol{k}_1} \hat{a}_{\boldsymbol{k}_3} + \delta(\boldsymbol{k}_1 - \boldsymbol{k}_3))(\hat{a}^\dagger_{\boldsymbol{k}_2} \hat{a}_{\boldsymbol{k}_4} + \delta(\boldsymbol{k}_2 - \boldsymbol{k}_4)) |0\rangle \\
&\quad + \langle 0| (\hat{a}^\dagger_{\boldsymbol{k}_2} \hat{a}_{\boldsymbol{k}_3} + \delta(\boldsymbol{k}_2 - \boldsymbol{k}_3)) |0\rangle \, \delta(\boldsymbol{k}_1 - \boldsymbol{k}_4) \\
&= \delta(\boldsymbol{k}_1 - \boldsymbol{k}_3)\delta(\boldsymbol{k}_2 - \boldsymbol{k}_4) + \delta(\boldsymbol{k}_2 - \boldsymbol{k}_3)\delta(\boldsymbol{k}_1 - \boldsymbol{k}_4), \qquad (32)
\end{aligned}$$

where simmilar techniques have reduced the inner product to a series of delta distributions.

If we apply the above inner products to the two-point correlator, we find,

$$
\begin{aligned}
W^{\phi}_{\eta_1,\eta_2}(\mathsf{x},\mathsf{x}') &= \mathcal{N}^2 \int \mathrm{d}^n\boldsymbol{k}_1\,\mathrm{d}^n\boldsymbol{k}_2\,\mathrm{d}^n\boldsymbol{k}_3\,\mathrm{d}^n\boldsymbol{k}_4\,\widetilde{\mathrm{d}^n\boldsymbol{k}}\,\widetilde{\mathrm{d}^n\boldsymbol{k}'} f_{\eta_1}(\boldsymbol{k}_1) f_{\eta_2}(\boldsymbol{k}_2) f_{\eta_1}(\boldsymbol{k}_3) f_{\eta_2}(\boldsymbol{k}_4) \\
&\quad \times e^{-\mathrm{i}|\boldsymbol{k}|t+\boldsymbol{k}\cdot\boldsymbol{x}} e^{\mathrm{i}|\boldsymbol{k}'|t'-\boldsymbol{k}'\cdot\boldsymbol{x}'} \delta(\boldsymbol{k}_3-\boldsymbol{k}')\delta(\boldsymbol{k}_4-\boldsymbol{k}_1)\delta(\boldsymbol{k}-\boldsymbol{k}_2) \\
&+ \mathcal{N}^2 \int \mathrm{d}^n\boldsymbol{k}_1\,\mathrm{d}^n\boldsymbol{k}_2\,\mathrm{d}^n\boldsymbol{k}_3\,\mathrm{d}^n\boldsymbol{k}_4\,\widetilde{\mathrm{d}^n\boldsymbol{k}}\,\widetilde{\mathrm{d}^n\boldsymbol{k}'} f_{\eta_1}(\boldsymbol{k}_1) f_{\eta_2}(\boldsymbol{k}_2) f_{\eta_1}(\boldsymbol{k}_3) f_{\eta_2}(\boldsymbol{k}_4) \\
&\quad \times e^{-\mathrm{i}|\boldsymbol{k}|t+\boldsymbol{k}\cdot\boldsymbol{x}} e^{\mathrm{i}|\boldsymbol{k}'|t'-\boldsymbol{k}'\cdot\boldsymbol{x}'} \delta(\boldsymbol{k}_3-\boldsymbol{k}_1)\delta(\boldsymbol{k}-\boldsymbol{k}_2)\delta(\boldsymbol{k}_4-\boldsymbol{k}') \\
&+ \mathcal{N}^2 \int \mathrm{d}^n\boldsymbol{k}_1\,\mathrm{d}^n\boldsymbol{k}_2\,\mathrm{d}^n\boldsymbol{k}_3\,\mathrm{d}^n\boldsymbol{k}_4\,\widetilde{\mathrm{d}^n\boldsymbol{k}}\,\widetilde{\mathrm{d}^n\boldsymbol{k}'} f_{\eta_1}(\boldsymbol{k}_1) f_{\eta_2}(\boldsymbol{k}_2) f_{\eta_1}(\boldsymbol{k}_3) f_{\eta_2}(\boldsymbol{k}_4) \\
&\quad \times e^{-\mathrm{i}|\boldsymbol{k}|t+\boldsymbol{k}\cdot\boldsymbol{x}} e^{\mathrm{i}|\boldsymbol{k}'|t'-\boldsymbol{k}'\cdot\boldsymbol{x}'} \delta(\boldsymbol{k}_3-\boldsymbol{k}')\delta(\boldsymbol{k}_4-\boldsymbol{k}_2)\delta(\boldsymbol{k}-\boldsymbol{k}_1) \\
&+ \mathcal{N}^2 \int \mathrm{d}^n\boldsymbol{k}_1\,\mathrm{d}^n\boldsymbol{k}_2\,\mathrm{d}^n\boldsymbol{k}_3\,\mathrm{d}^n\boldsymbol{k}_4\,\widetilde{\mathrm{d}^n\boldsymbol{k}}\,\widetilde{\mathrm{d}^n\boldsymbol{k}'} f_{\eta_1}(\boldsymbol{k}_1) f_{\eta_2}(\boldsymbol{k}_2) f_{\eta_1}(\boldsymbol{k}_3) f_{\eta_2}(\boldsymbol{k}_4) \\
&\quad \times e^{-\mathrm{i}|\boldsymbol{k}|t+\boldsymbol{k}\cdot\boldsymbol{x}} e^{\mathrm{i}|\boldsymbol{k}'|t'-\boldsymbol{k}'\cdot\boldsymbol{x}'} \delta(\boldsymbol{k}_3-\boldsymbol{k}_2)\delta(\boldsymbol{k}_4-\boldsymbol{k}')\delta(\boldsymbol{k}-\boldsymbol{k}_1) \\
&+ \mathcal{N}^2 \int \mathrm{d}^n\boldsymbol{k}_1\,\mathrm{d}^n\boldsymbol{k}_2\,\mathrm{d}^n\boldsymbol{k}_3\,\mathrm{d}^n\boldsymbol{k}_4\,\widetilde{\mathrm{d}^n\boldsymbol{k}}\,\widetilde{\mathrm{d}^n\boldsymbol{k}'} f_{\eta_1}(\boldsymbol{k}_1) f_{\eta_2}(\boldsymbol{k}_2) f_{\eta_1}(\boldsymbol{k}_3) f_{\eta_2}(\boldsymbol{k}_4) \\
&\quad \times e^{-\mathrm{i}|\boldsymbol{k}|t+\boldsymbol{k}\cdot\boldsymbol{x}} e^{\mathrm{i}|\boldsymbol{k}'|t'-\boldsymbol{k}'\cdot\boldsymbol{x}'} \Big(\delta(\boldsymbol{k}_1-\boldsymbol{k}_3)\delta(\boldsymbol{k}_2-\boldsymbol{k}_4)+\delta(\boldsymbol{k}_2-\boldsymbol{k}_3)\delta(\boldsymbol{k}_1-\boldsymbol{k}_4)\Big)\delta(\boldsymbol{k}-\boldsymbol{k}') \\
&+ \mathcal{N}^2 \int \mathrm{d}^n\boldsymbol{k}_1\,\mathrm{d}^n\boldsymbol{k}_2\,\mathrm{d}^n\boldsymbol{k}_3\,\mathrm{d}^n\boldsymbol{k}_4\,\widetilde{\mathrm{d}^n\boldsymbol{k}}\,\widetilde{\mathrm{d}^n\boldsymbol{k}'} f_{\eta_1}(\boldsymbol{k}_1) f_{\eta_2}(\boldsymbol{k}_2) f_{\eta_1}(\boldsymbol{k}_3) f_{\eta_2}(\boldsymbol{k}_4) \\
&\quad \times e^{\mathrm{i}|\boldsymbol{k}|t-\boldsymbol{k}\cdot\boldsymbol{x}} e^{-\mathrm{i}|\boldsymbol{k}|t+\boldsymbol{k}'\cdot\boldsymbol{x}'} \delta(\boldsymbol{k}_3-\boldsymbol{k})\delta(\boldsymbol{k}_4-\boldsymbol{k}_1)\delta(\boldsymbol{k}'-\boldsymbol{k}_2) \\
&+ \mathcal{N}^2 \int \mathrm{d}^n\boldsymbol{k}_1\,\mathrm{d}^n\boldsymbol{k}_2\,\mathrm{d}^n\boldsymbol{k}_3\,\mathrm{d}^n\boldsymbol{k}_4\,\widetilde{\mathrm{d}^n\boldsymbol{k}}\,\widetilde{\mathrm{d}^n\boldsymbol{k}'} f_{\eta_1}(\boldsymbol{k}_1) f_{\eta_2}(\boldsymbol{k}_2) f_{\eta_1}(\boldsymbol{k}_3) f_{\eta_2}(\boldsymbol{k}_4) \\
&\quad \times e^{\mathrm{i}|\boldsymbol{k}|t-\boldsymbol{k}\cdot\boldsymbol{x}} e^{-\mathrm{i}|\boldsymbol{k}|t+\boldsymbol{k}'\cdot\boldsymbol{x}'} \delta(\boldsymbol{k}_3-\boldsymbol{k}_1)\delta(\boldsymbol{k}'-\boldsymbol{k}_2)\delta(\boldsymbol{k}_4-\boldsymbol{k}) \\
&+ \mathcal{N}^2 \int \mathrm{d}^n\boldsymbol{k}_1\,\mathrm{d}^n\boldsymbol{k}_2\,\mathrm{d}^n\boldsymbol{k}_3\,\mathrm{d}^n\boldsymbol{k}_4\,\widetilde{\mathrm{d}^n\boldsymbol{k}}\,\widetilde{\mathrm{d}^n\boldsymbol{k}'} f_{\eta_1}(\boldsymbol{k}_1) f_{\eta_2}(\boldsymbol{k}_2) f_{\eta_1}(\boldsymbol{k}_3) f_{\eta_2}(\boldsymbol{k}_4) \\
&\quad \times e^{\mathrm{i}|\boldsymbol{k}|t-\boldsymbol{k}\cdot\boldsymbol{x}} e^{-\mathrm{i}|\boldsymbol{k}|t+\boldsymbol{k}'\cdot\boldsymbol{x}'} \delta(\boldsymbol{k}_3-\boldsymbol{k})\delta(\boldsymbol{k}_4-\boldsymbol{k}_2)\delta(\boldsymbol{k}'-\boldsymbol{k}_1) \\
&+ \mathcal{N}^2 \int \mathrm{d}^n\boldsymbol{k}_1\,\mathrm{d}^n\boldsymbol{k}_2\,\mathrm{d}^n\boldsymbol{k}_3\,\mathrm{d}^n\boldsymbol{k}_4\,\widetilde{\mathrm{d}^n\boldsymbol{k}}\,\widetilde{\mathrm{d}^n\boldsymbol{k}'} f_{\eta_1}(\boldsymbol{k}_1) f_{\eta_2}(\boldsymbol{k}_2) f_{\eta_1}(\boldsymbol{k}_3) f_{\eta_2}(\boldsymbol{k}_4) \\
&\quad \times e^{\mathrm{i}|\boldsymbol{k}|t-\boldsymbol{k}\cdot\boldsymbol{x}} e^{-\mathrm{i}|\boldsymbol{k}|t+\boldsymbol{k}'\cdot\boldsymbol{x}'} \delta(\boldsymbol{k}_3-\boldsymbol{k}_2)\delta(\boldsymbol{k}_4-\boldsymbol{k})\delta(\boldsymbol{k}'-\boldsymbol{k}_1). \qquad (33)
\end{aligned}
$$

While there are many terms here, they readily simplify using the same expression K Eq. (25) from the previous section: The first four summands in the bulky expression

Eq. (33) reduce to

$$
\begin{aligned}
&\mathcal{N}^2 \int \mathrm{d}^n\boldsymbol{k}_1\,\mathrm{d}^n\boldsymbol{k}_2\,\mathrm{d}^n\boldsymbol{k}_3\,\mathrm{d}^n\boldsymbol{k}_4\,\widetilde{\mathrm{d}^n\boldsymbol{k}}\,\widetilde{\mathrm{d}^n\boldsymbol{k}'} f_{\boldsymbol{\eta}_1}(\boldsymbol{k}_1) f_{\boldsymbol{\eta}_2}(\boldsymbol{k}_2) f_{\boldsymbol{\eta}_1}(\boldsymbol{k}_3) f_{\boldsymbol{\eta}_2}(\boldsymbol{k}_4) \\
&\quad \times e^{-\mathrm{i}|\boldsymbol{k}|t+\boldsymbol{k}\cdot\boldsymbol{x}} e^{\mathrm{i}|\boldsymbol{k}'|t'-\boldsymbol{k}'\cdot\boldsymbol{x}'} \delta(\boldsymbol{k}_3-\boldsymbol{k}')\delta(\boldsymbol{k}_4-\boldsymbol{k}_1)\delta(\boldsymbol{k}-\boldsymbol{k}_2) \\
&+ \mathcal{N}^2 \int \mathrm{d}^n\boldsymbol{k}_1\,\mathrm{d}^n\boldsymbol{k}_2\,\mathrm{d}^n\boldsymbol{k}_3\,\mathrm{d}^n\boldsymbol{k}_4\,\widetilde{\mathrm{d}^n\boldsymbol{k}}\,\widetilde{\mathrm{d}^n\boldsymbol{k}'} f_{\boldsymbol{\eta}_1}(\boldsymbol{k}_1) f_{\boldsymbol{\eta}_2}(\boldsymbol{k}_2) f_{\boldsymbol{\eta}_1}(\boldsymbol{k}_3) f_{\boldsymbol{\eta}_2}(\boldsymbol{k}_4) \\
&\quad \times e^{-\mathrm{i}|\boldsymbol{k}|t+\boldsymbol{k}\cdot\boldsymbol{x}} e^{\mathrm{i}|\boldsymbol{k}'|t'-\boldsymbol{k}'\cdot\boldsymbol{x}'} \delta(\boldsymbol{k}_3-\boldsymbol{k}_1)\delta(\boldsymbol{k}-\boldsymbol{k}_2)\delta(\boldsymbol{k}_4-\boldsymbol{k}') \\
&+ \mathcal{N}^2 \int \mathrm{d}^n\boldsymbol{k}_1\,\mathrm{d}^n\boldsymbol{k}_2\,\mathrm{d}^n\boldsymbol{k}_3\,\mathrm{d}^n\boldsymbol{k}_4\,\widetilde{\mathrm{d}^n\boldsymbol{k}}\,\widetilde{\mathrm{d}^n\boldsymbol{k}'} f_{\boldsymbol{\eta}_1}(\boldsymbol{k}_1) f_{\boldsymbol{\eta}_2}(\boldsymbol{k}_2) f_{\boldsymbol{\eta}_1}(\boldsymbol{k}_3) f_{\boldsymbol{\eta}_2}(\boldsymbol{k}_4) \\
&\quad \times e^{-\mathrm{i}|\boldsymbol{k}|t+\boldsymbol{k}\cdot\boldsymbol{x}} e^{\mathrm{i}|\boldsymbol{k}'|t'-\boldsymbol{k}'\cdot\boldsymbol{x}'} \delta(\boldsymbol{k}_3-\boldsymbol{k}')\delta(\boldsymbol{k}_4-\boldsymbol{k}_2)\delta(\boldsymbol{k}-\boldsymbol{k}_1) \\
&+ \mathcal{N}^2 \int \mathrm{d}^n\boldsymbol{k}_1\,\mathrm{d}^n\boldsymbol{k}_2\,\mathrm{d}^n\boldsymbol{k}_3\,\mathrm{d}^n\boldsymbol{k}_4\,\widetilde{\mathrm{d}^n\boldsymbol{k}}\,\widetilde{\mathrm{d}^n\boldsymbol{k}'} f_{\boldsymbol{\eta}_1}(\boldsymbol{k}_1) f_{\boldsymbol{\eta}_2}(\boldsymbol{k}_2) f_{\boldsymbol{\eta}_1}(\boldsymbol{k}_3) f_{\boldsymbol{\eta}_2}(\boldsymbol{k}_4) \\
&\quad \times e^{-\mathrm{i}|\boldsymbol{k}|t+\boldsymbol{k}\cdot\boldsymbol{x}} e^{\mathrm{i}|\boldsymbol{k}'|t'-\boldsymbol{k}'\cdot\boldsymbol{x}'} \delta(\boldsymbol{k}_3-\boldsymbol{k}_2)\delta(\boldsymbol{k}_4-\boldsymbol{k}')\delta(\boldsymbol{k}-\boldsymbol{k}_1) \\
&= \mathcal{N}^2 \Big(C_{\boldsymbol{\eta}_1\boldsymbol{\eta}_2} K_{\boldsymbol{\eta}_1}(\mathsf{x}') K_{\boldsymbol{\eta}_2}(\mathsf{x}) + K_{\boldsymbol{\eta}_2}(\mathsf{x}') K_{\boldsymbol{\eta}_2}(\mathsf{x}) \\
&\quad + C_{\boldsymbol{\eta}_1\boldsymbol{\eta}_2} K_{\boldsymbol{\eta}_2}(\mathsf{x}') K_{\boldsymbol{\eta}_1}(\mathsf{x}) + K_{\boldsymbol{\eta}_1}(\mathsf{x}') K_{\boldsymbol{\eta}_1}(\mathsf{x}) \Big),
\end{aligned}
\tag{34}
$$

where we have used the delta distributions to reduce the integrals. the final four summands in the bulky expression for the Wightman function is simply the complex conjugate of what is expressed above.

The middle term containing $\delta(\boldsymbol{k}-\boldsymbol{k}')$ contains the vacuum Wightman and the normalization constant Eq. (2.6),

$$
\begin{aligned}
&\mathcal{N}^2 \int \mathrm{d}^n\boldsymbol{k}_1\,\mathrm{d}^n\boldsymbol{k}_2\,\mathrm{d}^n\boldsymbol{k}_3\,\mathrm{d}^n\boldsymbol{k}_4\,\widetilde{\mathrm{d}^n\boldsymbol{k}}\,\widetilde{\mathrm{d}^n\boldsymbol{k}'} f_{\boldsymbol{\eta}_1}(\boldsymbol{k}_1) f_{\boldsymbol{\eta}_2}(\boldsymbol{k}_2) f_{\boldsymbol{\eta}_1}(\boldsymbol{k}_3) f_{\boldsymbol{\eta}_2}(\boldsymbol{k}_4) \\
&\qquad \times e^{-\mathrm{i}|\boldsymbol{k}|t+\boldsymbol{k}\cdot\boldsymbol{x}} e^{\mathrm{i}|\boldsymbol{k}'|t'-\boldsymbol{k}'\cdot\boldsymbol{x}'} \Big(\delta(\boldsymbol{k}_1-\boldsymbol{k}_3)\delta(\boldsymbol{k}_2-\boldsymbol{k}_4) + \delta(\boldsymbol{k}_2-\boldsymbol{k}_3)\delta(\boldsymbol{k}_1-\boldsymbol{k}_4) \Big) \delta(\boldsymbol{k}-\boldsymbol{k}') \\
&= \mathcal{N}^2 W^{\phi}_{\mathrm{VAC}} \Big(\int \mathrm{d}^n\boldsymbol{k}\, f_{\boldsymbol{\eta}_1}(\boldsymbol{k}) f_{\boldsymbol{\eta}_2}(\boldsymbol{k}) \int \mathrm{d}^n\boldsymbol{k}'\, f_{\boldsymbol{\eta}_1}(\boldsymbol{k}') f_{\boldsymbol{\eta}_2}(\boldsymbol{k}') \\
&\quad + \int \mathrm{d}^n\boldsymbol{k}\, (f_{\boldsymbol{\eta}_1}(\boldsymbol{k}))^2 \int \mathrm{d}^n\boldsymbol{k}'\, (f_{\boldsymbol{\eta}_2}(\boldsymbol{k}'))^2 \Big) \\
&= \mathcal{N}^2 W^{\phi}_{\mathrm{VAC}}(\mathsf{x},\mathsf{x}') \left(C^2_{\boldsymbol{\eta}_1\boldsymbol{\eta}_2} + 1 \right) \\
&= W^{\phi}_{\mathrm{VAC}}(\mathsf{x},\mathsf{x}')
\end{aligned}
\tag{35}
$$

In this previous series of equalities, the first equivalence follows from the definition of the vacuum Wightman and the method of reduction of integrals from the delta functions. The second equality follows from the definition of $C_{\boldsymbol{\eta}_1\boldsymbol{\eta}_2}$ found in Eq. (2.6). The final inequality follows from the form of the normalization constant $\mathcal{N}$ also found in Eq. (2.6).

If we combine the vacuum Eq. (35) and non vacuume Eq. (34) expressions we just combined, we can reduced the bulky expression of the Two-particle Wightman function Eq. (33) to

$$W^{\phi}_{\eta_1,\eta_2}(\mathsf{x},\mathsf{x}') = W^{\phi}_{\mathrm{VAC}}(\mathsf{x},\mathsf{x}') + \mathcal{N}^2\Big[C_{\boldsymbol{\eta}_1\boldsymbol{\eta}_2}\Big(K_{\boldsymbol{\eta}_1}(\mathsf{x}')K_{\boldsymbol{\eta}_2}(\mathsf{x}) + K_{\boldsymbol{\eta}_2}(\mathsf{x}')K_{\boldsymbol{\eta}_1}(\mathsf{x}) + c.c.\Big) + \Big(K_{\boldsymbol{\eta}_2}(\mathsf{x}')K_{\boldsymbol{\eta}_2}(\mathsf{x}) + K_{\boldsymbol{\eta}_1}(\mathsf{x}')K_{\boldsymbol{\eta}_1}(\mathsf{x}) + c.c.\Big)\Big] \tag{36}$$

4 Two point correlator of the quadratic coupling to a one-particle Fock state-1

In this section we will calculate the two-point correlator for the quadratic field operator when the field is in a one-particle fock-like state:

$$W^{\phi^2}_{k_0}(\mathsf{x},\mathsf{x}') = \langle 1_f| : \phi^2(\mathsf{x}) :: \phi^2(\mathsf{x}') : |1_{f_{k_0}}\rangle \tag{37}$$

The first step is to fill in the definitions in the above expression, starting with the mode expansion of the normal-ordered ϕ^2 operator,

$$: \phi^2(\mathsf{x}) := \int \widetilde{\mathrm{d}^n\boldsymbol{k}_1}\int \widetilde{\mathrm{d}^n\boldsymbol{k}_2}\Big(\hat{a}_{\boldsymbol{k}_1}\hat{a}_{\boldsymbol{k}_2}e^{-\mathrm{i}|\boldsymbol{k}_1|t+\boldsymbol{k}_1\cdot\boldsymbol{x}}e^{-\mathrm{i}|\boldsymbol{k}_2|t+\boldsymbol{k}_2\cdot\boldsymbol{x}} + \hat{a}^{\dagger}_{\boldsymbol{k}_1}\hat{a}_{\boldsymbol{k}_2}e^{\mathrm{i}|\boldsymbol{k}_1|t-\boldsymbol{k}_1\cdot\boldsymbol{x}}e^{-\mathrm{i}|\boldsymbol{k}_2|t+\boldsymbol{k}_2\cdot\boldsymbol{x}} + \hat{a}^{\dagger}_{\boldsymbol{k}_2}\hat{a}_{\boldsymbol{k}_1}e^{-\mathrm{i}|\boldsymbol{k}_1|t+\boldsymbol{k}_1\cdot\boldsymbol{x}}e^{\mathrm{i}|\boldsymbol{k}_2|t-\boldsymbol{k}_2\cdot\boldsymbol{x}} + \hat{a}^{\dagger}_{\boldsymbol{k}_1}\hat{a}^{\dagger}_{\boldsymbol{k}_2}e^{\mathrm{i}|\boldsymbol{k}_1|t-\boldsymbol{k}_1\cdot\boldsymbol{x}}e^{\mathrm{i}|\boldsymbol{k}_2|t-\boldsymbol{k}_2\cdot\boldsymbol{x}}\Big) \tag{38}$$

Inserting this into Eq. (37),

$$
\begin{aligned}
W_{k_0}^{\phi^2}(\mathsf{x},\mathsf{x}') = \int \mathrm{d}^n\boldsymbol{p} f_{\boldsymbol{k}_0}(\boldsymbol{p}) \int \mathrm{d}^n\boldsymbol{p}' f_{\boldsymbol{k}_0}(\boldsymbol{p}') \int \widetilde{\mathrm{d}^n\boldsymbol{k}_1} \int \widetilde{\mathrm{d}^n\boldsymbol{k}_2} \int \widetilde{\mathrm{d}^n\boldsymbol{k}_3} \int \widetilde{\mathrm{d}^n\boldsymbol{k}_4} \\
\times \langle 0| \hat{a}_{\boldsymbol{p}'} \Big(\hat{a}_{\boldsymbol{k}_1}\hat{a}_{\boldsymbol{k}_2} e^{-\mathrm{i}|\boldsymbol{k}_1|t+\boldsymbol{k}_1\cdot\boldsymbol{x}} e^{-\mathrm{i}|\boldsymbol{k}_2|t+\boldsymbol{k}_2\cdot\boldsymbol{x}} + \hat{a}^\dagger_{\boldsymbol{k}_1}\hat{a}_{\boldsymbol{k}_2} e^{\mathrm{i}|\boldsymbol{k}_1|t-\boldsymbol{k}_1\cdot\boldsymbol{x}} e^{-\mathrm{i}|\boldsymbol{k}_2|t+\boldsymbol{k}_2\cdot\boldsymbol{x}} \\
+ \hat{a}^\dagger_{\boldsymbol{k}_2}\hat{a}_{\boldsymbol{k}_1} e^{-\mathrm{i}|\boldsymbol{k}_1|t+\boldsymbol{k}_1\cdot\boldsymbol{x}} e^{\mathrm{i}|\boldsymbol{k}_2|t-\boldsymbol{k}_2\cdot\boldsymbol{x}} + \hat{a}^\dagger_{\boldsymbol{k}_1}\hat{a}^\dagger_{\boldsymbol{k}_2} e^{\mathrm{i}|\boldsymbol{k}_1|t-\boldsymbol{k}_1\cdot\boldsymbol{x}} e^{\mathrm{i}|\boldsymbol{k}_2|t-\boldsymbol{k}_2\cdot\boldsymbol{x}} \Big) \\
\times \Big(\hat{a}_{\boldsymbol{k}_3}\hat{a}_{\boldsymbol{k}_4} e^{-\mathrm{i}|\boldsymbol{k}_3|t+\boldsymbol{k}_3\cdot\boldsymbol{x}'} e^{-\mathrm{i}|\boldsymbol{k}_4|t'+\boldsymbol{k}_4\cdot\boldsymbol{x}'} + \hat{a}^\dagger_{\boldsymbol{k}_3}\hat{a}_{\boldsymbol{k}_4} e^{\mathrm{i}|\boldsymbol{k}_3|t-\boldsymbol{k}_3\cdot\boldsymbol{x}'} e^{-\mathrm{i}|\boldsymbol{k}_4|t'+\boldsymbol{k}_4\cdot\boldsymbol{x}'} \\
+ \hat{a}^\dagger_{\boldsymbol{k}_4}\hat{a}_{\boldsymbol{k}_3} e^{-\mathrm{i}|\boldsymbol{k}_3|t+\boldsymbol{k}_3\cdot\boldsymbol{x}'} e^{\mathrm{i}|\boldsymbol{k}_4|t-\boldsymbol{k}_4\cdot\boldsymbol{x}'} + \hat{a}^\dagger_{\boldsymbol{k}_3}\hat{a}^\dagger_{\boldsymbol{k}_4} e^{\mathrm{i}|\boldsymbol{k}_3|t-\boldsymbol{k}_3\cdot\boldsymbol{x}'} e^{\mathrm{i}|\boldsymbol{k}_4|t-\boldsymbol{k}_4\cdot\boldsymbol{x}'} \Big) \hat{a}^\dagger_{\boldsymbol{p}} |0\rangle
\end{aligned}
\tag{39}
$$

Expanding and dropping terms that aren't balanced in number of creation and annihilation operators yield

$$
\begin{aligned}
W_{k_0}^{\phi^2}(\mathsf{x},\mathsf{x}') = \int \mathrm{d}^n\boldsymbol{p} f_{\boldsymbol{k}_0}(\boldsymbol{p}) \int \mathrm{d}^n\boldsymbol{p}' f_{\boldsymbol{k}_0}(\boldsymbol{p}') \int \widetilde{\mathrm{d}^n\boldsymbol{k}_1} \int \widetilde{\mathrm{d}^n\boldsymbol{k}_2} \int \widetilde{\mathrm{d}^n\boldsymbol{k}_3} \int \widetilde{\mathrm{d}^n\boldsymbol{k}_4} \\
\times e^{\mathrm{i}|\boldsymbol{k}_3|t-\boldsymbol{k}_3\cdot\boldsymbol{x}'} e^{\mathrm{i}|\boldsymbol{k}_4|t-\boldsymbol{k}_4\cdot\boldsymbol{x}'} e^{-\mathrm{i}|\boldsymbol{k}_1|t+\boldsymbol{k}_1\cdot\boldsymbol{x}} e^{-\mathrm{i}|\boldsymbol{k}_2|t+\boldsymbol{k}_2\cdot\boldsymbol{x}} \langle 0| \hat{a}_{\boldsymbol{p}'}\hat{a}_{\boldsymbol{k}_1}\hat{a}_{\boldsymbol{k}_2}\hat{a}^\dagger_{\boldsymbol{k}_3}\hat{a}^\dagger_{\boldsymbol{k}_4}\hat{a}^\dagger_{\boldsymbol{p}} |0\rangle \\
+ \int \mathrm{d}^n\boldsymbol{p} f_{\boldsymbol{k}_0}(\boldsymbol{p}) \int \mathrm{d}^n\boldsymbol{p}' f_{\boldsymbol{k}_0}(\boldsymbol{p}') \int \widetilde{\mathrm{d}^n\boldsymbol{k}_1} \int \widetilde{\mathrm{d}^n\boldsymbol{k}_2} \int \widetilde{\mathrm{d}^n\boldsymbol{k}_3} \int \widetilde{\mathrm{d}^n\boldsymbol{k}_4} \\
\times e^{-\mathrm{i}|\boldsymbol{k}_3|t+\boldsymbol{k}_3\cdot\boldsymbol{x}'} e^{-\mathrm{i}|\boldsymbol{k}_4|t'+\boldsymbol{k}_4\cdot\boldsymbol{x}'} e^{\mathrm{i}|\boldsymbol{k}_1|t-\boldsymbol{k}_1\cdot\boldsymbol{x}} e^{\mathrm{i}|\boldsymbol{k}_2|t-\boldsymbol{k}_2\cdot\boldsymbol{x}} \langle 0| \hat{a}_{\boldsymbol{p}'}\hat{a}^\dagger_{\boldsymbol{k}_1}\hat{a}^\dagger_{\boldsymbol{k}_2}\hat{a}_{\boldsymbol{k}_3}\hat{a}_{\boldsymbol{k}_4}\hat{a}^\dagger_{\boldsymbol{p}} |0\rangle \\
+ \int \mathrm{d}^n\boldsymbol{p} f_{\boldsymbol{k}_0}(\boldsymbol{p}) \int \mathrm{d}^n\boldsymbol{p}' f_{\boldsymbol{k}_0}(\boldsymbol{p}') \int \widetilde{\mathrm{d}^n\boldsymbol{k}_1} \int \widetilde{\mathrm{d}^n\boldsymbol{k}_2} \int \widetilde{\mathrm{d}^n\boldsymbol{k}_3} \int \widetilde{\mathrm{d}^n\boldsymbol{k}_4} \\
\times e^{\mathrm{i}|\boldsymbol{k}_1|t-\boldsymbol{k}_1\cdot\boldsymbol{x}} e^{-\mathrm{i}|\boldsymbol{k}_2|t+\boldsymbol{k}_2\cdot\boldsymbol{x}} e^{\mathrm{i}|\boldsymbol{k}_3|t-\boldsymbol{k}_3\cdot\boldsymbol{x}'} e^{-\mathrm{i}|\boldsymbol{k}_4|t'+\boldsymbol{k}_4\cdot\boldsymbol{x}'} \langle 0| \hat{a}_{\boldsymbol{p}'}\hat{a}^\dagger_{\boldsymbol{k}_1}\hat{a}_{\boldsymbol{k}_2}\hat{a}^\dagger_{\boldsymbol{k}_3}\hat{a}_{\boldsymbol{k}_4}\hat{a}^\dagger_{\boldsymbol{p}} |0\rangle \\
+ \int \mathrm{d}^n\boldsymbol{p} f_{\boldsymbol{k}_0}(\boldsymbol{p}) \int \mathrm{d}^n\boldsymbol{p}' f_{\boldsymbol{k}_0}(\boldsymbol{p}') \int \widetilde{\mathrm{d}^n\boldsymbol{k}_1} \int \widetilde{\mathrm{d}^n\boldsymbol{k}_2} \int \widetilde{\mathrm{d}^n\boldsymbol{k}_3} \int \widetilde{\mathrm{d}^n\boldsymbol{k}_4} \\
\times e^{\mathrm{i}|\boldsymbol{k}_1|t-\boldsymbol{k}_1\cdot\boldsymbol{x}} e^{-\mathrm{i}|\boldsymbol{k}_2|t+\boldsymbol{k}_2\cdot\boldsymbol{x}} e^{-\mathrm{i}|\boldsymbol{k}_3|t+\boldsymbol{k}_3\cdot\boldsymbol{x}'} e^{\mathrm{i}|\boldsymbol{k}_4|t-\boldsymbol{k}_4\cdot\boldsymbol{x}'} \langle 0| \hat{a}_{\boldsymbol{p}'}\hat{a}^\dagger_{\boldsymbol{k}_1}\hat{a}_{\boldsymbol{k}_2}\hat{a}^\dagger_{\boldsymbol{k}_4}\hat{a}_{\boldsymbol{k}_3}\hat{a}^\dagger_{\boldsymbol{p}} |0\rangle \\
+ \int \mathrm{d}^n\boldsymbol{p} f_{\boldsymbol{k}_0}(\boldsymbol{p}) \int \mathrm{d}^n\boldsymbol{p}' f_{\boldsymbol{k}_0}(\boldsymbol{p}') \int \widetilde{\mathrm{d}^n\boldsymbol{k}_1} \int \widetilde{\mathrm{d}^n\boldsymbol{k}_2} \int \widetilde{\mathrm{d}^n\boldsymbol{k}_3} \int \widetilde{\mathrm{d}^n\boldsymbol{k}_4} \\
\times e^{-\mathrm{i}|\boldsymbol{k}_1|t+\boldsymbol{k}_1\cdot\boldsymbol{x}} e^{\mathrm{i}|\boldsymbol{k}_2|t-\boldsymbol{k}_2\cdot\boldsymbol{x}} e^{\mathrm{i}|\boldsymbol{k}_3|t-\boldsymbol{k}_3\cdot\boldsymbol{x}'} e^{-\mathrm{i}|\boldsymbol{k}_4|t'+\boldsymbol{k}_4\cdot\boldsymbol{x}'} \langle 0| \hat{a}_{\boldsymbol{p}'}\hat{a}^\dagger_{\boldsymbol{k}_2}\hat{a}_{\boldsymbol{k}_1}\hat{a}^\dagger_{\boldsymbol{k}_3}\hat{a}_{\boldsymbol{k}_4}\hat{a}^\dagger_{\boldsymbol{p}} |0\rangle \\
+ \int \mathrm{d}^n\boldsymbol{p} f_{\boldsymbol{k}_0}(\boldsymbol{p}) \int \mathrm{d}^n\boldsymbol{p}' f_{\boldsymbol{k}_0}(\boldsymbol{p}') \int \widetilde{\mathrm{d}^n\boldsymbol{k}_1} \int \widetilde{\mathrm{d}^n\boldsymbol{k}_2} \int \widetilde{\mathrm{d}^n\boldsymbol{k}_3} \int \widetilde{\mathrm{d}^n\boldsymbol{k}_4} \\
\times e^{-\mathrm{i}|\boldsymbol{k}_1|t+\boldsymbol{k}_1\cdot\boldsymbol{x}} e^{\mathrm{i}|\boldsymbol{k}_2|t-\boldsymbol{k}_2\cdot\boldsymbol{x}} e^{-\mathrm{i}|\boldsymbol{k}_3|t+\boldsymbol{k}_3\cdot\boldsymbol{x}'} e^{\mathrm{i}|\boldsymbol{k}_4|t-\boldsymbol{k}_4\cdot\boldsymbol{x}'} \langle 0| \hat{a}_{\boldsymbol{p}'}\hat{a}^\dagger_{\boldsymbol{k}_2}\hat{a}_{\boldsymbol{k}_1}\hat{a}^\dagger_{\boldsymbol{k}_4}\hat{a}_{\boldsymbol{k}_3}\hat{a}^\dagger_{\boldsymbol{p}} |0\rangle
\end{aligned}
\tag{40}
$$

Let us look at the three orderings of creation and anihilation operators (ignoring the labels on momenta),

$$\langle 0|\, \hat{a}_{\boldsymbol{p}_1} \hat{a}_{\boldsymbol{p}_2} \hat{a}_{\boldsymbol{p}_3} \hat{a}^\dagger_{\boldsymbol{p}_4} \hat{a}^\dagger_{\boldsymbol{p}_5} \hat{a}^\dagger_{\boldsymbol{p}_6} \,|0\rangle \ , \tag{41}$$

$$\langle 0|\, \hat{a}_{\boldsymbol{p}_1} \hat{a}^\dagger_{\boldsymbol{p}_2} \hat{a}^\dagger_{\boldsymbol{p}_3} \hat{a}_{\boldsymbol{p}_4} \hat{a}_{\boldsymbol{p}_5} \hat{a}^\dagger_{\boldsymbol{p}_6} \,|0\rangle \ , \text{ and} \tag{42}$$

$$\langle 0|\, \hat{a}_{\boldsymbol{p}_1} \hat{a}^\dagger_{\boldsymbol{p}_2} \hat{a}_{\boldsymbol{p}_3} \hat{a}^\dagger_{\boldsymbol{p}_4} \hat{a}_{\boldsymbol{p}_5} \hat{a}^\dagger_{\boldsymbol{p}_6} \,|0\rangle \ . \tag{43}$$

The first can be simplified in the following way:

$$\begin{aligned}
\langle 0|\, \hat{a}_{\boldsymbol{p}_1} \hat{a}_{\boldsymbol{p}_2} \hat{a}_{\boldsymbol{p}_3} \hat{a}^\dagger_{\boldsymbol{p}_4} \hat{a}^\dagger_{\boldsymbol{p}_5} \hat{a}^\dagger_{\boldsymbol{p}_6} \,|0\rangle &= \langle 0|\, \hat{a}_{\boldsymbol{p}_1} \hat{a}_{\boldsymbol{p}_2} \hat{a}^\dagger_{\boldsymbol{p}_4} \hat{a}_{\boldsymbol{p}_3} \hat{a}^\dagger_{\boldsymbol{p}_5} \hat{a}^\dagger_{\boldsymbol{p}_6} \,|0\rangle + \langle 0|\, \hat{a}_{\boldsymbol{p}_1} \hat{a}_{\boldsymbol{p}_2} \hat{a}^\dagger_{\boldsymbol{p}_5} \hat{a}^\dagger_{\boldsymbol{p}_6} \,|0\rangle\, \delta(\boldsymbol{p}_4 - \boldsymbol{p}_3) \\
&= \langle 0|\, \hat{a}_{\boldsymbol{p}_1} \hat{a}^\dagger_{\boldsymbol{p}_4} \hat{a}_{\boldsymbol{p}_2} \hat{a}^\dagger_{\boldsymbol{p}_5} \hat{a}_{\boldsymbol{p}_3} \hat{a}^\dagger_{\boldsymbol{p}_6} \,|0\rangle + \langle 0|\, \hat{a}_{\boldsymbol{p}_1} \hat{a}^\dagger_{\boldsymbol{p}_5} \hat{a}_{\boldsymbol{p}_3} \hat{a}^\dagger_{\boldsymbol{p}_6} \,|0\rangle\, \delta(\boldsymbol{p}_4 - \boldsymbol{p}_2) \\
&\quad + \langle 0|\, \hat{a}_{\boldsymbol{p}_1} \hat{a}^\dagger_{\boldsymbol{p}_4} \hat{a}_{\boldsymbol{p}_2} \hat{a}^\dagger_{\boldsymbol{p}_6} \,|0\rangle\, \delta(\boldsymbol{p}_5 - \boldsymbol{p}_3) + \langle 0|\, \hat{a}_{\boldsymbol{p}_1} \hat{a}^\dagger_{\boldsymbol{p}_6} \,|0\rangle\, \delta(\boldsymbol{p}_4 - \boldsymbol{p}_2)\delta(\boldsymbol{p}_5 - \boldsymbol{p}_3) \\
&\quad + \langle 0|\, \hat{a}_{\boldsymbol{p}_1} \hat{a}^\dagger_{\boldsymbol{p}_5} \hat{a}_{\boldsymbol{p}_2} \hat{a}^\dagger_{\boldsymbol{p}_6} \,|0\rangle\, \delta(\boldsymbol{p}_4 - \boldsymbol{p}_3) + \langle 0|\, \hat{a}_{\boldsymbol{p}_1} \hat{a}^\dagger_{\boldsymbol{p}_6} \,|0\rangle\, \delta(\boldsymbol{p}_4 - \boldsymbol{p}_3)\delta(\boldsymbol{p}_5 - \boldsymbol{p}_2) \\
&= \delta(\boldsymbol{p}_4 - \boldsymbol{p}_1)\delta(\boldsymbol{p}_5 - \boldsymbol{p}_2)\delta(\boldsymbol{p}_3 - \boldsymbol{p}_6) + \delta(\boldsymbol{p}_1 - \boldsymbol{p}_5)\delta(\boldsymbol{p}_3 - \boldsymbol{p}_6)\delta(\boldsymbol{p}_4 - \boldsymbol{p}_2) \\
&\quad + \delta(\boldsymbol{p}_4 - \boldsymbol{p}_1)\delta(\boldsymbol{p}_6 - \boldsymbol{p}_2)\delta(\boldsymbol{p}_5 - \boldsymbol{p}_3) + \delta(\boldsymbol{p}_1 - \boldsymbol{p}_6)\delta(\boldsymbol{p}_4 - \boldsymbol{p}_2)\delta(\boldsymbol{p}_5 - \boldsymbol{p}_3) \\
&\quad + \delta(\boldsymbol{p}_1 - \boldsymbol{p}_5)\delta(\boldsymbol{p}_2 - \boldsymbol{p}_6)\delta(\boldsymbol{p}_4 - \boldsymbol{p}_3) + \delta(\boldsymbol{p}_1 - \boldsymbol{p}_6)\delta(\boldsymbol{p}_4 - \boldsymbol{p}_3)\delta(\boldsymbol{p}_5 - \boldsymbol{p}_2),
\end{aligned} \tag{44}$$

where all equalities follow from applying the commutator and some arithmetic. The second expression can be simplified in the following way:

$$\begin{aligned}
\langle 0|\, \hat{a}_{\boldsymbol{p}_1} \hat{a}^\dagger_{\boldsymbol{p}_2} \hat{a}^\dagger_{\boldsymbol{p}_3} \hat{a}_{\boldsymbol{p}_4} \hat{a}_{\boldsymbol{p}_5} \hat{a}^\dagger_{\boldsymbol{p}_6} \,|0\rangle &= \langle 0|\, (\hat{a}^\dagger_{\boldsymbol{p}_2} \hat{a}_{\boldsymbol{p}_1} + \delta(\boldsymbol{p}_2 - \boldsymbol{p}_1))\hat{a}^\dagger_{\boldsymbol{p}_3} \hat{a}_{\boldsymbol{p}_4} (\hat{a}^\dagger_{\boldsymbol{p}_6} \hat{a}_{\boldsymbol{p}_5} + \delta(\boldsymbol{p}_6 - \boldsymbol{p}_5)) \,|0\rangle \\
&= \delta(\boldsymbol{p}_6 - \boldsymbol{p}_5)\delta(\boldsymbol{p}_3 - \boldsymbol{p}_4)\delta(\boldsymbol{p}_2 - \boldsymbol{p}_1)
\end{aligned} \tag{45}$$

The first equality applies from commuting the pairs of operators acting on the vacuum. The second is from annihilating the vacuum on either side and commuting the remaining two operators, which also annihilate the vacuum. The third expression is

$$\langle 0|\, \hat{a}_{\boldsymbol{p}_1} \hat{a}^\dagger_{\boldsymbol{p}_2} \hat{a}_{\boldsymbol{p}_3} \hat{a}^\dagger_{\boldsymbol{p}_4} \hat{a}_{\boldsymbol{p}_5} \hat{a}^\dagger_{\boldsymbol{p}_6} \,|0\rangle = \delta(\boldsymbol{p}_1 - \boldsymbol{p}_2)\delta(\boldsymbol{p}_3 - \boldsymbol{p}_4)\delta(\boldsymbol{p}_5 - \boldsymbol{p}_6), \tag{46}$$

where each successive pair of operators were be commuted to annihilate the vacuum, yielding the above result.

Applying these commutators to the two-point correlator Eq. (40) results in

$$
\begin{aligned}
W_{k_0}^{\phi^2}(\mathsf{x},\mathsf{x}') = &\int \mathrm{d}^n\boldsymbol{p} f_{\boldsymbol{k}_0}(\boldsymbol{p}) \int \mathrm{d}^n\boldsymbol{p}' f_{\boldsymbol{k}_0}(\boldsymbol{p}') \int \widetilde{\mathrm{d}^n\boldsymbol{k}_1} \int \widetilde{\mathrm{d}^n\boldsymbol{k}_2} \int \widetilde{\mathrm{d}^n\boldsymbol{k}_3} \int \widetilde{\mathrm{d}^n\boldsymbol{k}_4} \\
&\times e^{\mathrm{i}|\boldsymbol{k}_3|t-\boldsymbol{k}_3\cdot\boldsymbol{x}'} e^{\mathrm{i}|\boldsymbol{k}_4|t-\boldsymbol{k}_4\cdot\boldsymbol{x}'} e^{-\mathrm{i}|\boldsymbol{k}_1|t+\boldsymbol{k}_1\cdot\boldsymbol{x}} e^{-\mathrm{i}|\boldsymbol{k}_2|t+\boldsymbol{k}_2\cdot\boldsymbol{x}} \\
&\times \Big(\delta(\boldsymbol{p}'-\boldsymbol{k}_3)\delta(\boldsymbol{k}_1-\boldsymbol{k}_5)\delta(\boldsymbol{k}_2-\boldsymbol{p}) + \delta(\boldsymbol{p}'-\boldsymbol{k}_4)\delta(\boldsymbol{k}_1-\boldsymbol{k}_3)\delta(\boldsymbol{k}_2-\boldsymbol{p}) \\
&\quad + \delta(\boldsymbol{p}'-\boldsymbol{k}_3)\delta(\boldsymbol{k}_4-\boldsymbol{k}_2)\delta(\boldsymbol{k}_1-\boldsymbol{p}) + \delta(\boldsymbol{p}'-\boldsymbol{p})\delta(\boldsymbol{k}_1-\boldsymbol{k}_3)\delta(\boldsymbol{k}_2-\boldsymbol{k}_4) \\
&\quad + \delta(\boldsymbol{p}'-\boldsymbol{k}_4)\delta(\boldsymbol{k}_2-\boldsymbol{k}_3)\delta(\boldsymbol{k}_1-\boldsymbol{p}) + \delta(\boldsymbol{p}'-\boldsymbol{p})\delta(\boldsymbol{k}_2-\boldsymbol{k}_3)\delta(\boldsymbol{k}_1-\boldsymbol{k}_4) \Big) \\
&+ \int \mathrm{d}^n\boldsymbol{p} f_{\boldsymbol{k}_0}(\boldsymbol{p}) \int \mathrm{d}^n\boldsymbol{p}' f_{\boldsymbol{k}_0}(\boldsymbol{p}') \int \widetilde{\mathrm{d}^n\boldsymbol{k}_1} \int \widetilde{\mathrm{d}^n\boldsymbol{k}_2} \int \widetilde{\mathrm{d}^n\boldsymbol{k}_3} \int \widetilde{\mathrm{d}^n\boldsymbol{k}_4} \\
&\times e^{-\mathrm{i}|\boldsymbol{k}_3|t+\boldsymbol{k}_3\cdot\boldsymbol{x}'} e^{-\mathrm{i}|\boldsymbol{k}_4|t'+\boldsymbol{k}_4\cdot\boldsymbol{x}'} e^{\mathrm{i}|\boldsymbol{k}_1|t-\boldsymbol{k}_1\cdot\boldsymbol{x}} e^{\mathrm{i}|\boldsymbol{k}_2|t-\boldsymbol{k}_2\cdot\boldsymbol{x}} \delta(\boldsymbol{p}'-\boldsymbol{k}_1)\delta(\boldsymbol{k}_2-\boldsymbol{k}_3)\delta(\boldsymbol{k}_4-\boldsymbol{p}) \\
&+ \int \mathrm{d}^n\boldsymbol{p} f_{\boldsymbol{k}_0}(\boldsymbol{p}) \int \mathrm{d}^n\boldsymbol{p}' f_{\boldsymbol{k}_0}(\boldsymbol{p}') \int \widetilde{\mathrm{d}^n\boldsymbol{k}_1} \int \widetilde{\mathrm{d}^n\boldsymbol{k}_2} \int \widetilde{\mathrm{d}^n\boldsymbol{k}_3} \int \widetilde{\mathrm{d}^n\boldsymbol{k}_4} \\
&\times e^{\mathrm{i}|\boldsymbol{k}_1|t-\boldsymbol{k}_1\cdot\boldsymbol{x}} e^{-\mathrm{i}|\boldsymbol{k}_2|t+\boldsymbol{k}_2\cdot\boldsymbol{x}} e^{\mathrm{i}|\boldsymbol{k}_3|t-\boldsymbol{k}_3\cdot\boldsymbol{x}'} e^{-\mathrm{i}|\boldsymbol{k}_4|t'+\boldsymbol{k}_4\cdot\boldsymbol{x}'} \delta(\boldsymbol{p}'-\boldsymbol{k}_1)\delta(\boldsymbol{k}_2-\boldsymbol{k}_3)\delta(\boldsymbol{k}_4-\boldsymbol{p}) \\
&+ \int \mathrm{d}^n\boldsymbol{p} f_{\boldsymbol{k}_0}(\boldsymbol{p}) \int \mathrm{d}^n\boldsymbol{p}' f_{\boldsymbol{k}_0}(\boldsymbol{p}') \int \widetilde{\mathrm{d}^n\boldsymbol{k}_1} \int \widetilde{\mathrm{d}^n\boldsymbol{k}_2} \int \widetilde{\mathrm{d}^n\boldsymbol{k}_3} \int \widetilde{\mathrm{d}^n\boldsymbol{k}_4} \\
&\times e^{\mathrm{i}|\boldsymbol{k}_1|t-\boldsymbol{k}_1\cdot\boldsymbol{x}} e^{-\mathrm{i}|\boldsymbol{k}_2|t+\boldsymbol{k}_2\cdot\boldsymbol{x}} e^{-\mathrm{i}|\boldsymbol{k}_3|t+\boldsymbol{k}_3\cdot\boldsymbol{x}'} e^{\mathrm{i}|\boldsymbol{k}_4|t-\boldsymbol{k}_4\cdot\boldsymbol{x}'} \delta(\boldsymbol{p}'-\boldsymbol{k}_1)\delta(\boldsymbol{k}_2-\boldsymbol{k}_4)\delta(\boldsymbol{k}_3-\boldsymbol{p}) \\
&+ \int \mathrm{d}^n\boldsymbol{p} f_{\boldsymbol{k}_0}(\boldsymbol{p}) \int \mathrm{d}^n\boldsymbol{p}' f_{\boldsymbol{k}_0}(\boldsymbol{p}') \int \widetilde{\mathrm{d}^n\boldsymbol{k}_1} \int \widetilde{\mathrm{d}^n\boldsymbol{k}_2} \int \widetilde{\mathrm{d}^n\boldsymbol{k}_3} \int \widetilde{\mathrm{d}^n\boldsymbol{k}_4} \\
&\times e^{-\mathrm{i}|\boldsymbol{k}_1|t+\boldsymbol{k}_1\cdot\boldsymbol{x}} e^{\mathrm{i}|\boldsymbol{k}_2|t-\boldsymbol{k}_2\cdot\boldsymbol{x}} e^{\mathrm{i}|\boldsymbol{k}_3|t-\boldsymbol{k}_3\cdot\boldsymbol{x}'} e^{-\mathrm{i}|\boldsymbol{k}_4|t'+\boldsymbol{k}_4\cdot\boldsymbol{x}'} \delta(\boldsymbol{p}'-\boldsymbol{k}_2)\delta(\boldsymbol{k}_1-\boldsymbol{k}_3)\delta(\boldsymbol{k}_4-\boldsymbol{p}) \\
&+ \int \mathrm{d}^n\boldsymbol{p} f_{\boldsymbol{k}_0}(\boldsymbol{p}) \int \mathrm{d}^n\boldsymbol{p}' f_{\boldsymbol{k}_0}(\boldsymbol{p}') \int \widetilde{\mathrm{d}^n\boldsymbol{k}_1} \int \widetilde{\mathrm{d}^n\boldsymbol{k}_2} \int \widetilde{\mathrm{d}^n\boldsymbol{k}_3} \int \widetilde{\mathrm{d}^n\boldsymbol{k}_4} \\
&\times e^{-\mathrm{i}|\boldsymbol{k}_1|t+\boldsymbol{k}_1\cdot\boldsymbol{x}} e^{\mathrm{i}|\boldsymbol{k}_2|t-\boldsymbol{k}_2\cdot\boldsymbol{x}} e^{-\mathrm{i}|\boldsymbol{k}_3|t+\boldsymbol{k}_3\cdot\boldsymbol{x}'} e^{\mathrm{i}|\boldsymbol{k}_4|t-\boldsymbol{k}_4\cdot\boldsymbol{x}'} \delta(\boldsymbol{p}'-\boldsymbol{k}_2)\delta(\boldsymbol{k}_1-\boldsymbol{k}_4)\delta(\boldsymbol{k}_3-\boldsymbol{p}) \qquad (47)
\end{aligned}
$$

Next, we will apply the deltas distributions to reduce the number of integrals, resulting in

$$
\begin{aligned}
W^{\phi^2}_{k_0}(\mathsf{x},\mathsf{x}') = &\int \widetilde{\mathrm{d}^n\boldsymbol{p}} f_{\boldsymbol{k}_0}(\boldsymbol{p}) e^{-\mathrm{i}|\boldsymbol{p}|t+\boldsymbol{p}\cdot\boldsymbol{x}} \int \widetilde{\mathrm{d}^n\boldsymbol{p}'} f_{\boldsymbol{k}_0}(\boldsymbol{p}') e^{\mathrm{i}|\boldsymbol{p}'|t'-\boldsymbol{p}'\cdot\boldsymbol{x}'} \int \widetilde{\widetilde{\mathrm{d}^n\boldsymbol{k}}} e^{\mathrm{i}|\boldsymbol{k}|t'-\boldsymbol{k}\cdot\boldsymbol{x}'} e^{-\mathrm{i}|\boldsymbol{k}|t+\boldsymbol{k}\cdot\boldsymbol{x}} \\
&+ \int \widetilde{\mathrm{d}^n\boldsymbol{p}} f_{\boldsymbol{k}_0}(\boldsymbol{p}) e^{-\mathrm{i}|\boldsymbol{p}|t+\boldsymbol{p}\cdot\boldsymbol{x}} \int \widetilde{\mathrm{d}^n\boldsymbol{p}'} f_{\boldsymbol{k}_0}(\boldsymbol{p}') e^{\mathrm{i}|\boldsymbol{p}'|t'-\boldsymbol{p}'\cdot\boldsymbol{x}'} \int \widetilde{\widetilde{\mathrm{d}^n\boldsymbol{k}}} e^{\mathrm{i}|\boldsymbol{k}|t'-\boldsymbol{k}\cdot\boldsymbol{x}'} e^{-\mathrm{i}|\boldsymbol{k}|t+\boldsymbol{k}\cdot\boldsymbol{x}} \\
&+ \int \widetilde{\mathrm{d}^n\boldsymbol{p}} f_{\boldsymbol{k}_0}(\boldsymbol{p}) e^{-\mathrm{i}|\boldsymbol{p}|t+\boldsymbol{p}\cdot\boldsymbol{x}} \int \widetilde{\mathrm{d}^n\boldsymbol{p}'} f_{\boldsymbol{k}_0}(\boldsymbol{p}') e^{\mathrm{i}|\boldsymbol{p}'|t-\boldsymbol{p}'\cdot\boldsymbol{x}'} \int \widetilde{\widetilde{\mathrm{d}^n\boldsymbol{k}}} e^{\mathrm{i}|\boldsymbol{k}|t'-\boldsymbol{k}\cdot\boldsymbol{x}'} e^{-\mathrm{i}|\boldsymbol{k}|t+\boldsymbol{k}\cdot\boldsymbol{x}} \\
&+ \int \mathrm{d}^n\boldsymbol{p} f_{\boldsymbol{k}_0}(\boldsymbol{p}) f_{\boldsymbol{k}_0}(\boldsymbol{p}) \int \widetilde{\widetilde{\mathrm{d}^n\boldsymbol{k}_1}} e^{\mathrm{i}|\boldsymbol{k}_1|t-\boldsymbol{k}_1\cdot\boldsymbol{x}'} e^{-\mathrm{i}|\boldsymbol{k}_1|t+\boldsymbol{k}_1\cdot\boldsymbol{x}} \int \widetilde{\widetilde{\mathrm{d}^n\boldsymbol{k}_2}} e^{\mathrm{i}|\boldsymbol{k}_2|t-\boldsymbol{k}_2\cdot\boldsymbol{x}'} e^{-\mathrm{i}|\boldsymbol{k}_2|t+\boldsymbol{k}_2\cdot\boldsymbol{x}} \\
&+ \int \widetilde{\mathrm{d}^n\boldsymbol{p}} f_{\boldsymbol{k}_0}(\boldsymbol{p}) e^{-\mathrm{i}|\boldsymbol{p}|t+\boldsymbol{p}\cdot\boldsymbol{x}} \int \widetilde{\mathrm{d}^n\boldsymbol{p}'} f_{\boldsymbol{k}_0}(\boldsymbol{p}') e^{\mathrm{i}|\boldsymbol{p}'|t'-\boldsymbol{p}'\cdot\boldsymbol{x}'} \int \widetilde{\widetilde{\mathrm{d}^n\boldsymbol{k}}} e^{\mathrm{i}|\boldsymbol{k}|t'-\boldsymbol{k}\cdot\boldsymbol{x}'} e^{-\mathrm{i}|\boldsymbol{k}|t+\boldsymbol{k}\cdot\boldsymbol{x}} \\
&+ \int \mathrm{d}^n\boldsymbol{p} f_{\boldsymbol{k}_0}(\boldsymbol{p}) f_{\boldsymbol{k}_0}(\boldsymbol{p}) \int \widetilde{\widetilde{\mathrm{d}^n\boldsymbol{k}_1}} e^{\mathrm{i}|\boldsymbol{k}_1|t-\boldsymbol{k}_1\cdot\boldsymbol{x}'} e^{-\mathrm{i}|\boldsymbol{k}_1|t+\boldsymbol{k}_1\cdot\boldsymbol{x}} \int \widetilde{\widetilde{\mathrm{d}^n\boldsymbol{k}_2}} e^{\mathrm{i}|\boldsymbol{k}_2|t-\boldsymbol{k}_2\cdot\boldsymbol{x}'} e^{-\mathrm{i}|\boldsymbol{k}_2|t+\boldsymbol{k}_2\cdot\boldsymbol{x}} \\
&+ \int \widetilde{\mathrm{d}^n\boldsymbol{p}} f_{\boldsymbol{k}_0}(\boldsymbol{p}) e^{-\mathrm{i}|\boldsymbol{p}|t'+\boldsymbol{p}\cdot\boldsymbol{x}'} \int \widetilde{\mathrm{d}^n\boldsymbol{p}'} f_{\boldsymbol{k}_0}(\boldsymbol{p}') e^{\mathrm{i}|\boldsymbol{p}'|t-\boldsymbol{p}'\cdot\boldsymbol{x}} \int \widetilde{\widetilde{\mathrm{d}^n\boldsymbol{k}}} e^{-\mathrm{i}|\boldsymbol{k}|t+\boldsymbol{k}\cdot\boldsymbol{x}'} e^{\mathrm{i}|\boldsymbol{k}|t-\boldsymbol{k}\cdot\boldsymbol{x}} \\
&+ \int \widetilde{\mathrm{d}^n\boldsymbol{p}} f_{\boldsymbol{k}_0}(\boldsymbol{p}) e^{-\mathrm{i}|\boldsymbol{p}|t'+\boldsymbol{p}\cdot\boldsymbol{x}'} \int \widetilde{\mathrm{d}^n\boldsymbol{p}'} f_{\boldsymbol{k}_0}(\boldsymbol{p}') e^{\mathrm{i}|\boldsymbol{p}'|t-\boldsymbol{p}'\cdot\boldsymbol{x}} \int \widetilde{\widetilde{\mathrm{d}^n\boldsymbol{k}}} e^{-\mathrm{i}|\boldsymbol{k}|t+\boldsymbol{k}\cdot\boldsymbol{x}} e^{\mathrm{i}|\boldsymbol{k}|t'-\boldsymbol{k}\cdot\boldsymbol{x}'} \\
&+ \int \widetilde{\mathrm{d}^n\boldsymbol{p}} f_{\boldsymbol{k}_0}(\boldsymbol{p}) e^{-\mathrm{i}|\boldsymbol{p}|t'+\boldsymbol{p}'\cdot\boldsymbol{x}'} \int \widetilde{\mathrm{d}^n\boldsymbol{p}'} f_{\boldsymbol{k}_0}(\boldsymbol{p}') e^{\mathrm{i}|\boldsymbol{p}'|t-\boldsymbol{p}'\cdot\boldsymbol{x}} \int \widetilde{\widetilde{\mathrm{d}^n\boldsymbol{k}}} e^{-\mathrm{i}|\boldsymbol{k}|t+\boldsymbol{k}\cdot\boldsymbol{x}} e^{\mathrm{i}|\boldsymbol{k}|t'-\boldsymbol{k}\cdot\boldsymbol{x}'} \\
&+ \int \widetilde{\mathrm{d}^n\boldsymbol{p}} f_{\boldsymbol{k}_0}(\boldsymbol{p}) e^{-\mathrm{i}|\boldsymbol{p}|t'+\boldsymbol{p}\cdot\boldsymbol{x}'} \int \widetilde{\mathrm{d}^n\boldsymbol{p}'} f_{\boldsymbol{k}_0}(\boldsymbol{p}') e^{\mathrm{i}|\boldsymbol{p}'|t-\boldsymbol{p}'\cdot\boldsymbol{x}} \int \widetilde{\widetilde{\mathrm{d}^n\boldsymbol{k}}} e^{-\mathrm{i}|\boldsymbol{k}|t+\boldsymbol{k}\cdot\boldsymbol{x}} e^{\mathrm{i}|\boldsymbol{k}|t'-\boldsymbol{k}\cdot\boldsymbol{x}'} \\
&+ \int \widetilde{\mathrm{d}^n\boldsymbol{p}} f_{\boldsymbol{k}_0}(\boldsymbol{p}) e^{-\mathrm{i}|\boldsymbol{p}|t'+(\boldsymbol{p}\cdot\boldsymbol{x}'} \int \widetilde{\mathrm{d}^n\boldsymbol{p}'} f_{\boldsymbol{k}_0}(\boldsymbol{p}') e^{\mathrm{i}|\boldsymbol{p}'|t-\boldsymbol{p}'\cdot\boldsymbol{x}} \int \widetilde{\widetilde{\mathrm{d}^n\boldsymbol{k}}} e^{-\mathrm{i}|\boldsymbol{k}|t+\boldsymbol{k}\cdot\boldsymbol{x}} e^{\mathrm{i}|\boldsymbol{k}|t'-\boldsymbol{k}\cdot\boldsymbol{x}'} \qquad (48)
\end{aligned}
$$

The expressions, which only have one integral over a variable labeled by p or p' are vacuum contributions, and the remaining terms can be expressed using $K_{\boldsymbol{k}_0}(\mathsf{x})$ defined in Eq. (25). The result is (in order term for term with the previous expression)

$$
\begin{aligned}
W^{\phi^2}_{k_0}(\mathsf{x},\mathsf{x}') = &K^*_{\boldsymbol{k}_0}(\mathsf{x}) K_{\boldsymbol{k}_0}(\mathsf{x}') W^{\phi}_{\mathrm{VAC}}(\mathsf{x},\mathsf{x}') + K^*_{\boldsymbol{k}_0}(\mathsf{x}) K_{\boldsymbol{k}_0}(\mathsf{x}') W^{\phi}_{\mathrm{VAC}}(\mathsf{x},\mathsf{x}') \\
&+ K^*_{\boldsymbol{k}_0}(\mathsf{x}) K_{\boldsymbol{k}_0}(\mathsf{x}') W^{\phi}_{\mathrm{VAC}}(\mathsf{x},\mathsf{x}') + W^{\phi}_{\mathrm{VAC}}(\mathsf{x},\mathsf{x}') W^{\phi}_{\mathrm{VAC}}(\mathsf{x},\mathsf{x}') \\
&+ K^*_{\boldsymbol{k}_0}(\mathsf{x}) K_{\boldsymbol{k}_0}(\mathsf{x}') W^{\phi}_{\mathrm{VAC}}(\mathsf{x},\mathsf{x}') + W^{\phi}_{\mathrm{VAC}}(\mathsf{x},\mathsf{x}') W^{\phi}_{\mathrm{VAC}}(\mathsf{x},\mathsf{x}') \\
&+ K^*_{\boldsymbol{k}_0}(\mathsf{x}') K_{\boldsymbol{k}_0}(\mathsf{x}) W^{\phi}_{\mathrm{VAC}}(\mathsf{x},\mathsf{x}') + K^*_{\boldsymbol{k}_0}(\mathsf{x}') K_{\boldsymbol{k}_0}(\mathsf{x}) W^{\phi}_{\mathrm{VAC}}(\mathsf{x},\mathsf{x}') \\
&+ K^*_{\boldsymbol{k}_0}(\mathsf{x}') K_{\boldsymbol{k}_0}(\mathsf{x}) W^{\phi}_{\mathrm{VAC}}(\mathsf{x},\mathsf{x}') + K^*_{\boldsymbol{k}_0}(\mathsf{x}') K_{\boldsymbol{k}_0}(\mathsf{x}) W^{\phi}_{\mathrm{VAC}}(\mathsf{x},\mathsf{x}') \\
&+ K^*_{\boldsymbol{k}_0}(\mathsf{x}') K_{\boldsymbol{k}_0}(\mathsf{x}) W^{\phi}_{\mathrm{VAC}}(\mathsf{x},\mathsf{x}'), \qquad (49)
\end{aligned}
$$

which can be simplified by collecting like terms,

$$W^{\phi^2}_{k_0}(\mathsf{x},\mathsf{x}') = 4W^{\phi}_{\text{VAC}}(\mathsf{x},\mathsf{x}')\Big(K^*_{\boldsymbol{k}_0}(\mathsf{x})K_{\boldsymbol{k}_0}(\mathsf{x}') + c.c\Big) + 2\big(W^{\phi}_{\text{VAC}}(\mathsf{x},\mathsf{x}')\big)^2. \tag{50}$$

This is the expression we will use.

5 Two point correlator of the quadratic coupling to a two-particle Fock state-2

In this section we will calculate the following two-point correlator

$$W^{\phi^2}_{\eta_1,\eta_2}(\mathsf{x},\mathsf{x}') = \langle 2_f| : \phi^2(\mathsf{x}) :: \phi^2(\mathsf{x}') : |2_{f_{\eta_1,\eta_2}}\rangle\,. \tag{51}$$

Applying the field mode expansion and the definition for the two-particle state, we find

$$\begin{aligned}
W^{\phi^2}_{\boldsymbol{\eta}_1,\boldsymbol{\eta}_2}(\mathsf{x},\mathsf{x}') = \mathcal{N}^2 &\int \mathrm{d}^n\boldsymbol{p}_1 f_{\boldsymbol{\eta}_1}(\boldsymbol{p}_1)\int \mathrm{d}^n\boldsymbol{p}_2 f_{\boldsymbol{\eta}_2}(\boldsymbol{p}_2)\int \mathrm{d}^n\boldsymbol{p}_3 f_{\boldsymbol{\eta}_1}(\boldsymbol{p}_3)\int \mathrm{d}^n\boldsymbol{p}_4 f_{\boldsymbol{\eta}_2}(\boldsymbol{p}_4)\\
&\times\int \widetilde{\mathrm{d}^n\boldsymbol{k}_1}\int \widetilde{\mathrm{d}^n\boldsymbol{k}_2}\int \widetilde{\mathrm{d}^n\boldsymbol{k}_3}\int \widetilde{\mathrm{d}^n\boldsymbol{k}_4}\,\langle 0|\,\hat{a}_{\boldsymbol{p}_1}\hat{a}_{\boldsymbol{p}_2}\\
&\times\Big(\hat{a}_{\boldsymbol{k}_1}\hat{a}_{\boldsymbol{k}_2}e^{-\mathrm{i}|\boldsymbol{k}_1|t+\boldsymbol{k}_1\cdot\boldsymbol{x}}e^{-\mathrm{i}|\boldsymbol{k}_2|t+\boldsymbol{k}_2\cdot\boldsymbol{x}} + \hat{a}^\dagger_{\boldsymbol{k}_1}\hat{a}_{\boldsymbol{k}_2}e^{\mathrm{i}|\boldsymbol{k}_1|t-\boldsymbol{k}_1\cdot\boldsymbol{x}}e^{-\mathrm{i}|\boldsymbol{k}_2|t+\boldsymbol{k}_2\cdot\boldsymbol{x}}\\
&\quad + \hat{a}^\dagger_{\boldsymbol{k}_2}\hat{a}_{\boldsymbol{k}_1}e^{-\mathrm{i}|\boldsymbol{k}_1|t+\boldsymbol{k}_1\cdot\boldsymbol{x}}e^{\mathrm{i}|\boldsymbol{k}_2|t-\boldsymbol{k}_2\cdot\boldsymbol{x}} + \hat{a}^\dagger_{\boldsymbol{k}_1}\hat{a}^\dagger_{\boldsymbol{k}_2}e^{\mathrm{i}|\boldsymbol{k}_1|t-\boldsymbol{k}_1\cdot\boldsymbol{x}}e^{\mathrm{i}|\boldsymbol{k}_2|t-\boldsymbol{k}_2\cdot\boldsymbol{x}}\Big)\\
&\times\Big(\hat{a}_{\boldsymbol{k}_3}\hat{a}_{\boldsymbol{k}_4}e^{-\mathrm{i}|\boldsymbol{k}_3|t+\boldsymbol{k}_3\cdot\boldsymbol{x}'}e^{-\mathrm{i}|\boldsymbol{k}_4|t'+\boldsymbol{k}_4\cdot\boldsymbol{x}'} + \hat{a}^\dagger_{\boldsymbol{k}_3}\hat{a}_{\boldsymbol{k}_4}e^{\mathrm{i}|\boldsymbol{k}_3|t-\boldsymbol{k}_3\cdot\boldsymbol{x}'}e^{-\mathrm{i}|\boldsymbol{k}_4|t'+\boldsymbol{k}_4\cdot\boldsymbol{x}'}\\
&\quad + \hat{a}^\dagger_{\boldsymbol{k}_4}\hat{a}_{\boldsymbol{k}_3}e^{-\mathrm{i}|\boldsymbol{k}_3|t+\boldsymbol{k}_3\cdot\boldsymbol{x}'}e^{\mathrm{i}|\boldsymbol{k}_4|t-\boldsymbol{k}_4\cdot\boldsymbol{x}'} + \hat{a}^\dagger_{\boldsymbol{k}_3}\hat{a}^\dagger_{\boldsymbol{k}_4}e^{\mathrm{i}|\boldsymbol{k}_3|t-\boldsymbol{k}_3\cdot\boldsymbol{x}'}e^{\mathrm{i}|\boldsymbol{k}_4|t-\boldsymbol{k}_4\cdot\boldsymbol{x}'}\Big)\hat{a}^\dagger_{\boldsymbol{p}_3}\hat{a}^\dagger_{\boldsymbol{p}_4}\,|0\rangle
\end{aligned} \tag{52}$$

Expanding and dropping terms with unbalanced number of creation and annihilation

operators, we find the above expression is equvalent to

$$
\begin{aligned}
W^{\phi^2}_{\boldsymbol{\eta}_1,\boldsymbol{\eta}_2}(\mathsf{x},\mathsf{x}') = \mathcal{N}^2 &\int \mathrm{d}^n\boldsymbol{p}_1 f_{\boldsymbol{\eta}_1}(\boldsymbol{p}_1)\int \mathrm{d}^n\boldsymbol{p}_2 f_{\boldsymbol{\eta}_2}(\boldsymbol{p}_2)\int \mathrm{d}^n\boldsymbol{p}_3 f_{\boldsymbol{\eta}_1}(\boldsymbol{p}_3)\int \mathrm{d}^n\boldsymbol{p}_4 f_{\boldsymbol{\eta}_2}(\boldsymbol{p}_4)\\
&\times\int \widetilde{\mathrm{d}^n\boldsymbol{k}_1}\int \widetilde{\mathrm{d}^n\boldsymbol{k}_2}\int \widetilde{\mathrm{d}^n\boldsymbol{k}_3}\int \widetilde{\mathrm{d}^n\boldsymbol{k}_4} e^{-\mathrm{i}|\boldsymbol{k}_1|t+\boldsymbol{k}_1\cdot\boldsymbol{x}} e^{-\mathrm{i}|\boldsymbol{k}_2|t+\boldsymbol{k}_2\cdot\boldsymbol{x}} e^{\mathrm{i}|\boldsymbol{k}_3|t-\boldsymbol{k}_3\cdot\boldsymbol{x}'} e^{\mathrm{i}|\boldsymbol{k}_4|t-\boldsymbol{k}_4\cdot\boldsymbol{x}'}\\
&\quad\times\langle 0|\,\hat{a}_{\boldsymbol{p}_1}\hat{a}_{\boldsymbol{p}_2}\hat{a}_{\boldsymbol{k}_1}\hat{a}_{\boldsymbol{k}_2}\hat{a}^\dagger_{\boldsymbol{k}_3}\hat{a}^\dagger_{\boldsymbol{k}_4}\hat{a}^\dagger_{\boldsymbol{p}_3}\hat{a}^\dagger_{\boldsymbol{p}_4}\,|0\rangle\\
+\mathcal{N}^2 &\int \mathrm{d}^n\boldsymbol{p}_1 f_{\boldsymbol{\eta}_1}(\boldsymbol{p}_1)\int \mathrm{d}^n\boldsymbol{p}_2 f_{\boldsymbol{\eta}_2}(\boldsymbol{p}_2)\int \mathrm{d}^n\boldsymbol{p}_3 f_{\boldsymbol{\eta}_1}(\boldsymbol{p}_3)\int \mathrm{d}^n\boldsymbol{p}_4 f_{\boldsymbol{\eta}_2}(\boldsymbol{p}_4)\\
&\times\int \widetilde{\mathrm{d}^n\boldsymbol{k}_1}\int \widetilde{\mathrm{d}^n\boldsymbol{k}_2}\int \widetilde{\mathrm{d}^n\boldsymbol{k}_3}\int \widetilde{\mathrm{d}^n\boldsymbol{k}_4} e^{\mathrm{i}|\boldsymbol{k}_1|t-\boldsymbol{k}_1\cdot\boldsymbol{x}} e^{\mathrm{i}|\boldsymbol{k}_2|t-\boldsymbol{k}_2\cdot\boldsymbol{x}} e^{-\mathrm{i}|\boldsymbol{k}_3|t+\boldsymbol{k}_3\cdot\boldsymbol{x}'} e^{-\mathrm{i}|\boldsymbol{k}_4|t'+\boldsymbol{k}_4\cdot\boldsymbol{x}'}\\
&\quad\times\langle 0|\,\hat{a}_{\boldsymbol{p}_1}\hat{a}_{\boldsymbol{p}_2}\hat{a}^\dagger_{\boldsymbol{k}_1}\hat{a}^\dagger_{\boldsymbol{k}_2}\hat{a}_{\boldsymbol{k}_3}\hat{a}_{\boldsymbol{k}_4}\hat{a}^\dagger_{\boldsymbol{p}_3}\hat{a}^\dagger_{\boldsymbol{p}_4}\,|0\rangle\\
+\mathcal{N}^2 &\int \mathrm{d}^n\boldsymbol{p}_1 f_{\boldsymbol{\eta}_1}(\boldsymbol{p}_1)\int \mathrm{d}^n\boldsymbol{p}_2 f_{\boldsymbol{\eta}_2}(\boldsymbol{p}_2)\int \mathrm{d}^n\boldsymbol{p}_3 f_{\boldsymbol{\eta}_1}(\boldsymbol{p}_3)\int \mathrm{d}^n\boldsymbol{p}_4 f_{\boldsymbol{\eta}_2}(\boldsymbol{p}_4)\\
&\times\int \widetilde{\mathrm{d}^n\boldsymbol{k}_1}\int \widetilde{\mathrm{d}^n\boldsymbol{k}_2}\int \widetilde{\mathrm{d}^n\boldsymbol{k}_3}\int \widetilde{\mathrm{d}^n\boldsymbol{k}_4} e^{\mathrm{i}|\boldsymbol{k}_1|t-\boldsymbol{k}_1\cdot\boldsymbol{x}} e^{-\mathrm{i}|\boldsymbol{k}_2|t+\boldsymbol{k}_2\cdot\boldsymbol{x}} e^{\mathrm{i}|\boldsymbol{k}_3|t-\boldsymbol{k}_3\cdot\boldsymbol{x}'} e^{-\mathrm{i}|\boldsymbol{k}_4|t'+\boldsymbol{k}_4\cdot\boldsymbol{x}'}\\
&\quad\times\langle 0|\,\hat{a}_{\boldsymbol{p}_1}\hat{a}_{\boldsymbol{p}_2}\hat{a}^\dagger_{\boldsymbol{k}_1}\hat{a}_{\boldsymbol{k}_2}\hat{a}^\dagger_{\boldsymbol{k}_3}\hat{a}_{\boldsymbol{k}_4}\hat{a}^\dagger_{\boldsymbol{p}_3}\hat{a}^\dagger_{\boldsymbol{p}_4}\,|0\rangle\\
+\mathcal{N}^2 &\int \mathrm{d}^n\boldsymbol{p}_1 f_{\boldsymbol{\eta}_1}(\boldsymbol{p}_1)\int \mathrm{d}^n\boldsymbol{p}_2 f_{\boldsymbol{\eta}_2}(\boldsymbol{p}_2)\int \mathrm{d}^n\boldsymbol{p}_3 f_{\boldsymbol{\eta}_1}(\boldsymbol{p}_3)\int \mathrm{d}^n\boldsymbol{p}_4 f_{\boldsymbol{\eta}_2}(\boldsymbol{p}_4)\\
&\times\int \widetilde{\mathrm{d}^n\boldsymbol{k}_1}\int \widetilde{\mathrm{d}^n\boldsymbol{k}_2}\int \widetilde{\mathrm{d}^n\boldsymbol{k}_3}\int \widetilde{\mathrm{d}^n\boldsymbol{k}_4} e^{-\mathrm{i}|\boldsymbol{k}_1|t+\boldsymbol{k}_1\cdot\boldsymbol{x}} e^{\mathrm{i}|\boldsymbol{k}_2|t-\boldsymbol{k}_2\cdot\boldsymbol{x}} e^{\mathrm{i}|\boldsymbol{k}_3|t-\boldsymbol{k}_3\cdot\boldsymbol{x}'} e^{-\mathrm{i}|\boldsymbol{k}_4|t'+\boldsymbol{k}_4\cdot\boldsymbol{x}'}\\
&\quad\times\langle 0|\,\hat{a}_{\boldsymbol{p}_1}\hat{a}_{\boldsymbol{p}_2}\hat{a}^\dagger_{\boldsymbol{k}_2}\hat{a}_{\boldsymbol{k}_1}\hat{a}^\dagger_{\boldsymbol{k}_3}\hat{a}_{\boldsymbol{k}_4}\hat{a}^\dagger_{\boldsymbol{p}_3}\hat{a}^\dagger_{\boldsymbol{p}_4}\,|0\rangle\\
+\mathcal{N}^2 &\int \mathrm{d}^n\boldsymbol{p}_1 f_{\boldsymbol{\eta}_1}(\boldsymbol{p}_1)\int \mathrm{d}^n\boldsymbol{p}_2 f_{\boldsymbol{\eta}_2}(\boldsymbol{p}_2)\int \mathrm{d}^n\boldsymbol{p}_3 f_{\boldsymbol{\eta}_1}(\boldsymbol{p}_3)\int \mathrm{d}^n\boldsymbol{p}_4 f_{\boldsymbol{\eta}_2}(\boldsymbol{p}_4)\\
&\times\int \widetilde{\mathrm{d}^n\boldsymbol{k}_1}\int \widetilde{\mathrm{d}^n\boldsymbol{k}_2}\int \widetilde{\mathrm{d}^n\boldsymbol{k}_3}\int \widetilde{\mathrm{d}^n\boldsymbol{k}_4} e^{\mathrm{i}|\boldsymbol{k}_1|t-\boldsymbol{k}_1\cdot\boldsymbol{x}} e^{-\mathrm{i}|\boldsymbol{k}_2|t+\boldsymbol{k}_2\cdot\boldsymbol{x}} e^{-\mathrm{i}|\boldsymbol{k}_3|t+\boldsymbol{k}_3\cdot\boldsymbol{x}'} e^{\mathrm{i}|\boldsymbol{k}_4|t-\boldsymbol{k}_4\cdot\boldsymbol{x}'}\\
&\quad\times\langle 0|\,\hat{a}_{\boldsymbol{p}_1}\hat{a}_{\boldsymbol{p}_2}\hat{a}^\dagger_{\boldsymbol{k}_1}\hat{a}_{\boldsymbol{k}_2}\hat{a}^\dagger_{\boldsymbol{k}_3}\hat{a}_{\boldsymbol{k}_4}\hat{a}^\dagger_{\boldsymbol{p}_3}\hat{a}^\dagger_{\boldsymbol{p}_4}\,|0\rangle\\
+\mathcal{N}^2 &\int \mathrm{d}^n\boldsymbol{p}_1 f_{\boldsymbol{\eta}_1}(\boldsymbol{p}_1)\int \mathrm{d}^n\boldsymbol{p}_2 f_{\boldsymbol{\eta}_2}(\boldsymbol{p}_2)\int \mathrm{d}^n\boldsymbol{p}_3 f_{\boldsymbol{\eta}_1}(\boldsymbol{p}_3)\int \mathrm{d}^n\boldsymbol{p}_4 f_{\boldsymbol{\eta}_2}(\boldsymbol{p}_4)\\
&\times\int \widetilde{\mathrm{d}^n\boldsymbol{k}_1}\int \widetilde{\mathrm{d}^n\boldsymbol{k}_2}\int \widetilde{\mathrm{d}^n\boldsymbol{k}_3}\int \widetilde{\mathrm{d}^n\boldsymbol{k}_4} e^{-\mathrm{i}|\boldsymbol{k}_1|t+\boldsymbol{k}_1\cdot\boldsymbol{x}} e^{\mathrm{i}|\boldsymbol{k}_2|t-\boldsymbol{k}_2\cdot\boldsymbol{x}} e^{-\mathrm{i}|\boldsymbol{k}_3|t+\boldsymbol{k}_3\cdot\boldsymbol{x}'} e^{\mathrm{i}|\boldsymbol{k}_4|t-\boldsymbol{k}_4\cdot\boldsymbol{x}'}\\
&\quad\times\langle 0|\,\hat{a}_{\boldsymbol{p}_1}\hat{a}_{\boldsymbol{p}_2}\hat{a}^\dagger_{\boldsymbol{k}_2}\hat{a}_{\boldsymbol{k}_1}\hat{a}^\dagger_{\boldsymbol{k}_4}\hat{a}_{\boldsymbol{k}_3}\hat{a}^\dagger_{\boldsymbol{p}_3}\hat{a}^\dagger_{\boldsymbol{p}_4}\,|0\rangle\,. \qquad (53)
\end{aligned}
$$

Each of the inner products can be commuted to annihilate the vacuum:

$$\begin{aligned}
\langle 0|\, \hat{a}_{\boldsymbol{k}_a}\hat{a}_{\boldsymbol{k}_b}\hat{a}_{\boldsymbol{k}_c}\hat{a}_{\boldsymbol{k}_d}\hat{a}^\dagger_{\boldsymbol{k}_e}\hat{a}^\dagger_{\boldsymbol{k}_f}\hat{a}^\dagger_{\boldsymbol{k}_g}\hat{a}^\dagger_{\boldsymbol{k}_h}\,|0\rangle &= \delta(\boldsymbol{k}_a-\boldsymbol{k}_e)\delta(\boldsymbol{k}_b-\boldsymbol{k}_f)\delta(\boldsymbol{k}_c-\boldsymbol{k}_g)\delta(\boldsymbol{k}_d-\boldsymbol{k}_h)\\
&+\delta(\boldsymbol{k}_a-\boldsymbol{k}_e)\delta(\boldsymbol{k}_b-\boldsymbol{k}_h)\delta(\boldsymbol{k}_c-\boldsymbol{k}_f)\delta(\boldsymbol{k}_d-\boldsymbol{k}_g)\\
&+\delta(\boldsymbol{k}_a-\boldsymbol{k}_f)\delta(\boldsymbol{k}_b-\boldsymbol{k}_e)\delta(\boldsymbol{k}_c-\boldsymbol{k}_h)\delta(\boldsymbol{k}_d-\boldsymbol{k}_g)\\
&+\delta(\boldsymbol{k}_a-\boldsymbol{k}_g)\delta(\boldsymbol{k}_b-\boldsymbol{k}_e)\delta(\boldsymbol{k}_c-\boldsymbol{k}_f)\delta(\boldsymbol{k}_d-\boldsymbol{k}_h)\\
&+\delta(\boldsymbol{k}_a-\boldsymbol{k}_f)\delta(\boldsymbol{k}_b-\boldsymbol{k}_e)\delta(\boldsymbol{k}_c-\boldsymbol{k}_g)\delta(\boldsymbol{k}_d-\boldsymbol{k}_h)\\
&+\delta(\boldsymbol{k}_a-\boldsymbol{k}_e)\delta(\boldsymbol{k}_b-\boldsymbol{k}_g)\delta(\boldsymbol{k}_d-\boldsymbol{k}_h)\delta(\boldsymbol{k}_e-\boldsymbol{k}_f)\\
&+\delta(\boldsymbol{k}_a-\boldsymbol{k}_e)\delta(\boldsymbol{k}_b-\boldsymbol{k}_f)\delta(\boldsymbol{k}_c-\boldsymbol{k}_h)\delta(\boldsymbol{k}_d-\boldsymbol{k}_g)\\
&+\delta(\boldsymbol{k}_a-\boldsymbol{k}_h)\delta(\boldsymbol{k}_b-\boldsymbol{k}_e)\delta(\boldsymbol{k}_c-\boldsymbol{k}_f)\delta(\boldsymbol{k}_d-\boldsymbol{k}_g)\\
&+\delta(\boldsymbol{k}_a-\boldsymbol{k}_f)\delta(\boldsymbol{k}_b-\boldsymbol{k}_g)\delta(\boldsymbol{k}_c-\boldsymbol{k}_e)\delta(\boldsymbol{k}_d-\boldsymbol{k}_h)\\
&+\delta(\boldsymbol{k}_a-\boldsymbol{k}_g)\delta(\boldsymbol{k}_b-\boldsymbol{k}_f)\delta(\boldsymbol{k}_c-\boldsymbol{k}_e)\delta(\boldsymbol{k}_d-\boldsymbol{k}_h)\\
&+\delta(\boldsymbol{k}_a-\boldsymbol{k}_f)\delta(\boldsymbol{k}_b-\boldsymbol{k}_h)\delta(\boldsymbol{k}_c-\boldsymbol{k}_e)\delta(\boldsymbol{k}_d-\boldsymbol{k}_g)\\
&+\delta(\boldsymbol{k}_a-\boldsymbol{k}_h)\delta(\boldsymbol{k}_b-\boldsymbol{k}_f)\delta(\boldsymbol{k}_c-\boldsymbol{k}_e)\delta(\boldsymbol{k}_d-\boldsymbol{k}_g)\\
&+\delta(\boldsymbol{k}_a-\boldsymbol{k}_e)\delta(\boldsymbol{k}_b-\boldsymbol{k}_g)\delta(\boldsymbol{k}_c-\boldsymbol{k}_h)\delta(\boldsymbol{k}_d-\boldsymbol{k}_f)\\
&+\delta(\boldsymbol{k}_a-\boldsymbol{k}_g)\delta(\boldsymbol{k}_b-\boldsymbol{k}_e)\delta(\boldsymbol{k}_c-\boldsymbol{k}_h)\delta(\boldsymbol{k}_d-\boldsymbol{k}_f)\\
&+\delta(\boldsymbol{k}_a-\boldsymbol{k}_e)\delta(\boldsymbol{k}_b-\boldsymbol{k}_h)\delta(\boldsymbol{k}_c-\boldsymbol{k}_g)\delta(\boldsymbol{k}_d-\boldsymbol{k}_f)\\
&+\delta(\boldsymbol{k}_a-\boldsymbol{k}_h)\delta(\boldsymbol{k}_b-\boldsymbol{k}_e)\delta(\boldsymbol{k}_c-\boldsymbol{k}_g)\delta(\boldsymbol{k}_d-\boldsymbol{k}_f)\\
&+\delta(\boldsymbol{k}_a-\boldsymbol{k}_h)\delta(\boldsymbol{k}_b-\boldsymbol{k}_e)\delta(\boldsymbol{k}_c-\boldsymbol{k}_g)\delta(\boldsymbol{k}_d-\boldsymbol{k}_f)\\
&+\delta(\boldsymbol{k}_a-\boldsymbol{k}_g)\delta(\boldsymbol{k}_b-\boldsymbol{k}_h)\delta(\boldsymbol{k}_c-\boldsymbol{k}_e)\delta(\boldsymbol{k}_d-\boldsymbol{k}_f)\\
&+\delta(\boldsymbol{k}_a-\boldsymbol{k}_h)\delta(\boldsymbol{k}_b-\boldsymbol{k}_g)\delta(\boldsymbol{k}_c-\boldsymbol{k}_e)\delta(\boldsymbol{k}_d-\boldsymbol{k}_f), \qquad (54)
\end{aligned}$$

The second case is shorter:

$$\begin{aligned}
\langle 0|\, \hat{a}_{\boldsymbol{k}_a}\hat{a}_{\boldsymbol{k}_b}\hat{a}^\dagger_{\boldsymbol{k}_c}\hat{a}_{\boldsymbol{k}_d}\hat{a}^\dagger_{\boldsymbol{k}_e}\hat{a}_{\boldsymbol{k}_f}\hat{a}^\dagger_{\boldsymbol{k}_g}\hat{a}^\dagger_{\boldsymbol{k}_h}\,|0\rangle &= \delta(\boldsymbol{k}_a-\boldsymbol{k}_c)\delta(\boldsymbol{k}_b-\boldsymbol{k}_e)\delta(\boldsymbol{k}_d-\boldsymbol{k}_g)\delta(\boldsymbol{k}_f-\boldsymbol{k}_g)\\
&+\delta(\boldsymbol{k}_a-\boldsymbol{k}_e)\delta(\boldsymbol{k}_b-\boldsymbol{k}_c)\delta(\boldsymbol{k}_d-\boldsymbol{k}_g)\delta(\boldsymbol{k}_f-\boldsymbol{k}_h)\\
&+\delta(\boldsymbol{k}_a-\boldsymbol{k}_c)\delta(\boldsymbol{k}_b-\boldsymbol{k}_g)\delta(\boldsymbol{k}_d-\boldsymbol{k}_e)\delta(\boldsymbol{k}_f-\boldsymbol{k}_h)\\
&+\delta(\boldsymbol{k}_a-\boldsymbol{k}_c)\delta(\boldsymbol{k}_b-\boldsymbol{k}_e)\delta(\boldsymbol{k}_d-\boldsymbol{k}_h)\delta(\boldsymbol{k}_f-\boldsymbol{k}_g)\\
&+\delta(\boldsymbol{k}_a-\boldsymbol{k}_c)\delta(\boldsymbol{k}_b-\boldsymbol{k}_h)\delta(\boldsymbol{k}_d-\boldsymbol{k}_e)\delta(\boldsymbol{k}_f-\boldsymbol{k}_g)\\
&+\delta(\boldsymbol{k}_a-\boldsymbol{k}_e)\delta(\boldsymbol{k}_b-\boldsymbol{k}_c)\delta(\boldsymbol{k}_d-\boldsymbol{k}_g)\delta(\boldsymbol{k}_f-\boldsymbol{k}_g)\\
&+\delta(\boldsymbol{k}_a-\boldsymbol{k}_g)\delta(\boldsymbol{k}_b-\boldsymbol{k}_c)\delta(\boldsymbol{k}_d-\boldsymbol{k}_e)\delta(\boldsymbol{k}_f-\boldsymbol{k}_h)\\
&+\delta(\boldsymbol{k}_a-\boldsymbol{k}_h)\delta(\boldsymbol{k}_b-\boldsymbol{k}_c)\delta(\boldsymbol{k}_d-\boldsymbol{k}_e)\delta(\boldsymbol{k}_f-\boldsymbol{k}_g), \qquad (55)
\end{aligned}$$

And the third set of creation and annihilation operators is the simplest,

$$\begin{aligned}\langle 0|\,\hat{a}_{\boldsymbol{k}_a}\hat{a}_{\boldsymbol{k}_b}\hat{a}^\dagger_{\boldsymbol{k}_c}\hat{a}^\dagger_{\boldsymbol{k}_d}\hat{a}_{\boldsymbol{k}_e}\hat{a}_{\boldsymbol{k}_f}\hat{a}^\dagger_{\boldsymbol{k}_g}\hat{a}^\dagger_{\boldsymbol{k}_h}\,|0\rangle &= \delta(\boldsymbol{k}_a-\boldsymbol{k}_c)\delta(\boldsymbol{k}_b-\boldsymbol{k}_d)\delta(\boldsymbol{k}_e-\boldsymbol{k}_g)\delta(\boldsymbol{k}_f-\boldsymbol{k}_g)\\ &+\delta(\boldsymbol{k}_a-\boldsymbol{k}_d)\delta(\boldsymbol{k}_b-\boldsymbol{k}_c)\delta(\boldsymbol{k}_e-\boldsymbol{k}_g)\delta(\boldsymbol{k}_f-\boldsymbol{k}_h)\\ &+\delta(\boldsymbol{k}_a-\boldsymbol{k}_c)\delta(\boldsymbol{k}_b-\boldsymbol{k}_d)\delta(\boldsymbol{k}_e-\boldsymbol{k}_h)\delta(\boldsymbol{k}_f-\boldsymbol{k}_g)\\ &+\delta(\boldsymbol{k}_a-\boldsymbol{k}_d)\delta(\boldsymbol{k}_b-\boldsymbol{k}_c)\delta(\boldsymbol{k}_e-\boldsymbol{k}_h)\delta(\boldsymbol{k}_f-\boldsymbol{k}_g). \end{aligned} \tag{56}$$

Applying these commuted expression to the two-point correlator directly simplifying each of the integrals with the delta distributions results in

$$\begin{aligned}W^{\phi^2}_{\eta_1,\eta_2}(\mathsf{x},\mathsf{x}') &= 2\left(W^{\phi}_{|0\rangle}(\mathsf{x},\mathsf{x}')\right)^2+\mathcal{N}^2\Big[4W^{\phi}_{|0\rangle}(\mathsf{x},\mathsf{x}')(K_{\boldsymbol{\eta}_1}(\mathsf{x})K^*_{\boldsymbol{\eta}_1}(\mathsf{x}')+K_{\boldsymbol{\eta}_2}(\mathsf{x})K^*_{\boldsymbol{\eta}_2}(\mathsf{x}')+c.c.)\\ &+4W^{\phi}_{|0\rangle}(\mathsf{x},\mathsf{x}')C_{\boldsymbol{\eta}_1\boldsymbol{\eta}_2}\Big(K_{\boldsymbol{\eta}_1}(\mathsf{x})K^*_{\boldsymbol{\eta}_2}(\mathsf{x}')+K_{\boldsymbol{\eta}_2}(\mathsf{x})K^*_{\boldsymbol{\eta}_1}(\mathsf{x}')+cc\Big)\\ &+4\Big(K^*_{\boldsymbol{\eta}_1}(\mathsf{x})K^*_{\boldsymbol{\eta}_2}(\mathsf{x})K_{\boldsymbol{\eta}_1}(\mathsf{x}')K_{\boldsymbol{\eta}_2}(\mathsf{x}')+K_{\boldsymbol{\eta}_1}(\mathsf{x})K^*_{\boldsymbol{\eta}_2}(\mathsf{x})K^*_{\boldsymbol{\eta}_1}(\mathsf{x}')K_{\boldsymbol{\eta}_2}(\mathsf{x}')+c.c.\Big)\\ &+4|K^*_{\boldsymbol{\eta}_2}(\mathsf{x})|^2|K^*_{\boldsymbol{\eta}_1}(\mathsf{x}')|^2+4|K^*_{\boldsymbol{\eta}_1}(\mathsf{x})|^2|K^*_{\boldsymbol{\eta}_2}(\mathsf{x}')|^2\Big] \end{aligned} \tag{57}$$

6 Two-point correlator of the Scalar Density

The two-point correlator of the normal-ordered scalar density will play an important role in the Fermionic UDW model. Here, we will follow the procedure outlined in [28], most of which can be found in an appendix B of that work. However, in that work, the normal-ordering was not applied and the divergent expression was instead assumed to vanish in the massless limit.

Let us write out the full expression for the two-point correlator we are concerned with

$$W^{:\overline{\Psi}\Psi:,|\psi\rangle}(t,\boldsymbol{x},t'\boldsymbol{x}') = \langle\psi|:\overline{\Psi}(t,\boldsymbol{x})\Psi(t,\boldsymbol{x})::\overline{\Psi}(t',\boldsymbol{x}')\Psi(t',\boldsymbol{x}'):|\psi\rangle\,. \tag{58}$$

Let us work in particular in the vacuum, $|\psi\rangle = |0\rangle$.

First we will find the expression for the expression without normal-ordering, then we will subtract off the appropriate quantities to achieve the normal ordering operation. There will be two important expressions, called the Wightman functions for the Dirac field, in

which we hope to express the two-point correlator of the scalar density. The Wightman functions can be written in the following forms

$$\begin{aligned} S^{+}_{ab}(t,\boldsymbol{x},t',\boldsymbol{x}') &:= \langle 0|\psi_a(t,\boldsymbol{x})\overline{\psi}_b(t',\boldsymbol{x}')|0\rangle = \left\{\psi^{+}_a(t,\boldsymbol{x}),\overline{\psi}^{-}_b(t',\boldsymbol{x}')\right\} \\ &= \left(i\gamma^{\mu}\partial_{x^{\mu}} + m\right)_{ab} W^{\phi,|0\rangle}(t,\boldsymbol{x},,t',\boldsymbol{x}') \qquad (59) \\ S^{-}_{ab}(t,\boldsymbol{x},t',\boldsymbol{x}') &:= \langle 0|\overline{\psi}_b(t',\boldsymbol{x}')\psi_a(t,\boldsymbol{x})|0\rangle = \left\{\psi^{-}_a(t,\boldsymbol{x}),\overline{\psi}^{+}_b(t',\boldsymbol{x}')\right\} \\ &= -\left(i\gamma^{\mu}\partial_{x^{\mu}} + m\right)_{ab} W^{\phi,|0\rangle}(t',\boldsymbol{x}',t,\boldsymbol{x}) \qquad (60) \end{aligned}$$

where $W^{\phi,|0\rangle}(t,\boldsymbol{x},,t',\boldsymbol{x}')$ is the two point correlator of the massive scalar field, also known as the Scalar Wightman funciton, which can be concretely be expressed as

$$\begin{aligned} W^{\phi,|0\rangle}(t,\boldsymbol{x},t'\boldsymbol{x}') &= \langle 0|\,\psi(t,\boldsymbol{x})\phi(t',\boldsymbol{x}')\,|0\rangle \\ &= \frac{1}{2\pi}\left(\frac{m}{2\pi z(t,\boldsymbol{x},,t',\boldsymbol{x}')}\right)^{d/2-1} K_{d/2-1}\big(mz(t,\boldsymbol{x},,t',\boldsymbol{x}')\big). \qquad (61) \end{aligned}$$

where m is the mass, $K_{d/2-1}$ is the modified Bessel function of the second kind [78] and

$$z(t,\boldsymbol{x},,t',\boldsymbol{x}') := \sqrt{(\boldsymbol{x},-\boldsymbol{x},)^2 - (t-t'-i\epsilon)^2}\ . \qquad (62)$$

However, we are mostly interested in the massless Wightman, in which case we must understand $\lim_{m\to 0}$ of W. Consider

$$\lim_{m\to 0}(m)^{d/2-1} K_{d/2-1}\big(mz(t,\boldsymbol{x},,t',\boldsymbol{x}')\big) = 2^{\frac{d}{2}-2} z(t,\boldsymbol{x},,t',\boldsymbol{x}')^{2-d}\Gamma\left(\frac{d-2}{2}\right) \qquad (63)$$

when $d > 2$. The massless limit of $d = 2$ requires more careful consideration and the introduction of a IR cutoff, as discussed in [28]. The results give the following expression for the massless scalar Wightman function

$$W^{\phi,|0\rangle}(t,\boldsymbol{x},t'\boldsymbol{x}') = \begin{cases} \frac{\Gamma\left(\frac{d}{2}-1\right)}{4\pi^{d/2}\left(z(t,\boldsymbol{x},,t',\boldsymbol{x}')\right)^{d-2}} & \text{for } d>2, \\ -(2\pi)^{-1}\ln\left(\Lambda z(t,\boldsymbol{x},,t',\boldsymbol{x}')\right) & \text{for } d=2, \end{cases} \qquad (64)$$

where Λ regulates the IR divergence of the $d = 2$ expression.

We will now turn out attention to the two-point correlator of the (Normal ordered) scalar density, Equation 58. Writing out the normal ordering operation on the scalar density explicitly, we find,

$$\begin{aligned} :\overline{\Psi}(t,\boldsymbol{x})\Psi(t,\boldsymbol{x}): :=& \overline{\psi}^{+}_a(t,\boldsymbol{x})\psi^{+}_a(t,\boldsymbol{x}) + \overline{\psi}^{-}_a(t,\boldsymbol{x})\psi^{-}_a(t,\boldsymbol{x}) \\ &+ \overline{\psi}^{-}_a(t,\boldsymbol{x})\psi^{+}_a(t,\boldsymbol{x}) - \psi^{-}_a(t,\boldsymbol{x})\overline{\psi}^{+}_a(t,\boldsymbol{x}) \qquad (65) \end{aligned}$$

where repeated indices are summed and $\psi^{\pm}$ are the positive and negative frequency components of Ψ (and analagously for $\overline{\Psi}$)

$$\psi^{+}(t,\boldsymbol{x}) = \int \widetilde{dk} \sum_{s} b_s(\mathbf{k}) u^{(s)}_{\mathbf{k}}(t,\boldsymbol{x}) \ , \tag{66}$$

$$\psi^{-}(t,\boldsymbol{x}) = \int \widetilde{dk} \sum_{s} d^{\dagger}_s(\mathbf{k}) v^{(s)}_{\mathbf{k}}(t,\boldsymbol{x}) \ , \tag{67}$$

$$\overline{\psi}^{+}(t,\boldsymbol{x}) = \int \widetilde{dk} \sum_{s} d_s(\mathbf{k}) \overline{v}^{(s)}_{\mathbf{k}}(t,\boldsymbol{x}) \ , \tag{68}$$

$$\overline{\psi}^{-}(t,\boldsymbol{x}) = \int \widetilde{dk} \sum_{s} b^{\dagger}_s(\mathbf{k}) \overline{u}^{(s)}_{\mathbf{k}}(t,\boldsymbol{x}) \ . \tag{69}$$

and u are the mode functions as described in chapter 6.

$$\begin{aligned} W^{:\overline{\Psi}\Psi:,|0\rangle}(t,\boldsymbol{x},t'\boldsymbol{x}') = \langle 0| \Big(& \overline{\psi}^{+}_a(t,\boldsymbol{x})\psi^{+}_a(t,\boldsymbol{x}) + \overline{\psi}^{-}_a(t,\boldsymbol{x})\psi^{-}_a(t,\boldsymbol{x}) \\ & + \overline{\psi}^{-}_a(t,\boldsymbol{x})\psi^{+}_a(t,\boldsymbol{x}) - \psi^{-}_a(t,\boldsymbol{x})\overline{\psi}^{+}_a(t,\boldsymbol{x}) \Big) \\ \times \Big(& \overline{\psi}^{+}_b(t',\boldsymbol{x}')\psi^{+}_b(t',\boldsymbol{x}') + \overline{\psi}^{-}_b(t',\boldsymbol{x}')\psi^{-}_b(t',\boldsymbol{x}') \\ & + \overline{\psi}^{-}_b(t',\boldsymbol{x}')\psi^{+}_b(t',\boldsymbol{x}') - \psi^{-}_b(t',\boldsymbol{x}')\overline{\psi}^{+}_b(t',\boldsymbol{x}') \Big) |0\rangle \, . \end{aligned} \tag{70}$$

We may immediately drop many of these terms, since ψ^{+} anihilates the vacuum from the left and ψ^{-} anihilates it from the right (and similarly for $\overline{\psi}^{+\pm}$.

$$W^{:\overline{\Psi}\Psi:,|0\rangle}(t,\boldsymbol{x},t'\boldsymbol{x}') = \langle 0| \overline{\psi}^{+}_a(t,\boldsymbol{x})\psi^{+}_a(t,\boldsymbol{x})\overline{\psi}^{-}_b(t',\boldsymbol{x}')\psi^{-}_b(t',\boldsymbol{x}') |0\rangle \, . \tag{71}$$

We find that $\psi^{-}_b(t',\boldsymbol{x}')$ anti-commutes with both $\psi^{+}_a(t,\boldsymbol{x})$ and $\overline{\psi}^{-}_b(t',\boldsymbol{x}')$. Anticommuting twice, we pick up $(-1)^2$ so that

$$W^{:\overline{\Psi}\Psi:,|0\rangle}(t,\boldsymbol{x},t'\boldsymbol{x}') = \langle 0| \overline{\psi}^{+}_a(t,\boldsymbol{x})\psi^{-}_b(t',\boldsymbol{x}')\psi^{+}_a(t,\boldsymbol{x})\overline{\psi}^{-}_b(t',\boldsymbol{x}') |0\rangle \, . \tag{72}$$

Next, we can replace $\overline{\psi}^{+}_a(t,\boldsymbol{x})\psi^{-}_b(t',\boldsymbol{x}')$ with its anticommutator, since the commuted operator anihilates the vacuum from the right. The same can be said for $\psi^{+}_a(t,\boldsymbol{x})\overline{\psi}^{-}_b(t',\boldsymbol{x}')$. Therefore

$$W^{:\overline{\Psi}\Psi:,|0\rangle}(t,\boldsymbol{x},t'\boldsymbol{x}') = \langle 0| \{\overline{\psi}^{+}_a(t,\boldsymbol{x}), \psi^{-}_b(t',\boldsymbol{x}')\}\{\psi^{+}_a(t,\boldsymbol{x}), \overline{\psi}^{-}_b(t',\boldsymbol{x}')\} |0\rangle \, . \tag{73}$$

This expression allows for us to conveniently apply Equation 59 and Equation 60, resultign in

$$W^{:\overline{\Psi}\Psi:,|0\rangle}(t,\boldsymbol{x},t'\boldsymbol{x}') = \langle 0|\, S^-_{ab}(t',\boldsymbol{x}',t,\boldsymbol{x})S^+_{ab}(t,\boldsymbol{x},t',\boldsymbol{x}')\,|0\rangle\,. \tag{74}$$

Of course $S^\pm_{ab}$ are themselves scalars and so

$$W^{:\overline{\Psi}\Psi:,|0\rangle}(t,\boldsymbol{x},t'\boldsymbol{x}') = S^-_{ab}(t',\boldsymbol{x}',t,\boldsymbol{x})S^+_{ab}(t,\boldsymbol{x},t',\boldsymbol{x}'). \tag{75}$$

recalling that repeated indices are summed over and that $S^\pm_{ab}$ vanishes when $a \neq b$, , we have

$$S^-_{ab}S^+_{ab} = S^-_{11}S^+_{11} + S^-_{22}S^+_{22}$$

, Which is simply the trace:

$$W^{:\overline{\Psi}\Psi:,|0\rangle}(t,\boldsymbol{x},t'\boldsymbol{x}') = \mathrm{Tr}\Big(S^-(t',\boldsymbol{x}',t,\boldsymbol{x})S^+(t,\boldsymbol{x},t',\boldsymbol{x}')\Big). \tag{76}$$

Finally, we may cyclicly permute the argument of the trace to arrive at the expression in [28]:

$$W^{:\overline{\Psi}\Psi:,|0\rangle}(t,\boldsymbol{x},t'\boldsymbol{x}') = \mathrm{Tr}\Big(S^+(t,\boldsymbol{x},t',\boldsymbol{x}')S^-(t',\boldsymbol{x}',t,\boldsymbol{x})\Big). \tag{77}$$

Considering now that we wish to find a concrete expression for $W^{:\overline{\Psi}\Psi:,|0\rangle}$, let us further apply Equation 59. We will also consider the massless limit at this point as well. Noting that γ^μ are traceless and $\mathrm{Tr}(\gamma^\mu\gamma^\nu) = N_d\eta_{\mu\nu}$, one can show

$$W^{:\overline{\Psi}\Psi:,|0\rangle}(t,\boldsymbol{x},t'\boldsymbol{x}') = \frac{N_d(\Gamma(d/2))^2}{4\pi^d(z(t,\boldsymbol{x},t',\boldsymbol{x}'))^{2d-2}}. \tag{78}$$

7 Two-point correlator of a massive complex field (aggie project)

In this appendix, we will compute the Wightman function for a massive scalar field in $n+1$ spacetime dimensions. Then we will particularize to $3+1$ dimensions, as in Eq. (3.16).

Starting with $W_n^\phi(t,\boldsymbol{x},t',\boldsymbol{x}') = \mathrm{tr}[\hat{\phi}(t,\boldsymbol{x})\hat{\phi}^*(t',\boldsymbol{x}')\hat{\rho}_{\mathrm{EM}}^{(0)}]$, we perform a mode expansion of $\hat{\phi}$, which reduces to the following after applying the trace:

$$W_n^\phi(t,\boldsymbol{x},t',\boldsymbol{x}') = \frac{1}{2(2\pi)^n}\int \frac{\mathrm{d}^n\boldsymbol{k}}{\omega_{\boldsymbol{k}}} e^{i(\boldsymbol{k}\cdot(\boldsymbol{x}-\boldsymbol{x}')-\omega_{\boldsymbol{k}}(t-t'))}\,. \tag{79}$$

We now introduce a soft UV cutoff ϵ to regularize the expression:

$$W_n^\phi(\boldsymbol{x},t,\boldsymbol{x}',t') = \frac{1}{2(2\pi)^n}\int_{\mathbb{R}^n} \frac{\mathrm{d}^n\boldsymbol{k}}{\omega_{\boldsymbol{k}}} e^{\mathrm{i}(\omega_{\boldsymbol{k}}(t'-t+\mathrm{i}\epsilon)-\boldsymbol{k}\cdot(\boldsymbol{x}'-\boldsymbol{x}))}\,. \tag{80}$$

In the steps outlined below, we follow [114]. First, we transform to spherical coordinates with the vector $\boldsymbol{X} := \boldsymbol{x}'-\boldsymbol{x}$ lying along the z-axis. The resultant expression is independent of all integration variables except θ and $|\boldsymbol{k}|$, so then

$$W_n^\phi(X,T) = \frac{1}{2(2\pi)^n}\frac{2\pi^{\frac{n-1}{2}}}{\Gamma\left(\frac{n-1}{2}\right)}\int_0^\pi \mathrm{d}\theta \sin^{n-2}\theta \int_0^\infty \mathrm{d}^n|\boldsymbol{k}|\frac{|\boldsymbol{k}|^{n-1}}{\omega_{\boldsymbol{k}}} e^{\mathrm{i}(\omega_{\boldsymbol{k}}T-|\boldsymbol{k}|X\cos\theta)} \tag{81}$$

where $T := (t'-t+\mathrm{i}\epsilon)$ and $W_n^\phi(X,T) = W_n^\phi(0,0,X,T)$.

To find a general expression for the remaining angular integrals, we look to table of integrals by Gradshteyn [115]. Integral 3.387 is

$$\int_{-1}^1 \mathrm{d}s\,(1-s^2)^{\frac{n-3}{2}} e^{\mathrm{i}(-|\boldsymbol{k}|X)s} = \frac{\sqrt{\pi}2^{\frac{n-2}{2}}}{(-X)^{\frac{n-2}{2}}}\Gamma\left(\frac{n-1}{2}\right)|\boldsymbol{k}|^{-\frac{n-2}{2}} J_{\frac{n-2}{2}}(-|\boldsymbol{k}|X)\,, \tag{82}$$

which is valid under the assumption that $\mathrm{Re}(n) > 1$.

We change integration variables from θ to $s = \cos\theta$.

$$W_n^\phi(X,T) = \frac{1}{2(2\pi)^n}\frac{2\pi^{\frac{n-1}{2}}}{\Gamma\left(\frac{n-1}{2}\right)}\int_0^\infty \mathrm{d}^n|\boldsymbol{k}|\frac{|\boldsymbol{k}|^{n-1}}{\omega_{\boldsymbol{k}}} e^{\mathrm{i}\omega_{\boldsymbol{k}}T}\int_{-1}^1 \mathrm{d}s\,(1-s^2)^{\frac{n-3}{2}} e^{-\mathrm{i}|\boldsymbol{k}|Xs}. \tag{83}$$

Then the identity in Gradshteyn yields

$$W_n^\phi(X,T) = \frac{(-X)^{-\frac{n-2}{2}}}{2(2\pi)^{\frac{n}{2}}}\int_0^\infty \mathrm{d}|\boldsymbol{k}|\frac{|\boldsymbol{k}|^{\frac{n}{2}}}{\omega_{\boldsymbol{k}}} e^{\mathrm{i}\omega_{\boldsymbol{k}}T} J_{\frac{n-2}{2}}(-|\boldsymbol{k}|X) \tag{84}$$

This final integral over variable $|\boldsymbol{k}|$ can be found using yet another identity, 6.645, from Gradshteyn, [115, p 721]:

$$\int_1^\infty \mathrm{d}s \left(s^2-1\right)^{\frac{\left(\frac{n-2}{2}\right)}{2}} e^{-s(-\mathrm{i}mT)} J_{\frac{n-2}{2}}\left(-mX\sqrt{s^2-1}\right) = \frac{m^{\frac{n}{2}-1}\sqrt{\frac{2}{\pi}}\left(-X\right)^{\frac{n-2}{2}} K_{\frac{n}{2}-\frac{1}{2}}\left(\sqrt{\left(-mX\right)^2+\left(-\mathrm{i}mT\right)^2}\right)}{\left(\sqrt{\left(-mX\right)^2+\left(-\mathrm{i}mT\right)^2}\right)^{\frac{n-1}{2}}}, \tag{85}$$

The use of this integral becomes clearer upon a change from $|\boldsymbol{k}|$ as our integration variable to $s = \omega_{\boldsymbol{k}}/m$. In this form, the relationship to the identity in Gradshteyn is evident:

$$W_n^\phi(X,T) = \frac{m^{\frac{n}{2}}\left(-X\right)^{-\frac{n-2}{2}}}{2(2\pi)^{\frac{n}{2}}} \int_1^\infty \mathrm{d}s \left(s^2-1\right)^{\frac{\left(\frac{n-2}{2}\right)}{2}} e^{-s(-\mathrm{i}mT)} J_{\frac{n-2}{2}}\left(-mX\sqrt{s^2-1}\right). \tag{86}$$

Then the Wightman can be written as

$$W_n^\phi(X,T) = \frac{m^{\frac{n}{2}}}{(2\pi)^{\frac{n+1}{2}}} \frac{K_{\frac{n}{2}-\frac{1}{2}}\left(m\sqrt{X^2-T^2}\right)}{\sqrt{\boldsymbol{X}^2-T^2}^{\frac{n-1}{2}}}. \tag{87}$$

The final expression in the original coordinates is

$$W_n^\phi(\boldsymbol{x},t,\boldsymbol{x}',t') = \frac{m^{\frac{n}{2}}}{(2\pi)^{\frac{n+1}{2}}} \frac{K_{\frac{n}{2}-\frac{1}{2}}\left(m\sqrt{|\boldsymbol{x}'-\boldsymbol{x}|^2-(t'-t+\mathrm{i}\epsilon)^2}\right)}{\sqrt{|\boldsymbol{x}'-\boldsymbol{x}|^2-(t'-t+\mathrm{i}\epsilon)^2}^{\frac{n-1}{2}}} \tag{88}$$

In particular, the expression in $3+1$ dimensions is

$$W_3^\phi(\boldsymbol{x},t,\boldsymbol{x}',t') = m^{\frac{3}{2}} \frac{K_1\left(m\sqrt{|\boldsymbol{x}'-\boldsymbol{x}|^2-(t'-t+\mathrm{i}\epsilon)^2}\right)}{4\pi^2\sqrt{|\boldsymbol{x}'-\boldsymbol{x}|^2-(t'-t+\mathrm{i}\epsilon)^2}}. \tag{89}$$

We think it should actually be

$$W_3^\phi(\boldsymbol{x},t,\boldsymbol{x}',t') = m \frac{K_1\left(m\sqrt{|\boldsymbol{x}'-\boldsymbol{x}|^2-(t'-t+\mathrm{i}\epsilon)^2}\right)}{4\pi^2\sqrt{|\boldsymbol{x}'-\boldsymbol{x}|^2-(t'-t+\mathrm{i}\epsilon)^2}}. \tag{90}$$

8 Detailed Decoherence Calculation

In the previous section, we computed several different expressions for the purity. Each of these expressions depended on coefficients A and B, defined in Eq. (3.35).

We start with the expression for A in Eq. and insert the expression for $w(t,t')$ in Eq. Eq. (3.22):

$$A = \frac{e^2}{2V\Omega}\int_{-\infty}^{\infty}\mathrm{d}t\int_{-\infty}^{\infty}\mathrm{d}t' e^{-\mathrm{i}\Omega(t-t')}\chi\left(\tfrac{t}{T}\right)\chi\left(\tfrac{t'}{T}\right)\int \mathrm{d}^3\boldsymbol{x}\int \mathrm{d}^3\boldsymbol{x}' F(\boldsymbol{x})F(\boldsymbol{x}')\left(W_3^{\phi}(t,\boldsymbol{x},t',\boldsymbol{x}')\right)^2. \tag{91}$$

Next we insert the expression for the Wightman function in Eq. (90):

$$\begin{aligned} A =& \frac{e^2m^2}{32\pi^2V\Omega}\int_{-\infty}^{\infty}\mathrm{d}t\int_{-\infty}^{\infty}\mathrm{d}t' e^{-\mathrm{i}\Omega(t-t')}\chi\left(\tfrac{t}{T}\right)\chi\left(\tfrac{t'}{T}\right)\int \mathrm{d}^3\boldsymbol{x}\int \mathrm{d}^3\boldsymbol{x}' F(\boldsymbol{x})F(\boldsymbol{x}') \\ &\times \frac{K_1\left(m\sqrt{|\boldsymbol{x}'-\boldsymbol{x}|^2-(t'-t+\mathrm{i}\epsilon)^2}\right)^2}{(|\boldsymbol{x}'-\boldsymbol{x}|^2-(t'-t+\mathrm{i}\epsilon)^2)}. \end{aligned} \tag{92}$$

Now let us turn to our choice of switching and smearing. We will choose a box function for our switching. This function is compact and adds relatively little computation to the calculations. The Smearing function will have a cosine profile in the direction along the cavity, which matches the fundamental of the modes in the cavity. The profile along the other two orthogonal spatial directions will be a Gaussian function. The Gaussian function decays rapidly and makes for simple calculations, and also is quite close to the expectation for the fundamental mode of monochromatic light in a cavity. The exact forms of these functions we will use are

$$\chi\left(\tfrac{t}{T}\right) = \mathrm{rect}(t/T) \tag{93}$$

$$F(\boldsymbol{x}/\sigma) = e^{-\frac{|\boldsymbol{x}|^2}{\sigma^2}}\cos(\Omega z) = \frac{1}{2}e^{-\frac{|\boldsymbol{x}|^2}{\sigma^2}}(e^{i\Omega z}+e^{-i\Omega z}). \tag{94}$$

Here, T is the time that the switching function is "on" and σ is the length scale associated with the transverse width of the cavity, and z is the direction of propagation of the photons

(longitudinal direction). This gives

$$\begin{aligned}
A =& \frac{1}{4}\frac{e^2}{2V\Omega}\int_{-T/2}^{T/2}\mathrm{d}t\int_{-T/2}^{T/2}\mathrm{d}t' e^{-\mathrm{i}\Omega(t-t')} \\
&\times\int \mathrm{d}^3\boldsymbol{x}\int \mathrm{d}^3\boldsymbol{x}' e^{-\frac{\boldsymbol{x}^2}{\sigma^2}} e^{-\frac{(\boldsymbol{x}')^2}{\sigma^2}}(e^{i\Omega z}+e^{-i\Omega z})(e^{i\Omega z'}+e^{-i\Omega z'}) \\
&\times\left(\frac{mK_1\left(m\sqrt{|\boldsymbol{x}'-\boldsymbol{x}|^2-(t'-t+\mathrm{i}\epsilon)^2}\right)}{4\pi^2\sqrt{|\boldsymbol{x}'-\boldsymbol{x}|^2-(t'-t+\mathrm{i}\epsilon)^2}}\right)^2 \qquad (95)\\
=& \frac{1}{4}\frac{e^2}{2V\Omega}\int_{-T/2}^{T/2}\mathrm{d}t\int_{-T/2}^{T/2}\mathrm{d}t' e^{-\mathrm{i}\Omega(t-t')} \\
&\times\int \mathrm{d}^3\boldsymbol{x}\int \mathrm{d}^3\boldsymbol{x}' e^{-\frac{\boldsymbol{x}^2}{\sigma^2}} e^{-\frac{(\boldsymbol{x}')^2}{\sigma^2}}(e^{i\Omega(z+z')}+e^{-i\Omega(z-z')}+e^{i\Omega(z-z')}+e^{-i\Omega(z+z')}) \\
&\times\left(\frac{mK_1\left(m\sqrt{|\boldsymbol{x}'-\boldsymbol{x}|^2-(t'-t+\mathrm{i}\epsilon)^2}\right)}{4\pi^2\sqrt{|\boldsymbol{x}'-\boldsymbol{x}|^2-(t'-t+\mathrm{i}\epsilon)^2}}\right)^2 \qquad (96)
\end{aligned}$$

We now do a change of variables to de-nest the spatial integrals: $\boldsymbol{p}=\boldsymbol{x}+\boldsymbol{x}'$ and $\boldsymbol{q}=\boldsymbol{x}-\boldsymbol{x}'$, with a Jacobian $1/2^3$.

$$\begin{aligned}
A =& \frac{1}{2^3}\frac{1}{4}\frac{e^2}{2V\Omega}\int_{-T/2}^{T/2}\mathrm{d}t\int_{-T/2}^{T/2}\mathrm{d}t' e^{-\mathrm{i}\Omega(t-t')} \\
&\times\int_{-\infty}^{\infty}\mathrm{d}^3\boldsymbol{p} e^{-\frac{|\boldsymbol{p}|^2}{2\sigma^2}}\int_{-\infty}^{\infty}\mathrm{d}^3\boldsymbol{q} e^{-\frac{|\boldsymbol{q}|^2}{2\sigma^2}}(e^{i\Omega p_z}+e^{-i\Omega q_z}+e^{i\Omega q_z}+e^{-i\Omega p_z}) \\
&\times\left(\frac{mK_1\left(m\sqrt{|\boldsymbol{q}|^2-(t'-t+\mathrm{i}\epsilon)^2}\right)}{4\pi^2\sqrt{|\boldsymbol{q}|^2-(t'-t+\mathrm{i}\epsilon)^2}}\right)^2 . \qquad (97)
\end{aligned}$$

We will make use of the following:

$$e^{-\frac{|\boldsymbol{p}|^2}{2\sigma^2}} = e^{-\frac{|p_x|^2}{2\sigma^2}} e^{-\frac{|p_y|^2}{2\sigma^2}} e^{-\frac{|p_z|^2}{2\sigma^2}} \qquad (98)$$

$$\int_{-\infty}^{\infty} dp e^{-\frac{|p|^2}{2\sigma^2}} = \sqrt{2\pi}\sigma \qquad (99)$$

$$\int_{-\infty}^{\infty} dp e^{-\frac{|p|^2}{2\sigma^2}} e^{\pm i\Omega p} = \sqrt{2\pi}\sigma e^{-\frac{1}{2}\sigma^2\Omega^2} . \qquad (100)$$

Performing the integral over $\boldsymbol{p}$ gives

$$\begin{aligned} A =&(\sqrt{2\pi}\sigma)^3\frac{1}{2^3}\frac{1}{4}\frac{e^2}{2V\Omega}\int_{-T/2}^{T/2}\mathrm{d}t\int_{-T/2}^{T/2}\mathrm{d}t' e^{-\mathrm{i}\Omega(t-t')}\int_{-\infty}^{\infty}\mathrm{d}^3\boldsymbol{q}e^{-\frac{|\boldsymbol{q}|^2}{2\sigma^2}} \\ &\times(2e^{-\frac{1}{2}\sigma^2\Omega^2}+e^{-i\Omega q_z}+e^{i\Omega q_z})\left(\frac{mK_1\left(m\sqrt{|\boldsymbol{q}|^2-(t'-t+\mathrm{i}\epsilon)^2}\right)}{4\pi^2\sqrt{|\boldsymbol{q}|^2-(t'-t+\mathrm{i}\epsilon)^2}}\right)^2 . \end{aligned} \tag{101}$$

We now do a change of variables to break up the time integrals: $u=t+t'$, $v=t-t'$, with a Jacobian $1/2$. The exponential becomes

$$e^{-\mathrm{i}\Omega(t-t')}=e^{-\mathrm{i}\Omega v}. \tag{102}$$

Inserting this into A, we get

$$\begin{aligned} A =&\frac{1}{2}(\sqrt{2\pi}\sigma)^3\frac{1}{2^3}\frac{1}{4}\frac{e^2}{2V\Omega}\left(\int_0^T\mathrm{d}v\int_{v-T}^{-v+T}\mathrm{d}u+\int_{-T}^0\mathrm{d}v\int_{-v-T}^{v+T}\mathrm{d}u\right)e^{-\mathrm{i}\Omega v} \\ &\times\int_{-\infty}^{\infty}\mathrm{d}^3\boldsymbol{q}e^{-\frac{|\boldsymbol{q}|^2}{2\sigma^2}}(2e^{-\frac{1}{2}\sigma^2\Omega^2}+e^{-i\Omega q_z}+e^{i\Omega q_z})\left(\frac{mK_1\left(m\sqrt{|\boldsymbol{q}|^2-(v-\mathrm{i}\epsilon)^2}\right)}{4\pi^2\sqrt{|\boldsymbol{q}|^2-(v-\mathrm{i}\epsilon)^2}}\right)^2 . \end{aligned} \tag{103}$$

We can do a change of variables $v\to -v$ for the second term in the first line:

$$\begin{aligned} A =&\frac{1}{2}(\sqrt{2\pi}\sigma)^3\frac{1}{2^3}\frac{1}{4}\frac{e^2}{2V\Omega}\int_0^T\mathrm{d}v\int_{v-T}^{-v+T}\mathrm{d}u\int\mathrm{d}^3\boldsymbol{q}e^{-\frac{|\boldsymbol{q}|^2}{2\sigma^2}}(2e^{-\frac{1}{2}\sigma^2\Omega^2}+e^{-i\Omega q_z}+e^{i\Omega q_z}) \\ &\times\left(e^{-\mathrm{i}\Omega v}\left(\frac{mK_1\left(m\sqrt{|\boldsymbol{q}|^2-(v-\mathrm{i}\epsilon)^2}\right)}{4\pi^2\sqrt{|\boldsymbol{q}|^2-(v-\mathrm{i}\epsilon)^2}}\right)^2+e^{\mathrm{i}\Omega v}\left(\frac{mK_1\left(m\sqrt{|\boldsymbol{q}|^2-(-v-\mathrm{i}\epsilon)^2}\right)}{4\pi^2\sqrt{|\boldsymbol{q}|^2-(-v-\mathrm{i}\epsilon)^2}}\right)^2\right). \end{aligned} \tag{104}$$

Performing the integral over u gives.

$$\begin{aligned} A =&(\sqrt{2\pi}\sigma)^3\frac{1}{2^3}\frac{1}{4}\frac{e^2}{2V\Omega}\int_0^T\mathrm{d}v\ (T-v)\int\mathrm{d}^3\boldsymbol{q}e^{-\frac{|\boldsymbol{q}|^2}{2\sigma^2}}(2e^{-\frac{1}{2}\sigma^2\Omega^2}+e^{-i\Omega q_z}+e^{i\Omega q_z}) \\ &\times\left(e^{-\mathrm{i}\Omega v}\left(\frac{mK_1\left(m\sqrt{|\boldsymbol{q}|^2-(v-\mathrm{i}\epsilon)^2}\right)}{4\pi^2\sqrt{|\boldsymbol{q}|^2-(v-\mathrm{i}\epsilon)^2}}\right)^2+\left(e^{\mathrm{i}\Omega v}\frac{mK_1\left(m\sqrt{|\boldsymbol{q}|^2-(-v-\mathrm{i}\epsilon)^2}\right)}{4\pi^2\sqrt{|\boldsymbol{q}|^2-(-v-\mathrm{i}\epsilon)^2}}\right)^2\right). \end{aligned} \tag{105}$$

We now change into spherical coordinates by making the substitutions

$$\int_{-\infty}^{\infty} \mathrm{d}^3\boldsymbol{q} \to \int_0^{\infty} dq \int_0^{\pi} d\theta \int_0^{2\pi} d\phi \; q^2 \sin(\theta) = 4\pi \int_0^{\infty} dq \; q^2 \quad (106)$$

$$\int_{-\infty}^{\infty} \mathrm{d}^3\boldsymbol{q} e^{\pm i\Omega q_z} \to \int_0^{\infty} dq \int_0^{\pi} d\theta \int_0^{2\pi} d\phi \; q^2 \sin(\theta) e^{\pm i\Omega q \cos(\theta)} = 4\pi \int_0^{\infty} dq \; q^2 \mathrm{sinc}(q\Omega) \,, \quad (107)$$

where $q = |\boldsymbol{q}|$ and $\mathrm{sinc}(x) = \sin(x)/x$. This gives

$$\begin{aligned} A =& (4\pi) 2 \frac{1}{2} (\sqrt{2\pi}\sigma)^3 \frac{1}{2^3} \frac{1}{4} \frac{e^2}{2V\Omega} \int_0^T \mathrm{d}v \; (T-v) \int_0^{\infty} \mathrm{d}q \; e^{-\frac{q^2}{2\sigma^2}} \; q^2 \Big(e^{-\frac{1}{2}\sigma^2\Omega^2} + \mathrm{sinc}(q\Omega) \Big) \\ & \times \left(e^{-\mathrm{i}\Omega v} \left(\frac{m K_1\left(m\sqrt{q^2 - (v - \mathrm{i}\epsilon)^2} \right)}{4\pi^2 \sqrt{q^2 - (v-\mathrm{i}\epsilon)^2}} \right)^2 + e^{\mathrm{i}\Omega v} \left(\frac{m K_1\left(m\sqrt{q^2 - (-v - \mathrm{i}\epsilon)^2} \right)}{4\pi^2 \sqrt{q^2 - (-v-\mathrm{i}\epsilon)^2}} \right)^2 \right) \end{aligned} \quad (108)$$

Following a similar procedure as above, but for B in Eq. (3.35), we find that

$$\begin{aligned} B =& (4\pi) \frac{1}{2} (\sqrt{2\pi}\sigma)^3 \frac{1}{2^3} \frac{1}{4} \frac{e^2}{2V\Omega} \int_0^T \mathrm{d}v \int_{v-T}^{-v+T} \mathrm{d}u e^{-\mathrm{i}\Omega u} \int_0^{\infty} \mathrm{d}q e^{-\frac{q^2}{2\sigma^2}} \; q^2 \Big(e^{-\frac{1}{2}\sigma^2\Omega^2} + \mathrm{sinc}(q\Omega) \Big) \\ & \times \left(\left(\frac{m K_1\left(m\sqrt{q^2 - (v - \mathrm{i}\epsilon)^2} \right)}{4\pi^2 \sqrt{q^2 - (v-\mathrm{i}\epsilon)^2}} \right)^2 + \left(\frac{m K_1\left(m\sqrt{q^2 - (-v - \mathrm{i}\epsilon)^2} \right)}{4\pi^2 \sqrt{q^2 - (-v-\mathrm{i}\epsilon)^2}} \right)^2 \right) . \end{aligned} \quad (109)$$

Performing the integral over u gives.

$$\begin{aligned} B =& (4\pi) (\sqrt{2\pi}\sigma)^3 \frac{1}{2^3} \frac{1}{4} \frac{e^2}{2V\Omega} \int_0^T \mathrm{d}v \; \sin\big((T-v)\Omega\big) \int_0^{\infty} \mathrm{d}q e^{-\frac{q^2}{2\sigma^2}} \; q^2 \Big(e^{-\frac{1}{2}\sigma^2\Omega^2} + \mathrm{sinc}(q\Omega) \Big) \\ & \times \left(\left(\frac{m K_1\left(m\sqrt{q^2 - (v - \mathrm{i}\epsilon)^2} \right)}{4\pi^2 \sqrt{q^2 - (v-\mathrm{i}\epsilon)^2}} \right)^2 + \left(\frac{m K_1\left(m\sqrt{q^2 - (-v - \mathrm{i}\epsilon)^2} \right)}{4\pi^2 \sqrt{q^2 - (-v-\mathrm{i}\epsilon)^2}} \right)^2 \right) \end{aligned} \quad (110)$$